

THÈSE

En vue de l'obtention du

DOCTORAT DE L'UNIVERSITÉ DE TOULOUSE

Délivré par :

Institut National Polytechnique de Toulouse (Toulouse INP)

Discipline ou spécialité :

Energétique et Transferts

Présentée et soutenue par :

M. THOMAS LAFARGE

le jeudi 23 juin 2022

Titre :

Investigation of Lattice Boltzmann Methods applied to multiphase flows

---

Ecole doctorale :

Mécanique, Energétique, Génie civil, Procédés (MEGeP)

Unité de recherche :

Centre Européen de Recherche et Formation Avancées en Calcul Scientifique (CERFACS)

Directeur(s) de Thèse :

MME BÉNÉDICTE CUENOT

M. PIERRE BOIVIN

Rapporteurs :

M. FLORIAN DE VUYST, UNIVERSITE DE TECHNOLOGIE DE COMPIEGNE

M. FRANÇOIS DUBOIS, CNAM PARIS

Membre(s) du jury :

M. RÉMI ABGRALL, UNIVERSITE DE ZURICH, Président

MME BÉNÉDICTE CUENOT, CERFACS, Membre

M. NICOLAS ODIER, CERFACS, Membre

M. PIERRE BOIVIN, UNIVERSITE AIX-MARSEILLE 1, Membre

M. STEFANO PUGGELLI, GROUPE SAFRAN, Membre

M. UMBERTO D'ORTONA, CNRS MARSEILLE, Membre

Multiphase Lattice Boltzmann methods

Abstract The purpose of this thesis is the study of Lattice Boltzmann Methods (LBM), applied to multiphase flows. First, general principles of statistical physics and of Lattice Boltzmann Methods are introduced, followed by a historical review about Lattice Gas Automata. A state of the art of the multiphase flow simulation methods is then proposed, with a particular emphasize on diffuse interface methods. In particular, the phase field methods are introduced, and different methods allowing to numerically simulate surface tension are also presented. A second review concerning multiphase flow simulation in a Lattice Boltzmann framework is presented. More precisely, general principals are presented, and the four major methods, Color Gradient, Pseudo-Potential, Free Energy and HCZ, are successively presented. Lattice Boltzmann Methods advanced notions are then introduced, in particular, a Taylor expansion based method that allows to determine Lattice Boltzmann schemes equivalent macroscopic equation is described. A Gradient Color method theoretical study is proposed. First, an original reformulation of the algorithm allowing an improvement in computational efficiency is proposed. The Taylor expansion method is then applied to Gradient Color Method in order to determine the high order error induced by the numerical scheme. This expression allows to demonstrate how the degree of isotropy is essential to the scheme numerical stability. In particular, a numerical operator allowing to introduce an equation of states that differs from the athermal perfect gas equation is proposed. This operator efficiency is illustrated by being applied to academical testcases. The Taylor expansion method is also applied in order to show how the Color Gradient Method allows to solve an Allen-Cahn phase field equation. This theoretical result is then validated numerically. Finally, an original improved version of the Gradient Color Method is proposed. In this method, the efficient formulation and the isotropic Equation of State operator is used, and an original temporal correction term is proposed. This correction term improves the scheme numerical stability and allows to expands the method application range to higher density ratios. Finally, this method is validated through academical testcases.

Keywords: Mutltiphase flow, Colour Gradient, Lattice Boltzmann Methods

---

CERFACS

SAFRAN

Remerciements

Je souhaite tout d'abord remercier les membres du jury qui ont accepter d'évaluer mes travaux, Rémi Abgrall qui a accepté de présider le jour de la soutenance, les rapporteurs qui ont évalué le manuscrit : François Dubois, et Florian De Vuyst qui a même fait le déplacement jusqu'à Toulouse. Je remercie particulièrement Umberto d'Ortona pour sa relecture attentive du manuscrit et ses retours de qualités. Je remercie bien sûr mes superviseurs, Pierre pour tes conseils avisés, Stéfano pour ton aide malgré le fait que tu ais reçu reçu la patate chaude un peu malgré toi, et bien sûr Nicolas pour ton immense soutien au quotidien, ta relecture plus qu'attentive (et impitoyable) du manuscrit et ta gentillesse. Je te dois beaucoup, encore merci. Je n'oublie bien sûr pas Antony et Léa qui ont été là au début du projet, bon courage dans vos carrières respectives. Merci aux membres de la team Aéro qui sont toujours là pour une discussion intéressante et surtout pour aider les newbies en LBM, je pense tout particulièrement à Thomas Astoul, Florian, Gauthier (pour votre précieuse aide, notamment pour me mettre le pied à l'étrier), Minh (pour ton aide sur ProLB) et Lucien (pour tes discussions et conseils avisés). Merci aux membres du M2P2 pour leur accueil et les discussions intéressantes, notamment Gabriel et Thomas Coratger.
Je remercie également tout les gens imposables de l'Union Européenne qui ont rendu le projet Magister (et donc le versement de mon salaire pendant 3 ans) possible. Plus sérieusement, merci à Bridgette et Jorien pour la gestion du projet (et pour leur compréhension vis à vis des retards de deadline). Un grand merci à l'équipe informatique du Cerfacs CSG, qui est toujours là pour aider les Cerfacsiens en détresse avec efficacité et pédagogie. Merci à toute l'équipe administrative du Cerfacs pour leur aide au quotidien, et tout particulièrement à Super Chantal, dont la bonne humeur devenue légendaire illumine le quotidien du Cerfacs. Enfin, un grand merci aux collègues de Ct Ingénierie qui m'ont soutenu pendant la période plutôt intense de chevauchement entre fin de rédaction du manuscrit et début de nouveau job, merci pour votre soutien et votre compréhension.
D'un point de vue plus personnel, merci à tout ceux qui m'ont entouré pendant ces trois années quelques peu particulières. Je pense bien évidemment à mes parents, mes soeurs chéries et à toute la famille avec qui nous avons partagé (et partagerons encore longtemps) de beaux moments. Merci à vous, je vous aime. Je pense bien sûr aussi à ceux qui partagent ma vie Toulousaine. Les collègues du Cerfacs, que ce soit ceux avec qui j'ai pu partager des parties de mots croisées endiablées, des séances de thérapies collectives sur à quel point la vie de doctorant au Cerfacs c'est horrible, ou de grandes bières bien méritées. Merci aux copains du Wild Rose d'être toujours là quand y faut, vous êtes comme de la famille. Et surtout je n'oublie pas de remercier tout les beaux gosses du Tou'Win Rugby Club, merci pour votre luxuriance au quotidien.
Enfin, un grand merci au type qui se fait des soupes de pangolins au p'tit dej. T'es parfait mec, change rien.

Contents

Abstract iii

Remerciements v

Résumé en Français xi

Introduction 1

1. Lattice Boltzmann Methods 5
1.1. Introduction to statistical mechanics . . . 6
1.1.1. Distribution function . . . 6
1.1.2. Equilibrium function . . . 7
1.1.3. Boltzmann equation . . . 8
1.2. Macroscopic equivalent equation . . . 10
1.2.1. The Chapmann-Enskog development . . . 10
1.2.2. Equivalent macroscopic equation of the Boltzmann equation . . . 11
1.2.3. Equivalent macroscopic equation for the athermal case . . . 13
1.3. Discretization of Boltzmann Equation . . . 15
1.3.1. Hermite polynomial . . . 15
1.3.2. Velocity sets and coefficients . . . 16
1.3.2.1. D2Q9 velocity set . . . 17
1.3.2.2. D3Q19 velocity set . . . 20
1.3.3. Classical LBM . . . 21
1.4. Historical review . . . 23
1.4.1. The original Hardy de Pazzis Pommeau algorithm . . . 23
1.4.2. Algorithm equivalent macroscopic equations . . . 24
1.4.3. Enhanced HPP model . . . 25
1.4.4. A discussion around isotropy . . . 26
1.4.5. LGA's drawback . . . 27
1.4.6. From LGA to LBM . . . 28

2. Multiphase flows simulation 29
2.1. Surface tracking methods . . . 30
2.1.1. Front tracking . . . 30
2.1.2. Volume Of Fluids . . . 31
2.1.3. Level Set . . . 33
2.2. Diffuse Interface Method . . . 36
2.2.1. Phase field method . . . 36
2.2.1.1. Fundamental principles . . . 36
2.2.1.2. Cahn Hilliard and Allen-Cahn equations . . . 37
2.2.1.3. Allen-Cahn equation: a geometrical approach . . . 38
2.2.1.4. About mass conservation . . . 40
2.2.2. Multi fluids methods . . . 40

2.3. Surface tension . . . 44
2.3.1. Geometrical approach . . . 45
2.3.2. Free Energy approach . . . 46

3. Multiphase LBM **49**
3.1. General Introduction . . . 50
3.1.1. Surface Tension . . . 50
3.1.2. Numerical scheme for the spatial derivative operator . . . 52
3.1.3. Non-perfect Equation Of State . . . 54
3.1.4. Viscosity . . . 57
3.2. Rothman-Keller Method . . . 59
3.2.1. Algorithm presentation . . . 59
3.2.2. Historical review . . . 61
3.3. Free energy methods . . . 67
3.3.1. Introduction . . . 67
3.3.2. Discussion around the phase field equation . . . 69
3.3.3. Historical review . . . 70
3.4. Pseudo Potential . . . 71
3.4.1. Macroscopic equations . . . 71
3.4.2. Numerical Scheme . . . 72
3.4.3. Historical review . . . 73
3.5. HCZ . . . 76
3.5.1. Macroscopic equations . . . 76
3.5.2. Numerical Scheme . . . 77
3.5.3. Historical review . . . 79

4. Taylor expansion of the Lattice Boltzmann **81**
4.1. Advanced Collision Model . . . 82
4.1.1. Multiple Relaxation Time . . . 82
4.1.2. Regularized Collision Operators . . . 84
4.1.3. Bulk viscosity and MRT . . . 86
4.2. Body Force in LBM . . . 88
4.2.1. Body force schemes . . . 88
4.2.2. Body force and MRT schemes . . . 89
4.2.3. Correction terms in LBM . . . 90
4.3. Taylor expansion . . . 91
4.3.1. $0^{th} order$ . . . 92
4.3.2. $1^{st} order$ . . . 93
4.3.3. $2^{nd} order$ . . . 93
4.3.4. $3^{rd} order$ . . . 94

5. Colour Gradient algorithm theoretical analysis **95**
5.1. Algorithm reformulation . . . 96
5.2. Equation of State Operator . . . 99
5.2.1. Discussion . . . 99
5.2.2. Numerical illustration . . . 103
5.3. Recoloration equivalent phase field equation . . . 105
5.3.1. Discussion . . . 105
5.3.2. Numerical illustration . . . 106

6. Improved algorithm **109**
6.1. Improved algorithm . . . 110
6.1.1. Targeted macroscopic equations . . . 110
6.1.2. Algorithm presentation . . . 111
6.1.3. Correction term justification . . . 114
6.2. Numerical Results . . . 118
6.2.1. Poiseuille Flow . . . 118
6.2.2. Laplace test . . . 119
6.2.3. Oscillating droplet . . . 120
6.2.4. Rayleigh-Taylor instability . . . 123

Conclusion **125**

Appendices **127**
A. Appendix A . . . 129
B. Appendix B . . . 139
C. Appendix C . . . 141
D. Appendix D . . . 149

List of Figures **152**

List of Tables **155**

Bibliography **157**

Résumé en Français

L'objectif de cette thèse est l'étude des méthodes Boltzmann sur Réseau (dites LBM) appliquées aux écoulements multiphasiques. Dans un premier temps, des principes généraux concernant la physique statistique ainsi que les méthodes Boltzmann sur Réseaux sont introduits, ainsi qu'une revue historique des automates de gaz sur réseaux. Un état de l'art des méthodes de simulation des écoulement multiphasiques est ensuite proposé avec une intention particulière portée aux méthodes aux interfaces diffuses. En particulier, les méthodes de champs de phases (dites " phase field ") sont introduites, ainsi que les différentes méthodes permettant de simuler la numériquement le phénomène de tension de surface. Une seconde revue bibliographique portant sur la simulation des écoulement multiphasiques dans le contexte des schémas de Boltzmann sur réseau est présentée. Plus précisément, des principes généraux sont présentés, puis les quatre grandes familles de méthodes, gradient de couleur, énergie libre, pseudo-potentielle et HCZ sont détaillées successivement. Des notions avancées concernant les méthodes de Boltzmann sur Réseau sont ensuite introduites, en particulier une méthode basée sur le principe de développement de Taylor permettant de déterminer les équations macroscopiques équivalentes d'un schéma de Boltzmann sur réseau est décrite. Une étude théorique des méthodes du Gradient de Couleur est ensuite proposée. En premier lieu, une reformulation de l'algorithme permettant un gain en efficacité est proposée. La méthode de développement de Taylor est ensuite appliquée à la méthode du Gradient de Couleur afin de déterminer l'expression analytique des erreurs d'ordre élevée induite par le schéma numérique. Cette expression permet de démontrer l'importance du degré d'isotropie sur la stabilité du schéma numérique. En particulier, un opérateur numérique permettant d'introduire une équation d'état différente de l'équation d'état des gaz parfait athermale est proposée. L'efficacité de ce schéma isotropique est illustrée sur des cas académiques. La méthode du développement de Taylor est également appliquée afin de démontrer que la méthode du Gradient de Couleur est équivalent à la résolution d'une équation d'Allen-Cahn ce qui est vérifié numériquement. Enfin, une version améliorée de la méthode du Gradient de Couleur est proposée. En plus d'utiliser la reformulation et l'opérateur isotropique présentés plus haut, un opérateur de correction temporelle est proposé. Ce dernier permet de grandement améliorer la stabilité numérique du schéma et permet d'étendre le domaine d'applicabilité de la méthode à de plus hauts ratio de densité. Enfin, cette méthode est ensuite validée sur différents cas d'applications académiques.

Introduction

Aeronautics is one of the major french industries: 4 out of the 40 biggest french companies are dedicated to it (Airbus, Dassault, Safran and Thalès). The passengers number has been constantly growing years after years; while being previously only considered by wealthy people, this transportation mode became cheaper over the year, and is now affordable for middle classes [1]. Not only this activity has an economical importance, but it is also a national sovereignty matter for wide countries such as Russia or Australia, for which internal travels mainly rely on plane due to the country dimensions [2]. An obstacle to this development is that the aeronautical industry remains one of the most polluting industry per passenger per kilometers, when considering green house gases emissions, representing alone 4% of European Union's green house gases emissions [3]. As a consequence, aeronautical industry growth is a priori incompatible with the fight against climate change.
Recently, two policies are proposed to address this issue. The first one consists in reducing the total number of travels operated by planes, for example in France by banning flights that can be reasonably replaced by a train travel. The second consists in drastically reducing the greenhouse gas emissions. In the short term, airplane makers plan to launch a new aircraft generation with significantly reduced emissions, relying on lean combustion engines which are believed to be able to reduce CO_2 emissions by 25% [1]. However, such reduction won't be enough to reach national plans to fight climate change, such as the 2050 zero emission plan followed by the European Union. On the longer term, manufacturers plan on developing new hydrogen based sustainable aviation fuels, which are presented as "zero emission" solutions [4]. Both technical solutions rely on new aircraft engines combustion chamber architectures, allowing to use different fuel compositions or totally different fuels. An issue of the uppermost importance when designing combustion chamber is the prediction of thermo-acoustic instabilities [5], which may lead to severe damages. Thermo-acoustic instabilities have been shown to be impacted by the use of hydrogen [6]. It is also known that cowlings occur between the spray and the acoustics [7, 8]. For these reasons, the design of combustion chambers must account for these couplings and instabilities to ensure safety [9]. It must then account for the fuel injection and the spray formation. In order to characterize completely an engine architecture, a consistent injection model is necessary. One phenomenon in particular is of interest: primary atomization. In order to define this phenomenon, a discussion about aircraft engine structure is proposed.

Atomization in aircraft

Aeronautical civil aircraft engines consist in a stack of different components as illustrated in Figure 0.1. The fan, or propeller, located at the entrance, accelerates the incoming air and provides most of the engine thrust. The fan rotation is allowed through a primary air circuit, in which some amount of propelled air is taken, compressed in a compressor, heated in the combustion chamber thanks to the combustion of a fuel, and then expanded in a turbine which drives the shaft and consequently, the fan and compressor. A nozzle located downstream of the engine finally accelerates the air to increase the thrust. Note that compression is not essential to the engine operation but significantly increases combustion efficiency. When focusing on the combustion chamber, it is composed of a chamber as well as some fuel injectors, allowing to inject the fuel.
The liquid fuel is injected in the combustion chamber through fuel injectors, for which several concepts exist ([10]). The role of the injector is to transform the injected liquid fuel into a spray of small droplets, so that the exchange surface between the liquid fuel and the gaseous oxidizer is increased. This allows to increase the liquid evaporation rate, favoring the fuel-oxidizer mixing, and thus the combustion

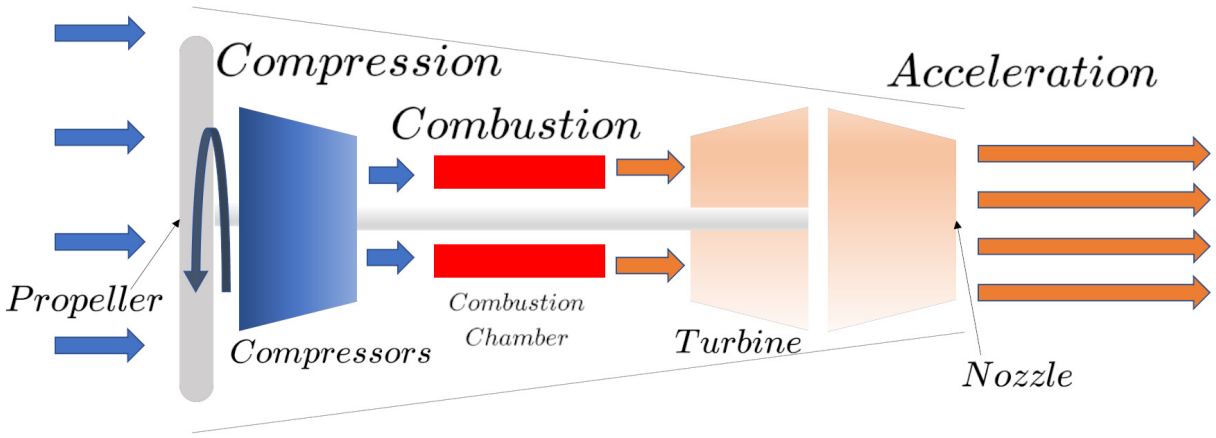


Figure 0.1. – Scheme of an aeronautical engine

efficiency. Figure 0.2 illustrates this process, when liquid fuel is injected in the combustion chamber through a pressure-swirl atomizer. The physics from which a spray of small droplets results from a

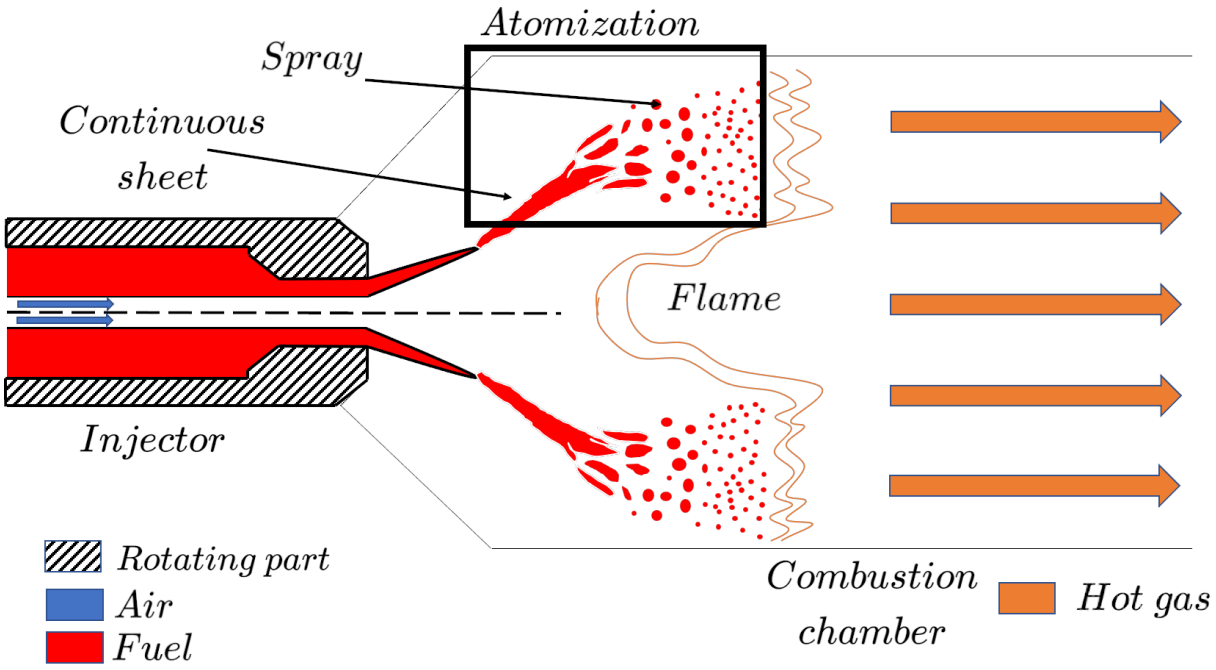


Figure 0.2. – Schematic of a pressure swirl injector in a combustion chamber

continuous liquid is called the atomization. It consists in a series of liquid-gas instabilities [10, 11] which remain not fully understood and hardly predictable for realistic configurations. As previously said, the atomization may significantly be influenced by acoustic, or thermo-acoustic instabilities [7, 12, 13]. An illustration of an actual spray at a pressure swirl injector exit is proposed Figure 0.3. For this reason, both atomization and combustion must be simultaneously investigated. Unfortunately, the experimental investigation of atomization in a closed, pressurized, reactive combustion chamber is a tough issue. This motivates the need for accurate numerical solvers able to predict atomization in a compressible and reactive environment.

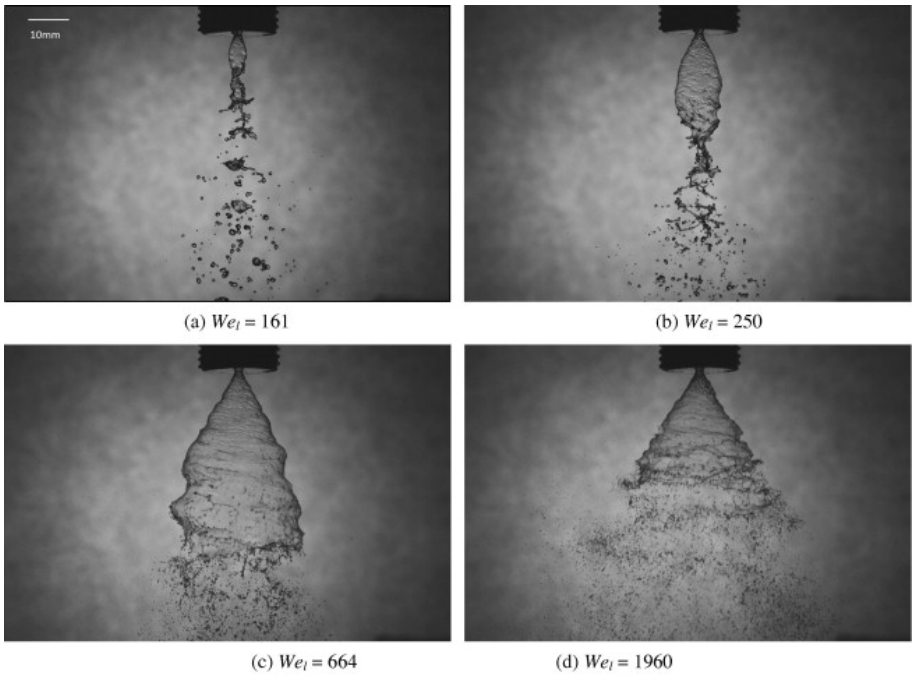


Figure 0.3. – Atomization process in a pressure swirled injector. From Surya Prakash et al. [14]

Numerical solvers

Because of the complexity resulting from non-linearity of Navier-Stokes equations, analytical solution are known only for simple academical cases such as a Poiseuille flow or a Couette flow. Proving existence and smoothness of a solution is part of the seven Millenium Prize Problems defined by the Clay Mathematical Institute, rewarded by a million dollars price [15]. The development of numerical methods and supercomputers allowed to overcome this lack of analytical solution by approximating Navier-Stokes solution through Computational Fluid Dynamics (CFD). Several numerical methods can be listed, such as finite volume, finite differences, spectral differences. Independently of the considered numerical method, high Reynold numbers (Re) flows simulation is only possible by paying a heavy price in term of computational time and memory. To reduce this costs, turbulence modeling has been proposed, such as Large Eddy Simulation (LES) [16], for which the smallest turbulent scales are modeled, or Reynold Averaged Numerical Simulation (RANS) [17], averaged in space and time. Navier-Stokes convection term and pressure term non-locality are an important unstability source. Simulating non-purely aerodynamic phenomena is also an active topic of investigation, such as for evaporation, frosting, or, the main topic of this document, multiphase flows.
Multiphase flows simulation is a challenging subject of investigation in fluid mechanics. In the present work, "multiphase flows" states for two immiscible phases, while "multiphase" can be more general. When two immsicible flows co-exist, a smooth transition occurs over a few atoms length. Since it is much smaller than the usual system's length of interests, the interface is considered infinitely fine. This introduces a discontinuity, which is a challenge to adress in numerical methods. Furthermore, as later detailled in the manuscript, a surface tension occurrs at the interface, which has a significant impact on the dynamics of the interface [18], making it a key factor in atomization study. For this force to be computed, the interface curvature needs to be accurately estimated, which is particularly challenging for complex flow topologies, such as interfacial waves, liquid ligaments, and associated break-up. Finally, atomization configurations also involve high Reynold numbers, high Weber numbers, significant shear and density gradient across the interface.

Lattice Boltzmann Method and Multiphase Flow

In the meantime, Lattice Boltzmann Method (LBM) has received a growing attention. Its basis have been originally proposed by the Cellular Automata community. Since Frish et *al*. [19] and d'Humières et *al*. [20] who introduced the Lattice Gas Automata (LGA) algorithm, Mc Namara and Zanetti [21] extended this work to propose a Lattice Boltzmann Method. Originally proposed for low-Mach aerodynamics, extensions to multi-phase flows rapidly came out. Rothman and Keller [22] proposed a LGA multiphase algorithm that has been adapted to a LBM framework by Gustensen et *al*. [23]. LBM received a growing interest motivated by its scalability and its low dissipation properties, making it particularly well-suited for acoustic long distance dispersion problems [24]. It also proved to be more computationally efficient than standard Navier-Stokes methods for aerodynamics problems for example. Its application to two-phase flows have also largely been undertaken, with several specific methodologies. Apart from the Colour Gradient Method [22] (also known as RK method from Rothman and Keller, their creators) Shan and Chen [25, 26] proposed a Pseudo-potential method. Swift et *al*. introduced the Free Energy method [27, 28] and He et *al*. [29] finally proposed the so-called HCZ method (from He, Chen and Zhang who first proposed the method), which recently received a lot of attention since the work of Fakhari et *al* [30–33] and Geier et *al*. [34]. Those methods were applied on a large range of cases: droplet impact [35], free jet [36], ternary fluid [37], drop impact on a liquid film [38], flow with surfactants [39] and also widely in porous flow [40]. HCZ method allows to simulate a large range of flows at both large density ratios and large Reynolds numbers [41], while other methods are limited to moderate density ratios and / or moderate Reynolds numbers. Despite the attractiveness of this last method, it takes place in an incompressible framework. The need to account for compressibility is of importance for atomization. For such problems, other methods than HCZ must be investigated. Because of its numerical efficiency [42], the Color Gradient Method is chosen here. However, the derivation of the equivalent macroscopic equations is not straightforward [43–45]. Considering that a lot of important steps in free energy and HCZ methods were made by appropriating methods among the Phase Field community[46, 47], the difficulty of obtaining a LBM equivalent equation for the Color-Gradient Method can be seen as an important drawback.

Dissertation outline

In the present work, a new numerically efficient, but equivalent formulation of the Color-Gradient method is proposed. In particular, it is adapted to an arbitrary Equation Of State (EOS), and a new physical interpretation of the method is proposed. Based on an innovative approach different from Subhedar et al. [45], the equivalent macroscopic equation associated to the recoloration step – accounting for phase segregation – is proposed. It is shown that the recoloration step allows to solve an advection-diffusion equation. Finally this work highlights a spurious temporal term, which can be corrected by a new correction term, significantly improving numerical stability, thus allowing to tackle density ratios as high as 1000.
This work is organized as follow: in Chapter 1, an introduction to Lattice Boltzmann method is proposed, in Chapter 2, a review of numerical methods to predict multiphase flows is proposed. Chapter 3 is a review of Lattice Boltzmann Methods applied to multiphase flows. Chapter 4 address the advanced LBM framework that must be detailed to understand how LBM macroscopic equations can be determined from a Taylor Expansion. In Chapter 5, a theoretical analysis of the colour gradient method is proposed and finally in Chapter 6 an improved algorithm is presented and is applied to academical test-cases.

Chapter 1

Lattice Boltzmann Methods

Overview

1.1. Introduction to statistical mechanics . . . 6
1.1.1. Distribution function . . . 6
1.1.2. Equilibrium function . . . 7
1.1.3. Boltzmann equation . . . 8
1.2. Macroscopic equivalent equation . . . 10
1.2.1. The Chapmann-Enskog development . . . 10
1.2.2. Equivalent macroscopic equation of the Boltzmann equation . . . 11
1.2.3. Equivalent macroscopic equation for the athermal case . . . 13
1.3. Discretization of Boltzmann Equation . . . 15
1.3.1. Hermite polynomial . . . 15
1.3.2. Velocity sets and coefficients . . . 16
1.3.3. Classical LBM . . . 21
1.4. Historical review . . . 23
1.4.1. The original Hardy de Pazzis Pommeau algorithm . . . 23
1.4.2. Algorithm equivalent macroscopic equations . . . 24
1.4.3. Enhanced HPP model . . . 25
1.4.4. A discussion around isotropy . . . 26
1.4.5. LGA's drawback . . . 27
1.4.6. From LGA to LBM . . . 28

At a time where the existence of the atom was still a burning subject of controversy among the scientific community, Ludwig Boltzmann (1844-1906) proposed the kinetic theory of gases [48]. By assuming fluids as an aggregation of atoms ruled by Newtonian mechanic laws, Boltzmann recovered phenomena such as heat, viscosity or magnetism. The statistical approach of gases covers most of the phenomena described by thermodynamic, such as heat transfer, thermal equilibrium, equations of state, etc. Even after more than a century, this work remains particularly relevant and is still used on a daily base in the modern science framework. In particular, one the main subject of discussion of the present work, Lattice Boltzmann Methods, rely on Boltzmann's kinetic theory. The present Chapter is organized as follow. First, statistical mechanics basic principles are presented Section 1.1, then the link between Boltzmann equations and Navier-Stokes equations are presented Section 1.2. The Lattice Boltzmann method is then introduced Section 1.3, and the chapter ends on a review of LBM's birth history Section 1.4.

1.1. Introduction to statistical mechanics

1.1.1. Distribution function

The classical approach to represent a fluid is to consider a continuum system, described by several macroscopic quantities, such as the density ρ ($kg.m^{-3}$), the velocity $\vec{u}$ ($m.s^{-1}$), the total mass energy E ($m^2.s^{-2}$). The state of a fluid is fully known if those macroscopic fields are known. The temperature T (K) can be used rather than E. The dynamic of the fluid is influenced by the pressure p ($kg.m^{-1}.s^{-2}$) which is a function of ρ and T. The law describing the relationship between p, ρ and T is called the Equation Of State (EOS).
A fluid system can also be described from a microscopic and discontinuous point a view by calculating every atom's position and instant velocity. Such an approach would necessitate an excessive amount of computation power given the particles quantity in a typical flow (2.1 10^{22} particles in a single gram of air). Note that for each atom, the position (x, y, z) and the velocity $\vec{\xi} = (\xi_x, \xi_y, \xi_z)$ need to be determined, which makes 6 variables per particle. An intermediate scale exists between the microscopic and the macroscopic one: the fluid can be described through a statistical approach thanks to a density function f.
This statistical description of the fluid stands in a particular framework. Atoms are supposed to be all identical and mono-atomic. As a consequence of this mono-atomic assumption, no inner-rotation or inner-vibration movement are possible, making the particles translation the only source of kinetic energy.
In this model, the state of a fluid at a given point of space is fully described by a distribution function $f(\vec{x}, \vec{\xi}, t)$. It is a function of time t, space $\vec{x}$ and of the microscopic velocities $\vec{\xi}$, it is homogeneous to a density per velocity cubed ($kg.m^{-6}.s^3$). Its integration over the microscopic velocity space correspond to the density of particles going to a particular speed. Its integration over $[\xi_{x,1}, \xi_{x,2}]$, $[\xi_{y,1}, \xi_{y,2}]$, $[\xi_{z,1}, \xi_{z,2}]$ given by $\int_{\xi_{x,1}}^{\xi_{x,2}} \int_{\xi_{y,1}}^{\xi_{y,2}} \int_{\xi_{z,1}}^{\xi_{z,2}} f(\vec{x}, \vec{\xi}, t) d\xi_x d\xi_y d\xi_z$ corresponds to the density of particles at the location $\vec{x}$ at the time t whose velocity belongs to $[\xi_{x,1}, \xi_{x,2}]$, $[\xi_{y,1}, \xi_{y,2}]$ and $[\xi_{z,1}, \xi_{z,2}]$.
In a simpler way, $f(\vec{x}, \vec{\xi}, t) d\vec{\xi}$ is the density of particles going at the velocity $\vec{\xi}$ in a volume of $d\vec{\xi}$. The way this function describes a fluid behavior can seem obscure, but in fact f can be linked to the macroscopic quantities through integration relationships. If $f(\vec{x}, \vec{\xi}, t) d\vec{\xi}$ is the density of particles going at a given speed, then its integration over all the microscopic space gives the density of particles going at any speed, which is the total density of particles. Then density at a given point is given by:

$$\rho(\vec{x}, t) = \int_{-\infty}^{\infty} \int_{-\infty}^{\infty} \int_{-\infty}^{\infty} f(\vec{x}, \vec{\xi}, t) d\xi_x d\xi_y d\xi_z \tag{1.1}$$

In order to make the notations slightly less heavy the triple integration over microscopic space is noted: $\int_{\infty}^{\infty}\int_{\infty}^{\infty}\int_{\infty}^{\infty} *d\xi_x d\xi_y d\xi_z = \iiint *d\vec{\xi}$.
If $f(\vec{x},\vec{\xi},t)d\vec{\xi}$ corresponds to the density of particles going at the velocity $\vec{\xi}$, then $\vec{\xi}f(\vec{x},\vec{\xi},t)d\vec{\xi}$ corresponds to the momentum of those particles. Then its integration gives the average momentum of all the particles. Finally the fluid macroscopic velocity can be given by:

$$\rho(\vec{x},t)\vec{u}(\vec{x},t) = \iiint \vec{\xi}f(\vec{x},\vec{\xi},t)d\vec{\xi} \tag{1.2}$$

In a similar manner, the macroscopic total mass energy is given by:

$$\rho(\vec{x},t)E(\vec{x},t) = \frac{1}{2}\iiint |\vec{\xi}|^2 f(\vec{x},\vec{\xi},t)d\vec{\xi} \tag{1.3}$$

This total energy accounts for the internal energy e, and the kinetic energy :

$$\rho E = \rho\left(e + \frac{1}{2}|u|^2\right) \tag{1.4}$$

It can be verified that the internal energy can also be calculated through an integral equation such as:

$$\rho e(\vec{x},t) = \frac{1}{2}\iiint |\vec{\xi}-\vec{u}|^2 f(\vec{x},\vec{\xi},t)d\vec{\xi} \tag{1.5}$$

This internal energy term is of importance in this work since it can be proven to be related to the pressure. The $\vec{\xi}-\vec{u}$ is the particles velocity relatively to the mean velocity. Hereinafter, it will be noted:

$$\vec{v} = \vec{\xi}-\vec{u} \tag{1.6}$$

It can be shown through a demonstration proposed in Appendix A.1, that in the mono-molecular framework, internal energy and pressure are proportional according to:

$$p = \frac{2}{3}\rho e \tag{1.7}$$

If perfect gas law is assumed, internal energy can be written as:

$$e = \frac{3p}{2\rho} = \frac{3rT}{2} = \frac{3k_B}{2m} \tag{1.8}$$

With r the specific gas constant ($m^2s^{-2}K^{-1}$), T the temperature (in Kelvin K), k_B the Boltzmann's constant and m the mass of one particle.

1.1.2. Equilibrium function

As detailed in Section 1.1.3, a differential equation for f describing the flow dynamic can be defined. It relies on the assumption of the existence of an equilibrium state in which all the directions of the relative velocity $\vec{v}$ are equally probable. This equilibrium state is described by an equilibrium distribution function function f^{eq}, which expression is central in the present work. Relying on the isotropic assumption, the expression of the equilibrium distribution function can be determined. The detail of the demonstration is proposed in Appendix A.2. The equilibrium function's expression is given by:

$$f^{eq} = \frac{\rho}{(2\pi rT)^{\frac{3}{2}}}e^{-\frac{|\vec{v}|^2}{2rT}} \tag{1.9}$$

This function f_i^{eq} is the Maxwell-Boltzmann distribution. A first expression of f^{eq} has been proposed by Maxwell [49] and corresponds to the demonstration of Appendix A.2, then a more rigorous demonstration has been later proposed by Boltzmann [48].
Note that the successive moments of f^{eq} respects the conditions of isotropy proposed by Wolfram Eq. (1.96). In the LGA framework, to obtain the density it was necessary to sum c_i over all the microscopic velocities, in this kinetic theory framework the integration operation is necessary. The first successive moments of f^{eq} in $\vec{u}$ frame of reference follow:

$$\iiint f^{eq}(\vec{x},\vec{\xi},t)d\vec{\xi} = \rho \tag{1.10}$$

$$\iiint v_\alpha f^{eq}(\vec{x},\vec{\xi},t)d\vec{\xi} = 0 \tag{1.11}$$

$$\iiint v_\alpha v_\beta f^{eq}(\vec{x},\vec{\xi},t)d\vec{\xi} = \rho rT\delta_{\alpha\beta} \tag{1.12}$$

$$\iiint v_\alpha v_\beta v_\gamma f^{eq}(\vec{x},\vec{\xi},t)d\vec{\xi} = \rho rT\left(u_\alpha\delta_{\beta\gamma} + u_\beta\delta_{\alpha\gamma} + u_\gamma\delta_{\alpha\beta}\right) \tag{1.13}$$

$$\iiint v_\alpha v_\beta v_\gamma v_\mu f^{eq}(\vec{x},\vec{\xi},t)d\vec{\xi} = \rho\frac{(rT)^2}{2}\left(\delta_{\alpha\beta}\delta_{\gamma\mu} + \delta_{\alpha\gamma}\delta_{\beta\mu} + \delta_{\beta\gamma}\delta_{\alpha\mu}\right) \tag{1.14}$$

Since the function f^{eq} is anti-symmetrical, the odd moments are always equal to 0. Then it can be shown though a recursive demonstration that the isotropic relationship are always verified, i.e.:

$$\iiint v_{x_1}v_{x_2}...v_{x_{2n}}f^{eq}d\vec{\xi} = \Delta^{(2n)} \tag{1.15}$$

Such a condition is not surprising since the equilibrium function f^{eq} relies on isotropic assumptions.

1.1.3. Boltzmann equation

In the statistical mechanics framework, a large quantity of particles have their own velocity, which consequently leads to the occurrence of collisions. When two particles or more collide, their trajectories are modified depending on their relative velocities and positions at the impact. Collisions between particles are a complex phenomenon, which is not directly computed in LBM, but modeled. To do so, Boltzmann proposed to account for collisions in a collision operator Ω in the conservation equation of the distribution function f, following:

$$\partial_t f + \xi_\alpha\partial_\alpha f + \frac{F_\alpha}{\rho}\frac{\partial f}{\partial_{\xi_\alpha}} = \Omega \tag{1.16}$$

with F_α the α component of a body force $\vec{F}$, and Ω is the collision operator. The formulation of this operator is complex, involving a double integral in space and time, and not used in practise. Its formulation is not given here, but some of its properties must be underlined. In the hypothesis of hard sphere colliding in a perfectly elastic way, mass, momentum and the internal energy of the particles are conserved:

$$\iiint \Omega(\vec{x},\vec{\xi},t)d\vec{\xi} = 0 \tag{1.17}$$

$$\iiint \xi_{\alpha,i}\Omega(\vec{x},\vec{\xi},t)d\vec{\xi} = 0 \tag{1.18}$$

$$\iiint |\vec{\xi}-\vec{u}|^2\Omega(\vec{x},\vec{\xi},t)d\vec{\xi} = 0 \tag{1.19}$$

If momentum and internal energy are conserved, it can be shown that total energy is also conserved:

$$\iiint \vec{\xi}^2 \Omega(\vec{x}, \vec{\xi}, t) d\vec{\xi} = 0 \tag{1.20}$$

A simpler form of the collision operator was proposed by Bathnagar Gross & Krook [50], who proposed to write the collision operator as:

$$\Omega(f(\vec{x}, \vec{\xi}, t)) = -\frac{1}{\tau}\left(f(\vec{x}, \vec{\xi}, t) - f^{eq}(\vec{x}, \vec{\xi}, t)\right) \tag{1.21}$$

where f is the distribution function and f^{eq} is the distribution function at the equilibrium, detailed in the next subsection. In this model, the collision term is seen as a relaxation toward the equilibrium with a characteristic time scale τ. It is the simplest possible collision model.

1.2. Macroscopic equivalent equation

1.2.1. The Chapmann-Enskog development

Independently proposed by Chapmann and Enskog [51], it can be shown that the Navier Stokes equation can be derived from the Boltzmann equation. This approach is called the Chapmann-Enskog development and is detailed here. It generally relies on a development in Knudsen number, noted Kn. The Knudsen number is defined as the ratio between the mean free path L_{mfp} and a characteristic length of the flow, L_0:

$$Kn = \frac{L_{mfp}}{L_0} \tag{1.22}$$

This number allows to evaluate the validity of the continuous approach to describe the fluid. If $L_0 \gg L_{mfp}$ i.e. if $Kn \ll 1$ then the continuous approach is valid. Otherwise the field is considered as rarefied and then Navier-Stokes equations (or other conservation equations taking place in a continuous framework) cannot be used to describe such a flow. This dimensionless number is of great importance when doing a dimension analysis of the Boltzmann equation. The Chapmann-Enskog development considers the Boltzmann equations in the BGK hypothesis framework, and first consists in normalizing the variables of interest. These variables are the space coordinates $\vec{x}$, the time t, the microscopic velocities $\vec{\xi}$, the relaxation time τ, the partition function f and the body force $\vec{F}$. A characteristic velocity ξ_0 is defined. Giving the existence of two space scales L_0 and L_{fmp}, two characteristic time scales can be defined from the characteristic velocity:

$$t_0 = \frac{L_0}{\xi_0}, \quad t_{mfp} = \frac{L_{mfp}}{\xi_0} \tag{1.23}$$

Since the collision process is a microscopic phenomenon, the associated relaxation time is normalized thanks to t_{mfp} while the time scale t is normalized using t_0. Finally

$$\begin{array}{lll} \tilde{t} = t\dfrac{\xi_0}{L_0} & \vec{\tilde{x}} = \vec{x} & \vec{\tilde{\xi}} = \vec{\xi}/\xi_0 \\ \tilde{\tau} = \tau\dfrac{\xi_0}{L_{mfp}} & \vec{\tilde{F}} = \vec{F}\dfrac{L_0}{\xi_0^2\rho_0} & \tilde{f} = f\dfrac{\xi_0^3}{\rho_0} \end{array} \tag{1.24}$$

Where the $\tilde{.}$ variables refer to the dimensionless variables. Then the dimensionless counterpart of the Boltzmann equation Eq. (1.16) comes as:

$$Kn\left(\partial_t \tilde{f} + \vec{\tilde{\xi}_\alpha}\partial_{\tilde{x}_\alpha}\tilde{f} + \tilde{F}_\alpha\partial_{\tilde{\xi}_\alpha}\tilde{f}\right) = -\frac{1}{\tilde{\tau}}\left(\tilde{f} - \tilde{f}^{eq}\right) \tag{1.25}$$

It comes that when the Knudsen number tends toward 0, then $\tilde{f} = \tilde{f}^{eq}$. Then the greater Kn becomes the more the partition function $\tilde{f}$ deviates from the equilibrium function $\tilde{f}^{eq}$. This stays true for f and f^{eq}. It is then reasonable to write the partition function as a sum in Knudsen number such as:

$$f = f^{(0)} + Knf^{(1)} + Kn^2 f^{(2)} + ... \tag{1.26}$$

with $f^{(0)} = f^{eq}$. Since by definition: $\iiint f^{(eq)} d\vec{\xi} = \iiint f^{(0)} d\vec{\xi} = \rho$, it comes that:

$$\iiint \left(f - f^{(0)}\right) d\vec{\xi} = 0 \tag{1.27}$$

$$\iiint \left(f - f^{(0)}\right) \xi_\alpha d\vec{\xi} = 0 \tag{1.28}$$

$$\iiint |\vec{\xi} - \vec{u}|^2 \left(f - f^{(0)}\right) d\vec{\xi} = 0 \tag{1.29}$$

The previous relationships are true for $\sum_i Kn^n f^{(n)}$, an important assumption that is made here, is that the previous relationships are true for each $f^{(n)}$, and not only for all the sum:

$$\begin{aligned} \iiint f^{(n)} d\vec{\xi} = 0 \qquad n \geq 1 \\ \iiint f^{(n)} \xi_\alpha d\vec{\xi} = 0 \end{aligned} \tag{1.30}$$

The different derivative operators are also expanded in Knudsen number:

$$\partial_t = Kn\partial_{t^{(1)}} + Kn^2\partial_{t^{(2)}} + ... \tag{1.31}$$

In practice this relationship is truncated at the order 2, which is equivalent to assume the existence of two time scales as in the work of Da Silva et al. [52] : one diffuse time scale $t^{(1)}$ and one convective time scale $t^{(2)}$. The spatial derivative is also expanded in Knudsen number.

$$\partial_\alpha = Kn\partial_{\alpha^{(1)}} + Kn^2\partial_{\alpha^{(2)}} + ... \tag{1.32}$$

Previous equation Eq. (1.32) is truncated up to the order 1, which gives $\partial_\alpha = \epsilon\partial_{\alpha^{(1)}}$

1.2.2. Equivalent macroscopic equation of the Boltzmann equation

Applying Eqs. (1.26, 1.31, 1.32) to the Boltzmann equation Eq. (1.16), one can obtain the expansion of the Boltzmann equation in Knudsen number:

$$\begin{aligned} \frac{1}{\tau}\left(f^{(0)} - f^{eq}\right) + Kn\left(\partial_{t^{(1)}} f^{(0)} + \xi_\alpha \partial_{\alpha^{(1)}} f^{(0)} + \frac{1}{\tau} f^{(1)}\right) \\ + Kn^2\left(\partial_{t^{(2)}} f^{(0)} + \partial_{t^{(1)}} f^{(1)} + \xi_\alpha \partial_{\alpha^{(1)}} f^{(1)} + \frac{1}{\tau} f^{(2)}\right) + Kn^3 ... = 0 \end{aligned} \tag{1.33}$$

The last assumption that will be made, is that Eq. (1.33) must be verified for each order in Knudsen. For instance, at the order 0 in Knudsen, this equation becomes:

$$f_i^{(0)} = f_i^{eq} \tag{1.34}$$

which has already been stated. Now the Boltzmann equation will be investigated for every degree in Knudsen.

Order 1 in Knudsen

Eq. (1.33) first order in Knudsen comes as:

$$\partial_{t^{(1)}} f^{(0)} + \xi_\alpha \partial_{\alpha^{(1)}} f^{(0)} = -\frac{1}{\tau} f^{(1)} \tag{1.35}$$

Using Eq. (1.30), it comes that $\iiint f^{(1)} d\vec{\xi} = 0$. Then the integration of Eq. (1.35) gives:

$$\partial_{t^{(1)}} \iiint f^{eq} d\vec{\xi} + \partial_{\alpha^{(1)}} \iiint \xi_\alpha f^{eq} d\vec{\xi} = \iiint f^{(1)} d\vec{\xi} \tag{1.36}$$

Giving that $\iiint f^{(1)} d\vec{\xi} = 0$ according to Eq. (1.30), it comes:

$$\partial_{t^{(1)}} \rho + \partial_{\alpha^{(1)}} \rho u_\alpha = 0 \tag{1.37}$$

Eq. (1.37) evidences that Boltzmann equation allows to recover the mass conservation equation. Similarly, a momentum conservation equation can also be recovered by integrating Eq. (1.35) multiplied by the microscopic velocity ξ_α:

$$\partial_{t^{(1)}} \rho u_\alpha + \partial_{\alpha^{(1)}} \left(\rho u_\alpha u_\beta + \rho r T \delta_{\alpha\beta}\right) = 0 \tag{1.38}$$

Finally, an expression for the total energy can be deduced by integrating Eq. (1.35) multiplied by $|\vec{\xi}|^2$. It comes:

$$\partial_{t^{(1)}} \rho E + \partial_{\alpha^{(1)}} \left(\rho E u_\alpha\right) = 0 \tag{1.39}$$

By manipulating Eq. (1.39) and Eq. (1.38), an equation for the internal energy can also be obtained:

$$\partial_{t^{(1)}} \rho e + \partial_{\alpha^{(1)}} \left(\rho e u_\alpha\right) + p \partial_{\alpha^{(1)}} u_\alpha = 0 \tag{1.40}$$

Remembering that $e = \dfrac{3rT}{2}$, the previous equation Eq. (1.40) can be expressed in term of the temperature field:

$$\partial_{t^{(1)}} \rho r T + \partial_{\gamma^{(1)}} \left[\rho r T u_\gamma\right] + \frac{2\rho r T}{3} \partial_{\gamma^{(1)}} u_\gamma = 0 \tag{1.41}$$

We see that the first order in Knudsen of the Boltzmann equation is equivalent to the Euler equation system.

Order 2 in Knudsen

It can actually be demonstrated that the Boltzmann equation is equivalent to the Navier-Stokes equations: the viscous effects come from the non-equilibrium part of the partition function at the order 2 in Knudsen.
Before developing the Boltzmann equation to the order 2 in Knudsen, the knowledge of $f^{(1)}$ is necessary. To do so manipulating Eq. (1.35) gives:

$$f^{(1)} = -\tau \left(\partial_{t^{(1)}} f^{eq} + \xi_\alpha \partial_{\alpha^{(1)}} f^{(eq)}\right) \tag{1.42}$$

Now the expression of $f^{(1)}$ is known, the second order in Knudsen counterpart of Eq. (1.33) can be expressed as:

$$\partial_{t^{(2)}} f_i^{(0)} + \partial_{t^{(1)}} f_i^{(1)} + \xi_\alpha \partial_{\alpha^{(1)}} f_i^{(1)} = -\frac{1}{\tau} f_i^{(2)} \tag{1.43}$$

Since $\iiint \tilde{f}_i^{(1)} d\vec{\xi} = \iiint \xi_\alpha \tilde{f}_i^{(1)} d\vec{\xi} = \iiint \tilde{f}_i^{(2)} d\vec{\xi} = 0$ the integration of Eq. (1.43) on the microscopic velocity space provides:

$$\partial_{t^{(2)}} \rho = 0 \tag{1.44}$$

Similarly, multiplying Eq. (1.43) by the microscopic velocity and integrating provides:

$$\partial_{t^{(2)}} \rho u_\alpha = \partial_{\beta^{(1)}} \left[\tau \Pi_{\alpha\beta}^{(1)}\right] \tag{1.45}$$

with $\Pi_{\alpha\beta}^{(1)} = \iiint f^{(1)} \xi_\alpha \xi_\beta d\vec{\xi}$ which is the order two moment of $f^{(1)}$. Thanks to Eq. (1.42), this term can be expressed in term of moments of the equilibrium function, i.e. in term of the macroscopic values. It comes that:

$$\begin{aligned}\Pi_{\alpha\beta}^{(1)} &= \partial_{t^{(1)}} \iiint \xi_\alpha \xi_\beta f^{eq} d\vec{\xi} + \partial_{\gamma^{(1)}} \iiint \xi_\alpha \xi_\beta \xi_\gamma f^{eq} d\vec{\xi} \\ &= \underbrace{\partial_{t^{(1)}} \rho u_\alpha u_\beta}_{(1)} + \partial_{t^{(1)}} \rho r T \delta_{\alpha\beta} + \partial_{\gamma^{(1)}} \left(\rho u_\alpha u_\beta u_\gamma + \rho r T \left[u_\alpha \delta_{\beta\gamma} + u_\beta \delta_{\alpha\gamma} + u_\gamma \delta_{\alpha\beta}\right]\right)\end{aligned} \tag{1.46}$$

(1) can be determined using Eq. (1.38):

$$\begin{aligned}(1) = \partial_{t^{(1)}}\left(\rho u_\alpha u_\beta\right) = \rho u_\alpha \partial_{t^{(1)}}\left(u_\beta\right) + u_\beta \partial_{t^{(1)}}\left(\rho u_\alpha\right) \\ = -\partial_{\gamma^{(1)}}\left(\rho u_\alpha u \beta u_\gamma\right) - u_\alpha \partial_{\beta^{(1)}}\left(\rho r T\right) - u_\beta \partial_{\alpha^{(1)}}\left(\rho r T\right)\end{aligned} \tag{1.47}$$

By injecting Eq. (1.47) into Eq. (1.46) it comes that:

$$\Pi^{(1)}_{\alpha\beta} = \rho r T\left(\partial_{\alpha^{(1)}} u_\beta + \partial_{\beta^{(1)}} u_\alpha\right) + \left(\underbrace{\partial_{t^{(1)}} \rho r T + \partial_{\gamma^{(1)}}\left[\rho r T u_\gamma\right]}_{Eq.(1.41) = -\frac{2}{3}\rho r T \partial_{\gamma^{(1)}} u_\gamma}\right)\delta_{\alpha\beta} \tag{1.48}$$

It finally comes that put to the order 2 in Knudsen, the Boltzmann equation comes as:

$$\partial_{t^{(2)}}\left(\rho u_\alpha\right) = \partial_\beta\left[\tau \rho r T\left(\partial_\alpha u_\beta + \partial_\beta u_\alpha - \frac{2}{3}\partial_\gamma u_\gamma \delta_{\alpha\beta}\right)\right] \tag{1.49}$$

Equivalent macroscopic equation

Then, remembering that $\partial_t = Kn\partial_{t^{(1)}} + Kn^2\partial_{t^{(2)}}$ the equivalent macroscopic equation can be obtained by summing the two counterpart of the temporal derivative. For instance, the momentum equation can be obtained by summing Eq. (1.38) and Eq. (1.49). The equivalent system of the Boltzmann equation is made of three equations. The continuity equation:

$$\partial_t \rho + \partial_\alpha \rho u_\alpha = 0 \tag{1.50}$$

the momentum conservation equation:

$$\partial_t \rho u_\alpha + \partial_\beta\left(\rho u_\alpha u_\beta + \rho r T \delta_{\alpha\beta}\right) = \partial_\beta\left[\tau(\rho r T)\left(\partial_\alpha u_\beta + \partial_\beta u_\alpha - \frac{2}{3}\partial_\gamma u_\gamma \delta_{\alpha\beta}\right)\right] \tag{1.51}$$

and the total energy conservation equation (the detail of the calculation are not given here):

$$\partial_t \rho E + \partial_\alpha\left(\rho E + p\right) u_\alpha = \partial_\beta\left[\tau p \frac{5r}{2}\partial_\alpha T + \tau \rho r T\left(\partial_\alpha u_\beta + \partial_\beta u_\alpha - \frac{2}{3}\partial_\gamma u_\gamma \delta_{\alpha\beta}\right)\right] \tag{1.52}$$

The equations Eqs. (1.50, 1.51, 1.52) show that a Navier-Stokes system can be expressed from the Boltzmann equation. In this framework, the pressure is defined through the perfect gas equation: $p = \rho r T$ and the kinetic viscosity is a function of the relaxation time: $\nu = \tau r T$. Note that the general form of the stress tensor is given by:

$$\mu\left(\partial_\alpha u_\beta + \partial_\beta u_\alpha\right) + \left(\mu_b - \frac{2}{3}\mu\right)\partial_\gamma u_\gamma \delta_{\alpha\beta} \tag{1.53}$$

with μ the dynamic viscosity and μ_b the bulk viscosity. The bulk viscosity corresponds to the viscous stress associated to the dilatation. A common hypothesis called the Stokes hypothesis consists in assuming that $\mu_b = 0$. This hypothesis is often made with no justification, in the present case, Eq. (1.51) shows that a mono-atomic gas close from the equilibrium respects the Stokes hypothesis.

1.2.3. Equivalent macroscopic equation for the athermal case

The previous subsection 1.2.2 presented the relations between the Boltzmann equation and the macroscopic equations, in which temperature is involved. Standard Lattice Boltzmann method is

historically athermal. The present subsection details the relations with the athermal macroscopic equations. In the standard LBM proposed by He et al. [53] the equilibrium function is given by:

$$f_i^{eq} = \rho w_i \left[1 + \frac{u_\alpha \xi_{\alpha,i}}{c_s^2} + u_\alpha u_\beta \frac{\xi_{\alpha,i}\xi_{\beta,i} - c_s^2 \delta_{\alpha\beta}}{2c_s^4}\right] \tag{1.54}$$

Using the same approach as before, it can be shown that the mass conservation equation takes a similar form:

$$\partial_t \rho + \partial_\alpha \rho u_\alpha = 0 \tag{1.55}$$

But the momentum equation is modified to:

$$\partial_t \rho u_\alpha + \partial_\beta \left(\rho u_\alpha u_\beta + \rho c_s^2 \delta_{\alpha\beta}\right) = \partial_\beta \left[\rho c_s^2 \Delta t(\tau - 1/2)\left(\partial_\alpha u_\beta + \partial_\beta u_\alpha\right) - \partial_\gamma \rho u_\alpha u_\beta u_\gamma\right] \tag{1.56}$$

Compared with the thermal case Eq. (1.51), two important differences must be noted. The viscous constraint term is modified to:

$$\mathcal{T}_{\alpha\beta} = \rho c_s^2 \Delta t\left(\tau - 1/2\right)\left(\partial_\alpha u_\beta + \partial_\beta u_\alpha\right) \tag{1.57}$$

It can be compared to the general formulation Eq. (1.53). It comes that in the athermal case, the Stokes's hypothesis is no longer verified since $\mu_b = \frac{2}{3}\mu$. The reason of this difference between the thermal case and the athermal case is discussed hereinafter.
In the thermal approach, temperature is defined through the second order moment of the density function:

$$\rho|\vec{u}| + \rho r T = \iiint |\vec{\xi}|^2 f d\vec{\xi} \tag{1.58}$$

In order to guaranty the internal energy conservation principle, the collision operator must respect: $\iint |\vec{\xi}|^2 \Omega d\vec{\xi} = 0$. This implies that Eq. (1.58) must also be verified for f^{eq}: $\rho|\vec{u}| + \rho r T = \iiint |\vec{\xi}|^2 f^{eq} d\vec{\xi}$
From the two last equations it comes that

$$\iiint |\vec{\xi}|^2 \left(f - f^{eq}\right) d\vec{\xi} = 0 \tag{1.59}$$

Eq. (1.59) can also be generalised to $f^{(1)}$: $\iiint |\vec{\xi}|^2 f^{(1)} d\vec{\xi} = 0$. It happens that this last integrate is the trace of the tensor $\Pi^{(1)}$. Then it comes that in the thermal framework:

$$Tr\left(\Pi^{(1)}\right) = 0 \tag{1.60}$$

This last tensor being proportional to the stress tensor, it comes that the trace of the stress tensor is also equal to 0, making the Stokes's assumption true.
From the last demonstration, it comes that the fact to involve a temperature field in LBM is a sufficient condition for the Stokes's assumption to be true. It is then natural that in the athermal framework, this assumption is no longer true.
The other difference between the current model and the thermal one is the presence of the spurious term: $\partial_\gamma \rho u_\alpha u_\beta u_\gamma$ in Eq. (1.56). It comes from the fact that the equilibrium function is only truncated to the order three when the knowledge of the order three of the equilibrium function is involve into the calculation of the stress tensor. This error term is discussed more in detail into Section 1.3.

1.3. Discretization of Boltzmann Equation

We saw earlier Eq. (1.16), that $\bar{f}_i$ is solution of the Boltzmann equation. But the attentive reader would have note that there is a slight difference with the Boltzmann equation Eq. (1.21). In the second one, f is a continuous variable in space while f_i is a finite number of fields associated with a microscopic variable. In section(1.2), we could see the Boltzmann equation allows to simulate a Navier-Stokes system, but is it the case for Eq. (1.21), the discrete Boltzmann equation? The capability of a discrete system to recover the macroscopic equation of the continuous one is linked to the capability of the discrete system to estimate accurately the moments of the partition function f. At this stage it is interesting to introduce the Hermite polynomial, as they are an essential tool to discretize the equilibrium function equation in the microscopic velocity space.

1.3.1. Hermite polynomial

Most of the discussion detailed hereinafter was tackled by Kruger et al [54]. The expression of the Hermite polynomial (and the one that is used in practice) is given by:

$$\begin{array}{cc} H_0 = 1 & H_\alpha = \xi_\alpha \\ H_{\alpha\beta} = \xi_\alpha\xi_\beta - c_s^2\delta_{\alpha\beta} & H_{\alpha\beta\gamma} = \xi_\alpha\xi_\beta\xi_\gamma - c_s^2\left[\xi_\alpha\delta_{\beta\gamma} + \xi_\beta\delta_{\alpha\gamma} + \xi_\gamma\delta_{\alpha\beta}\right] \end{array} \tag{1.61}$$

Here, c_s is a constant of the scheme that is set by the user. Those polynomials form a base of the function space, then any arbitrary function h can be expressed as a serie of Hermite polynomial:

$$h(\vec{\xi}) = \tilde{w}(\vec{\xi})\sum_{n=0}^{\infty}\frac{\vec{\tilde{a}}^{(n)}}{n!(c_s)^{2n}}\vec{\tilde{H}}^{(n)}(\vec{\xi}) \quad \vec{\tilde{a}}^{(n)} = \int h(\vec{\xi})\vec{\tilde{H}}^{(n)}(\vec{\xi})d\vec{\xi} \tag{1.62}$$

The equilibrium function can then fully be expressed in term of Hermite's polynomial. The most important property of the Hermite polynomial is that it is possible to calculate integrals of polynomial functions by summing values at a finite number of discrete points. Thanks to a rule named the Gauss-Hermite quadrature, there is a number of abscissa x_i and a number of number of coefficient w_i for which the integral of a polynomial function P (of degree N) can be exactly estimated through:

$$\int_{-\infty}^{+\infty} w(x)P^{(N)}(x)dx = \sum_i^n w_i P^{(N)}(x_i) \tag{1.63}$$

where the x_i are the roots of the Hermite polynomial $H^{(N)}(x)$ and the w_i are functions of these roots. The point is, the higher the rank of the polynomial P is, the higher the number of roots of the polynomial $\vec{H}^{(N)}$ then the higher is the number of x_i necessary to retrieve exactly the integral of $P^{(N)}$. Put it in the other way, the higher is the order of the Hermite polynomial which integral we want to refund exactly, the higher is the number of points necessary to do so. It means that there will be limitations depending with the number of points and velocity available.
Thanks to those considerations we can define a discrete function which sums are equal to the integral of the partition function:

$$f_i = \frac{w_i}{w(\vec{\xi})}f(\xi_i) \tag{1.64}$$

Similarly a discrete equilibrium function can be expressed. It is a common practice to truncate the Hermite polynomial expansion to the order 2. The first equilibrium function that was proposed under this form was proposed by Qian et al.[55] in the athermal case

$$f_i^{eq} = w_i\rho\left[1 + \frac{u_\alpha\xi_\alpha}{c_s^2} + u_\alpha u_\beta\frac{\xi_\alpha\xi_\beta - c_s^2\delta_{\alpha\beta}}{2c_s^4}\right] \tag{1.65}$$

This equilibrium has been widely used after it was proposed, and it can be considered as the standard function for Lattice Boltzmann Methods. The attentive reader would have note that no pressure term seems to be involved in the equilibrium function. In practice, to obtain the proper value of the pressure, a CFL condition is imposed. The ratio between the space step and the temporal step is given by:

$$\frac{\Delta x}{\Delta t} = \sqrt{3} c_s \tag{1.66}$$

The motivation between the previous condition is given in Appendix A.

1.3.2. Velocity sets and coefficients

Similarly as in Lattice Gas Automata, the shape of the lattice and the chosen velocity set is of primary importance in the Lattice Boltzmann Method. In practice, a velocity set is created thanks to the lattice the particles evolves on. Similarly with the lattice Gas Automata, the idea is to choose only velocities for which particles located on the lattice will still be located on the lattice after a time step Δt. Doing this way, no special treatment is necessary to locate the particles since they are on the nodes. Mathematically, it reads that for a given particle located on a lattice (2D in this example but could be 1D or 3D) with a constant space step Δx, if the particle going at the velocity $\vec{\xi_i}$ is located at the node which coordinates are (x, y), then to guaranty that after the time Δt the particle will still be on the lattice, the velocity must read: $\xi_{\alpha,i} = \frac{\Delta x}{\Delta t} \vec{x_\alpha} n_\alpha$ with n_α an integer and $\vec{x_\alpha}$ a unit vector parallel to the x_α direction. This last relationship tells that the properties of the scheme, in this case the norm of the microscopic velocities, are linked with the ratio between the dimensional step and the temporal step (also called the Courant number). This principle is illustrated Figure 1.1. It means

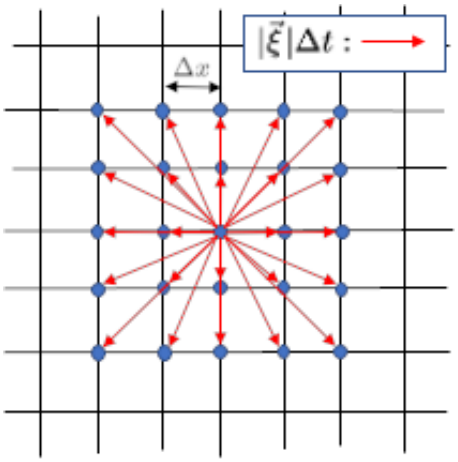


Figure 1.1. – Illustration of some possible velocities on a 2D cartesian grid

that to be sure to recover correctly the different moments of the equilibrium function, the Courant number must be chosen wisely. Before the Hermite truncature rules was discovered, the w_i and the

velocity set was set up by using isotropic relationships:

$$\begin{gathered}\sum_i w_i = 1 \\ \sum_i \xi_\alpha w_i = 0 \\ \sum_i \xi_\alpha \xi_\beta w_i = c_s^2 \\ \sum_i \xi_\alpha \xi_\beta \xi_\gamma w_i = 0 \\ \sum_i \xi_\alpha \xi_\beta \xi_\gamma \xi_\mu w_i = c_s^4(\delta_{\alpha\beta}\delta_{\gamma\mu} + \delta_{\alpha\gamma}\delta_{\beta\mu} + \delta_{\beta\gamma}\delta_{\alpha\mu}) \\ \sum_i \xi_\alpha \xi_\beta \xi_\gamma \xi_\mu \xi_\theta w_i = 0\end{gathered} \tag{1.67}$$

It must be noted that the condition $\sum_i \xi_{\alpha,i}\xi_{\beta,i}w_i = c_s^2$ only stands in the case where the pressure is linked to the CFL number as in the previous discussion. Otherwise, the value $\sum_i \xi_{\alpha,i}\xi_{\beta,i}w_i$ is set according to the desired CFL. Even if the mathematical framework of the Quadrature rule is more rigorous, the coefficient w_i and the value of the Courant number obtained through this methods are exactly the same. Then it seems that there is a tight bound between the isotropy of a Lattice Boltzamnn scheme and its capability to recover high degree polynomial.
As a matter of fact, both of those capability are linked with the number of microscopic velocities in the velocity set. Now, commonly used velocity set are presented and discussed. Each velocity set is characterised by the dimension of the system it simulates (noted d) and the number q of discrete velocity. It is then given by D_dQ_q. The higher q is, the more computationally expensive a scheme becomes, but also the higher are the degrees of moments the scheme is capable to recover correctly. For example, in 3D, D_3Q_{15} needs less memory allocation and less calculation per iteration than D_3Q_{19} which is itself less memory intensive and less computation time consuming than D_3Q_{27}. The most commonly used velocity sets are the one where only the first neighbours are involved. For instance in D2Q9 the values of the partition function located at (x, y) at the time t is calculated only from partition functions located at $(x\pm1, y\pm1)$ at the time $t-1$. This choice makes the parallelization of the algorithm easy, and the scalability of the algorithm makes it a good candidate for High Performance Computing (HPC). The question of the relative efficiency of Lattice Boltzmann schemes compared with classical numerical methods is a currently controversial and uncertain topic. The properties of the most commonly used sets are given in Figure 1.2. In the following part, we focus on the two velocity sets that will be used in this work D_2Q_9 and D_3Q_{19}.

1.3.2.1. D2Q9 velocity set

An illustration of a D2Q9 velocity set is proposed Figure 1.3. As underlined by its name, it is composed of 9 velocities and takes place in a 2 dimensional framework. Among the 9 velocities, one corresponds to a velocity equal to zero, and the other ones are the velocities corresponding to velocities pointing toward the corners of a square and toward the middle of its sides. The formulation of those velocities is given by:

$$\vec{\xi_i} = \frac{\Delta x}{\Delta t}\begin{cases}(0,0) & i = 0 \\ (\pm1, 0)\ or\ (0, \pm1) & i = 1, 3, 5, 7 \\ (\pm1, \pm1)\ or\ (\pm1, \mp1) & i = 2, 4, 6, 8\end{cases} \tag{1.68}$$

Notation	Velocities c_i	Number	Length $\|c_i\|$	Weight w_i
D1Q3	(0)	1	0	2/3
	(± 1)	2	1	1/6
D2Q9	$(0,0)$	1	0	4/9
	$(\pm 1,0),(0,\pm 1)$	4	1	1/9
	$(\pm 1,\pm 1)$	4	$\sqrt{2}$	1/36
D3Q15	$(0,0,0)$	1	0	2/9
	$(\pm 1,0,0),(0,\pm 1,0),(0,0,\pm 1)$	6	1	1/9
	$(\pm 1,\pm 1,\pm 1)$	8	$\sqrt{3}$	1/72
D3Q19	$(0,0,0)$	1	0	1/3
	$(\pm 1,0,0),(0,\pm 1,0),(0,0,\pm 1)$	6	1	1/18
	$(\pm 1,\pm 1,0),(\pm 1,0,\pm 1),(0,\pm 1,\pm 1)$	12	$\sqrt{2}$	1/36
D3Q27	$(0,0,0)$	1	0	8/27
	$(\pm 1,0,0),(0,\pm 1,0),(0,0,\pm 1)$	6	1	2/27
	$(\pm 1,\pm 1,0),(\pm 1,0,\pm 1),(0,\pm 1,\pm 1)$	12	$\sqrt{2}$	1/54
	$(\pm 1,\pm 1,\pm 1)$	8	$\sqrt{3}$	1/216

Figure 1.2. – Properties of the principal velocity sets (from [54], which compiled informations from Succi [56] and Qian et d'Humières [55]

As proposed in Figure 1.2, the weighted coefficients are given by:

$$w_i = \begin{cases} 4/9 & i = 0 \\ 1/9 & i = 1,3,5,7 \\ 1/36 & i = 2,4,6,8 \end{cases} \tag{1.69}$$

In two dimension, it is the largest velocity set that involves only the first neighbours. As in this velocity set $q = 9$, 9 is also the number of moments that can be recovered. It means that if we would like to recover all of the moments, for example by taking an equilibrium function with an infinite number of components:

$$f_i^{perfect,eq} = w_i \sum_{n=0}^{\infty} \frac{a^{(n),eq}}{n! c_s^{2n}} H^{(n)} \tag{1.70}$$

in practice only 9 moments would be recovered, i.e.:

$$\begin{array}{lll} m_0^{eq} = \rho & m_x^{eq} = \rho u_x & m_y^{eq} = \rho u_y \\ m_{xy}^{eq} = \rho u_x u_y & m_{xx}^{eq} = \rho u_x^2 & m_{yy}^{eq} = \rho u_y^2 \\ m_{xxy}^{eq} = \rho u_x^2 u_y & m_{yyx}^{eq} = \rho u_x u_y^2 & \\ m_{xxyy}^{eq} = \rho u_x^2 u_y^2 & & \end{array} \tag{1.71}$$

with $m_j^{eq} = \sum_i f_i^{eq} H_{j,i}$ and $j \in \{0, x, y, xy, xx, yy, xxy, yyx, xxyy\}$. All the other moments would be equal to 0. The mechanism making this is the fact that in D_2Q_9, not all Hermite's polynomial moments can be recovered. For example, due to the fact that only first neighbours are involved, then $\xi_\alpha^3 = c_s^2 \xi_\alpha$, which makes that $H_{xxx,i} = 0$ for all the microscopic velocities in D_2Q_9, and then straightforwardly $\sum_i f_i^{eq} H_{xxx,i} = 0$. It must be noted that the relationship $H_{xxx,i} = 0$ is not due to the discretization

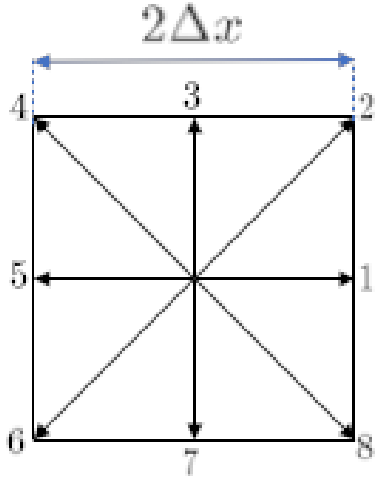


Figure 1.3. – Illustration of a D_2Q_9 velocity set

process, because 0 is the value of the continuous Hermite polynomial at this coordinates, then to recover correctly the moments H_{xxx} and H_{yyy} a velocity set should include at list second neighbours (i.e. microscopic velocities under the form $\vec{\xi} = n_x \frac{\Delta x}{\Delta t}\vec{x} + n_y \frac{\Delta x}{\Delta t}\vec{y}$ with $n_x = 2$ or $n_y = 2$).
In practice the consequence is well known. If we take a look at the equivalent macroscopic equation to the order Δt^2 for the momentum:

$$\partial_t m_\alpha^{eq} + \partial_\beta \left(m_{\alpha\beta}^{eq} + c_s^2 m_0^{eq} \delta_{\alpha\beta} \right) = \Delta t \rho c_s^2 \left(\tau - 1/2 \right) \left[\partial_t m_{\alpha\beta}^{eq} + \partial_\gamma \left(m_{\alpha\beta\gamma}^{eq} + c_s^2 \left(m_\alpha^{eq} \delta_{\beta\gamma} + m_\beta^{eq} \delta_{\alpha\gamma} \right) \right) \right] \tag{1.72}$$

It can be seen that the right part of the equation involves order three moments of the equilibrium function ($m_{\alpha\beta\gamma}^{eq}$), then if the third moments are not recovered correctly, spurious term might appear in the previous equation. In the perfect case, the Navier-Stokes equation for isothermal flow is recovered perfectly and the right term of the previous equation is given by:

$$\partial_\beta \Pi_{\alpha\beta}^{(1),eq} = \rho c_s^2 \left(\partial_\alpha u_\beta + \partial_\beta u_\alpha \right) \tag{1.73}$$

But in the D_2Q_9, even by using all the components of the equilibrium function, the second moment of the non-equilibrium function is given by:

$$\Pi_{\alpha\beta}^{(1),eq} = \partial_\beta \left[\rho c_s^2 \left(\partial_\alpha u_\beta + \partial_\beta u_\alpha \right) \right] - \partial_\alpha^2 \partial_\alpha \rho u_\alpha^3 \delta_{\alpha\beta} \tag{1.74}$$

It comes that a spurious term proportional to the velocity cubed appears. This term is of similar nature that the $\rho u_\alpha u_\beta u_\gamma$ terms that appears when using the algorithm of He et al.
This spurious term is often refereed as a Mach number (Ma) cubed error, because in dimensionless units, this error term takes the following form: $\partial_\alpha^2 \frac{\rho u_\alpha^3}{3\sqrt{3} c_s^3}$ which is proportional to the Mach number.
The consequence of this spurious term is the fact that LBM's precision tends to fall at high Mach number, but the method stays relevant to simulate compressible field at low velocity flows, and in particular for acoustic flows. This is the reason why Lattice Boltzmann methods are often recalled as "weakly compressible scheme" because they simulate compressible flow but only for low-Mach number flows, i.e., flows where the compressible effect are of less importance. It is also sometimes said that LBM lakes of Galilean invariance, this affirmation is motivated by the presence of this spurious term. Among the multiphase community, "weakly compressible" could also refer to the capability of given numerical methods to simulate two phase flows where only one phase is compressible like in Kajzer et Pozorski [57].

1.3.2.2. D3Q19 velocity set

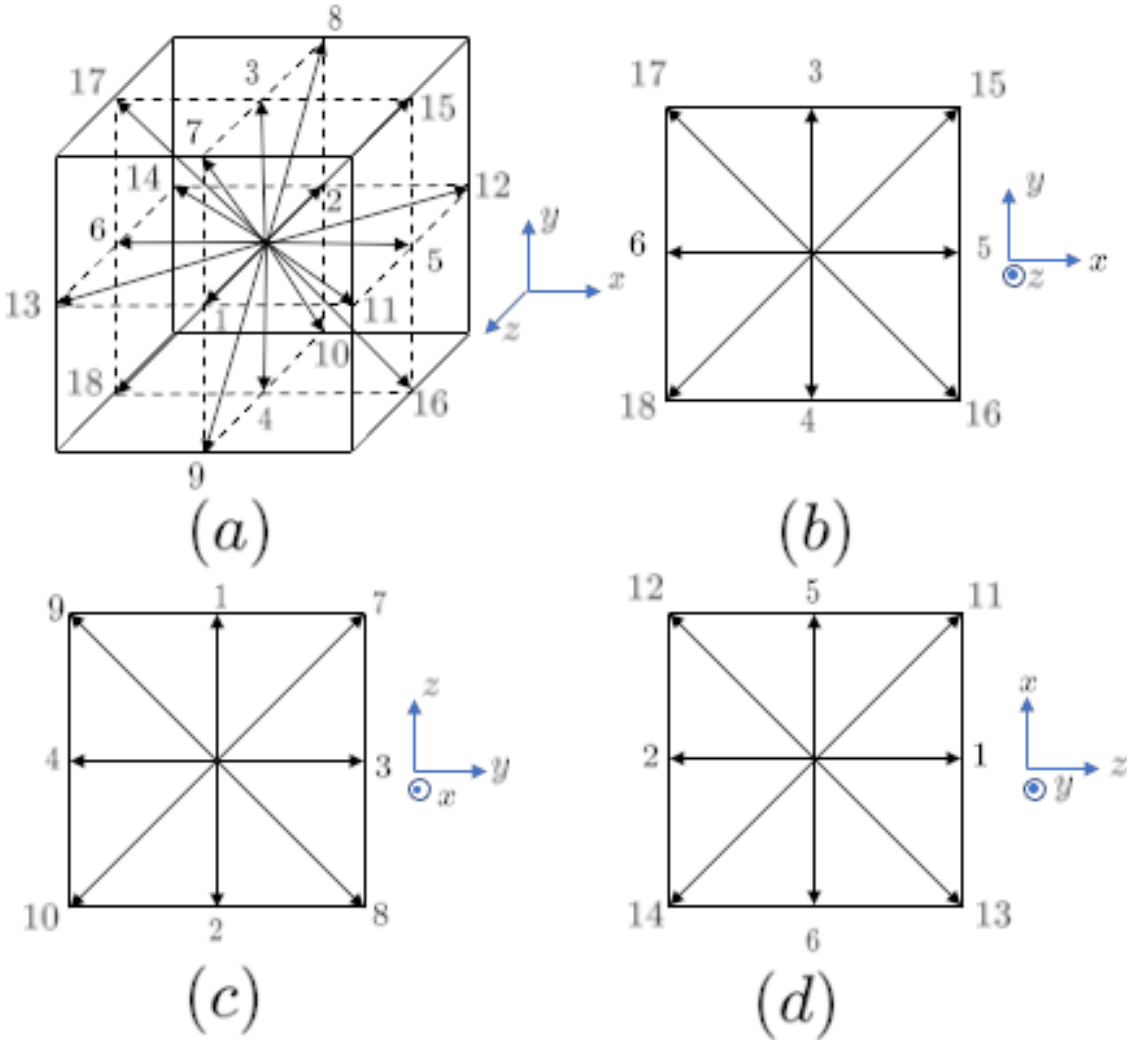


Figure 1.4. – Illustration of the D_3Q_{19} velocity set. (a) is the velocity set itself (b) projection in the (x, y) plane (c) projection in the (y, z) plane (d) projection in the (z, x) plane

As its name suggests, the D_3Q_{19} velocity set takes place in a 3 dimensional framework and is made of 19 velocities. An illustration of the D_3Q_{19} is proposed in figure 1.4. It can be interpreted as three D_2Q_9 put together. All the velocities only involve the first neighbours. In 3D, the largest scheme that involves only first neighbours is the D_3Q_{27} scheme. The difference between the D_3Q_{19} and the D_3D_{27} are the summits of the cubes in which the points are inscribed, that are not present in D_3Q_{19}.
Such as in D_2Q_9, only 19 moments can be recovered in D_3Q_{19}. They are listed here: H_0, H_x, H_y, H_z, H_{xy}, H_{xz}, H_{yz}, H_{xx}, H_{yy}, H_{zz}, H_{xxy}, H_{xxz}, H_{yyx}, H_{yyx}, H_{yyz}, H_{zzx}, H_{xxyy}, H_{yyzz} and H_{xxzz}. But another difficulty rises from this velocity set, it is the breaking of the relationships of orthogonality between the Hermite's polynomial. This concerns mainly the $H_{\alpha\alpha\beta}$ and $H_{\alpha\alpha\beta\beta}$. In particular, we have:

$$\sum_i w_i \frac{H_{xxy,i} H_{zzy,i}}{2c_s^6} = -0.5 \neq 0 \tag{1.75}$$

and

$$\sum_i w_i \frac{H_{xxy,i} H_{zzy,i}}{2c_s^6} = -0.5 \neq 0$$
$$\sum_i w_i \frac{H_{xxyy,i} H_{xxzz,i}}{4c_s^8} = \sum_i w_i \frac{H_{xxyy,i} H_{yyzz,i}}{4c_s^8} = -0.25 \neq 0$$
$$\sum_i w_i \frac{H_{xxyy,i} H_{zz,i}}{4c_s^8} = -0.75 \neq 0$$

The consequence of that, is that the equilibrium function must not be written anymore as a composition of Hermite polynomial. Instead, a new orthogonal base of polynomials should be constructed. For instance, the following one was obtained using a Gram-Schmidt algorithm:

$$a_0 = 1$$
$$a_1 = H_x \quad a_2 = H_y \quad a_3 = H_z$$
$$a_4 = H_{xx} \quad a_5 = H_{yy} \quad a_6 = H_{zz}$$
$$a_7 = H_{xy} \quad a_8 = H_{yz} \quad a_9 = H_{xz}$$
$$a_{10} = H_{xxy} \quad a_{11} = H_{xxy} + 2H_{zzy}$$
$$a_{12} = H_{xxz} \quad a_{13} = H_{xxz} + 2H_{yyz} \quad a_{14} = H_{yyx} \quad a_{15} = H_{yyx} + 2H_{zzx}$$
$$a_{16} = 2H_{xxyy} + c_s^2 H_{zz} \quad a_{17} = 14H_{xxzz} + 7c_s^2 H_{yy} + 4H_{xxyy} + 2c_s^2 H_{zz}$$
$$a_{18} = 10H_{yyzz} + 5c_s^2 H_{xx} + 4H_{xxyy} + 2c_s^2 H_{zz} + 4H_{xxzz} + 2c_s^2 H_{yy}$$

In practice, this base is not very convenient to use, then it is more practical to define the polynomial whose moments in Hermite are defined like:

$$\sum_i w_i H_{*,i} X_{o,i} = \delta_{*o} \tag{1.76}$$

We have:

$$X_{xxyy} = \frac{3 * (2H_{xxyy} + c_s^2 H_{zz}) + 4 (H_{xxyy} + H_{xxzz} + H_{yyzz}) + 2c_s^2 (H_{xx} + H_{yy} + H_{zz})}{27c_s^8} \tag{1.77}$$

$$X_{xxy} = \frac{2H_{xxy} + H_{zzy}}{3c_s^6} \tag{1.78}$$

$$X_{xx} = \frac{H_{xx}}{2c_s^4} + \frac{c_s^2}{2} X_{yyzz} \tag{1.79}$$

Finally, the moments linked to H_{xxx}, H_{yyy} and H_{zzz} cannot be recovered properly for the same reason as the D_2Q_9 velocity sets. For this reason, a similar spurious terms appear in the Navier-Stokes equation.

1.3.3. Classical LBM

In Section 1.3.1 and Section 1.3.2, different mechanisms allowing to discretize Boltzmann equation were proposed. This leads to the Lattice Boltzmann Methods, that can simulate fluid flows by solving Boltzmann equation. The words "Lattice Boltzmann Method" refers to a whole family of methods rather than a specific algorithm. For the sake of clarity, one particular algorithm is chosen and defined as the Classic LBM. The specific algorithm is the one proposed by He et Luo [58] detailed hereafter. In the approach of He and Luo [58], a density and velocity field must be specified at the initialization.

The distribution function is initialized at equilibrium, i.e. $f_i(t=0) = f_i^{eq}(\rho(t=0), \vec{u}(t=0))$. The mainloop starts with the computation of the equilibrium function f_i^{eq} calculated from the value of the macroscopic fields. For instance, in the model proposed by He et Luo [58], the equilibrium function is given by:

$$f_i^{eq} = \rho w_i \left(1 + \frac{u_\alpha \xi_{\alpha,i}}{c_s^2} + u_\alpha u_\beta \frac{\xi_{\alpha,i}\xi_{\beta,i} - c_s^2 \delta_{\alpha\beta}}{2c_s^4}\right) \tag{1.80}$$

where w_i is a set of coefficients depending with the lattice. A proper introduction is proposed in section 1.3.2. The density function f_i is supposed to be in a state f_i^* after the collision step following:

$$f_i^* = f_i - \frac{1}{\tau}(f_i - f_i^{eq}) \tag{1.81}$$

Then the streaming step occurs:

$$f_i(x + \xi_{\alpha,i}\Delta t, t + \Delta t) = f_i^*(x,t) \tag{1.82}$$

Finally the new macroscopic fields are calculated thanks to the the distribution function at $t + \Delta t$:

$$\rho(x, t+\Delta t) = \sum_i f_i(x, t+\Delta t) \qquad u_\alpha(x, t+\Delta t) = \frac{\sum_i \xi_\alpha f_i(x, t+\Delta t)}{\rho(x, t+\Delta t)} \tag{1.83}$$

An illustration of this algorithm is proposed Figure 1.5. He and Luo [58] showed that this algorithm

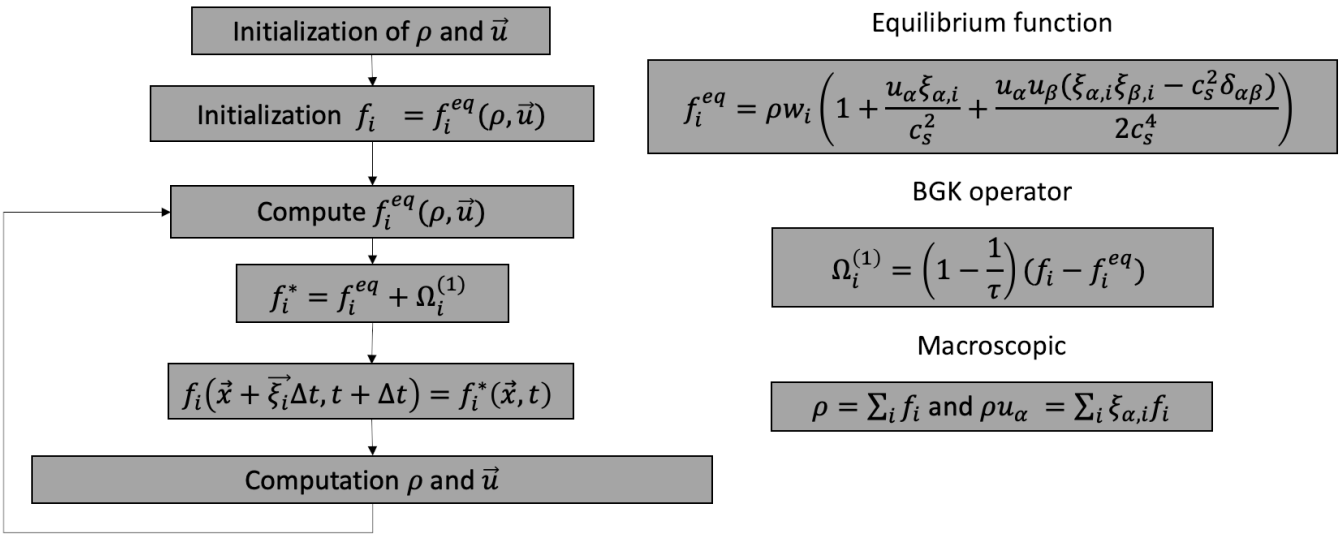


Figure 1.5. – Illustration of the classic athermal LBM algorithm proposed by He et Luo [59]

can be related to the Boltzmann equation. By introducing $\bar{f}_i = f_i - \frac{1}{2\tau}(f_i - f_i^{eq})$, it can be shown that:

$$\partial_t \bar{f}_i + \xi_\alpha \partial_\alpha \bar{f}_i = -\frac{\Delta t}{\tau - 1/2}\left(\bar{f}_i - f_i^{eq}\right) + O(\Delta t^2) \tag{1.84}$$

which is equivalent to the Boltzmann equation. The demonstration is proposed in Appendix A.3. It shows that classical LBM is equivalent to the solving of the Boltzmann equation with a 2^{nd} order accuracy in time. It is interesting to note that historically, this link has been made *a posteriori*. Before going further in the analysis of Lattice Boltzmann Method, an introduction to statistical mechanic is necessary.

1.4. Historical review

In Section 3.1, Lattice Boltzmann Method was described as a numerical method allowing to solve the Boltzmann equation. However, the historical truth is that the link between Lattice Boltzmann Methods and Boltzmann equation was made *a posteriori* by He et Luo [58–60]. This makes LBM unique among others numerical methods since the algorithm was born without knowing what differential equation it solves. This can seem peculiar to the reader used to more common numerical methods and could refrain from a deep understanding of the method. For these reasons, it is of interest to describe the historical background that leaded to LBM's birth. LBM was originally thought as an improvement of the Lattice Gas Automata, a cellular automaton designed to simulate fluid flows. A review of Lattice Gas Automata history and how Lattice Boltzmann Method emerged from this alogorithm is proposed in the present Section.
In the 70's, motivated by the "fast development of integrated circuits and computers", Hardy, Pomeau and de Pazzis proposed to simulate fluid flows in a molecular dynamic framework. In a succession of three papers [61–63], they proposed a so-called "Maxwell model" to simulate molecular dynamic. The uniqueness of the model is that, rather than trying to determine the exact velocity and position of the simulated particles, only few locations distributed regularly across space are allowed, and the velocities are quantified. In this model only a finite number of velocities are allowed for the particles. The motivations are mainly numerical, at the time of the first paper (1972) velocities and positions are known with limited precision due to the technical restriction of the electronic components. By assuming constant velocities and positions, the precision of the simulation remains constant in time.

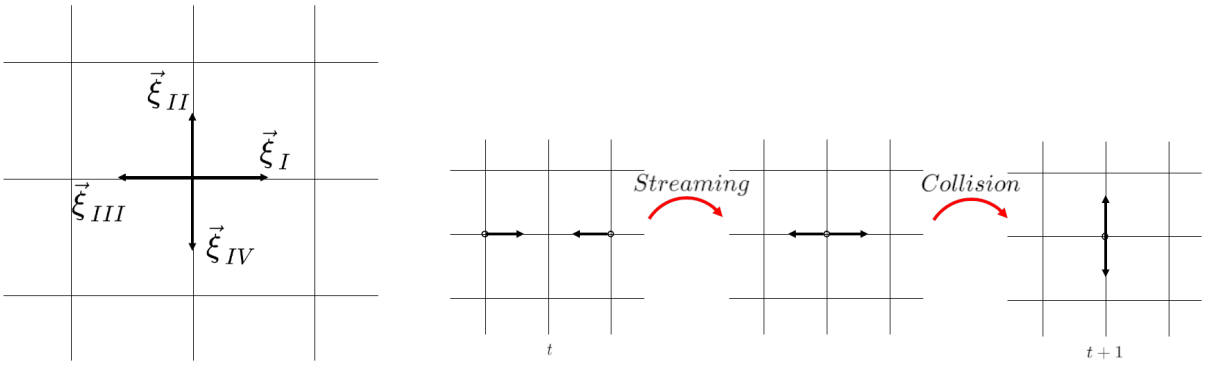
1.4.1. The original Hardy de Pazzis Pommeau algorithm

This first model is described as follows:

- (1): The model is a two-dimensional fluid of N identical particles with one of the four unit velocities.
- (2): ($\vec{\xi_I}$, $\vec{\xi_{II}}$, $\vec{\xi_{III}}$ and $\vec{\xi_{IV}}$). $\vec{\xi_I}$ and $\vec{\xi_{III}}$ corresponding to the horizontal direction and $\vec{\xi_{II}}$ and $\vec{\xi_{IV}}$ the vertical one. The velocity set is illustrated Figure 1.6(a).
- (3): At the time t, if a particle is located at a given node and going at a velocity $\vec{\xi_i}$, then this particle will move to the closest node in the $\vec{\xi_i}$ direction. This process is called streaming. If after streaming only one particle is located at the node, then this is the state of the node at time $t+1$
- (4): If after streaming, two particles are located at the same node, collision occurs. The collisions involve two particles and are instantaneous. Collision occurs only between particles with opposite velocities. Cases with three particles are ignored. For instance, if after streaming two particles are located on a given node, and if these two particles' velocities are $\vec{\xi_I}$ and $\vec{\xi_{III}}$ respectively, then a collision occurs.
- (5): When collision occurs, the velocities of the two particles are modified. After collision, the direction of the particles' velocities are modified to their orthogonal directions. For instance, in the cases described in (4), after collision the velocities of the two particles are changed to $\vec{\xi_{II}}$ and $\vec{\xi_{IV}}$. The system being reversible, when after streaming two particles going at velocities $\vec{\xi_{II}}$ and $\vec{\xi_{IV}}$ coexists, then the velocities change to $\vec{\xi_I}$ and $\vec{\xi_{III}}$. Cases where two particles going at a same velocity on the same node are excluded. A collision process is illustrated Figure 1.6(b).

To give a mathematical background to this algorithm, four $c_i(x,t)$ functions are defined (one per velocity), equal to 1 if a particle having the i^{th} velocity is present at the node of coordinates x at the time t. Then, the algorithm gives:

$$c_i(\vec{x}, t+\Delta t) = c_i^*(\vec{x} - \vec{\xi_i}\Delta t, t) \tag{1.85}$$



(a) 4 velocities in Hardy et al. model [61]

(b) Stream and collide process for two particles in the Maxwell model

Figure 1.6. – (a): Velocity set in the original "Maxwell model"; (b) An example of a collision at time t (From Hardy et al. [62])

$c_i^*(x,t)$ being equal to 1 if a particle going at the i^{th} velocity is present at the node of coordinates x at the time t. This collision operator is given by:

$$\begin{aligned} c_1^* &= c_1(1-c_3) + c_2c_4 \\ c_2^* &= c_2(1-c_4) + c_1c_3 \\ c_3^* &= c_3(1-c_1) + c_2c_4 \\ c_4^* &= c_4(1-c_2) + c_1c_3 \end{aligned} \tag{1.86}$$

One fundamental property of this collision step is the fact that it doesn't create mass or momentum, meaning that if we define $N = \sum_i c_i$ the number of particles at a given node, $J_x = c_1 - c_3$ and $J_y = c_2 - c_4$ the average velocities at a given point, then:

$$N^* = N, \quad J_x^* = J_x \quad and \quad J_y^* = J_y \tag{1.87}$$

N^*, J_x^* and J_y^* corresponding to N, J_x and J_y after the collision step.

1.4.2. Algorithm equivalent macroscopic equations

Two properties of the gas can be simulated such as the existence of an equilibrium state and the fact that the system tends towards it, despite an imprecision growing through time. It can be shown that this model can be related to the Navier-Stokes equations.
To do so, one should consider the presence probability function $P(c_i(\vec{x},t))$ of a particle to be present at (x,t), with the velocity $\vec{\xi_i}$. Contrarily to $c_i(x,t)$, $P(c_i)$ is continuous. Eq. (1.85) can be rewritten through Taylor expansion:

$$P(c_i) - P(c_i^*) = \partial_t P(c_i) + \xi_\alpha \partial_\alpha P(c_i^*) + O(\Delta t) \tag{1.88}$$

Eq. (1.88) can be summed over the i indices, using Eq. (1.87), leading to a macroscopic equation. The obtained relationship deals with the probability of presence, it is interesting to write the equations in term of expected value: $\rho_{LGA} = E(N)$ and $\rho_{LGA} u_{LGA,\alpha} = E(J_\alpha)$, with $E.$ the expected value. Then the obtained equation is:

$$\partial_t \rho_{LGA} + \partial_\alpha \rho_{LGA} u_{LGA,\alpha} = O(\Delta t) \tag{1.89}$$

An equation for the momentum can also be deduced from Eq. (1.88)(giving certain constraints given by Hardy et al. [63]):

$$\partial_t \rho_{LGA} u_{LGA,\alpha} + 1/2 \partial_\alpha \rho_{LGA} = O(\Delta t) \tag{1.90}$$

With a bit of imagination, Eq. (1.89) and Eq. (1.90) can be seen as Euler equations with the pressure given as $1/2\rho_{LGA}$ and without the convection term.

1.4.3. Enhanced HPP model

It was pointed out by the authors themselves [61] that the lack of isotropy makes it impossible to reproduce the viscous behaviour of a fluid. This model, refereed as HPP (from Hardy, Pomeau et de Pazzis who proposed the first model) is mainly known as Lattice Gas Automate (LGA). The model was improved afterward by Frish et al. [19], where a hexagonal lattice is proposed. The improvement of the grid isotropy allowed to solve many problems pointed out by Hardy et al. [61]. An illustration of the grid is proposed in Figure (1.7). It is a six velocities model, the velocities are given by:

$$\vec{\xi_i} = \begin{cases} cos\left(\dfrac{i\pi}{3}\right) \\ sin\left(\dfrac{i\pi}{3}\right) \end{cases} \quad i \in [1, 2, ..., 6] \tag{1.91}$$

D'Humières et Lallemand [20] noted that in the original HPP model, no degree of freedom was allowed

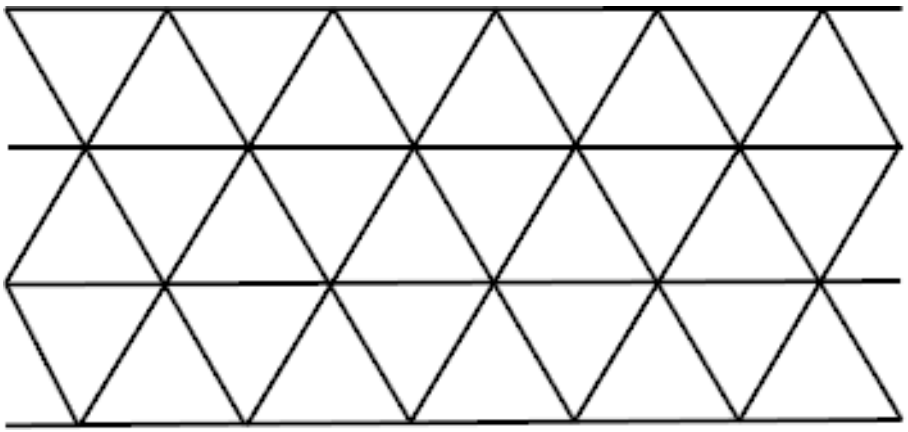


Figure 1.7. – Hexagonal grid proposed by Frish et al [19]

for the description of the collision model. In the 6 velocities framework, different collision models are possible. Moreover, they proposed the possibility to add a resting particle to the model, i.e. a particle having velocity $\vec{\xi_0} = \vec{0}$ that stays still during the streaming phase, but that influences the output of the collision phase.
The importance of the resting particle is pointing out by Frish et al. [64]. The authors highlight the appearance of spurious conservation laws. In particular, it can be shown that if only two particles collisions occur, the total mass over a vertical or horizontal line is preserved. Without a resting particle, three particles collisions are not likely to happen, implying spurious mass conservation over straight lines.
They showed that if the original model couldn't really reproduce the behavior of a Navier-Stokes system Eq. (1.90), the following equation is true:

$$\partial_t \rho_{LGA} u_{LGA,\alpha} + \partial_\beta \left(g(\rho_{LGA}) \rho_{LGA} u_{LGA,\alpha} u_{LGA,\beta} + p\delta_{\alpha\beta} \right) = \\ \mu_{LGA} \left(\partial_\alpha u_{LGA,\beta} + \partial_\beta u_{LGA,\alpha} \right) + \mu_{LGA,b} \partial_\gamma u_{LGA,\gamma} \tag{1.92}$$

with $g(\rho_{LGA})$ a spurious term, p the pressure, μ_{LGA} the shear viscosity and $\mu_{LGA,b}$ the second viscosity. All these expressions are functions of ρ_{LGA} but depends on the used collision model and on the number of velocities (6 without resting particles and 7 with). Independently from the chosen collision model, HPP algorithms are always capable of simulating approximately the Euler part of the Navier-Stokes equation, but the way particles interacts with each others during the collision step influences the viscosity of the system. A similar result was proposed by Frish and Rivet [65]. In the same paper [20], d'Humières and Lallemand showed that they could simulate realistically a 2D duct, or observe Von-Karman instabilities behind a flat plate.

1.4.4. A discussion around isotropy

How to explain the superior performance of the hexagonal grid compared with the squared one? By analogy with numerical schemes like finite difference or spectral difference, it seems natural that increasing the number of degrees of freedom also increases the scheme accuracy. In the case of LGA, this link is not straightforward since no partial derivative equation is solved. Wolfram [66] tackled this issue by showing the influence of the lattice on the system capability to retrieve Navier-Stokes equation. He showed that the higher the degree of isotropy of a system is, the closer the equivalent macroscopic equations are from the Navier-Stokes equations.
Wolfram defined a criterion allowing to define the "degree of isotropy" of a lattice, relying on a family of tensors E^n, n being an integer. He then defined relationships that $E^{(n)}$ should respect. For instance, if the relationships are verified for $E^{(0)}$, $E^{(1)}$ and $E^{(2)}$, then the lattice is isotropic up to the order 2. Wolfram showed that the hexagonal lattice is isotropic up to the order 4 while the squared lattice is only isotropic up to the order 2. The consequence being that the hexagonal lattice has a better capability to retrieve Navier-Stokes equations, but also some spurious terms are removed, making the simulation both more accurate and more numerically stable. The conditions for a lattice to be isotropic are described hereafter.
First, the family of tensors $E^{(n)}$ is defined. $E^{(n)}$ is a tensor of order n, meaning that it contains D^n elements where D is the dimension of the system. For instance, in a $2D$ framework $E^{(3)}$ is a concatenation of 2 matrices of dimension $2 * 2$. The elements of the tensor $E^{(n)}$ is given by:

$$E^{(n)}_{x_1,x_2,x_3,...,x_n} = \sum_{i=1}^{6} \xi_{(x_1,i)}\xi_{(x_2,i)}\xi_{(x_3,i)}...\xi_{(x_n,i)} \tag{1.93}$$

The x_k corresponds to a coordinates (in a $2D$ framework, it must be equal to x or y) , $\xi_{x_k,i}$ being the velocity projection of $\vec{\xi_i}$ in the x_k direction. For instance, for the hexagonal lattice $\xi_{x,0} = 1/2$ $\xi_{y,0} = \dfrac{\sqrt{3}}{2}$. To illustrate, the matrix $E^{(2)}$ can be calculated for the hexagonal lattice.

$$E^{(2)}_{xx} = \sum_{i}^{6} \xi^2_{x,i} = 0.5^2 + (-0.5)^2 + (-1)^2 + (-0.5)^2 + (0.5)^2 + 1^2 = 3 \tag{1.94}$$

The matrix $E^{(2)}$ is given by:

$$E^{(2)} = \begin{pmatrix} 3 & 0 \\ 0 & 3 \end{pmatrix} \tag{1.95}$$

From the definition of this operator, an isotropic condition can be defined. A lattice is said isotropic in the particular context of LGA and LBM methods when it respects the following relationships:

$$\begin{aligned} E^{(2n+1)} &= 0 \\ E^{(2n)} &= C^{(2n)}\Delta^{(2n)} \end{aligned} \tag{1.96}$$

with $C^{(2n)}$ a constant and $\Delta^{(2n)}$ a composition of Kronecker operator defined by the following recursive relationship:

$$\begin{aligned} \Delta^{(0)} &= 1 \\ \Delta^{(2n)}_{i_1,i_2,i_3,...,i_n} &= \sum_{j=2}^{2n} \delta_{i_1 i_j} \Delta^{(2n-2)}_{i_2,i_3,...,i_{j-1},i_{j+1},...,i_{2n}} \end{aligned} \tag{1.97}$$

where δ_{ij} the Kronecker's function being equal to 1 if $i = j$ and 0 otherwise. A lattice is said to be isotropic up to the order k if the relationship Eq. (1.96) is respected for $E^{(k)}$.
For instance, for the hexagonal grid, it comes that, $E^{(1)}_{\alpha} = 0$. From Eq. (1.95), it comes that $E^{(2)}_{\alpha\beta} = 3\delta_{\alpha\beta}$. Also, $E^{(3)}_{\alpha\beta\gamma} = 0$, $E^{(4)}_{\alpha\beta\gamma\mu} = \dfrac{3}{4}\left(\delta_{\alpha\beta}\delta_{\gamma\mu} + \delta_{\alpha\gamma}\delta_{\beta\mu} + \delta_{\alpha\mu}\delta_{\beta\gamma}\right)$ and $E^{(5)}_{\alpha\beta\gamma\mu\lambda}$=0. Then it comes that the

hexagonal lattice is isotropic up to the order 5.
Wolfram proposed to use the isotropy of a lattice as a criterion to evaluate its performance. Using this criterion, he proposed the possibility to use lattices in which the different velocities don't necessarily have the same norm.
In addition, Wolfram shows that to simulate accurately a Navier-Stokes system, the lattice must ensure:

$$\begin{aligned} E^{(1)}_{\alpha} &= 0 \\ E^{(2)}_{\alpha\beta} &= A\delta_{\alpha\beta} \\ E^{(3)}_{\alpha\beta\gamma} &= 0 \end{aligned} \tag{1.98}$$

where A is a constant. More importantly, Wolfram showed that an error proportional to u^4 can be cancelled if the tensor E respects:

$$-\frac{E^{(4)}_{\alpha\beta\gamma\gamma}}{E^{(2)}_{\alpha\beta}} = \sigma \tag{1.99}$$

σ being a constant of the lattice. For the details of the demonstration the interested reader is directed to the original paper [66]. The previous conditions can be reformulated into the following one:

$$E^{(4)}_{\alpha\beta\gamma\mu} = B\left(\delta_{\alpha\beta}\delta_{\gamma\mu} + \delta_{\alpha\gamma}\delta_{\beta\mu} + \delta_{\alpha\mu}\delta_{\beta\gamma}\right) \tag{1.100}$$

with B a constant. It appears that the different conditions in Eqs. (1.98, 1.100) are isotropic conditions [67].
This work showed the close bound between the quality of a LGA simulation (capability to retrieve Navier-Stokes equation, numerical stability, lack of spurious currents,...) and the isotropy of the lattice.

1.4.5. LGA's drawback

In section 1.4.3, the link between LGA and Navier-Stokes system has been shown, by making the hypothesis that the functions c_i involved in Eq. (1.85) are random variables. One could question this hypothesis since the rules of the automaton are strictly deterministic. In practice, for a number of points large enough, the system becomes complex enough so that it seems random. Another issue is that particle probability of presence cannot be directly measured, but Eq. (1.92) is given for the expected value of the random values then this probability has to be measured. To do so, d'Humières [20] proposed to calculate the average of c_i in a given spatial domain and to consider this calculated average as an estimation of the expected value of c_i (seen as an averaged variable). The computation of the average value relies on the hypothesis of the system ergodicity, which cannot be proved for real flows, but however is usually assumed. It is notably an important hypothesis in the general framework of statistical physic.
It should be noted that if the particle probability of presence is not constant in time or space, the spatial averaging can only provide a rough approximation of the actual average. As a consequence, the flow mean variations must occur slowly for an accurate prediction with LGA.
Moreover, Higuera and Jimenez [68] pointed out that LGA leads to a high level of fluctuation due to the limited number of lattice points in the space averaging. In particular, they show how the higher the Reynolds number is, the higher number of cells used in the spatial averaging must be for the simulation to be numerically stable, leading to a significant increase of the computational cost.
In addition to this default, d'Humières and Lallemand [20] pointed out the lake of numerical stability for Reynolds up to 10^3, and the drop in accuracy for compressible flows. A detailled discussion about Lattice Gas Automata is proposed by Frish et al. [64].

1.4.6. From LGA to LBM

As discussed, the Lattice Gas Automata has many defaults. For this reasons, McNamara and Zanetti [21] proposed a Boltzmann alternative for the Lattice Gas Automata, that is said to produce less spurious noise than the automaton. If in LGA, the state of the fluid was described by the Boolean function c_i equal to 1 or 0 if a particle is present or not, the authors proposed a continuous function noted f_i whose value can continuously vary from 0 to 1. It means that f_i can be interpreted as the density of particles with a velocity $\vec{\xi_i}$ rather than a boolean term. In their approach, both density and momentum can be directly determined using the following identities:

$$\sum_i f_i = \rho \tag{1.101}$$

and $\sum_i \xi_{\alpha,i} f_i = \rho u_\alpha$ In this framework, no space averaging is needed. The evolution rule for the function f_i is:

$$f_i(x, t + \Delta t) = f_i(x - \xi_{\alpha,i}\Delta t, t) + \Omega_i(x - \xi_{\alpha,i}\Delta t, t) \tag{1.102}$$

with Ω_i a collision function that is the continuous counterpart of the collisions rules given by the LGA community [20] [64], and $\xi_{\alpha,i}$ is a microscopic velocity. Higuera and Jimenez [68] proposed to approximate the collision term for low Reynolds and Knudsen number through:

$$\Omega_i = \frac{1}{\tau_{ij}} \left(f_j - f_j^{eq} \right) \tag{1.103}$$

where f_j^{eq} is an equilibrium function which formulation was proposed by Wolfram [66], and τ_{ij} is a matrix of dimensionless coefficients that characterize the collision scheme. In this framework, the existence of a local equilibrium is assumed. In that particular context, a state is said to be at equilibrium if density function f_i only depends with the macroscopic values (ρ and ρu_α). The formulation in Eq. (1.103) is closed from an approximation proposed in the statistical physic framework by Bhatnagar, Gross and Krook [50]. They propose that τ_{ij} is proportional to the identity matrix, which leads the algorithm proposed in Eq. (1.102) to become:

$$f_i(x, t + \Delta t) = f_i(x - \xi_{\alpha,i}\Delta t, t) - \frac{1}{\tau} \left(f_i(x - \xi_{\alpha,i}\Delta t, t) - f_i^{eq}(x - \xi_{\alpha,i}\Delta t, t) \right) \tag{1.104}$$

with τ a unique coefficient. This description constitues the core of the Lattice Boltzmann Method. This leaded several years later to the method proposed by He and Luo [58] detailled in Section 1.3.3.

Chapter 2

Multiphase flows simulation

Overview

2.1. Surface tracking methods 30
2.1.1. Front tracking 30
2.1.2. Volume Of Fluids 31
2.1.3. Level Set 33
2.2. Diffuse Interface Method 36
2.2.1. Phase field method 36
2.2.2. Multi fluids methods 40
2.3. Surface tension 44
2.3.1. Geometrical approach 45
2.3.2. Free Energy approach 46

Interfacial two-phase flows are defined by the occurrence of two immiscible phase at different states, namely a liquid and a gas. The interface between phases is very thin, - typically a few atoms length - much smaller than the characteristic system length, and is considered infinitely thin. Moreover, a difference of attractive forces between the liquid and the gas occurs at the interface, inducing a surface forces: surface tension. This surface tension has a significant impact on the flow dynamic [69], and is also involved the physics of atomization [70]. Numerical simulations of interfacial flows are a challenge, for several reasons. First, large and sharp density gradients occur across the interface, which must be discretized on the mesh and taken into account in the numerical method. For atomization applications, massive shear occurs at the interface, which add difficulties. Finally, the interface curvature must be known with accuracy to predict surface tension, which requires accurate numerical schemes.
Several methodologies have been proposed to deal with such flows. On One hand, sharp interface methods consider separated phases with discontinuities and jump conditions at the interface. On the other hand, diffuse interface methods have also been proposed, in which a continuous transition from one phase to the other occurs. To allow such a continuous transition, the interface is artificially thickened over several grid points, which consequently reduces interfacial gradients and associated mesh constraints required for their discretization.
In this chapter, these two main approaches are presented. A specific section is dedicated to the description of surface tension operator.

2.1. Surface tracking methods

2.1.1. Front tracking

Front tracking methods are the first proposed in the literature to address interfacial flows, and consist in the explicit interface tracking through the use of markers. The Marker And Cells (MAC) proposed in Harlow and Welsh [71, 72] consists in a staggered grid, where pressure and velocity are defined at different locations, on which incompressible Navier-Stokes equations are solved through dedicated numerical scheme not presented here:

$$\vec{\nabla}\vec{u} = 0 \tag{2.1}$$

$$\partial_t \rho u_\alpha + \partial_\beta \left(\rho u_\alpha u_\beta + p\delta_{\alpha\beta}\right) = \mu \left(\partial_\alpha u_\beta + \partial_\beta u_\alpha\right) \tag{2.2}$$

A specificity of this method is the use of a staggered grid: the velocity fields and the pressure field are defined at different locations of the computational grid similarly as in the well known Patankar's SIMPLE algorithm [73].
A specific flag is associated to each cell, depending on the presence of each phases among the following:

- Full (F)
- Empty (E)
- Boundary (B)
- Interface (I)

The flags are assigned thanks to massless markers that are streamed with the flow. If a cell doesn't contain any marker, then it is assigned the (E) flag. If a cell contain at least one marker, but is in contact with at least one (E) cell, then it is considered as an interface cell (flagged (I)). A cell that contains one marker or more, and that is not a (I) cell is assigned with a (F) flag. The (B) flag corresponds to a boundary and they are assigned by the user beforehand, their statue stays unchanged all along the simulation. The algorithm is illustrated in Figure 2.1. The methodology has been later improved by Amdsen and Harlow [74] who proposed the Simplified MAC (SMAC) where a more efficient algorithm, as the name suggests it, is proposed. A significant improvement was made

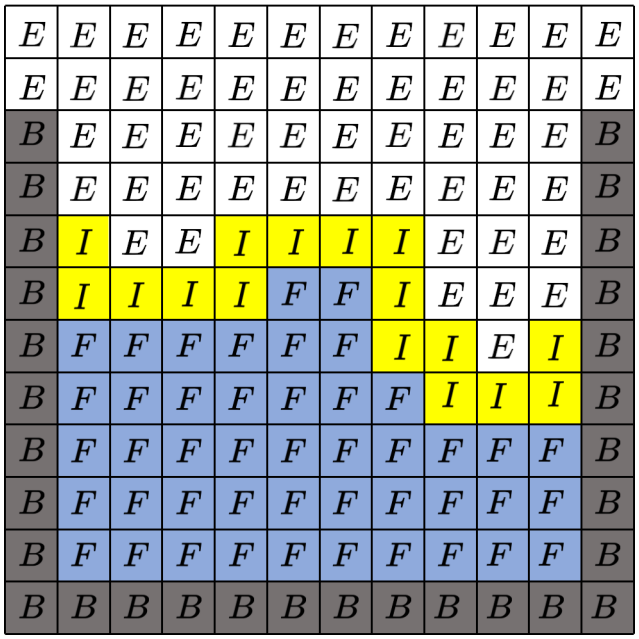


Figure 2.1. – Illustration of the flag system for a MAC algorithm

by Tomé and McKee [75] who proposed the GENSMAC approach, in which markers are specifically dedicated to the interface dynamic description. Mangiavacchi et al. [76] proposed to take into account surface tension. McKee et al. [77] proposed a review of these front tracking methods.
Promising results were obtained, such as droplet splashing in a denser and more viscous fluid proposed by De Sousa et al. [78] in Figure 2.2. However, these methodologies suffer from a lack of accuracy for complex flows topologies, such as the ones occurring in atomization

2.1.2. Volume Of Fluids

The Volume of Fluid (VoF) method belongs to the surface tracking methods, and is one of the most common approaches chosen in the interfacial flow numerical community. This eulerian method was first proposed by Nichols and Hirt [79] inspired by the work of Noh et al. [80].
While front tracking methods were historically the first to be proposed in the literature, this method's family tends to be computationally expansive, and to have mass conservation issues. Volume of Fluids methods intent to fix these mass conservation issues while being less computationally intensive than Front tracking methods.
In this framework, the total density ρ and the velocity $\vec{u}$ are determined by solving the incompressible continuity equation:

$$\partial_\alpha u_\alpha = 0 \tag{2.3}$$

and the momentum conservation equation given by:

$$\partial_t \rho u_\alpha + \partial_\beta \left(\rho u_\alpha u_\beta + p\delta_{\alpha\beta}\right) = \mu \left(\partial_\alpha u_\beta + \partial_\beta u_\alpha\right) + F_\alpha^\sigma \tag{2.4}$$

F_α^σ being a body force accounting for surface tension. The interface location is known from the liquid mass fraction Y_1 advection, following:

$$\partial_t Y_1 + u_\alpha \partial_\alpha Y_1 = 0 \tag{2.5}$$

Total density ρ is then recovered through:

$$\rho = \rho_1 Y_1 + \rho_2 \left(1 - Y_1\right) \tag{2.6}$$

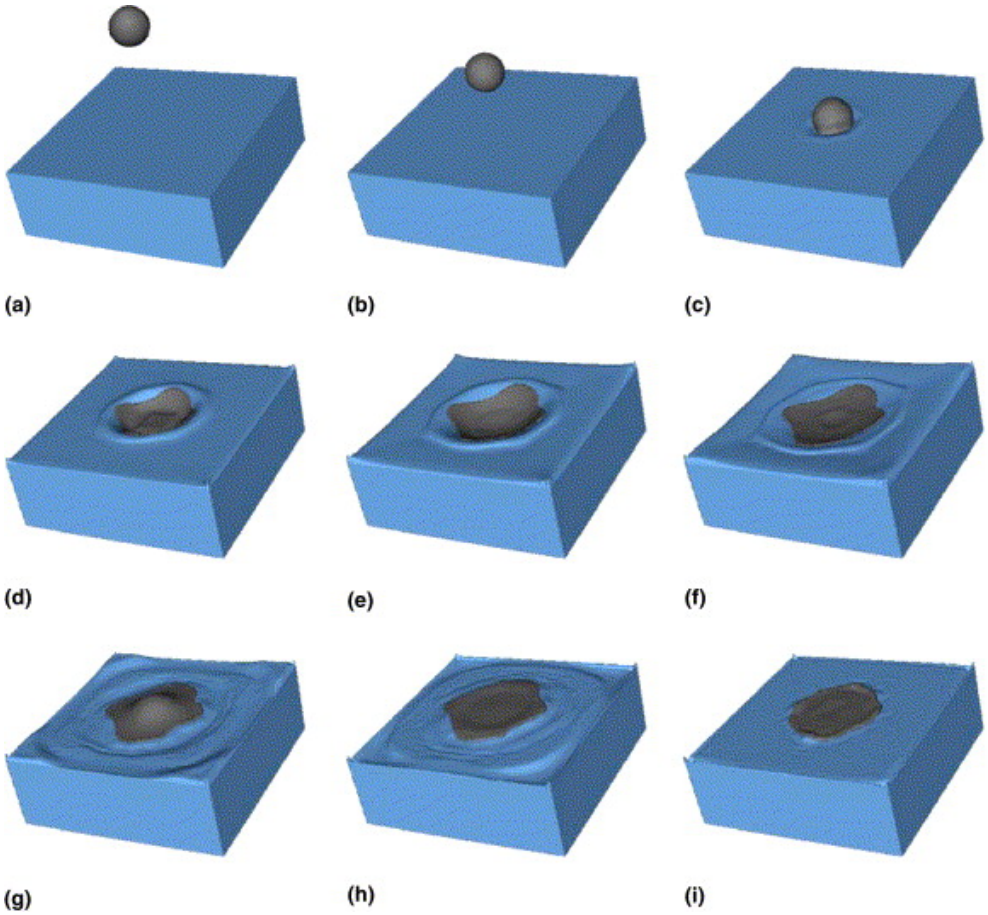
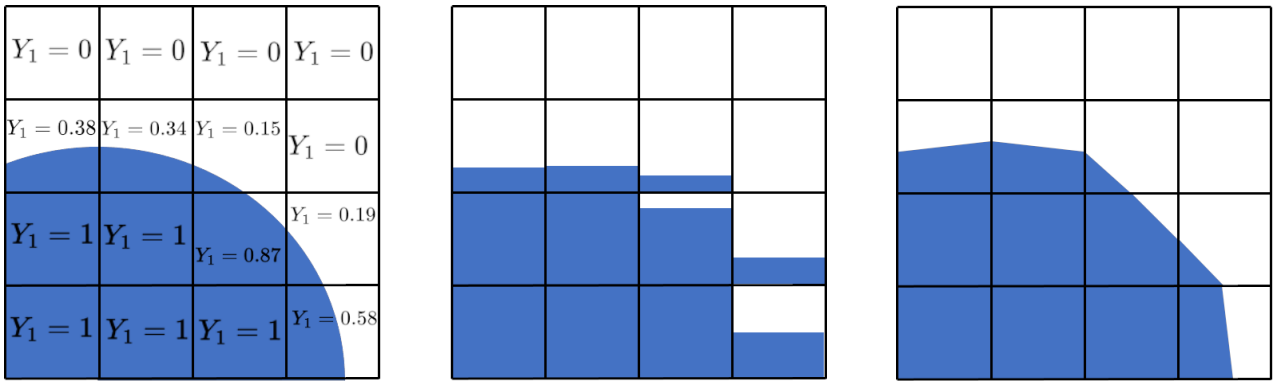


Figure 2.2. – Splashing droplet into a denser and more viscous fluid. Figure from [78]

where ρ_1 and ρ_2 are the respective density of phase 1 and phase 2. The numerical method must ensure the interface sharpness. In practice, the numerical method induces interface dissipation. Two VOF have been developed to deal with an accurate interface prediction: VOF with interface reconstruction, and VOF with flux reconstruction. Flux reconstruction methods consist in the use of high order numerical schemes to limit numerical dissipation. These methods are detailed here, the interested reader may see Ubbink and Issa [81], Lafaurie et al. [82], Tsui et al. [83] and Patel et al. [84].
Interface reconstruction methods assume interfacial cells with liquid mass fraction Y_1 such that $0 < Y_1 < 1$, and with an unknown interface topology to be reconstructed. More or less complex algorithms have been proposed, depending on their order of accuracy, as shown in Figure 2.3.
The first and simplest reconstruction algorithm, the Simple Line Interface Calculation (SLIC), was introduced by Noh and Woodward [80]. It assumes a linear, and horizontal or vertical interface reconstruction, as illustrated in Figure 2.3(b).
This methodology was further improved by Youngs [85] who introduced the Piece-wise Linear Interface Calculation (PLIC), illustrated in Figure 2.3(c). This method requires to precisely estimate the interface direction in order to predict accurately the interface dynamics. The interface normal vector reconstruction is a topic in itself, the interested reader is referred to Pilliof and Puckett [86], Mosso et al. [87], Dyadechko and Shashkov [88] or Sussman and Puckett [89].
VOF methods are fully mass conservative, even for interfacial flows at high density ratio and high Reynolds numbers. The flapping of a two phase jet for air and water at $Re = 8701$ performed by Schmidt et al. [90] is shown in Figure 2.4. In this study [90], the authors showed a good agreement with experimental results for both the atomization mechanism and the droplet probability density function.



(a) Reference

(b) Simple Linear Interface Calculation (SLIC) method

(c) Piece-wise Linear Interface Method (PLIC)

Figure 2.3. – Illustration of an interface reconstruction process. (a) the reference phase field Y_1 with the actual interface location. (b) Reconstructed interface obtained through a SLIC algorithm (c) Reconstructed interface obtained through a piece wise linear method

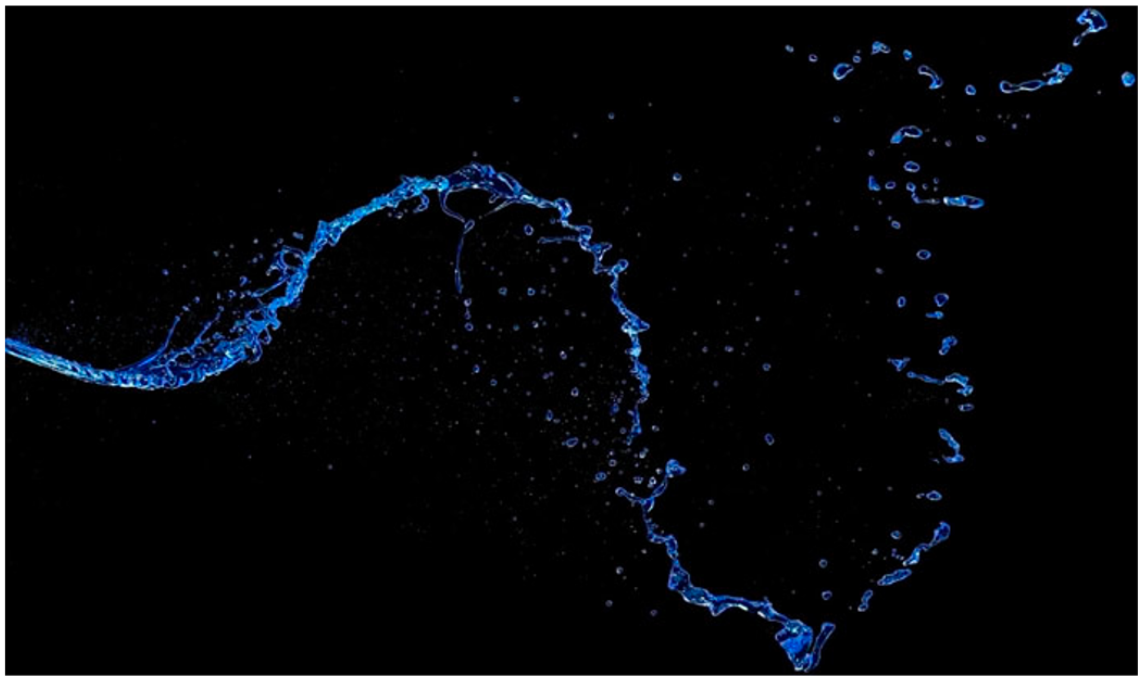


Figure 2.4. – Atomization of an air-water oscillating liquid jet with a VOF method. The open-source code Gerris [91] is used. Illustration from Schmidt et al. [90]

2.1.3. Level Set

Originally proposed by Osher and Sethian [92] for flame front propagation, and later adapted for two-phase flows by Mulder and Osher [93], the Level Set method consists in the advection of the scalar signed distance function Φ defined Eq. (2.7):

$$|\Phi(\vec{x}, t)| = \min_{\vec{x_I} \in \Gamma} |\vec{x} - \vec{x_I}| \tag{2.7}$$

where Γ is the interface and x_I the interface location. The function ϕ is called the Level Set function, naming the method. It is computed by solving Eq. (2.8):

$$\partial_t \Phi + u_\alpha \partial_\alpha \phi = 0 \tag{2.8}$$

Similarly as in VOF methods, the density ρ and velocity $\vec{u}$ are recovered through a continuity equation and momentum conservation equation Eq. (2.9) and Eq. (2.10)

$$\partial_t \rho + \partial_\alpha \rho u_\alpha = 0 \tag{2.9}$$

$$\partial_t \rho u_\alpha + \partial_\beta \left(\rho u_\alpha u_\beta + p\delta_{\alpha\beta}\right) = \mu \left(\partial_\alpha u_\beta + \partial_\beta u_\alpha\right) + F_\alpha^\sigma \tag{2.10}$$

where F_α^σ accounts for surface tension. The interface location is given by the isocontour of $\phi = 0$. This function is signed such as its sign changes depending with the phase it is located in.
To remain a distance function, the level-set function must satisfy $\vec{\nabla}\Phi = 1$. However, the advection through a complex flow does not always ensure such condition. Sussman and Puckett [94] proposed to add a redistanciation step in the phase field calculation algorithm. In this enhanced algorithm, an intermediate function $\Phi^*(\vec{x}, t)$ is first calculated as the solution of Eq. (2.8). The phase field $\Phi(\vec{x}, t+1)$ is calculated as the stationary solution of the following system, Eq. (2.11):

$$\partial_\tau \Phi = sign\left(\Phi^*\right)\left(1 - |\vec{\nabla}\Phi|\right) \quad \text{with} \quad \Phi(\vec{x}, 0) = \Phi^*\left(\vec{x}, t\right) \tag{2.11}$$

The main drawback of level-Set method is the lack of mass conservation, which results from this redistanciation step. The redistanciation induces non-physical interface displacements, and thus spurious mass transfer between phases. To address this issue Olson and Kreis [95] proposed a so-called Conservative Level Set (CLS). This improvement consists in the consideration of a hyperbolic tangent distance function Ψ:

$$\Psi\left(\vec{x}, t\right) = \frac{1}{2}\left(tanh\left(\frac{\Phi(\vec{x}, t)}{2\epsilon}\right) + 1\right) \tag{2.12}$$

where ϵ is a characteristic length that controls the interface thickness. Ψ is calculated by solving a convection equation and the interface is located at $\Phi = (\vec{x}, t) = 0$, i.e. $\Psi = (\vec{x}, t) = 0.5$. The conservative equation is similar to Eq. (2.8):

$$\partial_t \Psi + \partial_\alpha \left(\Psi u_\alpha\right) = 0 \tag{2.13}$$

In order to ensure $|\vec{\nabla}\Phi| = 1$, which reads for the new function $\partial_\alpha \Psi = \dfrac{\Psi\left(1 - \Psi\right)}{\epsilon}$. Similarly as in Sussman et al. [94], Olson and Kreiss [96] proposed an enhanced algorithm using an intermediate function Ψ^* solution of Eq. (2.13). $\Psi(\vec{x}, t+1)$ is defined as the stationary solution of Eq. (2.14):

$$\partial_\tau \psi = \partial_\alpha \left(\epsilon \left(\partial_\alpha \Psi n_\alpha\right) n_\alpha - \Psi\left(1 - \Psi\right) n_\alpha\right) \tag{2.14}$$

where $\vec{n}$ is the interface normal vector defined Eq. (2.15)

$$\vec{n} = \frac{\vec{\nabla}\Psi}{|\vec{\nabla}\Psi|} \tag{2.15}$$

The main strength of the Level Set Method is the capability to easily construct a normal vector and consequently compute curvature thanks to the Ψ or the Φ field. The curvature κ can be computed through:

$$\kappa = \vec{\nabla}.\left(\vec{n}\right) \tag{2.16}$$

Desjardins et al. [97] nonetheless proposed to rely on Ψ rather than Φ to compute the interface normal:

$$\vec{n} = \frac{\vec{\nabla}\Phi}{|\vec{\nabla}\Phi|} \tag{2.17}$$

This methodology, refereed as the Accurate Conservative Level-Set (ACLS) is shown to significantly improve the results, allowing the computation of rather large density gradients, and high Reynolds and Weber numbers, as shown in Figure 2.5 for which $Re = 3000$, $We = 10000$, and the density ratio is 40. Despite the improvements, the ACLS is not fully conservative, leading to a 3% mass loss in the original paper.

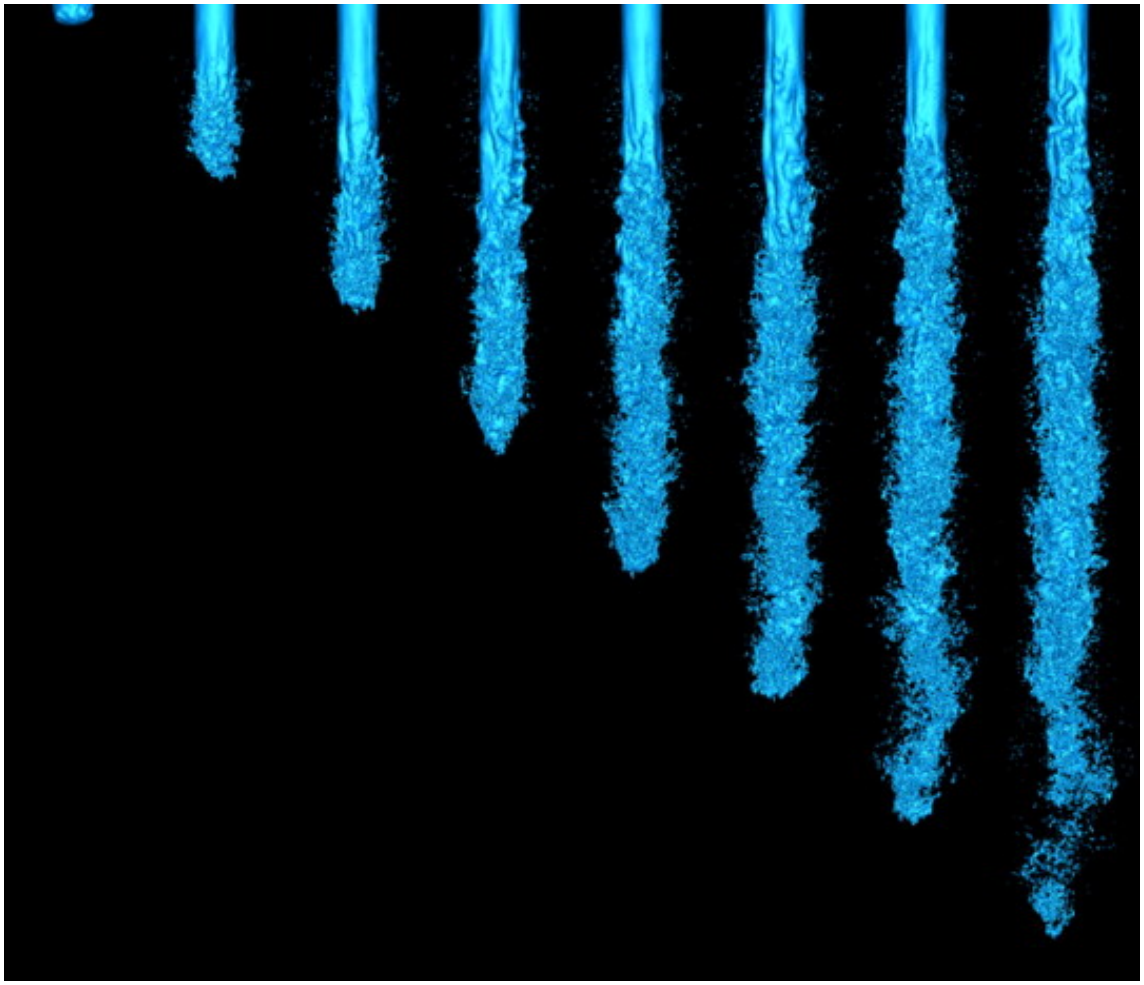


Figure 2.5. – Simulation of the atomization of a liquid Diesel using ACLS method. Picture from Desjardins et al. [97]

2.2. Diffuse Interface Method

Diffuse interface methods consist in the consideration of a continuous change in physical properties across the interface. This continuous change is dictated by a thermodynamic approach, or a phase field method, either a multi-fluids method, described in the following.

2.2.1. Phase field method

2.2.1.1. Fundamental principles

The phase field methods inherit from the original work of van der Waals [98], Korteweg [99], Cahn and Hilliard [100] and allow to track the interface through a thermodynamic variable characteristic of the considered phase. Several phase fields functions have been considered in the literature, either the density ρ, the liquid mass fraction Y_{liq}, or the liquid volume fraction α_{liq}. The specific phase field, noted ϕ, defined by Eq. (2.18):

$$\phi = Y_1 - Y_2 \tag{2.18}$$

where Y_k corresponds to the k^{th} mass fraction, is of particular importance in the present work, and $\phi = \pm 1$ in pure phase. In pure phase 1, ϕ takes the value 1 and in pure phase 2, ϕ is equal to -1. In his original work [98], Van der Walls proposed to consider density ρ, as the phase field, but his work can be generalised to any phase field variable. His work relies on the Helmholtz free energy defined by Eq. (2.19)

$$F = U - TS \tag{2.19}$$

where U is the internal energy, T the temperature and S the entropy. The volume free energy writes f_H, and is a function of the temperature T, the density ρ and the composition ϕ.
Van Der Waals made three assumptions. It was assumed that the phase field and its successive spatial derivatives are independent variables, the study takes place in an isothermal framework (then f_H doesn't depend on the temperature anymore), and f_H is a function of the phase field, but also of the phase field's spatial derivative ($f_H\left(\rho, \phi, \vec{\nabla}\phi\right)$). Based on symmetry assumption, it can be shown that:

$$F = \iiint \left[f_H\left(\rho, \phi, 0\right) + \lambda_\phi \left(\vec{\nabla}\phi\right)^2 \right] dx^3 \tag{2.20}$$

where λ_ϕ is a constant. It can be seen that free energy can be divided into two components. A "pure fluid" component $f_{H,0} = f_H\left(\rho, \phi, 0\right)$ and an "interfacial" component $f_H^\sigma = \lambda_\phi \left(\vec{\nabla}\phi\right)^2$. The interested reader can find the calculation's detail in Cahn and Hilliard's work [100]. From last equation, a volume free energy function can be defined:

$$f_{FE} = f_{H,0} + f_H^\sigma \tag{2.21}$$

Homogeneous free energy

It was pointed out by Gibbs [101] that for the two phases to be at equilibrium, the pure fluid free energy $f_{H,0}$ should reach a minimum in pure phases. For the phase field ϕ defined by Eq. (2.18), the free energy $f_{H,0}$ must verify:

$$\partial_\phi f_{H,0}|_{\phi=1} = \partial_\phi f_{H,0}|_{\phi=-1} = 0 \tag{2.22}$$

The free-energy can be freely set by the user, as long as Eq. (2.22) is satisfied. In Section 2.3, it is discussed that pressure can be computed from free energy, then $f_{H,0}$'s definition can be considered as an equation of state. Many formalisms have been proposed in the literature for $f_{H,0}$, among which:

$$f_{H,0} = F_0 \left(1 - \phi^2\right)^2 \tag{2.23}$$

where F_0 is a constant set by the user. This expression is sometimes expressed as a function of the phase mass fraction:

$$f_{H,0} = F_0 Y_1^2 (1 - Y_1)^2 \tag{2.24}$$

It must be noted that the present work takes place in an isothermal framework, making the present model unable to take into consideration thermal effect. Caginal [102] and then Boettinger et al.[103] proposed an improved free energy formalism that takes into account a thermal behavior.

Free energy potential

From Gibbs [101], it comes that for a system to be at thermodynamical equilibrium, its total free energy must reach a minimum. At equilibrium, the phase field ϕ_{eq} must satisfy:

$$F(\phi_{eq}) = \min_{\phi} (F(\phi)) \tag{2.25}$$

It can be shown that the previous condition reduces to the following differential equation Eq. (2.26). A rigorous demonstration was proposed by Nayigizente [104].

$$\partial_\phi f_{H,0} - \partial_\alpha (\lambda_\phi \partial_\beta \phi) = 0 \tag{2.26}$$

From the last condition, it is useful to define a phase field potential defined by:

$$\mu_\phi = \partial_\phi f_{H,0} - \partial_\alpha (\lambda_\phi \partial_\beta \phi) \tag{2.27}$$

Note that in pure phase $\partial_\beta \phi = 0$, which induces $\partial_\phi f_{H,0} = 0$, which satisfies the Gibbs condition Eq. (2.22).
On a side note, when $f_{H,0}$ is specifically defined through Eq. (2.23) and in a flat interface case, the partial derivative equation Eq. (2.26) can be solved analytically. Eq. (2.26) reduces to:

$$\phi(x) = \frac{1 + \tanh\left(\sqrt{\frac{F_0}{2\alpha}} x\right)}{2} \tag{2.28}$$

2.2.1.2. Cahn Hilliard and Allen-Cahn equations

As discussed in Cahn et al. [105], a family of methods can be constructed from the definition of the phase field potential μ_ϕ defined by Eq. (2.27). The phase field will be solution of a specific equation based on the previous principles. This equation controls the interface shape. Two main families of equations have been proposed in the literature, the Cahn-Hilliard [106] and the Allen-Cahn [107] equations, detailled hereafter.

Cahn-Hilliard equation

The work of Cahn and Hilliard takes place in the context of metallurgy, and spinodal decomposition between phases. It assumes a concentration flux $\vec{J_\Phi}$ occuring during this spinodal decomposition, to homogenise the system. This flux is assumed to be proportional to the phase field potential gradient following:

$$J_{\phi,\alpha} = M \partial_\alpha \mu_\phi \tag{2.29}$$

where M is the so-called mobility factor, which controls the interface dynamics. The Cahn-Hilliard equation is obtained by assuming that temporal variation of the phase field corresponds to the concentration flux spatial gradient:

$$\partial_t \phi = \partial_\alpha J_{\phi,\alpha} = \partial_\alpha \left[M \left(\partial_\phi f_{H,0} - \partial_\gamma \lambda_\phi \partial_\beta \phi \right) \right] \tag{2.30}$$

As Cahn and Hilliard work takes place in a metallurgical framework, it doesn't take into account a convective term. Eq. (2.30) was generalised to fluid mechanics by Antanovski [108], who proposed:

$$\partial_t \rho\phi + \partial_\alpha \left(\rho\phi u_\alpha\right) = \partial_\alpha \left[M\partial_\alpha \left(\partial_\phi f_{H,0} - \partial_\beta \lambda_\phi \partial_\gamma \phi\right)\right] \tag{2.31}$$

Unlike the Cahn-Hilliard equation Eq. (2.30), the generalisation by Antanovski Eq. (2.31) is written in a conservative form. In the incompressible framework, both ϕ and $\rho\phi$ can be considered as transported field. However, in the compressible framework, the formulation by Antanovski Eq. (2.31) must be considered to ensure mass conservation. These equations involve the 4th order derivative of ϕ, which may be an issue in term of numerical cost. On the other hand, Eq. (2.31) has the advantage to be unconditionally mass conservative. More details about mass conservation are provided in Section 2.2.1.4.

Allen-Cahn equation

The fact that the Cahn-Hilliard equation implies a 4^{th} order spatial derivative can be numerically costly. To prevent this issue, Allen and Cahn [107] proposed a 2^{nd} order equation. In this equation, temporal derivative of the phase field is directly proportional to the phase field potential:

$$\partial_t \phi = M\mu_\phi \tag{2.32}$$

The generalization to a fluid dynamic framework proposed by Yang et al. [109] following:

$$\partial_t \rho\phi + \partial_\alpha \left(\rho\phi u_\alpha\right) = M\left[\partial_\phi f_{H,0} - \partial_\alpha \lambda_\phi \partial_\beta \phi\right] \tag{2.33}$$

It must be noted that the coefficient M is also called the mobility factor as in an Allen-Cahn framework. Note anyway that these two coefficients have different natures, and don't have the same units.
Compared to the Cahn-Hilliard equation, the Allen-Cahn equation is less computationally expensive since it only involves a second order spatial derivative. However, its main drawback is that it doesn't necessarily ensure mass conservation. More details are provided in Section 2.2.1.4

2.2.1.3. Allen-Cahn equation: a geometrical approach

Original Sun and Beckermann model

Another class of phase field methods has been proposed by Sun and Beckermann [46]. In the literature, this approach is often called "Allen-Cahn" equation despite being significantly different from the approach described Section 2.2.1.2. To distinguish this methodology from the original Allen-Cahn formulation, it is refereed in this present work as the geometrical Allen-Cahn approach. Sun and Beckermann work takes place in an incompressible context. The authors assumed the right hand side of the phase field transport equation to be proportional to the local interface curvature, following:

$$\partial_t \phi + \partial_\alpha \phi u_\alpha = M\kappa|\vec{\phi}| \tag{2.34}$$

where M is the mobility factor, and κ the interface curvature. Similarly as in Level-Set method, the curvature is estimated from the interface normal:

$$\vec{n} = \frac{\vec{\nabla}\phi}{|\vec{\nabla}\phi|} \tag{2.35}$$

The interface curvature writes

$$\kappa = \vec{\nabla}.\vec{n} = \frac{1}{|\vec{\nabla}\phi|}\left[\partial_\alpha^2 \phi - \frac{\left(\partial_\alpha \phi\right)\left(\partial_\alpha |\vec{\nabla}\phi|\right)}{|\vec{\nabla}\phi|}\right] \tag{2.36}$$

They furthermore proposed to assume that the diffuse interface follows an hyperbolic tangent profile following [46]:

$$\phi = -\tanh\left(\frac{n_{dist}}{\sqrt{2}W}\right) \tag{2.37}$$

where n_{dist} is the normal distance to the interface and W the interface characteristic width. Since $f' = 1 - f^2$ for $tanh$, Eq. (2.36) can be recast as:

$$\vec{\nabla}\phi = -\partial_n\phi = \frac{1-\phi^2}{\sqrt{2}W} \tag{2.38}$$

$$\frac{\left(\vec{\nabla}\phi.\vec{\nabla}\right)|\vec{\nabla}\phi|}{|\vec{\nabla}\phi|} = -\frac{\phi\left(1-\phi^2\right)}{W^2} \tag{2.39}$$

Finally, the phase field transport equation writes:

$$\partial_t\phi + \partial_\alpha\left(\phi u_\alpha\right) = M\left[\partial^2_\alpha\phi + \frac{\phi\left(1-\phi^2\right)}{W^2}\right] \tag{2.40}$$

The main advantage is that the interface thickness is controlled by the user through the parameter W. By construction, in a flat interface case the phase field tends to a hyperbolic tangent profile. As will be discussed in the following subsection (Section 2.2.1.4), this methodology however does not ensure mass conservation. To address this issue, Chiu and Lin [47] proposed an improved conservative model.

Chiu and Lin conservative model

Chiu and Lin [47] proposed to add a correction term in Eq. (2.40) following:

$$\partial_t\phi + \partial_\alpha\left(\phi u_\alpha\right) = M\left[\partial^2_\alpha\phi - |\vec{\nabla}\phi|\partial_\alpha\left(\frac{\partial_\alpha\phi}{|\vec{\nabla}\phi|}\right) - \frac{\phi\left(1-\phi^2\right)}{W^2}\right] \tag{2.41}$$

which can be reduced as:

$$\partial_t\phi + \partial_\alpha\left(\phi u_\alpha\right) = M\partial_\alpha\left[\partial_\alpha\phi - \frac{\phi\left(1-\phi\right)}{W}\frac{\partial_\alpha\phi}{|\vec{\nabla}\phi|}\right] \tag{2.42}$$

The previous equation is of paramount important in the current work. Similarly, like the equation proposed by Sun and Beckerman [46], it can be shown that for a flat interface this equation tends to a tangent hyperbolic profile. It must also be reminded that the $\frac{\partial_\alpha\phi}{|\vec{\nabla}\phi|}$ term in the equation's right term corresponds to the normal vector α direction n_α.
By construction, this equation is purely conservative. Note that Eq. (2.42) has been proposed in the incompressible framework. In a compressible framework, this conservation equation must write:

$$\partial_t\rho\phi + \partial_\alpha\left(\rho\phi u_\alpha\right) = M\partial_\alpha\left[\partial_\alpha\phi - \frac{\phi(1-\phi)}{W}n_\alpha\right] \tag{2.43}$$

so that each phase mass fraction are conserved. It must be noted that M from (2.43) and M from (2.42) corresponds to different physical value, despite being noted in a similar manner among the literature. In particular, they don't have the same dimension.

2.2.1.4. About mass conservation

In a compressible framework, Cahn-Hilliard and Allen-Cahn equations are associated to the mass conservation equation:

$$\partial_t \rho + \partial_\alpha (\rho u_\alpha) = 0 \tag{2.44}$$

This equation assures total mass conservation. On the other hand, $\rho\phi$ variation corresponds to the mass transfer from one phase to the other. The phase field conservation equation must avoid spurious mass transfer to ensure mass conservation. In a Cahn-Hilliard or an Allen-Cahn framework, the interface thickening can only occur if mass transfers are locally allowed. This mass transfer doesn't necessarily break the mass conservation principle if its integral on the whole domain is zero. The general form of a phase field equation is reminded here:

$$\partial_t \rho\phi + \partial_\alpha (\rho u_\alpha) = \omega \tag{2.45}$$

When integrated on the whole spatial domain, Eq. (2.45) writes:

$$\partial_t \iiint_D \rho\phi dV + \iint_S \rho\phi u_\alpha n_{S,\alpha} dS = \iiint_D \omega dV \tag{2.46}$$

where $\iiint_D dV$ is the integral all over space, $\iiint_S n_{S,\alpha} dS$ is the integral all over the domain's limit and $\vec{n_S}$ is the domain limit normal vector.
In the Cahn-Hilliard case, $w = \partial_\alpha j_\alpha$. Using the Grad-Ostrogradsky theorem the integrated source term can be reduced to:

$$\iiint_D \omega dV = \iint_S j_\alpha n_{S,\alpha} dS \tag{2.47}$$

If the phase field flux is null at the domain's boundary, the phase field production integral is null. It shows how a system including a Cahn-Hilliard equation is unconditionally mass conservative.
In the Allen-Cahn framework, $w = M\mu_\phi = M(\partial_\phi f_{H,0} - \partial_\alpha \lambda_\phi \partial_\beta \phi)$, then the production term reduces to:

$$\iiint_D \omega dV = \underbrace{\iint_D M\partial_\phi f_{H,0}}_{(1)} - \underbrace{\iint_S M\lambda_\phi \partial_\beta \phi n_{\alpha,S} dS}_{(2)} \tag{2.48}$$

In the last equation, (2) can be equal to zero with the good boundary conditions choice, but (1) is not necessarily equal to 0. For instance, if $f_{H,0}$ is set thanks to (2.26), the Allen-Cahn equation is not conservative. Based on Rubinstein et al.'s work [110], conservative Allen-Cahn phase field equations were proposed [111] [112]
In particular, Chiu and Lin equation (Eq. (2.42)) is mass conservative since it takes an Allen-Cahn equation's form, with a production term w equal to a gradient term.

2.2.2. Multi fluids methods

Multi-fluids methods are another popular class of diffuse interface methods. Originally proposed in Drew & Segel [113], Baer and Nunziato [114] derived a seven transport equation model intending to model deflagration to detonation transition. This method is extended to a two phase immiscible framework by Saurel and Abgrall [115].
In this methods, a unique equation system describe the whole fluid. The interface is not explicitly considered, it simply corresponds to sharp spatial gradient zones. But contrary to phase field methods, the theoretical background doesn't rely on the free energy approach. In Saurel and Abgrall's [115] work, each fluid mass, momentum and energy are considered independently, and each of them are

determined through a specific transport equation. It means that this model allows to simulate fluids in a non-equilbrium state mechanically and energetically. The original equations system is given by:

$$\partial_t \left(\alpha_1 \rho_1\right) + \partial_\alpha \left(\alpha_1 \rho_1 u_{1,\alpha}\right) = 0 \tag{2.49}$$

$$\partial_t \left(\alpha_2 \rho_2\right) + \partial_\alpha \left(\alpha_2 \rho_2 u_{2,\alpha}\right) = 0 \tag{2.50}$$

$$\partial_t \left(\alpha_1 \rho_1 u_{\alpha,1}\right) + \partial_\beta \left(\alpha_1 \left[\rho_1 u_{\alpha,1} u_{\beta,1} + p_1\right]\right) = -p_{int} \partial_t \alpha_2 - K_u \left(u_{\alpha,1} - u_{\alpha,2}\right) \tag{2.51}$$

$$\partial_t \left(\alpha_2 \rho_2 u_{\alpha,2}\right) + \partial_\beta \left(\alpha_2 \left[\rho_2 u_{\alpha,2} u_{\beta,2} + p_2\right]\right) = -p_{int} \partial_t \alpha_1 + K_u \left(u_{\alpha,1} - u_{\alpha,2}\right) \tag{2.52}$$

$$\partial_t \left(\alpha_1 \rho_1 e_1\right) + \partial_\alpha \left(\alpha_1 \left(\rho_1 e_1 + p_1\right) u_1\right) = -p_{int} u_{int} \partial_t \alpha_2 - K_u u_{int} \left(u_1 - u_2\right) - K_p p_{int} \left(p_2 - p_1\right) \tag{2.53}$$

$$\partial_t \left(\alpha_2 \rho_2 e_2\right) + \partial_\alpha \left(\alpha_2 \left(\rho_2 e_2 + p_2\right) u_2\right) = p_{int} u_{int} \partial_t \alpha_2 + K_u u_{int} \left(u_1 - u_2\right) + K_p p_{int} \left(p_2 - p_1\right) \tag{2.54}$$

$$\partial_t \alpha_2 + u_{\alpha,int} \partial_\alpha \alpha_2 = K_p \left(p_2 - p_1\right) \tag{2.55}$$

with α_k being k^{th} phase volume fraction, ρ_k density, u_k velocity, e_k the internal energy. K_u and K_p are relaxation terms, $\vec{u}_{int}$ corresponds to the interface velocity and p_{int} the interface pressure. The formulation for p_{int} and u_{int} is a subject of discussion in itself.
In this model, the two phases are not supposed to be at mechanical and thermal equilivbium, so that two different velocities (u_1 and u_2) and internal energies (e_1 and e_2) are transported.
To reduce the computational cost of this seven equations model, Kapila et al. [116] then Saurel et al. [117][118] successively reduced this formulation to a 6 and 5-equation model.
More recently, Saurel et al. [119] have proposed a 4-equation model, and Pelletier et al. [120] a 3-equation model. Emphasis is put on these last two formulations, because of their similarities to the models found in phase-field LBM.

Four equation model

The 4-equation model proposed in Saurel et al. [119] writes:

$$\partial_t \rho + \partial_\alpha \rho u_\alpha = 0 \tag{2.56}$$

$$\partial_t \alpha_1 \rho + \partial_\alpha \alpha_1 \rho u_\alpha = 0 \tag{2.57}$$

$$\partial_t \rho u_\alpha + \partial_\beta \left(\rho u_\alpha u_\beta + p \delta_{\alpha\beta}\right) = 0 \tag{2.58}$$

$$\partial_t \alpha_1 \rho e + \partial_\alpha \left(\alpha_1 \left(\rho e + p\right) u_\alpha\right) = 0 \tag{2.59}$$

The model assumes mechanical equilibrium ($\vec{u}_1 = \vec{u}_2 = \vec{u}$ and $p_1 = p_2 = p$) and thermal equilibrium ($e_1 = e_2 = e$). While Eqs. (2.56, 2.58, 2.59) respectively account for the conservation of the mixture density ρ, momentum $\rho\vec{u}$ and energy e, Eq. (2.57) accounts for the conservation of a given phase mass fraction, and plays the role of a phase field equation.
This formulation can be improved to account for surface tension and viscous effects, such as proposed

in Gaillard et al. [121] and Carmona's PhD [122]. Furthermore, mass transfer can also be accounted for through Eq.(2.57) as proposed in Chiapolino et al. [123] who studied the effect of evaporation for a coaxial supercritical jet as shown in Figure 2.6.
Another way to interpret the 4-equation model, is to consider that there is a colorless flow (which density is ρ and momentum is $\rho\vec{u}$) which is solved independently, while on the other hand, a phase field equation is solved. The fluid is then "colored" thanks to this phase field. Such an interpretation is similar to Level-Set [92] model's original philosophy.

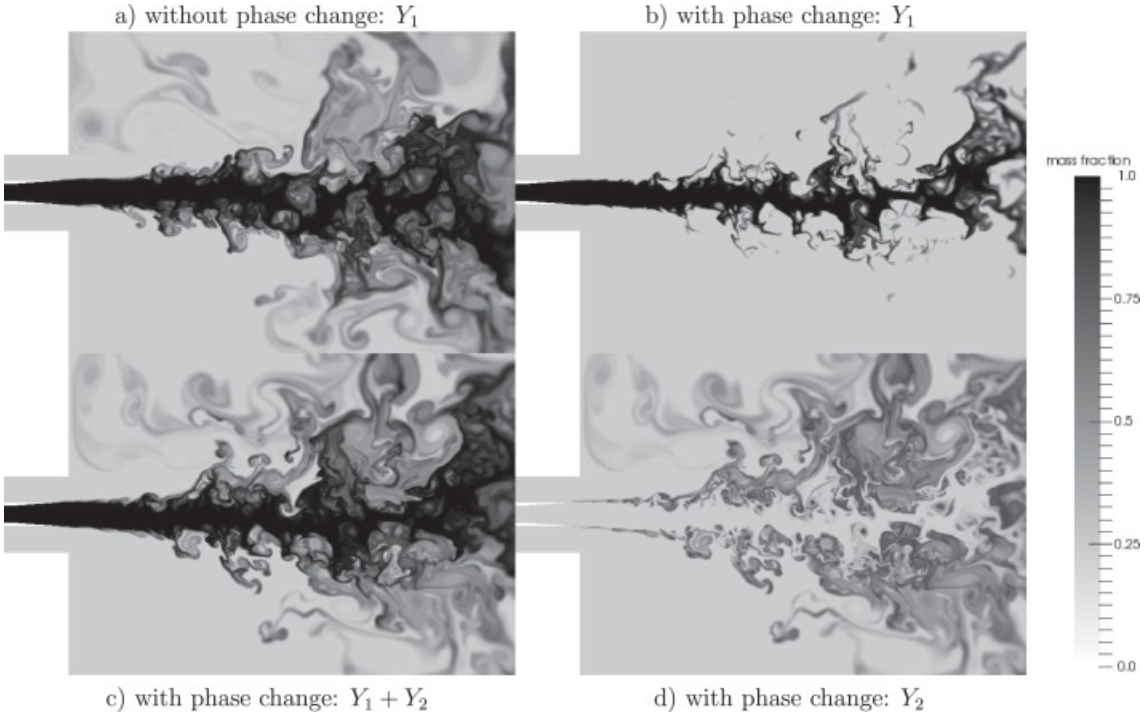


Figure 2.6. – Fragmentation of a liquid O_2 jet by a coaxial high-speed H_2 current. From Chiapolino et al. [123]

Three equations

The 4-equation multi-fluid model can even be reduced to a 3-equation model. Relying on Barret et al. [124], Pelleterier et al. [120] proposed Eqs. (2.60, 2.61, 2.62):

$$\partial_t \rho + \partial_\alpha \rho u_\alpha = 0 \tag{2.60}$$

$$\partial_t \rho u_\alpha + \partial_\beta \left(\rho u_\alpha u_\beta + p\delta_{\alpha\beta}\right) = 0 \tag{2.61}$$

$$\partial_t \rho e + \partial_\alpha \left(\left(\rho e + p\right) u_\alpha\right) = 0 \tag{2.62}$$

This model assumes mechanical and thermal equilibrium between phases, as well as equality of chemical potentials between phases. This set of equations is similar to a classical aerodynamical system. Similarly as in the 4-equations model, it can be improved to account for surface tension [125].
A detailed description of the strategies allowing to account for surface tension in diffuse interface methods is proposed in the following subsection.
Despite taking place in the free energy framework, the second gradient methods developed by Jamet et al. [126] can be classified as a three equation method. An improved second gradient method has

been recently proposed by Nayigizente et al. [127], allowing to increase the numerical stability of these technique. An illustration of a droplet splashing case using Nayigizente et al. [127] is proposed in Figure 2.7. In this figure, the numerical results are confronted to Ashgriz et al. [128] experimental results. This method has been used in the work of Laroche et al. [125].

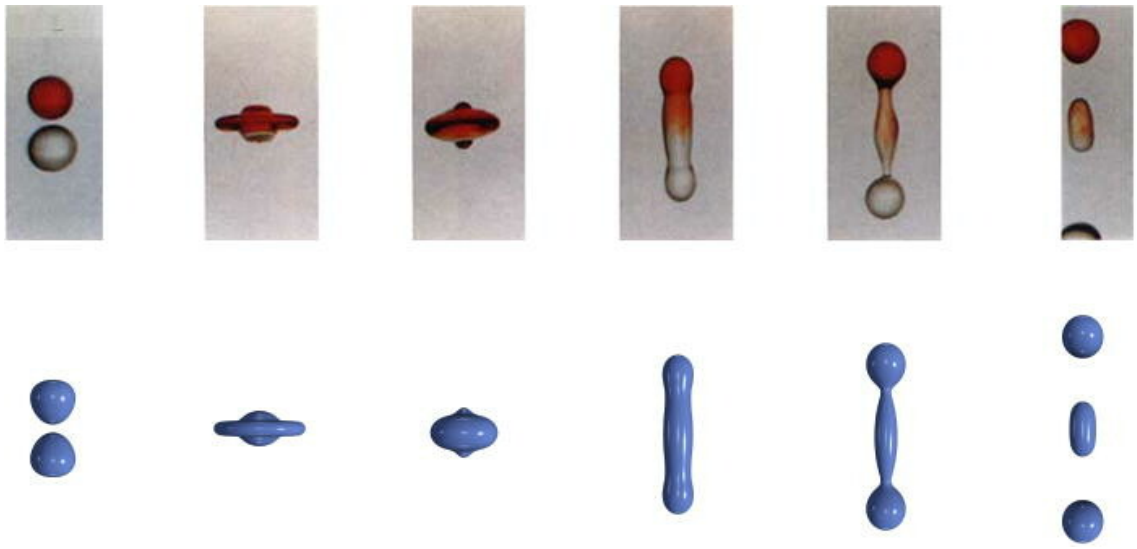


Figure 2.7. – 3-equation simulation of a bubble coaslescence and separation confronted to experimental results [128]. Figure from Nayigizente et al. [127]

Table 2.1. – Surface tension value for different fluids [132]

Fluids	Temperature (∘C)	$\sigma(kg.s^{-2})$
water-air	20	72.86
water-air	21.5	72.75
water-air	25	71.99
ethanol-air	20	22.39
kerosene-air [133]	20	23.0
water-oil	20	37.2
mercury-air	20	486.5

2.3. Surface tension

In the last two sections, methodologies allowing to numerically deal with a liquid-gas interface, either sharp or diffuse, have been presented. However, the modeling of surface tension has only been evoked. In pure phases, each particles are submitted to an isotropic attractive force between particles. For interfacial particles, an imbalance of these attractive forces occurs, leading to a surface force, referred as surface tension. A practical consequence of this force is the appearance of a pressure jump across the interface. Giving the nature of this force, the interface topology highly influences the pressure jump value. This pressure jump happens to be proportional to the local curvature as predicted by the Laplace Law [129]:

$$\Delta p = \sigma \left(\frac{1}{R_1} + \frac{1}{R_2} \right) \tag{2.63}$$

where Δp is the pressure jump, R_1 and R_2 the local curvatures of the interface and σ the surface tension coefficient. The coefficient σ is a function of temperature (it tends to slightly decrease when temperature rises [130][131]), but it mainly depends on the two considered fluids. Typical values are given Table 2.1.

Modeling surface tension is particularly challenging; in practice, this force appears only at the interface location. In most models, interface is not considered infinitely thin, making Laplace Law unusable in practice. To overcome this issue, surface tension must be modeled. In 1901 (at a time where international scientific papers were written in french), Korteweg [99] proposed a model to introduce surface tension in a Navier-Stokes system.

Based on symmetry considerations, and on van der Walls work [98], it was proposed that momentum conservation equation takes the following form:

$$\partial_t \left(\rho u_\alpha \right) + \partial_\beta \left(\rho u_\alpha u_\beta + p \delta_{\alpha\beta} + p^\sigma_{\alpha\beta} \right) = \partial_\beta \mathcal{T}_{\alpha\beta} \tag{2.64}$$

where p is the thermodynamic pressure, $\mathcal{T}_{\alpha\beta}$ is the stress tensor, and $p^\sigma_{\alpha\beta}$ a surface tension tensor. Korteweg also proposed that surface tension should take the following form:

$$p^\sigma_{\alpha\beta} = \left[\alpha_K \left(\partial_\alpha \rho \right)^2 - \gamma_K \partial^2_\alpha \rho \right] \delta_{\alpha\beta} + \beta_K \partial_\alpha \rho \partial_\beta \rho - \mu_K \partial^2_{\alpha\beta} \rho \tag{2.65}$$

α_K, β_K, γ_K and μ_K being constant coefficients. While in practice Korteweg model is not used, the idea that surface tension can be introduced through a stress tensor is of interest. An other way to interpret Korteweg's work is to model surface tension as a body force. In this case, the momentum conservation equation becomes:

$$\partial_t \rho u_\alpha + \partial_\beta \left(\rho u_\alpha u_\beta + p \delta_{\alpha\beta} \right) = \partial_\beta \mathcal{T}_{\alpha\beta} + F^\sigma_\alpha \tag{2.66}$$

with F^σ_α a surface tension body force which should respect $F^\sigma_\alpha = -\partial_\beta p^\sigma_{\alpha\beta}$ to account for surface tension. Based on these principles, two approaches are mainly found in the literature. They rely on totally

different theoretical frameworks, the first being based on a geometrical approach, while the second relies on the Van der Waals [98] free energy approach. These two approaches are detailed in the following. For the interested reader, less commonly used operators are discussed and proposed by Kim [134].

2.3.1. Geometrical approach

The geomretrical approach has been originally introduced by Brackbill et al. [135], and intends to model the Laplace pressure jump (Eq.(2.63)) on the basis on the interface topology. Brackbill et al. [135] proposed the so-called Continuum Surface Force (CSF), extended in Guyffier et al. [136] to a Continuous Surface Stress (CSS).

Continuous Surface Force

Brackbill et al. [135] proposed to rely on a continuous phase field function to estimate the interface normal, and consequently the interface curvature. Density is chosen as a phase field function in their original work, after a filtering operation on a bounded support h. This allows the introduction of a continuous density across the interface. The interface normal writes:

$$\vec{n} = \frac{\vec{\nabla}\phi}{|\vec{\nabla}\phi|} \tag{2.67}$$

where ϕ is the continuous phase field function. The volume force, equivalently body force, writes:

$$F_\alpha = \sigma\kappa n_\alpha \tag{2.68}$$

where σ is the surface tension coefficient, κ is the local curvature and $\vec{n}$ is the interface normal vector. Local curvature value can be determined through the interface normal vector through:

$$\kappa = -\left(\vec{\nabla}.\vec{n}\right) \tag{2.69}$$

The authors demonstrate that the volume force Eq. (2.68) tends to the actual surface tension as the transition region h (equivalent to the interface width) tends to zero. It should be noted that the phase field used to determined the fluid local composition can be different from the phase field used to determine interface normal vector.

Continuous Surface Stress

In the Continuous Surface Stress (CSS), surface tension is modeled through a surface tension tensor. The momentum conservation equation follows Eq.(2.66) and the body force satisfies:

$$F_\alpha^\sigma = -\partial_\beta\left(p_{\alpha\beta}^\sigma\right) \tag{2.70}$$

The pressure tensor $p_{\alpha\beta}^\sigma$ is chosen so that:

$$\partial_\beta p_{\alpha\beta}^\sigma = \sigma\kappa\delta_{int}n_\alpha \tag{2.71}$$

with δ_{int} being a function equal to 1 at the interface location and equal to 0 otherwise. The pressure tensor can be formulated:

$$p_{\alpha\beta}^\sigma = -\sigma\left(\delta_{\alpha\beta} - n_\alpha n_\beta\right)\delta_{int} \tag{2.72}$$

The function locating the interface δ_{int} is given by:

$$\delta_{int} = \frac{|\vec{\nabla}\phi|}{2} \tag{2.73}$$

where ϕ is a continuous phase field function across the interface. Similarly as in Brackbill et al. [135], the interface normal vector $\vec{n}$ is given by Eq. (2.67). Injecting $\vec{n}$ and δ_{int} definitions in Eq. (2.72), Gueyffier et al. [136] surface tension tensor writes:

$$p^{\sigma}_{\alpha\beta} = -\frac{\sigma}{2|\vec{\nabla}\phi|}\left[-\left(\partial_\gamma\phi\right)^2\delta_{\alpha\beta} + \partial_\alpha\phi\partial_\beta\phi\right] \tag{2.74}$$

Similarly as for Brackbill et al. [135] body force formulation, Eq. (2.74) can be generalized to any continuous and derivable phase field ϕ.

2.3.2. Free Energy approach

The second approach allowing to introduce surface tension in a system relies on Van der Walls [98] free energy principle. As detailed in Section 2.2.1, the idea introduced by Van der Walls is that the interface implies a surface additional free energy. The massic free energy f_{HE} is reminded, it writes:

$$f_{FE} = f_{H,0} + \lambda_\phi\left(\vec{\nabla}\phi\right)^2 \tag{2.75}$$

where $f_{H,0}$ is the pure fluid free energy component, λ surface tension coefficient, and ϕ a phase field function. As shown in Antanovski [108], or thoroughly detailed in the second gradient theory by Jamet [137] and more recently in Nayigizente's PhD thesis [104], a surface tension tensor can be deduced from the free energy. The momentum conservation can be formulated:

$$\partial_t\left(\rho u_\alpha\right) + \partial_\beta\left(\rho u_\alpha u_\beta + p\delta_{\alpha\beta} + p^{\sigma}_{\alpha\beta}\right) = \partial_\beta\mathcal{T}_{\alpha\beta} \tag{2.76}$$

with:

$$p = \phi\frac{\partial f_{H,0}}{\partial\phi} \tag{2.77}$$

and

$$p^{\sigma}_{\alpha\beta} = \lambda_\phi\left(\left[\phi\partial^2_\gamma\phi + \frac{1}{2}\left(\partial_\gamma\phi\right)^2\right]\delta_{\alpha\beta} - \partial_\alpha\phi\partial_\beta\phi\right) \tag{2.78}$$

The present formulation is referred to as free energy surface tension tensor form.

Potential formulation

A potential μ_ϕ can be derived from the free energy f_{HE}, so that:

$$\mu_\phi = \partial_\phi f_{H,0} - \partial_\alpha\left(\lambda_\phi\partial_\alpha\phi\right) \tag{2.79}$$

this potential allows to write:

$$\partial_\beta\left(p\delta_{\alpha\beta}p^{\sigma}_{\alpha\beta}\right) = \phi\partial_\alpha\mu_\phi \tag{2.80}$$

It means that from the free tensor formulation, a body force formulation can be deduced:

$$F^{\sigma}_{\alpha} = \phi\partial_\alpha\left(\partial^2_\gamma\phi\right) \tag{2.81}$$

This formulation is referred as the free energy potential formulation. From a physical point of a view, the free energy surface tension tensor and potential formulations are strictly equivalent. However, differences may appear from a numerical point of view. The free energy potential formulation is a popular operator, particularly among the HCZ community [30][138][139], presented hereafter in Section 3.5.

Relation between λ and the surface tension coefficient σ

An important note is that in Gueyffier's [136] and Brackbill's [135] operators, the coefficient σ in their operators corresponds to the desired surface tension coefficient given in Laplace Law Eq.(2.63). The present coefficient λ_ϕ (Eq. (2.75)) is not directly proportional to the surface tension coefficient, since in the free energy framework, the homogeneous component of surface tension in the diffuse interface also contributes to the pressure jump. As a consequence, surface tension σ and λ_ϕ are through:

$$\sigma = \int_{\phi_1}^{\phi_2} \lambda \partial_x \phi d\phi \tag{2.82}$$

with ϕ_1 and ϕ_2 phase field values in pure phase 1 and 2 respectively.

Chapter 3

Multiphase LBM

Overview

3.1. General Introduction **50**
3.1.1. Surface Tension 50
3.1.2. Numerical scheme for the spatial derivative operator 52
3.1.3. Non-perfect Equation Of State 54
3.1.4. Viscosity 57
3.2. Rothman-Keller Method **59**
3.2.1. Algorithm presentation 59
3.2.2. Historical review 61
3.3. Free energy methods **67**
3.3.1. Introduction 67
3.3.2. Discussion around the phase field equation 69
3.3.3. Historical review 70
3.4. Pseudo Potential **71**
3.4.1. Macroscopic equations 71
3.4.2. Numerical Scheme 72
3.4.3. Historical review 73
3.5. HCZ **76**
3.5.1. Macroscopic equations 76
3.5.2. Numerical Scheme 77
3.5.3. Historical review 79

3.1. General Introduction

Multiphase flows and Lattice Boltzmann methods have a particularly tight relationship which appeared very early, as soon as Lattice Gas Automata was proposed. In 1988, Rothmann and Keller [22] proposed a method that could simulate two phases, that was generalised to Lattice Boltzmann Method few years after [23]. As pointed out in the previous chapter two strategies stand out of the crowd to simulate multiphase flows, the surface tracking methods or the diffuse interface methods. Few attempts were made to apply surface tracking principles in a lattice Boltzmann framework [140–142] while most LBM multiphase studies consider diffuse interface methods approaches. The different multiphase methods for LBM are usually divided into four famillies: Rothmann-Keller methods [22] (also called Color Gradient methods, or more rarely Chromodynamic methods), pseudo-potential method [25, 26](or Shan and Chen method), free energy methods [27, 28] and HCZ methods [29]. Other methods were proposed among the literature such as the ones proposed by He & Luo [143] or Nourgaliev [144] but they are not detailed here. A thorough review of the Lattice Boltzmann Methods for multiphase flows can be found in [145, 146]. Note that some numerical approaches of interest for multiphase flows have been originally intended for porous flows, which share numerous physical similarities. A review of Lattice Boltzmann Method and porous flows is available [40].
Before the description of all these specific methods for multiphase LBM, the description of few common issues is provided in this first section. The numerical introduction of surface tension in the LBM framework, the spatial derivative operator, the introduction of non-perfect equation of state and of viscosity are detailled hereafter.

3.1.1. Surface Tension

As discussed in the Chapter 2, one of the fundamental feature of multiphase flow is the presence of surface tension. As discussed in Section 2.3, several ways to model surface tension are possible in any numerical formalism. From the mathematical point of view, surface tension can take two forms, it can rather be seen as a stress tensor as in the work of Gueyffier [136] but it can also be seen as a body force as in Brackbill [135]. The impact of these two formalisms has been recently discussed by Zhang et al. [147]. In the following, only the numerical aspect is discussed, then it will be assumed for the sake of generality that surface tension takes the following form:

$$F_\alpha^\sigma = \partial_\beta p_{\alpha\beta}^\sigma \tag{3.1}$$

as it is the most general form.

Body force scheme

A dedicated section on the inclusion of a body in LBM is proposed in section 4.2. Surface tension can be included in the momentum conservation equation through a source term using Guo's scheme [148] or He's scheme [53], detailed hereafter in Section 4.2. In the case of the body force, the situation is rather simple since the process has already been discussed in Section 4.2, then a source term is included using Guo's scheme or He's scheme. It must be noted that even though this solution is simpler, it is numerically more intensive since in all the body-force surface tension schemes involve a 2^{nd} order spatial derivative. For instance, the body force proposed by Brackbill et al. [135] is given by:

$$F_\alpha^\sigma = \sigma \partial_\alpha \left[\frac{\partial_\gamma \phi}{|\vec{\nabla}\phi|} \right] \tag{3.2}$$

with ϕ the order parameter. In practice, a second order spatial derivative term cannot be calculated directly without implying high order scheme, lowering the scalability of the algorithm. In practice, two successive first order spatial derivative must be calculated, also lowering the scalability of the algorithm, and then the numerical efficiency.

Tensor scheme

To circumvent this numerical efficiency issue the use of a tensor scheme can be preferred, i.e. expressing the surface tension as $P^{\sigma}_{\alpha\beta}$. Note that LBM allow an easy implementation of tensor terms. There are two main ways to do so. First, we remind that the conservation equation for the first moment of the distribution function writes:

$$\partial_t \rho u_\alpha + \partial_\beta \left[m^{eq}_{\alpha\beta} + m^{eq}_0 \delta_{\alpha\beta} + (\tau_{\alpha\beta} - 1/2) S_{\alpha\beta} \right] = O(\Delta t) \tag{3.3}$$

with $S_{\alpha\beta}$ the 2^{nd} order Hermites moments of the source term, i.e. $S_{\alpha\beta} = \sum_i H_{\alpha\beta,i} S_i$, and m^{eq}_* the moments of the equilibrium function, i.e. $\sum_i H_{*,i} f^{eq}_i$, and $\tau_{\alpha\beta}$ the relaxation times associated to the moments of $H_{\alpha\beta}$. There are two ways to include a tensor to Eq. (3.3). The first one consists in adding a source term which 2^{nd} order moments are given by:

$$S^{\sigma}_{\alpha\beta} = \frac{p^{\sigma}_{\alpha\beta}}{\tau_{\alpha\beta} - 1/2} \tag{3.4}$$

A source term that fulfills the previous condition is:

$$S_i = \frac{p^{\sigma}_{\alpha\beta}}{\tau_{\alpha\beta} - 1/2} \frac{H_{\alpha\beta,i}}{2c_s^4} \tag{3.5}$$

This source term is sometimes interpreted as a "second collision term", that takes into account intermolecular interaction and that originates surface-tension. This strategy is used for example in the colour gradient community, for example by Gustensen [23].

Equilibrium scheme

The other way to add a tensor is to modify the equilibrium function and to add a term which 2^{nd} order moment is equal to the desired tensor. For instance:

$$f^{eq}_i = \rho w_i \left(H_{0,i} + \frac{H_{\alpha,i} u_\alpha}{c_s^2} + \frac{u_\alpha u_\beta H_{\alpha\beta,i}}{2c_s^4} \right) + p^{\sigma}_{\alpha\beta} \frac{H_{\alpha\beta,i}}{2c_s^4} \tag{3.6}$$

This strategy is for example considered in the original free energy method proposed in Swift et al. [27, 28]. It must be noted that equilibrium scheme and tensor scheme are mathematically strictly equivalent, the only difference being the fact that in the second approach, the relaxation time is involved, which might increase the complexity of the source term expression in a MRT framework when dealing with different bulk and shear viscosity, as shown in Lafarge et al. [149].

The advantage of the tensor and the equilibrium scheme is that it necessitates only a first order spatial derivative computation, contrarily to the body force approach that needs a second order spatial derivative. The associated drawback of these methods is however the appearance of a spurious term at the order Δt in the momentum conservation equation. Considering a tensor scheme, the equivalent macroscopic equation developed at the order Δt^2 writes:

$$\partial_t \rho u_\alpha + \partial_\beta \left(\rho u_\alpha u_\beta + \rho c_s^2 \delta_{\alpha\beta} + p^{\sigma}_{\alpha\beta} \right) = \Delta t \partial_\beta \left[\rho c_s^2 (\tau - 1/2) \left(\partial_\alpha u_\beta + \partial_\beta u_\alpha \right) + E r^{\sigma}_{\alpha\beta} \right] + O(\Delta t^2) \tag{3.7}$$

with the spurious error term given by:

$$E r^{\sigma}_{\alpha\beta} = (\tau_{\alpha\beta} - 1/2) \left(u_\alpha \partial_\gamma p^{\sigma}_{\beta\gamma} + u_\beta \partial_\gamma p^{\sigma}_{\alpha\gamma} \right) \tag{3.8}$$

In practice, surface tension force being relatively low in absolute value, the resultant error term is relatively low, and then is often neglected. Note that spurious currents due to a similar error will be observed when using a non-perfect EoS, as later detailed in Section 3.1.3.

Schemes comparison

Zhang et al. [147] have shown that the choice of surface tension model (among free energy, Brackbill et al. [135], Gueyffier et al. [136], etc...) has more influence on numerical stability than the choice of the scheme introducing surface tension.

3.1.2. Numerical scheme for the spatial derivative operator

At least one spatial derivative computation is required in all the schemes (two concerning the body force one) and is a key element in the method. This point is discussed here. A first approach to compute a spatial derivative might be use of a simple finite difference scheme, for instance in a 2D framework :

$$\begin{aligned} \partial_x c_{|(x,y)} &= \frac{c(x+\Delta x, y) - c(x-\Delta x, y)}{2\Delta x} \\ \partial_y c_{|(x,y)} &= \frac{c(x, y+\Delta x) - c(x, y-\Delta x)}{2\Delta x} \end{aligned} \tag{3.9}$$

By calculating surface tension with such a scheme, topological errors are however observed even for simple cases. Leclaire et al. [150] pointed out that a droplet in a quiescent atmosphere doesn't converge toward a spherical shape if the gradient calculation scheme is not wisely chosen.

Leclaire's discretization scheme

The scheme traditionally used by the Color Gradient community was proposed by Gunstensen et al.[23] and was given by:

$$\partial_\alpha c_{|(x,y)} = \sum_{i=1}^{8} \frac{\xi_{\alpha,i} c(x+\xi_{x,i}\Delta t, y+\xi_{y,i}\Delta t))}{18 c_s^2 \Delta t} \tag{3.10}$$

Leclaire et al. [150] proposed to use the weighting coefficients w_i used to define the lattices. For instance in a D_2Q_9 scheme, the spatial gradient scheme is given by:

$$\partial_\alpha c_{|(x,y)} = \sum_{i=1}^{8} \frac{w_i \xi_{\alpha,i} c(x+\xi_{x,i}\Delta t, y+\xi_{y,i}\Delta t))}{c_s^2 \Delta t} \tag{3.11}$$

For each discretization schemes, a given level of isotropy can be defined. Gradient schemes were introduced in increasing order, meaning scheme introduced by Eq. (3.9) is less isotropic than gradient scheme introduced by Eq. (3.10) which is itself less isotropic than the scheme introduced by Eq. (3.11). For the sake of clarity, similarly as Leclaire et al. [150] it is said that these scheme have degrees of isotropy of 0, 1 and 2. From Leclaire [150], operator of degree of isotropy 3 and 4 can also be introduced. The operator of degree of isotropy 3 is defined by:

$$\partial_\alpha c_{|(x,y)} = \sum_{i=1}^{13} \frac{w_i^{(D2Q13)} \xi_{\alpha,i} c(x+\xi_{x,i}\Delta t, y+\xi_{y,i}\Delta t))}{c_s^2 \Delta t} \tag{3.12}$$

where $w_i^{(D2Q13)}$ are the weighting coefficients of the D_2Q_{13} velocity set. Similarly, the 4^{th} order of isotropic gradient operator is defined by:

$$\partial_\alpha c_{|(x,y)} = \sum_{i=1}^{25} \frac{w_i^{(D2Q25)} \xi_{\alpha,i} c(x+\xi_{x,i}\Delta t, y+\xi_{y,i}\Delta t))}{c_s^2 \Delta t} \tag{3.13}$$

where $w_i^{(D2Q25)}$ are the weighting coefficients of the D_2Q_{25} velocity set. Note that usually there are only nine microscopic velocities, here ξ_i for $i > 8$ corresponds to a D_2Q_{25} microscopic velocities.

Eq	(3.10)	(3.11)	(3.10)
Degree of isotropy	1	2	4
Maximum velocity $(m.s^{-1})$	$2.19 * 10^{-2}$	$5.94 * 10^{-4}$	$6.70 * 10^{-5}$

Table 3.1. – Maximum velocity corresponding to the spurious currents in the interface as a function of the degree of isotropy

The effect of the isotropy of the spatial gradient scheme can be evidenced on the static droplet test-case, in which a droplet of phase 1 is initialized with a square shape in a quiescient atmosphere of phase 2. Both phases have the same density. The expected final solution is a spherical droplet of phase 1. The solver used is the one that will be presented in Chapter 5, only the discretization operator is modified in order to observe the effect of the degree of isotropy. The different topology obtained after 10.000 iterations can be observed Figure 3.1. It comes clearly that when the degree of isotropy

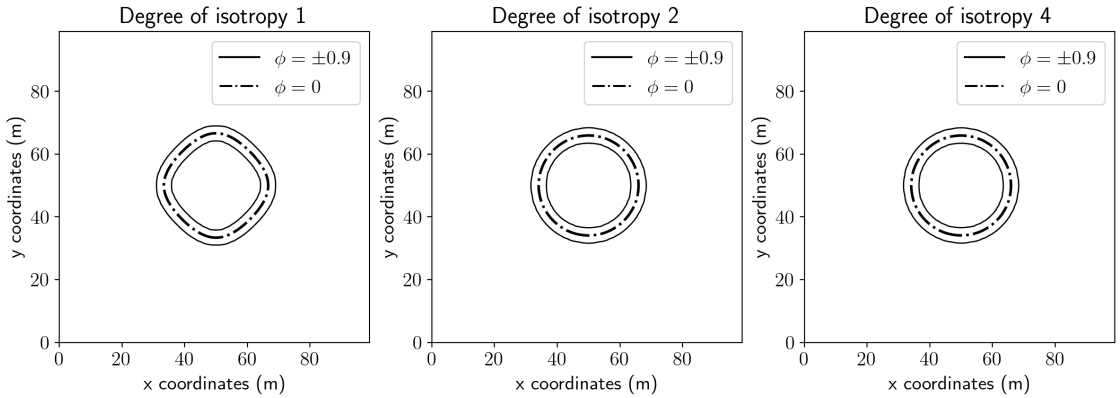


Figure 3.1. – Topology obtained for the squared shape droplet test after 10.000 iterations for different degree of isotropy. Degree of isotropy 1 (left), degree of isotropy 2 (center) Degree of isotropy 4 (right)

is too low, the solver cannot simulate accurately a still bubble. On the other side, it appears that from the only topological point of view, increasing the degree of isotropy can be useless as the degree of isotropy 2 already proposes a consistent shape.
The scheme used for calculating surface tension is not only interesting from the topological point of view. As pointed out by Shan [151] in a pseudo-potential framework, the discretization scheme used to approximate the spatial operator also has an impact on the spurious current appearing at the interface.
As in most diffuse interface methods, spurious currents and spurious vorticity appears inside the interface. In the static droplet test-case presented here, no velocity is expected once the droplet has reached a steady state. In practice, spurious currents and vorticity however appear, as shown in Figure 3.2. The velocity maxima are summarized in Table 3.1 for the 3 considered cases, which evidences a direct impact of the degree of isotropy on the resulting spurious currents. We can see that to pass from the degree of isotropy 1 to the degree of isotropy 2 reduces the spurious currents by two order of magnitudes.

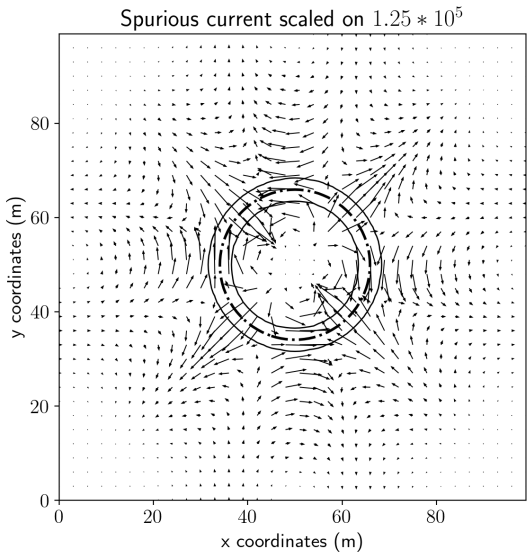


Figure 3.2. – Spurious current in the interface for a degree of isotropy 2

Lee's discretization scheme

This discussion about the discretization has also been carried out by the free energy community. In particular, Lee and Lin [152] and then Lee and Fisher [138] proposed a number of operators. The first one is the biased first derivative:

$$\partial_\alpha c^B_{(x,y)} = \sum_i \frac{w_i \xi_{\alpha,i}[-c(x+2\xi_{x,i}\Delta t, y+2\xi_{y,i}\Delta t) + 4c(x+\xi_{x,i}\Delta t, y+\xi_{y,i}\Delta t) - 3c(x,y)]}{2c_s^2 \Delta t} \tag{3.14}$$

The second one is the central first derivative (that is equivalent to the one proposed by Leclaire et al. [150]) Eq. (3.11):

$$\partial_\alpha c^C_{(x,y)} = \sum_i \frac{w_i \xi_{\alpha,i}[c(x+\xi_{x,i}\Delta t, y+\xi_{y,i}\Delta t) - c(x-\xi_{x,i}\Delta t, y-\xi_{y,i}\Delta t)]}{2c_s^2 \Delta t} \tag{3.15}$$

Lee and Fisher [138] proposed a mixed operator:

$$\partial^M_\alpha c = \frac{\partial^B_\alpha c + \partial^C_\alpha c}{2} \tag{3.16}$$

They showed that the use of this mixed operator coupled with a potential approach and a force term numerical scheme allowed to obtain spurious currents as low as 10^{-15} while a similar scheme but discretized with a forward difference scheme leaded to spurious current of 10^{-4} (The units are not specified in their work). This operator is widely used in the literature for its property to reduce spurious current, despite the fact it involves neighbours as far as two spatial steps.

3.1.3. Non-perfect Equation Of State

However, in multiphase flows, a dedicated equation of state must be accounted for, at least for the liquid phase. As discussed in Section 1.3, in the classic LBM algorithm, the EOS doesn't need to be set since a term equal to $\partial_\beta \rho c_s^2$ is implied by the moment cascade.

Body force scheme

As a term in ρc_s^2 is already implied by LBM, a natural way to impose a pressure field equal to p consists in imposing a suppressors term equal to $\partial_\beta \left(p - \rho c_s^2\right)$ in Navier-Stokes momentum conservation equation. Then the discussion becomes similar to the one proposed earlier about surface tension. The first solution, as proposed by Luo [153] consists in applying a force term equal to:

$$F_\alpha = \partial_\alpha \left(p - \rho c_s^2\right) \tag{3.17}$$

Pressure scheme

The second way originally proposed by Swift et al. [27] in a free energy framework consists in modifying the second moments of the equilibrium function to ensure that:

$$\sum_i H_{\alpha\beta,i} f_i^{eq} = \rho u_\alpha u_\beta + (p - \rho c_s^2)\delta_{\alpha\beta} \tag{3.18}$$

To do so, the equilibrium function is modified to:

$$f_i^{eq} = \rho w_i \left(1 + \frac{\xi_{\alpha,i} u_\alpha}{c_s^2} + u_\alpha u_\beta \frac{\xi_{\alpha,i}\xi_{\beta,i} - c_s^2\delta_{\alpha\beta}}{2c_s^4}\right) + (p - \rho c_s^2)\frac{H_{\gamma\gamma,i}}{2c_s^4} \tag{3.19}$$

This scheme is refereed to as the "pressure scheme". Similarly as for surface tension, the scheme consisting in modifying the pressure through the equilibrium induces a spurious term in the macroscopic equation, as shown in Holdych et al. [154]. They used a Chapman-Enskog method leading to:

$$\partial_t \rho u_\alpha + \partial_\beta \left[\rho u_\alpha u_\beta + p\delta_{\alpha\beta}\right] = \partial_\beta \Delta t(\tau - 1/2) \left[\rho c_s^2 \left(\partial_\alpha u_\beta + \partial_\beta u_\alpha\right) - \underbrace{u_\alpha \partial_\beta \left(p - \rho c_s^2\right) - u_\beta \partial_\alpha \left(p - \rho c_s^2\right)}_{spurious\ term}\right] \tag{3.20}$$

This spurious term is responsible for lack of numerical stability, as well as spurious currents. Wagner et al. [155] discussed rather the pressure scheme should be prefered to the body force scheme. It was shown that the body force scheme should be preferred as it produces the less spurious currents.
Pooley et al. [156] proposed an improved form of the pressure scheme which produces less spurious current that the original one. In this new scheme, the equilibrium function is given by:

$$\begin{gathered} f_i^{eq} = w_i \left(\frac{p}{c_s^2} + \rho \left[\frac{\xi_{\alpha,i} u_\alpha}{c_s^2} + u_\alpha u_\beta \frac{\xi_{\alpha,i}\xi_{\beta,i} - c_s^2\delta_{\alpha\beta}}{2c_s^4}\right]\right) \quad i \in 1,..,8 \\ f_0^{eq} = \rho - \sum_{i=1}^{8} f_i^{eq} \end{gathered} \tag{3.21}$$

This formulation has been largely used among the literature particularly by the free energy community [35, 54, 157]. We propose here a slightly more convenient notation of the Pooley's equilibrium function, since it fits in one line.

$$f_i^{eq} = \rho w_i \left(1 + \frac{u_\alpha \xi_\alpha}{c_s^2} + u_\alpha u_\beta \frac{\xi_{\alpha,i}\xi_{\beta,i} - c_s^2\delta_{\alpha\beta}}{2c_s^4}\right) + (p - \rho c_s^2)\frac{w_i - \delta_{i0}}{c_s^2} \tag{3.22}$$

Note that mathematically both formulation are strictly equivalent.
Che-SiDik and Tanahasi [158] proposed a correction to the spurious term appearing in the momentum equation when using the pressure scheme, and applied in a multiphase framework by Leclaire et al. [159] through a correction term. Another solution is to add a third order term in the equilibrium function as proposed by Li et al. [160] in a compressible framework, then transposed into a multiphase framework by Wen et al. [161]. A deeper discussion on the correction term to modify the pressure is proposed in Chapter 5.

He's pressure based scheme

Two other approaches to modify the equation of state have been proposed in the literature, and rely on a pressure-based formulation. The idea is to modify the 0^{th} moment of the distribution function, so that:

$$\sum_i f_i = p/c_s^2 \tag{3.23}$$

This scheme proposed in He et al. [29] usually refereed to as the HCZ model, from the name of the authors (He, Chen, Zhang), is currently one of the most stable in the literature.
This methods starts from the discrete Boltzmann equation that is reformulated here:

$$D_t f_i = \Omega_i - \frac{(\xi_\alpha - u_\alpha)\,\partial_\alpha(p - \rho c_s^2)}{\rho c_s^2} f_i^{eq} \tag{3.24}$$

where the microscopic particular derivative D_t^* defined as $D_t* = \partial_t * + \xi_\alpha \partial_\alpha *$. In this method, a body force is introduced by assuming that $\dfrac{\partial f}{\partial \xi_\alpha} \approx \dfrac{\partial f^{eq}}{\partial \xi_\alpha} = (\xi_\alpha - u_\alpha) f_i^{eq}$. In addition, the body force is introduced in Eq. (3.25) through a term proportional to $\partial_\alpha(p - \rho c_s^2)$ in the right-hand side, leading to:

$$\partial_t f_i + \xi_\alpha \partial_\alpha f_i = D_t f_i = \Omega_i - \frac{(\xi_\alpha - u_\alpha)\,\partial_\alpha(p - \rho c_s^2)}{\rho c_s^2} f_i^{eq} \tag{3.25}$$

A new distribution function g_i is introduced, defined as:

$$g_i = f_i c_s^2 + (p - \rho c_s^2) w_i \tag{3.26}$$

It comes that the 0^{th} moment of the g_i function is given by: $\sum_i g_i = p/c_s^2$. By introducing g_i into the Boltzmann equation (3.25), the conservation equation respected by g_i is given by:

$$\partial_t g_i + \xi_{\alpha,i} \partial_\alpha g_i - \partial_t \left(p - \rho c_s^2\right) - \xi_{\alpha,i} \partial_\alpha (p - \rho c_s^2) = c_s^2 D_t f_i \tag{3.27}$$

This equation, Eq. (3.27) cannot be used as a scheme because of the temporal derivative. The flow is assumed to be incompressible. The continuity equation $\partial_\alpha u_\alpha = 0$ leads to:

$$\partial_t \rho = -u_\alpha \partial_\alpha \rho \tag{3.28}$$

$$\partial_t p = -u_\alpha \partial_\alpha p \tag{3.29}$$

Integrating those previous equations into (3.27), it comes:

$$D_t g_i = -\frac{g_i - g_i^{eq}}{\tau} + (\xi_\alpha - u_\alpha) \left[\frac{f_i^{eq}}{\rho} F_s - \left(\frac{f_i^{eq}}{\rho} - w_i \right) \partial_\alpha (p - \rho c_s^2) \right] \tag{3.30}$$

F_s being a body force introducing surface tension, g_i^{eq} being the equilibrium function of g_i defined by:

$$g_i^{eq} = c_s^2 f_i^{eq} + (p - \rho c_s^2) w_i = w_i \left[p + \rho c_s^2 \left(\frac{\xi_{\alpha,i} u_\alpha}{c_s^2} + u_\alpha u_\beta \frac{\xi_{\alpha,i}\xi_{\beta,i} - c_s^2 \delta_{\alpha\beta}}{2 c_s^4} \right) \right] \tag{3.31}$$

This formulation is very close to the one proposed by Pooley et al. [156] in the pressure scheme framework (3.21). This scheme implies several changes in the macroscopic equations. In particular, it can be shown, through a Chapman-Enskog method, that the equivalent macroscopic equation for g_i^{eq} 0^{th} order becomes:

$$\frac{1}{\rho c_s^2} \partial_t p + \partial_\alpha u_\alpha = 0 \tag{3.32}$$

In practice, the time derivative of the pressure stays small, which means that the incompressible hypothesis made to design this scheme is pretty much respected. This scheme takes a particular place among the Lattice Boltzmann Method because it alters a fundamental property of LBM being compressibility. Using this scheme, the flow becomes (almost) incompressible.

Farag's pressure based

The last way to change the Equation of State in Lattice Boltzmann method is the pressure based method proposed by Farag et al. [162] in a compressible framework. It is a pressure-based model coupled with a predictor-corrector approach. Similarly as in the approach of He et al. [29] the equilibrium function is given by:

$$f_i^{eq} = w_i \left[p/c_s^2 + \rho \left(\frac{\xi_{\alpha,i} u_\alpha}{c_s^2} + u_\alpha u_\beta \frac{\xi_{\alpha,i}\xi_{\beta,i} - c_s^2 \delta_{\alpha\beta}}{2c_s^4} \right) \right] \tag{3.33}$$

Similarly with the HCZ scheme the 0^{th} moment of the f_i population is given by:

$$\sum_i f_i = p/c_s^2 \tag{3.34}$$

It can be shown that the macroscopic equation obtained for this 0^{th} moment is given by:

$$\partial_t \frac{p}{c_s^2} + \partial_\alpha \rho u_\alpha = O(\Delta t^2) \tag{3.35}$$

In order to respect the continuity equation, the density field is obtained through the following equation:

$$\rho(\vec{x}, t + \Delta t) = \sum_i f_i(\vec{x}, t + \Delta t) + \rho(\vec{x}, t) - \frac{p(\vec{x}, t)}{c_s^2} \tag{3.36}$$

It has been recently shown [163] that this scheme is equivalent to the one proposed by Pooley et al. [156].

About the CFL condition

On a side note, the CFL condition that is often associated with LBM itself is given by:

$$\frac{\Delta x}{\Delta t} = \sqrt{3} c_s \tag{3.37}$$

with c_s the speed of sound. It has been discussed in Section 1.3, that this CFL condition allows to directly include the pressure in the numerical scheme, saving some computational effort and improving the numerical stability. In a multiphase framework, the pressure field is no more equal to ρc_s^2, therefore the present CFL condition doesn't need to be imposed anymore which means that the CFL number can be freely imposed.

3.1.4. Viscosity

To simulate two different fluids, it is necessary to be able to simulate two different viscosities. In the present framework, the properties of the fluid have to vary continuously from the value in one phase to the value in the other phase. In practice, this means that the viscosity field has to be a function of the phase field. In the Lattice Boltzmann framework, the viscosity is imposed by the value of the relaxation time. In the classical LBM framework [53], viscosity and relaxation time are related through:

$$\tau = \frac{\nu}{\Delta t c_s^2} + 1/2 \tag{3.38}$$

To impose a viscosity that is a function of space, the relaxation time also becomes a function of space. The schemes allowing a variable viscosity are detailed in this subsection.
One of the first schemes in the Lattice Boltzmann framework was introduced by Grunau et al. [164]

in the Rothmann-Keller framework. In this model, the viscosity is a function of the phase field $\phi = \frac{\rho_1 - \rho_2}{\rho} = Y_1 - Y_2$

$$\nu = \begin{cases} \nu_1 & \phi > \epsilon \\ D_0 + D_1\phi + D_2\phi^2 & \epsilon \geqslant \phi > 0 \\ D_0 + D_3\phi + D_4\phi^2 & 0 \geqslant \phi > -\epsilon \\ \nu_2 & \phi < -\epsilon \end{cases} \tag{3.39}$$

Where ϵ is a trigger value, chosen by the user, which must be chosen close to 1. This value should be chosen in accordance with the interface thickness, which depends on the considered model. D_0, D_1, D_2, D_3 and D_4 are constants that are set in order to guaranty the continuity of ν and of its partial derivative $\frac{\partial \nu}{\partial \phi}$.
In practice, this model is barely used nowadays since it's pretty complex and that the interface thickness is not known a priori, making the variable ϵ hard to set wisely. For this reason, Tolke et al. [165] proposed to make ν directly proportional to the phase field:

$$\nu = \frac{\nu_1 + \nu_2}{2} + \frac{\nu_1 - \nu_2}{2}\phi \tag{3.40}$$

Another operator was proposed later by Leclaire et al. [166] who showed the following operator to be more stable:

$$\frac{1}{\nu} = \frac{1 + \phi}{2\nu_1} + \frac{1 - \phi}{2\nu_2} \tag{3.41}$$

3.2. Rothman-Keller Method

The first algorithm that was ever proposed to simulate multiphase flows in a Lattice Boltzmann framework is the colour gradient method or RK (from Rothmann and Keller) method. It was proposed by Rothman and Keller [22] in a LGA framework. Behind the name "Color Gradient Method" coexist a large number of methods, that evolved along time. Since the algorithm has changed through time, the recent formalism have little in common with the first ones, and it becomes difficult to precisely define what precisely characterises this approach. In practice, the words Color Gradient refer to a community of methods rather than a precise one. Note that practises among this same community may differ from a research team to another. Anyway, for the sake of understanding, a single formalism which sounds relevant in this work is considered here: the color gradient algorithm proposed in Leclaire et al. [159] in 2013.

3.2.1. Algorithm presentation

This model is a two phase model, where each phase is described by a color (blue or red). The system is described by a mixture density ρ equals to the sum of the two phase densities, i.e. $\rho = \rho^B + \rho^C$, the momentum of the two fluids ρu_α (noting that the two fluids velocities are supposed to be at equilibrium, then $\vec{u_1} = \vec{u_2}$), and the density of the coloured populations $\rho^{(R)}$ and $\rho^{(B)}$.

Equivalent macroscopic equation

Concerning the equivalent macroscopic equations, the color gradient belongs to the phase fields methods. The density and the momentum are solution of the following equations:

$$\partial_t \rho + \partial_\alpha \rho u_\alpha = 0 \tag{3.42}$$

$$\partial_t \rho u_\alpha + \partial_\beta \left(\rho u_\alpha u_\beta + p\delta_{\alpha\beta} + p^\sigma_{\alpha\beta} \right) = \Delta t \partial_\beta \left((\tau - 1/2)\rho c_s^2 \left(\partial_\alpha u_\beta + \partial_\beta u_\alpha \right) \right) \tag{3.43}$$

In the momentum conservation equation, the surface tension term is modeled using the Gueyffier et al. model [136]. As a reminder, this operator is given by:

$$p^\sigma_{\alpha\beta} = \sigma \left[\delta_{\alpha\beta} - n_\alpha n_\beta \right] \delta_{interface} \tag{3.44}$$

with $\vec{n} = \dfrac{\vec{C}}{|\vec{C}|}$, $\delta_{interface} = \dfrac{|\vec{C}|}{2}$. $\vec{C}$ being the so-called colour gradient that gives its name to the method. This vector aims at locating the interface and points towards the normal to the interface. It is equal to the special derivative of the phase field:

$$\vec{C} = \vec{\nabla}\phi \tag{3.45}$$

where the phase field is given by

$$\phi = \frac{\rho^{(R)} - \rho^{(B)}}{\rho} \tag{3.46}$$

To guaranty mechanical equilibrium, the pressure term is set to:

$$p = \rho^{(R)} c_s^{(R)^2} + \rho^{(B)} c_s^{(B)^2} \tag{3.47}$$

Where $c_s^{(k)}$ is the speed of sound in the fluid of colour k. In order to guaranty mechanical equilibrium between the two phases, those speeds of sounds must respect:

$$\frac{c_s^{(1)}}{c_s^{(2)}} = \sqrt{\frac{\rho_{2,0}}{\rho_{1,0}}} \tag{3.48}$$

where $\rho_{1,0}$ and $\rho_{2,0}$ are the density of fluid 1 and fluid 2 in homogeneous state.
One of the first difficulty coming from the Colour Gradient algorithm, is that the equivalent macroscopic equation of the coloured density and is a subject of discussion in itself [45] [167] [168]. This subject has been at the center of the author's work and it has been shown [149] that the equivalent macroscopic equation for the phase field is:

$$\partial_t \rho\phi + \partial_\alpha \rho\phi u_\alpha = \partial_\alpha \left[\frac{p\Delta t}{2} \left(\partial_\alpha \phi - \frac{\beta\left(1-\phi^2\right)}{2} \frac{C_\alpha}{|\vec{C}|} \right) \right] \tag{3.49}$$

with β being a constant that is set freely by the user. At this point, the present scheme could be strictly equivalent to a free energy method. The particularity of the algorithm comes from the numerical scheme that is used to solve this set of equations Eqs. (3.42, 3.43, 3.49)

Numerical scheme

The numerical scheme consists in the consideration of two distinct population distribution functions, R_i and B_i. Furthermore, a colorless distribution function f_i is also defined, as $f_i = R_i + B_i$. In this scheme, the colorless distribution function f_i carries the information for the total density ρ and the momentum ρu_α while R_i and B_i only carries the information of the individual phases.
As in classical LBM, f_i follows a stream and collide algorithm. The novelty compared to classical LBM is the introduction of surface tension, and eventually non-perfect equation of state. In Leclaire's [159] algorithm, surface tension is introduced through a tensor scheme as described in Section 3.1.1. It means that a dedicated collision term is introduced, whose second order moments equal the Gueyffier's tensor (detailed Eq. (3.53)). Considering the equation of state, the non-perfect pressure term is introduced through a pressure scheme, i.e. by modifying the equilibrium function. The collision phase for the colourless distribution function is given by:

$$f_i^* = f_i^{eq} + \left(1 - \frac{1}{\tau}\right)\left(f_i - f_i^{eq} + 0.5S_i\right) + 0.5S_i \tag{3.50}$$

where S_i is a source term. The equilibrium function is given by Pooley and Furtado's [156] formalism:

$$f_i^{eq} = \rho w_i \left(1 + \frac{u_\alpha \xi_\alpha}{c_s^2} + u_\alpha u_\beta \frac{\xi_{\alpha,i}\xi_{\beta,i} - c_s^2\delta_{\alpha\beta}}{2c_s^4}\right) + (p - \rho c_s^2)\frac{w_i - \delta_{i0}}{c_s^2} \tag{3.51}$$

The source term S_i consists in two contributions, one accounting for surface tension, another to correct the spurious term resulting from the use of a non-perfect equation of state (Eq. (3.18))

$$S_i = S_i^\sigma + S_i^{Er} \tag{3.52}$$

The surface tension term S_i^σ is simply Gueyffier's [136] tensor projected on the second order Hermite's polynomials. Similarly the correction source term S_i^{Er} is the projection of the error term in the Hermite's polynomials base:

$$S_i^\sigma = p_{\alpha\beta}^\sigma \frac{H_{\alpha\beta,i}}{2c_s^4} \tag{3.53}$$

As shown in Eq. (3.44), the spatial derivative of the phase field ϕ is required to evaluate $p_{\alpha\beta}^\sigma$. This spatial derivative is computed following:

$$\partial_\alpha \phi_{|(\vec{x},t)} = \sum_i \frac{w_i}{c_s^2} \xi_\alpha \phi(\vec{x} + \vec{\xi}_i \Delta t, t) \tag{3.54}$$

The corrective source term is given by:

$$S_i^{Er} = \left(u_\alpha \partial_\beta \rho c_s^2 + u_\beta \partial_\alpha \rho c_s^2\right) \frac{H_{\alpha\beta,i}}{2c_s^4} \tag{3.55}$$

The presented algorithm is close to a classical LBM algorithm. The specificity of the RK method lies in the "recoloration step", during which the two colored distribution functions are evaluated from the colorless one. The idea is to "paint" the colourless distribution functions thanks to the mass fraction of the corresponding coloured density. The recolored distribution functions are given by:

$$\begin{aligned} R_i &= Y_R f_i^* + \Omega_i^{(3)} \\ B_i &= Y_B f_i^* - \Omega_i^{(3)} \end{aligned} \tag{3.56}$$

where Y_k is k^{th} species mass fraction. In addition of this coloration process, a source term is added, noted $\Omega_i^{(3)}$.

$$\Omega_i^{(3)} = \beta \frac{1-\phi^2}{2} \frac{C_\alpha}{|\vec{C}||\vec{\xi_i}|} \tag{3.57}$$

where β is a free parameter set freely by the user. It is linked to the interface width as discussed Eq. (3.49). This last source term acts as an anti-diffusive term for the interface thickness, so that red particles tend to be sent in the red region when located in the blue region.
The recoloration step is a smart way to solve a diffusion-advection equation when using a classical Lattice Boltzmann algorithm. The algorithm proposed by Leclaire [159] is summarized in Figure 3.3

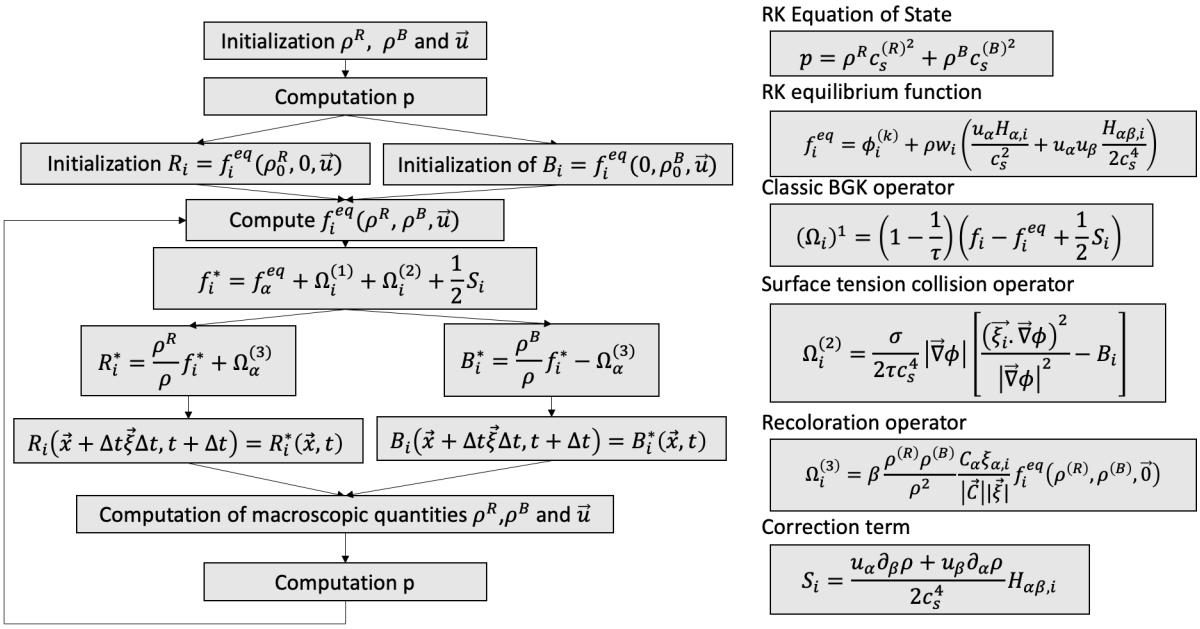


Figure 3.3. – Illustration of the algorithm proposed by Leclaire et al. [159]

3.2.2. Historical review

In this section, the progressive evolution that leaded to Leclaire's model is presented in detail. Also, the most recent features and the differences that appeared in the community are presented.

Original LGA Rothmann and Keller algorithm

As already said, the Rothmann Keller [22], or Colour Gradient algorithm is the first multiphase algorithm that was proposed in the literature. It was proposed in a Lattice Gas Automata framework and relies on a microscopic description of the interactions between the two phases. In this model, there are two kinds of particles characterized by their colours, respectively blue and red. The state at

a given node is described by two boolean functions b_i and r_i which are equal to 1 if a particle going at the velocity ξ_i is present at the considered node. The interactions between the two phases are modeled by an innovative collision operator. This new collision operator is defined thanks to two new fields: the color flux $\vec{q}$ and the color field $\vec{C}$. All these functions are given by:

$$q_\alpha = \sum_i \xi_{\alpha,i} \left[r_i - b_i \right] \tag{3.58}$$

and:

$$C_\alpha = \sum_i \xi_{\alpha,i} \sum_j \left[r_j(\vec{x} + \vec{\xi_i}) - b_j(\vec{x} + \vec{\xi_i}) \right] \tag{3.59}$$

The authors assume the existence of a repulsive force W between the particles that is equal to:

$$W = -C_\alpha q_\alpha \tag{3.60}$$

The state of the system after collision (r^*, b^*) is chosen among the possible states in order to minimize the repulsive force W:

$$W(r^*, b^*) = \min_{(r^{**}, b^{**})} W(r^{**}, b^{**}) \tag{3.61}$$

The state after collision is chosen among state respecting:

$$\sum_i r_i^{**} = \sum_i r_i \quad \sum_i b_i^{**} = \sum_i b_i \tag{3.62}$$

and:

$$\sum_i \xi_{\alpha,i}(r_i^{**} + b_i^{**}) = \sum_i \xi_{\alpha,i}(r_i + b_i) \tag{3.63}$$

This ensures the mass conservation of both red and blue particles, as well as the global momentum of the two phases.
This model replicates two specific behaviors of multiphase flows: the immiscibility and the Laplace law. To illustrate the algorithm's capability to simulate immiscibility a spinodal decomposition test is conducted in Rothman and Keller [22]. This numerical test consists in initializing a flow with a homogeneous concentration of blue and red particles. Immiscibility leads these two populations to segregate. The results from the article of Rothman and Keller [22] are proposed in Figure 3.4

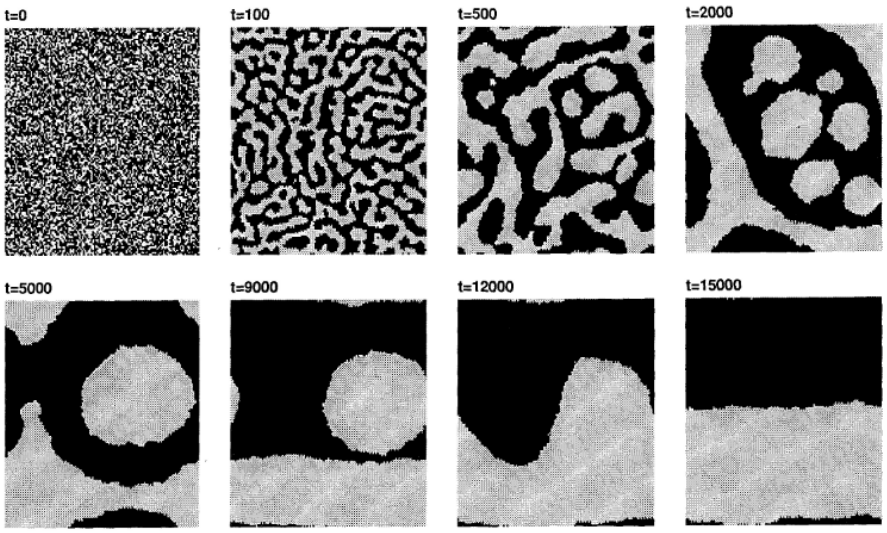


Figure 3.4. – Illustration of a spinodal decomposition simulated by the RK LGA method (from [22])

Gustensen's LBM model

The LBM counterpart of this method was proposed by Gunstensen et al. [23]. In this algorithm, a colorless population f_i is considered and two colored populations R_i and B_i. The colorless population is collided according to the following rule:

$$f_i^* = f_i + \Omega_i^1 + \Omega_i^{(2)} \tag{3.64}$$

where $\Omega_i^{(1)}$ is the "classical" BGK collision operator $\Omega_i^{(1)} = -\frac{1}{\tau}\left(f_i - f_i^{eq}\right)$, and $\Omega_i^{(2)}$ is a second operator that allows to introduce surface tension. It is given by:

$$\Omega_i^{(2)} = A|\vec{C}|cos\left[2(\theta_i - \theta_C)\right] \tag{3.65}$$

Where $\vec{C}$ is the same colour gradient operator defined by Rothman and Keller (3.59), θ_i is the angle of the lattice i, and θ_C is the angle of the colour gradient. To understand this term, it must be underlined that in this work, the color gradient $\vec{C}$ is interpreted as a marker of the interface. Moreover, the direction of $\vec{C}$ is normal to the interface. Then the second collision operator $\Omega_i^{(2)}$ must be understood as a term that creates a pressure jump normal to the interface: it doesn't introduce density nor momentum, but it reorients the flow parallel to the interface in the normal direction.
After this collision operator, the population B_i and R_i are calculated through the so-called "recoloration operator". This step is similar to the one proposed by Rothmann and Keller since it also consists in an optimisation process:

$$W(R_i^*, B_i^*) = \underset{R_i^{**}, B_i^{**}}{max}\left[\sum_i \left(R_i^{**} - B_i^{**}\right)\xi_{\alpha,i}\right] C_\alpha \tag{3.66}$$

where C_α is defined Eq. (3.59), and where R_i^{**} and B_i^{**} must respect:

$$\begin{gathered} R_i^{**} + B_i^{**} = f_i^* \\ R_i^{**} = R_i \end{gathered} \tag{3.67}$$

This ensures the conservation of both the two populations, and consequently of the total mass. The two population R_i and B_i are then streamed using the classical relationship:

$$\begin{gathered} R_i(\vec{x} + \vec{\xi}\Delta t, t + \Delta t) = R_i^*(\vec{x}, t) \\ B_i(\vec{x} + \vec{\xi}\Delta t, t + \Delta t) = B_i^*(\vec{x}, t) \end{gathered} \tag{3.68}$$

This algorithm proposed by Gunstensen et al. is the original LBM colour gradient algorithm. The whole approach relies on a bottom-up approach, meaning that the microscopic interactions are modeled in such a way that it allows to retrieve the desired macroscopic behavior. The main drawback is that the recoloration operator cannot be related to a continuous equation, so that the recoloration step cannot be associated to a macroscopic equation.
This algorithm has been gradually improved along time, allowing to improve the original formulation's drawback, or adding new features. In practice, the algorithm has three main parts that can be modified: the equilibrium function, the surface tension term and the recoloration operator.

Equilibrium function

When proposed by Gunstensen et al. [23], the algorithm only allowed to simulate density match cases. For this reason, Grunau et al. [164] introduced an original equilibrium equation that allows the two phases to have different densities. The proposed solution is:

$$f_i^{eq} = \phi_i^{(k)} + \rho w_i\left(\frac{\xi_{\alpha,i}u_\alpha}{c_s^2} + u_\alpha u_\beta\frac{\xi_{\alpha,i}\xi_{\beta,i} - c_s^2\delta_{\alpha\beta}}{2c_s^4}\right) \tag{3.69}$$

with $\phi_i^{(k)}$ an operator that depends on the velocity set, for instance in D_2Q_9 is given by:

$$\phi^{(k)} = \rho^{(k)} \begin{cases} \alpha_i^{(k)} & i = 0 \\ \dfrac{1-\alpha_i^{(k)}}{5} & i = 1,3,5,7 \\ \dfrac{1-\alpha_i^{(k)}}{20} & i = 2,4,6,8 \end{cases} \tag{3.70}$$

With $\alpha^{(k)}$ a user defined constant. The operator is chosen to ensure:

$$\begin{aligned} \sum_i \phi^k &= \rho^{(k)} \\ \sum_i \xi_{\alpha,i}\phi^k &= 0 \\ \sum_i \xi_{\alpha,i}\xi_{\beta,i}\phi^k &= \frac{3\rho_k(1-\alpha^{(k)})}{5} \end{aligned} \tag{3.71}$$

Giving the last equation, the scheme proposed by Grunau et al. can be interpreted as an equilibrium scheme where the pressure is given by:

$$p = \frac{3\rho_k(1-\alpha^{(k)})}{5} \tag{3.72}$$

An other way to interpret the previous equation is to consider that in this scheme the speed of sound for each phase is set independently, then the pressure expression comes as:

$$p = \rho_k {c_s^{(k)}}^2 \tag{3.73}$$

with ${c_s^{(k)}}^2 = \dfrac{3(1-\alpha^{(k)})}{5}$.

Leclaire et al. [150] pointed out that this condition can be restrictive. It means that the speed of sound is lower in the denser fluid, the consequence is that for flows with high density ratios, the speed of sound in the denser fluid can become relatively low. For instance, in a common case such as water in air under atmospheric pressure, the density of the denser fluid is $\rho_1 = 1000kg.m^{-3}$, the other one as a density of $\rho_2 = 1kg.m^{-3}$. In normal condition of pressure and temperature, the speed of sound in air is approximately $c_s^{(2)} = 340m.s^{-1}$. By calculating the speed of sound in water using (3.48) we obtain $c_s^{(1)} = 10.8m.s^{-1}$. In order to ensure incompressibility, the Mach number must remain lower than 0.3, i.e. the denser fluid velocity must be lower than $3.22m.s^{-1}$ in the denser fluid. Furthermore, it can be noted that a density ratio of 1000 is reached for a gas and a liquid, which makes the eventual compressibility in the denser fluid absolutely not physical. Leclaire et al. generalised this equilibrium function to an arbitrary number of phases [166] and to a 3D framework [169].

Even if it might not be straightforward, the equilibrium function proposed by Grunau et al. (3.69) is equivalent to the scheme proposed by Pooley and Furtado [156] given Eq. (3.21). When discussing about the different schemes to introduce a non-perfect equation of gas, it was pointed out that a spurious term appears in the stress tensor. As shown in Huang et al. [170], this spurious term induces discontinuous velocities across the interface for high density ratio. An enhanced equilibrium function was introduced by Leclaire et al. [159]. As shown in Eq. (3.18):

$$Er^{EOS} = \Delta t(\tau - 1/2)\partial_\beta \left(u_\alpha \partial_\beta \left(p - \rho c_s^2 \right) + u_\beta \partial_\alpha \left(p - \rho c_s^2 \right) \right) \tag{3.74}$$

Leclaire et al. note that the main contribution to the previous error term comes from the spatial derivatives of the density, then they added a correction term to the equilibrium function. This correction term, noted Φ_i, introduces a stress equal to the error term. The enhanced equilibrium function

is given by:

$$f_i^{eq} = \phi_i^{(k)} + \rho w_i \left(\frac{\xi_{\alpha,i} u_\alpha}{c_s^2} + u_\alpha u_\beta \frac{\xi_{\alpha,i}\xi_{\beta,i} - c_s^2 \delta_{\alpha\beta}}{2c_s^4} \right) + \Phi_i \tag{3.75}$$

Saïto et al. [36, 171] proposed an enhanced version of the equilibrium function proposed by Leclaire et al. [159], that takes into account 3^{rd} order terms that correct the Mach cubed error introduced in Eq. (1.56). This new feature allowed an improvement of the numerical stability at high density ratio. More recently Wen et al. [161] proposed an improved equilibrium function that allowed to improve the accuracy at high density ratio. This method will be a subject of discussion in Chapter 5.

Recoloration operator

Latva-Kokko and Rothmann [172] pointed out that the recoloration step as proposed by Rothmann and Keller has an important drawback called "lattice pinning". It appears that when the velocity field is not high enough, the interface tends not to be able to move and is "pinned" to the lattice. For instance, in the case of a little structure of "red" particles evolving into a quiescent atmosphere of "blue" particles, the red particles tends to move into a figure height-shaped curve which create a spurious periodic flow at this location. This phenomenon becomes significant when simulating little bubbles.
Inspired by the work of D'Ortona et al. [173] and Tolke et al. [165], Latva-Kokko and Rothmann [172] proposed an improved recoloration operator that takes the following form:

$$\begin{aligned} R_i^* &= \frac{\rho^{(R)}}{\rho} f_i^* + \beta \frac{\rho^{(R)}\rho^{(B)}}{\rho^2} f_i^{eq}(\rho^{(R)}, \rho^{(B)}, \vec{u} = \vec{0}) cos(\varphi_i) \\ B_i^* &= \frac{\rho^{(R)}}{\rho} f_i^* - \beta \frac{\rho^{(B)}\rho^{(R)}}{\rho^2} f_i^{eq}(\rho^{(R)}, \rho^{(B)}, \vec{u} = \vec{0}) cos(\varphi_i) \end{aligned} \tag{3.76}$$

where β is a user defined parameter, φ_i is the angle between the color gradient $\vec{C}$ and the i^{th} lattice $\vec{\xi_i}$. Then the cosinus of φ_1 is given by:

$$cos(\varphi_i) = \frac{\xi_{\alpha,i} C_\alpha}{|\vec{C}||\vec{\xi_i}|} \tag{3.77}$$

The β term in Eq. (3.76) must be a positive number superior to 0. In practice,when $\beta > 1$, instabilities arise and $0 < \beta < 1$ is recommended. Latva-Kokko [172] showed that the profile obtained in the case of a flat interface could be predicted with such a recoloration operator. They showed that the density of red fluid in the case of a flat interface is given by:

$$\rho^{(R)} = \rho \frac{e^{K(\beta)(x - x_0)}}{1 + e^{K(\beta)}(x - x_0)} \tag{3.78}$$

with $K(\beta) = \frac{2}{3}(1 + \sqrt{2})\beta$ and e the exponential function. While not being straightforward, it can be shown that β is linked to the inverse of the interface thickness.
From the physical point of view, β can be interpreted as a repelling term, when blue particles are present in a region of red particles in majority, blue particles tend to be sent to the other side of the interface. Then, a flow of material is created across the interface. As can be evidenced from Eq. (3.77) the 0^{th} moment of the recoloration operator is equal to 0, then no additional quantity of blue and red are created. In addition, as the different recoloration operators have the same magnitude but have opposite signs, the recoloration operator doesn't create any flux for the colorless distribution f_i.
An improvement of this operator has been proposed by Haliday et al [174], who proposed:

$$\Omega_i^{(3)} = \beta \frac{\rho^{(R)}\rho^{(B)}}{\rho^2} \frac{C_\alpha \xi_{\alpha,i}}{|\vec{C}|} f_i^{eq}(\rho^{(R)}, \rho^{(B)}, \vec{u} = \vec{0}) \tag{3.79}$$

This improves the operator's properties of isotropy and the authors showed less spurious currents than with the formulation of Latva-Kokko et al. [172].

Surface tension operator

The surface tension collision operator $\Omega_i^{(2)}$ has also been modified along the literature. First, Grunau et al. [164] pointed out that (3.65) can equivalently be expressed as:

$$\Omega_i^{(2)} = \frac{A}{2}|\vec{C}|\left[w_i\frac{(\xi_{\alpha,i}C_\alpha)^2}{|\vec{C}|^2} - \frac{3}{4}\right] \tag{3.80}$$

where Reis and Philips [43] showed that through a slight modification of the previous formulation, the present operator can be shown to be equivalent to the Continuous Stress Tensor proposed by Gueyfier et al. [136]:

$$\Omega_i^{(2)} = \frac{A}{2}|\vec{C}|\left[w_i\frac{(\xi_{\alpha,i}C_\alpha)^2}{|\vec{C}|^2} - B_i\right] \tag{3.81}$$

where B_i is a correction term given in D_2Q_9 by:

$$B_i = \begin{cases} -4/27 & i = 0 \\ 2/27 & i = 1,3,5,7 \\ 5/108 & i = 2,4,6,8 \end{cases} \tag{3.82}$$

They showed that the second moment of Eq. (3.81) is given by:

$$\sum_i \xi_{\alpha,i}\xi_{\beta,i}\Omega_i^{(2)} = \frac{A}{2|\vec{C}|}\left(C_\alpha C_\beta - |\vec{C}|^2\delta_{\alpha\beta}\right) \tag{3.83}$$

Liu et al. [44] finally proposed to relate the coefficient A and Gueyffier et al. [136] surface tension coefficient σ given in Eq. (2.74)

$$\sigma = 2c_s^4 A(\tau - 1/2) \tag{3.84}$$

Note that Eq. (3.84) slightly differs from the original paper [44] since they used a different scheme to introduce a source term than in the present formulation.
It comes that the scheme introduced by Reis and Philips [43] corresponds to a tensor scheme coupled to the formalism of Gueyffier et al. [136], but the colour gradient formulation can also be coupled to a body force approach and rely on the Continous Stress Force of Brackbill et al. [135] as proposed by Lishchuk et al. [175][176] or by Ba et al. [177].
Liu et al. [44], Leclaire et al. [178] and Ba et al. [177] showed that the order paramater ϕ can differ from $\rho^R - \rho^B$. Liu et al. [44] for instance showed that:

$$\phi = \frac{\rho^{(R)} - \rho^{(B)}}{\rho^{(R)} + \rho^{(B)}} \tag{3.85}$$

leads to a better stability. Leclaire et al. [178] proposed:

$$\phi = \frac{\rho^{(R)}/\rho_0^{(R)} - \rho^{(B)}/\rho_0^{(B)}}{\rho^{(R)}/\rho_0^{(R)} + \rho^{(B)}/\rho_0^{(B)}} \tag{3.86}$$

.

3.3. Free energy methods

Free energy methods are the second family of methods that have been proposed in the literature by Swift et al. [27, 28]. In practice, this model is not often used recently, the HCZ formalism, presented Section 3.5 is preferred. As a lot of HCZ models inherit from these free energy methods, their description is proposed in this subsection.
The very identity of the free energy methods lies in the physical model used to introduce a non-perfect equation of state, and to introduce surface tension. Note that the introduction of surface tension is part of the introduction of a non-perfect EOS in these approaches. As it was discussed in Chapter 2, in the free energy model the Helmholtz free energy is given by:

$$E = E_0 + \frac{\lambda}{2}|\vec{\nabla}\phi|^2 \tag{3.87}$$

where E_0 is the bulk free energy, λ is a surface tension term and ϕ is the order parameter. As it as been discussing previously, the consequence of this Helmholtz energy is the appearance of a tensor term that can also be expressed as a body force following Eq. (3.1):

$$F_\alpha = \partial_\beta p_{\alpha\beta} = \partial_\beta \left(p_0\delta_{\alpha\beta} + p^\sigma_{\alpha\beta}\right) \tag{3.88}$$

where p_0 is a non-perfect equation of state and $p^\sigma_{\alpha\beta}$ is the free energy surface tension tensor. This pressure term can equivalently be expressed deriving from a potential μ:

$$F_\alpha = \phi\partial_\alpha\mu \tag{3.89}$$

Since the free energy (Eq. (3.87)) is divided in two terms, the potential can also be expressed in two parts: $\mu = \mu_0 - \vec{\nabla}\left(\lambda\vec{\nabla}\phi\right)$.
The model proposed in Swift et al. [27] for multicomponents system is described hereafter.

3.3.1. Introduction

Macroscopic equations

The considered macroscopic equations are the same than in color gradient:

$$\partial_t\rho + \partial_\alpha\rho u_\alpha = 0 \tag{3.90}$$

$$\partial_t\rho u_\alpha + \partial_\beta\left(\rho u_\alpha u_\beta + p\delta_{\alpha\beta} + p^\sigma_{\alpha\beta}\right) = \Delta t\partial_\beta\left[\rho c_s^2\left(\tau - 1/2\right)\left(\partial_\alpha u_\beta + \partial_\beta u_\alpha\right)\right] \tag{3.91}$$

with $p^\sigma_{\alpha\beta}$ being the pressure resulting from the excess of free energy at the interface:

$$p^\sigma_{\alpha\beta} = \lambda\left[\left(-\rho\partial^2_\gamma\rho - \frac{1}{2}\left(\partial_\gamma\rho\right)^2\right)\delta_{\alpha\beta} + \partial_\alpha\rho\partial_\beta\rho\right] \tag{3.92}$$

In Eq. (3.91), p_0 is the pressure provided by the equation of state. Swift et al. [27] proposed to consider the van der Walls Equation of State adapted to an isothermal framework:

$$p = \frac{\rho r T_0}{1 - \rho b} - a\rho^2 \tag{3.93}$$

where T_0 is the user defined temperature of the system, $a = \dfrac{27(rT_c)^2}{64p_c}$, $b = \dfrac{rT_c}{8p_c}$, T_c and p_c being the temperature and the pressure at critical temperature. This model is a two phase one species model, and can be compared to three equations models such as the one by Pelleter et al. [120]. In this

model, there are no order parameter ϕ to distinguish phases. The difference can be made because the equation $p(\rho) = p_0$ has two roots, then at mechanical equilibrium (i.e. in a field with a uniform pressure) the density can take only two values. At a given point, the nature of the phase we are located in is determined by the value of the density.
It should be noted, that in a second paper [28], Swift et al. improved their model to account for two separate phases, that do not result from a thermodynamical equilibrium, introducing a transport equation for the phase field:

$$\partial_t \rho\phi + \partial_\alpha \rho\phi u_\alpha = M\left(\Gamma\partial^2_\beta \mu_0 - \partial_\alpha\left[\phi\partial_\beta\left(p_0\delta_{\alpha\beta} + p^\sigma_{\alpha\beta}\right)\right]\right) \tag{3.94}$$

where Γ is a free parameter set by the user, M is the mobility factor also set by the user, and μ_0 the difference of chemical potential between the two phases. In practice, it is given by:

$$\mu_0 = \frac{T}{2}\ln\left(\frac{1+\phi}{1-\phi}\right) - \lambda\partial^2_\gamma\rho\phi - \frac{\lambda}{2}\phi \tag{3.95}$$

where ϕ is the phase field. In practice, the previous equation is not used due to a lack of physical background. Free energy recent methods rather use Allen-Cahn equation or Cahn-Hilliard equation as in Semprebon et al. [157] or Wohrwag et al. [35]. The numerical scheme for this fee energy method is described in the following.

Numerical scheme

Similarly as in the Rothmann-Keller algorithm, the three equations system is solved thanks to two distribution functions. As in RK, a colorless distribution function f is also considered, which first two moments respectively correspond to the total density ρ and the total momentum ρu_α:

$$\sum_i f_i = \rho \tag{3.96}$$

$$\sum_i \xi_{\alpha,i} f_i = \rho u_\alpha \tag{3.97}$$

In the approach of Swift et al. [28], a second distribution function g_i is introduced, which 0^{th} moment is proportional to the phase field:

$$\sum_i g_i = \rho\phi \tag{3.98}$$

A stream and collide algorithm is applied to the main population f_i to recover mass and momentum conservation. The collision step writes:

$$f_i^* = f_i^{eq} + \left(1 - \frac{1}{\tau_1}\right)(f_i - f_i^{eq}) \tag{3.99}$$

where τ_1 is the relaxation time for the main population, related to the kinematic viscosity through: $\tau_1 = \dfrac{\nu}{c_s^2} + 1/2$. The non-perfect equation of state and the pressure resulting from surface tension are introduced by the "equilibrium scheme". The equilibrium function f_i^{eq} is modified to account for the pressure p resulting from the equation of state and p^σ resulting from surface tension:

$$f_i^{eq} = \rho w_i\left(H_{0,i} + \frac{H_{\alpha,i}u_\alpha}{c_s^2} + u_\alpha u_\beta\frac{H_{\alpha\beta,i}}{2c_s^4}\right) + (p\delta_{\alpha\beta} + p^\sigma_{\alpha\beta})\frac{H_{\alpha\beta}}{2c_s^4} \tag{3.100}$$

The streaming phase is given by:

$$f_i(\vec{x}, t+\Delta t) = f_i^*(\vec{x} - \vec{\xi}_{\alpha,i}\Delta t, t) \tag{3.101}$$

The second population also follows a stream and collide algorithm. It is given by:

$$g_i^* = g_i^{eq} + \left(1 - \frac{1}{\tau_2}\right)(g_i - g_i^{eq}) \tag{3.102}$$

where τ_2 is the relaxation time of the second population g_i, related to the mobility factor through:

$$M = \Delta t\,(\tau_2 - 1/2) \tag{3.103}$$

The equilibrium distribution function for g_i is given by:

$$g_i^{eq} = \rho\phi w_i \left(1 + \frac{\xi_{\alpha,i}u_\alpha}{c_s^2} + u_\alpha u_\beta \frac{H_{\alpha\beta,i}}{2c_s^4}\right) + w_i\left(\Gamma\mu_0 - \rho\phi c_s^2\right)\frac{H_{\alpha\alpha,i}}{2c_s^4} \tag{3.104}$$

The streaming phase for g_i is similar to the one for f_i:

$$g_i(\vec{x}, t + \Delta t) = g_i^*(\vec{x} - \vec{\xi}_{\alpha,i}\Delta t, t) \tag{3.105}$$

The algorithm is illustrated as follow in Figure 3.5.

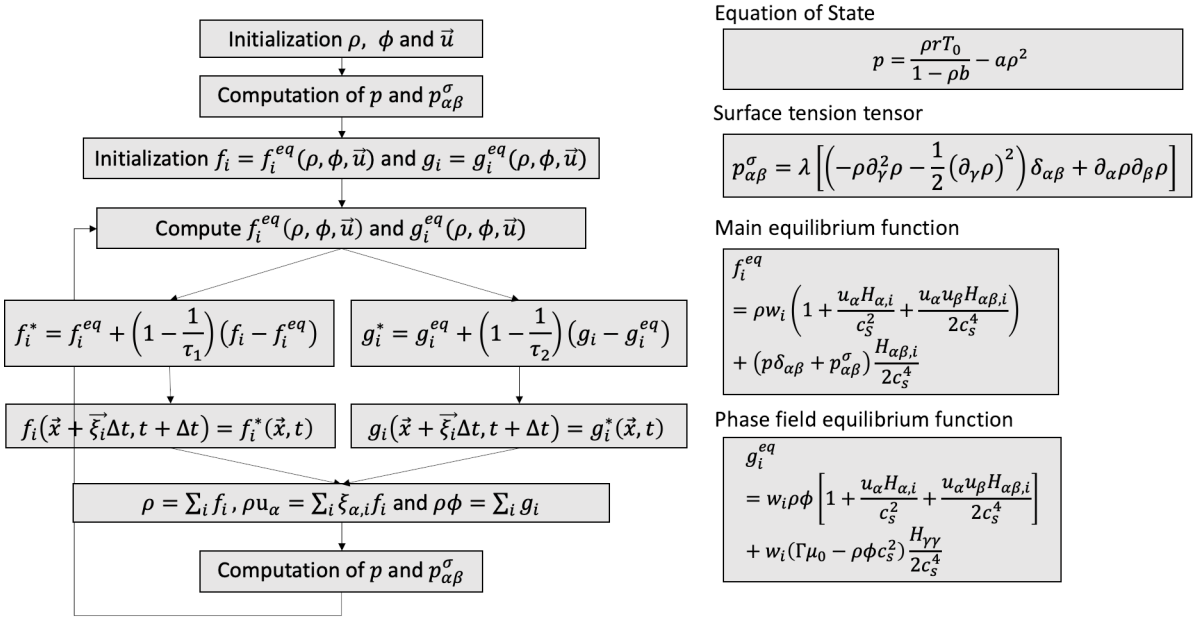


Figure 3.5. – Illustration of the free energy algorithm proposed by Swift et al. [28]

3.3.2. Discussion around the phase field equation

The attentive reader would have noted that in the macroscopic transport equation of the phase field, Eq. (3.94) a pressure term proportional to $p_0\delta_{\alpha\beta} + p^{\sigma}_{\alpha\beta}$ appears in the right-hand side. On the other hand, no pressure term is involved in the equilibrium function g_i^{eq} defined Eq. (3.104). This pressure term in the macroscopic equation results from the numerical scheme itself. It is shown here that this term allows to solve an advection-diffusion equation for the phase field ϕ.
Both f_i and g_i follow the same algorithm, the only difference is that f_i has two moments of interest (ρ and ρu_α) while g_i has only one. The consequence is that the first moment of g_i is no longer equal to the first moment of g_i^{eq}. The consequence is that the first moment of the non equilibrium function is no longer equal to zero. It can be shown through a Taylor expansion that the first moment of the non equilibrium function is given by:

$$\sum_i \xi_{\alpha,i}\,(g_i - g_i^{eq}) = \Delta t\tau_2\left[\partial_t\sum_i \xi_{\alpha,i}g_i + \partial_{\alpha\beta}\sum_i(\xi_{\alpha,i}\xi_{\beta,i}g_i^*)\right] + O(\Delta t^2) \neq 0 \tag{3.106}$$

It can be shown that a term proportional to Δt appears in the phase field equation:

$$\partial_t \rho\phi + \partial_\alpha \rho\phi u_\alpha = \Delta t \partial_\beta \left((\tau_2 - 1/2) \left[\partial_t^2 \rho\phi - \partial_{\alpha\beta} \sum_i \xi_{\alpha,i} \xi_{\beta,i} g_i^{eq} \right] \right) + O(\Delta t^2) \tag{3.107}$$

Eq. (3.107) can be simplified by developing $\partial_t^2 \rho\phi$. From Eq. (3.107) it comes:

$$\partial_t^2 \rho\phi = -\partial_\alpha \left(\partial_t \rho u_\alpha \right) + O(\Delta t) = \partial_\alpha \left[\partial_\beta \rho\phi u_\alpha u_\beta + \phi \partial_\beta \left(p\delta_{\alpha\beta} + p^\sigma_{\alpha\beta} \right) \right] + O(\Delta t) \tag{3.108}$$

By remembering that g_i^{eq} 2^{nd} moment is known and given by:

$$\sum_i \xi_{\alpha,i} \xi_{\beta,i} g_i^{eq} = \rho\phi u_\alpha u_\beta + \left(p\delta_{\alpha\beta} + p^\sigma_{\alpha\beta} \right) \tag{3.109}$$

and by making the hypothesis that in practice $p^\sigma_{\alpha\beta}$, the pressure implied by surface tension is far weaker than the pressure implied by the Equation of State, then $p\delta_{\alpha\beta} + p^\sigma_{\alpha\beta} \simeq p\delta_{\alpha\beta}$, it can be shown that Swift et al. [28] equivalent phase field equation is given by:

$$\partial_t \rho\phi + \partial_\alpha \rho\phi u_\alpha = \partial_\alpha \left(\Delta t (\tau_2 - 1/2) \left[p \partial_\alpha \phi \right] \right) \tag{3.110}$$

We recognize a diffusion-advection equation, and it shows that this kind of equation can be solved through a Lattice Boltzmann stream and collide algorithm.

3.3.3. Historical review

This model was first proposed by Swift et al. [27, 28]. A free energy method in an incompressible framework is proposed in Inamuro et al. [179]. Based on a generalisation of a binary fluid mixture model [180], Inamuro et al. proposed an iterative step at the end of the stream and collide algorithm allowing to simulate an incompressible equation. Simulations at high density ratio were proposed recently based on this method [38, 181, 182].
The work of Pooley and Furtado [156] that was already discussed takes place in a free energy framework. More recently, those methods were generalised to ternary flows [35, 157].

3.4. Pseudo Potential

The Shan-Chen model or pseudo-potential model was the second LBM multiphase model proposed by Shan and Chen in 1993 and 1994 [25, 26]. The method rely on a bottom-up approach, which means that the model intends to simulate the particles microscopic behavior rather than the macroscopic physic (as done in free energy for example). Pseudo-potential model is based on the idea, that immiscibility and surface tension come from interparticle forces occurring between particles of different phases. It must be noted that some non-perfect equation of state, including the van der Walls Equation of State, rely on the hypothesis of the existence of interparticle forces.
They are mainly two popular approaches, the single chemical component (SCMP) and the multiple chemical component approach (MCMP). Both are similar, therefore only SCMP is presented. The method by Yuan and Schaeffer [183] is presented here and is considered as the reference method.

3.4.1. Macroscopic equations

The present method can be compared to the 3-equation model [120]. The macroscopic unknowns are ρ the total density and the velocity $\vec{u}$. A pressure term p is introduced through an Equation of State. The knowledge of the order parameter (i.e. phases mass fraction) is not necessary. Similarly to Color gradient and free energy methods, the considered macroscopic equations are:

$$\partial_t \rho + \partial_\alpha \rho u_\alpha = 0 \tag{3.111}$$

$$\partial_t \rho u_\alpha + \partial_\beta \left(\rho u_\alpha u_\beta + p\delta_{\alpha\beta} + p^\sigma_{\alpha\beta} \right) = \partial_\beta \left(\rho c_s^2 \Delta t \left(\tau - 1/2 \right) \left(\partial_\alpha u_\beta + \partial_\beta u_\alpha \right) \right) \tag{3.112}$$

where p is an arbitrary Equation Of State. Surface tension is introduced through the free-energy tensor scheme introduced Section 2.3 Eq. (2.78). Its formulation is recalled here:

$$p^\sigma_{\alpha\beta} = \frac{\Delta t^3}{2} G c_s^4 \left(\psi \nabla^2 \psi + \frac{1}{2} |\vec{\nabla}\psi|^2 \right) \delta_{\alpha\beta} - \frac{\Delta t^3}{2} G c_s^4 \partial_\alpha \psi \partial_\beta \psi \tag{3.113}$$

With ψ being the so called pseudo-potential, and G a constant set by the user. This is a free-energy tensor, in which the phase field is the pseudo-potential. This pseudo-potential is related to the pressure through [184]:

$$\psi = \sqrt{\frac{2(p - \rho c_s^2)}{c_s^2 G}} \tag{3.114}$$

From the macroscopic point of view, the present method is almost identical to a free energy method. The difference lies in the numerical scheme used to implement it, as will be detailed later on. The macroscopic momentum conservation equation Eq. (3.112) can also be written:

$$\partial_t \rho u_\alpha + \partial_\beta \left(\rho u_\alpha u_\beta + \rho c_s^2 \delta_{\alpha\beta} \right) = \partial_\beta \left(\rho c_s^2 \Delta t \left(\tau - 1/2 \right) \left(\partial_\alpha u_\beta + \partial_\beta u_\alpha \right) \right) + F^{SC}_\alpha \tag{3.115}$$

where F^{SC}_α is a body force that introduces both surface tension and the pressure from the non-perfect equation of state. This body force is given by:

$$F^{SC}_\alpha = -\partial_\beta \left(\underbrace{\frac{\Delta t}{2} G c_s^2 \psi^2 \delta_{\alpha\beta}}_{EOS\ term} + \underbrace{\frac{\Delta t^3}{2} G c_s^4 \left(\psi \nabla^2 \psi + \frac{1}{2} |\vec{\nabla}\psi|^2 \right) \delta_{\alpha\beta} - \frac{\Delta t^3}{2} G c_s^4 \partial_\alpha \psi \partial_\beta \psi}_{Surface\ tension\ term} \right) \tag{3.116}$$

When the pseudo-potential is defined through Eq. (3.114), the EOS term in Eq. (3.116) reduces to $\partial_\beta \left(p - \rho c_s^2 \right)$. The consequence is that surface tension cannot be controlled at will, advanced methods, such as the one proposed by Sbragaglia et al. [185] are necessary in order to allow a decoupling between surface tension and the pressure from the EOS.

Phase Composition

The very specificity of this method among the LBM multiphase community is that the fluid composition doesn't need to be determined. The density ρ gradually changes from ρ_1 to ρ_2, thanks to the equation of state.
Thermodynamic consideration allow to determine the phase composition from the global quantities p and ρ of the total system. The liquid composition can be determined at a given location through the Maxwell construction rule. It is given by:

$$\int_{1/\rho_1}^{1/\rho_2} pd\frac{1}{\rho} = p_0\left(\frac{1}{\rho_2} - \frac{1}{\rho_1}\right) \tag{3.117}$$

where p_0 is the constant pressure resulting from the equation of state, ρ_1 and ρ_2 the respective densities of the two phases.
Note that the global mass conservation is ensured through the continuity equation Eq. (3.111), but contrarily to free-energy methods, no transport equation is considered for the specific mass phase. This may lead to non-physical mass transfer from one phase to the other.

3.4.2. Numerical Scheme

Contrarily to the Free Energy methods, and RK, the Shan-Chen method is a one population method. It relies on a single particle distribution function f_i. It follows a classical LBM approach, in which f_i's 0^{th} moment and 1^{st} moments are

$$\sum_i f_i = \rho \tag{3.118}$$

$$\sum_i \xi_{\alpha,i} f_i = \rho u_\alpha \tag{3.119}$$

The f_i particle population follows a classical stream and collide algorithm given by:

$$f_i^* = f_i - \frac{1}{\tau}\left(f_i - f_i^{eq}\right) + S_i \tag{3.120}$$

The equilibrium function is the same as in classical LBM and is given by:

$$f_i^{eq} = \rho w_i \left[1 + \frac{u_\alpha \xi_{\alpha,i}}{c_s^2} + u_\alpha u_\beta \frac{\xi_{\alpha,i}\xi_{\beta,i} - c_s^2\delta_{\alpha\beta}}{2c_s^4}\right] \tag{3.121}$$

The source term S_i from Eq. (3.120) is a source term that allows the introduction of a body force, using Guo et al.'s force scheme [148]. Noting that in the original paper of Yuan et Schaefer [184], Shan and Chen [25] forcing term is used. Source terms used to introduce body forces is a whole subject of discussion already tackled in Section 4.2. It is notably discussed that Guo's source term is an improved version of Shan and Chen source term, and must be prefered to introduce a body force. Guo's term writes:

$$S_i = \left(1 - \frac{1}{2\tau}\right)\left(\frac{\xi_{\alpha,i}F_\alpha^{SC}}{c_s^2} + \left(F_\alpha^{SC}u_\beta + F_\beta^{SC}u_\alpha\right)\frac{\xi_{\alpha,i}\xi_{\beta,i} - c_s^2\delta_{\alpha\beta}}{2c_s^4}\right) \tag{3.122}$$

where F^{SC} is the interparticle force given in Eq. (3.116).

Interparticle force

The calculation of the interpaticle force is a subject of discussion in itself. The original scheme proposed in the work of Shan and Chen [25] is given by:

$$F_\alpha^{SC}(\vec{x},t) = -G\psi(\vec{x},t)\sum_i w_i\psi\left(\vec{x} + \vec{\xi}_{\alpha,i}\Delta t, t\right)\xi_{\alpha,i} \tag{3.123}$$

where G and ψ were introduced respectively in Eq. (3.113) and in Eq. (3.114). The attentive reader would have recognized a spatial derivative scheme in Eq. (3.123). It can be shown that:

$$\sum_i w_i \psi \left(\vec{x} + \vec{\xi}_{\alpha,i}\Delta t, t\right) \xi_{\alpha,i} = \Delta t c_s^2 \partial_\alpha \psi - \frac{\Delta t^3}{6} \Delta t^3 c_s^4 \psi \partial_\alpha \left(\partial_\beta^2 \psi\right) + O(\Delta t^4) \tag{3.124}$$

Using previous equation, it comes that the numerical scheme given in Eq. (3.123) is equivalent to the force term involved in the macroscopic momentum conservation equation Eq. (3.116). The pseudo-potential approach is summarized in Figure 3.6

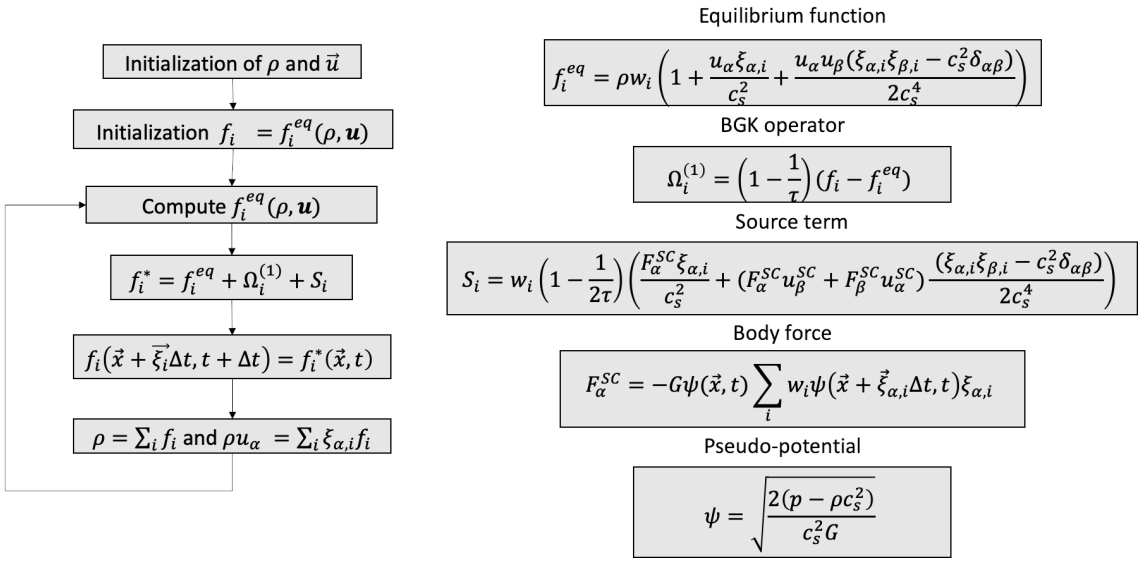


Figure 3.6. – Pseudo-potential algorithm inspired from Yuan and Schaefer [183]

3.4.3. Historical review

Pseudo potential

In their original papers, Shan and Chen [25][26] proposed two pseudo-potential forms to account for interparticle forces following:

$$\psi = \rho_0 \left[1 - exp\left(-\rho/\rho_0\right)\right] \tag{3.125}$$

and also:

$$\psi = \psi_0 \left[-exp\left(-\rho_0/\rho\right)\right] \tag{3.126}$$

where ρ_0 and ψ_0 are arbitrary constants. The second model Eq. (3.126) is said to be able to simulate an isothermal process.
In 1998, He et al. [53] proposed an Enskog model to simulate a van der Walls interaction potential, which is somehow similar to the present pseudo-potential model. The model proposed in Yuan and Schaefer [183] and described in this Section 3.4 is nowaday widely used to account for interparticle forces in a LBM framework.

Body force

One of the main drawback of the present pseudo potential method is the presence of important spurious currents located at the interface. To reduce them, Gong and Chen [186] proposed in 2012

the β model. It relies on the fact that the Shan-Chen body force truncated at the order 3 in Δt can be written under two formulations:

$$F_\alpha^{SC} = -G\Delta t\psi\partial_\alpha\psi + O(\Delta t^3) = -\frac{G}{2}\partial_\alpha\psi^2 + O(\Delta t^3) \tag{3.127}$$

The idea of the β model is to use a combination of these two formulations following:

$$F_\alpha^{SC}(\vec{x},t) = \beta\psi(\vec{x},t)\sum_i w_i\psi\left(\vec{x}+\vec{\xi}_{\alpha,i}\Delta t, t+\Delta t\right)\xi_{\alpha,i} + (1-\beta)\sum_i w_i\psi^2\left(\vec{x}+\vec{\xi}_{\alpha,i}\Delta t, t+\Delta t\right)\xi_{\alpha,i} \tag{3.128}$$

where β is a weighting parameter. Zarghami et al. [187] showed that $\beta = 1.25$ allows to significantly reduce these spurious currents.
Another issue raised earlier is the fact that surface tension cannot be freely set, reducing the method applicability range. Sbragaglia et al. [185] proposed an improvement involving the second neighbours in the Shan Chen body force, following:

$$F_\alpha^{SC} = -\psi(\vec{x},t)\sum_i w_i\left[G_1\psi\left(\vec{x}+\vec{\xi}_{\alpha,i}\Delta t, t\right) + G_2\psi\left(\vec{x}+2\vec{\xi}_{\alpha,i}\Delta t, t\right)\right] \tag{3.129}$$

It was proposed by Benzi et al. [188] that the potential expression should be modified to:

$$\psi = \sqrt{\frac{2\left(p-\rho c_s^2\right)}{c_s^2\left(G_1+2G_2\right)}} \tag{3.130}$$

Huang et al. [189] showed that this framework allows to modify the surface tension tensor:

$$p_{\alpha\beta}^\sigma = \frac{\Delta t^3}{2}c_s^4\left(G_1+8G_2\right)\left[\left(\psi\nabla^2\psi + \frac{1}{2}|\vec{\nabla}\psi|^2\right)\delta_{\alpha\beta} - \frac{1}{2}c_s^4\partial_\alpha\psi\partial_\beta\psi\right] \tag{3.131}$$

Li and Lio's scheme

The drawbacks of relying on the second neighbour is the loss of locality, which reduces the LBM scalability. For this reason, Li and Luo [190], then Xu et al. [191] for a 3D framework rather proposed to introduce an additional source term S_i^{Li}

$$S_i^{Li} = Q_{\alpha\beta}\frac{H_{\alpha\beta,i}}{2c_s^4} \tag{3.132}$$

where $Q_{\alpha\beta}$ is a stress tensor in the momentum conservation equation, computed through:

$$Q_{\alpha\beta} = \kappa\frac{G}{2}\psi(\vec{x},t)\sum_i w_i\left(\psi(\vec{x}+\vec{\xi}_\alpha\Delta t, t) - \psi(\vec{x},t)\right)\xi_{\alpha,i}\xi_{\beta,i} \tag{3.133}$$

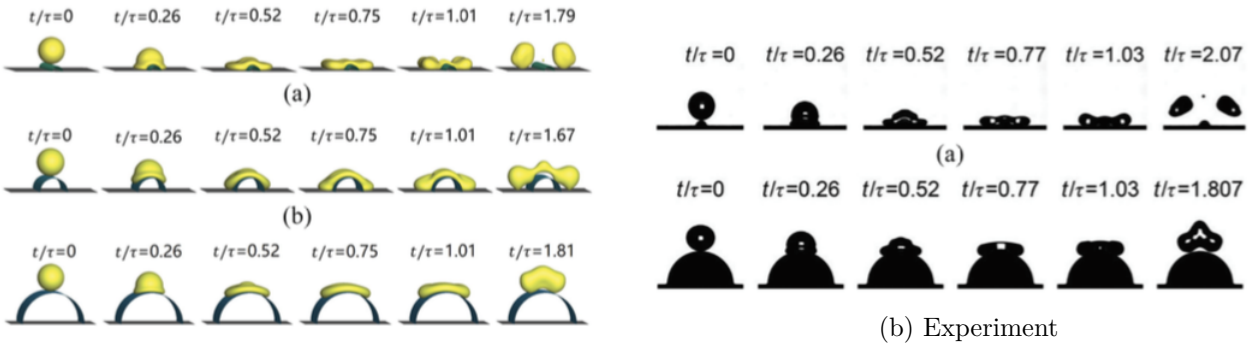
where κ is a free parameter. It can be shown that $Q_{\alpha\beta}$ is equivalent to:

$$Q_{\alpha\beta} = G\kappa c_s^4\frac{\Delta t^2}{4}\psi\left[\partial_\gamma^2\psi\delta_{\alpha\beta} + 2\partial_{\alpha\beta}^2\psi\right] + O(\Delta t^4) \tag{3.134}$$

and is therefore a surface tension tensor. When this source term is used the surface tension tensor $p_{\alpha\beta}^\sigma$ in momentum conservation equation Eq. (3.112) becomes [192]:

$$p_{\alpha\beta}^\sigma = G\frac{c_s^4\Delta t^2}{2}\left(\left[\left(\Delta t - \frac{\kappa}{2}\right)\psi\partial_\gamma^2\psi + \frac{\Delta t}{2}|\partial_\gamma\psi|^2\right]\delta_{\alpha\beta} - (\Delta t-\kappa)\,\partial_\alpha\psi\partial_\beta\psi + \frac{\kappa}{2}\partial_{\alpha\beta}^2\psi^2\right) \tag{3.135}$$

Despite the fact that the present formulation differs from the classical free energy tensor, surface tension can be freely set through setting κ's value. This method allows to significantly improve numerical stability at high density ratio, as shown in Fei et al. [192] who where able to compute bouncing bubbles at density ratio of 1000, as shown in Figure 3.7



(a) Simulation

(b) Experiment

Figure 3.7. – Comparison between a Shan-Chen method and experimentation. Study of the impact of a droplet an a hydrophobic surface. Figure from Fei et al. [192]

3.5. HCZ

Introduced by He, Chang, and Zhang [29] the HCZ model is one of the most widely used in the literature. The particularity of this method is that it describes incompressible flows while most of the other methods describe compressible ones. As for all the previously presented method, the HCZ denomination regroups a wide range of practices. The approach of Fakhari et al. [32] is retained as a reference, and described in this subsection.

3.5.1. Macroscopic equations

The macroscopic equations, consisting in a continuity equation, the momentum conservation equation and the phase field conservation are detailed in this subsection.

Continuity equation

The considered continuity equation writes:

$$\partial_t p + \rho c_s^2 \partial_\alpha u_\alpha = 0 \tag{3.136}$$

For the previous equation to describe an incompressible flow, it must reduce to $\partial_\alpha = 0$, which means that the temporal variation of the pressure term p must be equal to 0: $\partial_t p = 0$. For this model to be relevant, the pressure variation must be kept close from 0, which in practice is not possible since pressure is a function of the phase field which is not constant. For this reason, the pressure term p presented here is only a numerical artifact that won't vary much as soon as the Mach number (Ma) stays low. The non-perfect equation of state and surface tension are both introduced by a chemical potential in the momentum conservation equation.

Momentum conservation equation

The momentum conservation equation writes:

$$\partial_t \rho u_\alpha + \partial_\beta \left(\rho u_\alpha u_\beta + p\delta_{\alpha\beta}\right) = \mu_\phi \partial_\alpha \phi + \partial_\beta \left(\Delta t(\tau - 1/2)\rho c_s^2 \left(\partial_\alpha u_\beta + \partial_\beta u_\alpha\right)\right) \tag{3.137}$$

Where μ_ϕ is the chemical potential introduced in Gurtin et al. [193], allowing to account for non-perfect equation of state and surface tension. The chemical potential is defined by:

$$\mu_\phi = 4\beta\phi(\phi - 1)(\phi - 1/2) - \kappa\partial_\alpha^2 \phi \tag{3.138}$$

As usual, the chemical potential is divided into two counterparts. The first contribution $\phi(\phi - 1)(\phi - 1/2)$ describes the potential in pure phases. It can be noted that $\mu(\phi = 0) = \mu(\phi = 1) = 0$. The last counterpart $-\kappa\partial_\alpha^2\phi$ accounts for surface tension, and corresponds to the classical formulation of the free energy approach.
As previously introduced, the thermodynamical state is entirely described by the potential μ, the pressure only being a numerical artifact allowing incompressibility.

Phase field equation

Finally, the phase field conservation equation follows the Allen-Cahn equation presented by Chiu and Lin [47]:

$$\partial_t \phi + \partial_\alpha \phi u_\alpha = \partial_\alpha \left[M\left(\partial_\alpha \phi - \frac{4\phi(1-\phi)}{W} n_\alpha\right)\right] \tag{3.139}$$

where M is the mobility coefficient defined and W the interface thickness, it was presented in Section 2.2, Eq. (2.42). This equation ensures mass conservation. It is a 2^{nd} order spatial derivative, which is

less expensive to compute than the 4^{th} order spatial derivative Cahn-Hilliard equation.
The total density follows

$$\rho = \rho_L + \phi(\rho_H - \rho_L) \tag{3.140}$$

where ρ_H and ρ_L are the density in each respective phase.

3.5.2. Numerical Scheme

The numerical scheme relies on two particles density functions, g_i allowing to resolve continuity and momentum conservation equations, h_i allowing to resolve the phase field conservation equation. It is furthermore a pressure-based algorithm, which moments follow:

$$\sum_i f_i = p \tag{3.141}$$

$$\sum_i \xi_{\alpha,i} f_i = \rho c_s^2 u_\alpha \tag{3.142}$$

$$\sum_i h_i = \phi \tag{3.143}$$

For notation convenience the function Γ_i is introduced:

$$\Gamma_i = w_i \left[1 + \frac{\xi_{\alpha,i} u_\alpha}{c_s^2} + u_\alpha u_\beta \frac{H_{\alpha\beta,i}}{2c_s^4}\right] \tag{3.144}$$

Its three first moments are given by $\sum_i \Gamma_i = 1$, $\sum_i \xi_{\alpha,i}\Gamma_i = u_\alpha$, $\sum_i \xi_{\alpha,i}\xi_{\beta,i}\Gamma_i = u_\alpha u_\beta$. It can be interpreted as the "classical" equilibrium function divided by the density.

Phase field equation

As proposed by Geier et al. [34], the Allen-Cahn equation is solved through a stream and collide algorithm applied to the distribution h_i. The collision phase is given by:

$$h_i^* = h_i^{eq} + \left(1 - \frac{1}{\tau_\phi}\right)(h_i - h_i^{eq}) \tag{3.145}$$

where τ_ϕ is the relaxation time associated to h_i. It can be shown through a Chapman-Enskog method that τ_ϕ is related to the mobility factor through:

$$M = \Delta t(\tau_\phi + 1/2)c_s^2 \tag{3.146}$$

The equilibrium function introduced in Eq. (3.145) is given by:

$$h_i^{eq} = \phi\Gamma_i + w_i M \frac{4\phi(1-\phi)}{W}\frac{\xi_\alpha n_\alpha}{c_s^2} \tag{3.147}$$

This equilibrium function is divided into two terms. The second one allows to control the interface thickness W through the mobility factor M in the Allen-Cahn equation. The streaming phase is given by:

$$h_i(\vec{x}, t + \Delta t) = h_i^*(\vec{x} - \vec{\xi_i}\Delta t, t) \tag{3.148}$$

This numerical scheme was proposed by Geier et al. [34] and is said to solve the Allen-Cahn equations. As discussed in Appendix B.1, this is not exactly the case.

Hydrodynamic equations

The hydrodynamic pressure-based equations are solved thanks to the distribution function g_i, which follows a stream and collide algorithm. The equilibrium function g_i^{eq} is modified to account for the pressure based scheme, and some correction terms proposed in He et al. [29] and discussed above in Section 3.1.3 are introduced. Collision is given by:

$$g_i^* = g_i^{eq} + \left(1 - \frac{1}{\tau}\right)\left(g_i - g_i^{eq} + \frac{1}{2}S_i\right) \tag{3.149}$$

The equilibrium function g_i^{eq} is given by:

$$g_i^{eq} = \rho\Gamma + (p - \rho c_s^2)w_i \tag{3.150}$$

The source term S_i is given hereinafter:

$$S_i = \Delta t\left[(\Gamma_i - w_i)(\rho_H - \rho_L)c_s^2 + \Gamma_i\mu_\phi\right](\xi_\alpha - u_\alpha)\,\partial_\alpha\phi + \Delta t\Gamma_i(\xi_{\alpha,i} - u_\alpha)F_\alpha \tag{3.151}$$

This source term has two components. The first term, is equivalent to the term introduced in section 3.1.3, and is equal to $(\Gamma_i - w_i)(\xi_\alpha - u_\alpha)\left(\partial_\alpha p - \partial_\alpha\rho c_s^2\right)$. The second part $\Delta t\Gamma_i(\xi_{\alpha,i} - u_\alpha)F_\alpha$ allows to account for a body force F_α, such as gravity for instance. The streaming step remains unchanged and is given by:

$$g_i(\vec{x}, t + \Delta t) = g_i^*(\vec{x} - \vec{\xi_i}\Delta t, t) \tag{3.152}$$

The macroscopic fields account for the source term S_i and F_α through the O^{th} and the 1^{st} moments of g_i:

$$u_\alpha = \frac{1}{\rho c_s^2}\sum_i g_i\xi_{\alpha,i} + \frac{\Delta t\left(\mu_\phi\partial_\alpha\phi + F_\alpha\right)}{2\rho} \tag{3.153}$$

$$p = \sum_i g_i + \frac{\Delta t}{2}\left(\rho_H - \rho_L\right)c_s^2 u_\alpha\partial_\alpha\phi \tag{3.154}$$

The algorithm is summarized in Figure 3.8.

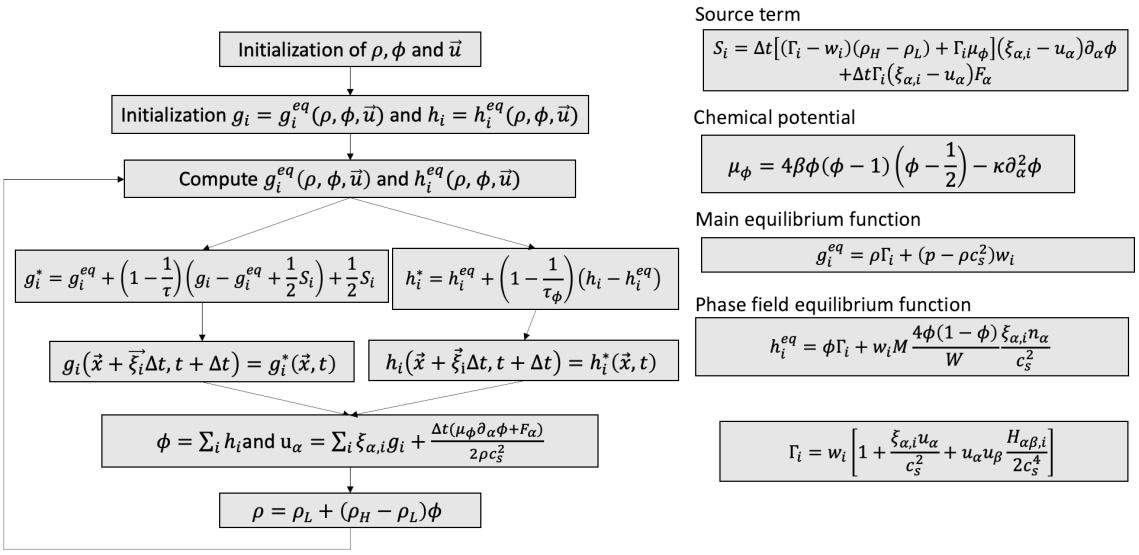


Figure 3.8. – Schematic of the HCZ algorithm from Fakhari et al. [31]

3.5.3. Historical review

This method was first proposed in He, Chen and Zhang [29], and was originally coupled to a Van Der Walls equation of state. It is the first LBM multiphase method stable enough to simulate a Rayleigh-Taylor instability at a Reynold number as high as 2000. Lee and Lin [152] proposed to use high order discretization scheme to compute the phase field gradient, in order to increase numerical stability. It was then proposed by Lee and Fisher [138] to use the chemical potential scheme for setting the equation of state and the surface tension term. Lee and Liu [194][139] proposed a wall boundary condition based on the free energy principles. These last methods were generalised to advanced collision models by Lycett-Brown et al. [195] (for cascaded collision model) and Fakhari and Lee [30] (for MRT collision model). Still in a HCZ framework, Fakhari et al. [31] [196] proposed adaptative mesh refinement for LBM, noting that the Boltzmann equation is solved through a Lax-Wendroff scheme and not through the classical stream and collide algorithm. In a recent work Mitchell et al. [41] proposed a HCZ method adapted to Zu and He's scheme [197].
The work of Premnath and Abraham [198] and Mc Cracken and Abraham [199][200] that generalised Lee and Lin's [152] method to 2D axisymmetric flows must also be underlined. Still in a 2D-axisymmetric flow, the recent work of Mukherjee et al. [39] allows to simulate high Reynolds break up phenomenon at high density ratio. It is in this framework that Lycett-Brown and Luo [195] proposed the cascaded Lattice Boltzmann Method
Among the multiphase LBM methods, HCZ have the best performances in term of numerical stability. For instance, in the work of Mitchel et al. [41], a Rayleigh-Taylor instability could be simulated for a density ratio of 1000 and Reynolds number of 3000, illustrated in Figure 3.9

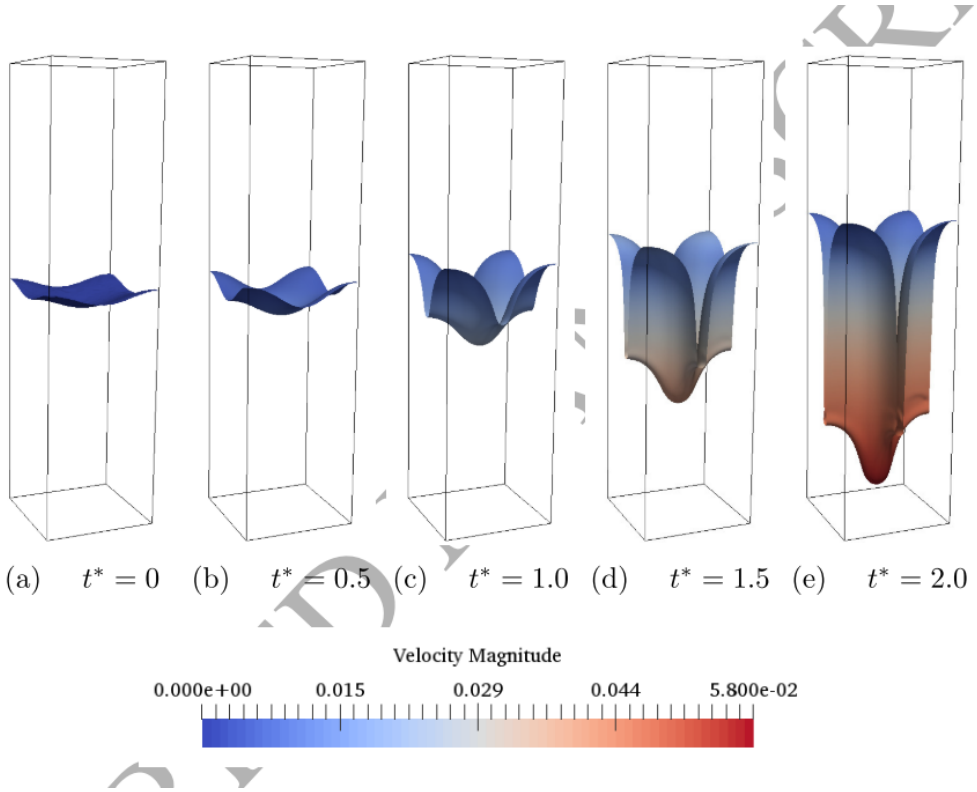


Figure 3.9. – The evolution of the three-dimensional Rayleigh-Taylor instability with density ratio of 1000 and Reynold number of 3000. Figure from [41]

Chapter 4

Taylor expansion of the Lattice Boltzmann

Overview

4.1. Advanced Collision Model . . . **82**
4.1.1. Multiple Relaxation Time . . . 82
4.1.2. Regularized Collision Operators . . . 84
4.1.3. Bulk viscosity and MRT . . . 86
4.2. Body Force in LBM . . . **88**
4.2.1. Body force schemes . . . 88
4.2.2. Body force and MRT schemes . . . 89
4.2.3. Correction terms in LBM . . . 90
4.3. Taylor expansion . . . **91**
4.3.1. $0^{th} order$ . . . 92
4.3.2. $1^{st} order$ . . . 93
4.3.3. $2^{nd} order$ . . . 93
4.3.4. $3^{rd} order$ . . . 94

In the first chapter, the Chapman-Enskog method was introduced. This method allows to recover the equivalent macroscopic equation of the Boltzmann Equation. It shows that if a distribution function is solution of the Boltzmann equation, then its first moments are solution of a Navier-Stokes equations system.
It was demonstrated in Appendix A.3 that the distribution function calculated through the Lattice Boltzmann algorithm is solution of a Boltzmann Equation. Then it comes that LBM only approximates a Boltzmann equation up to a given truncation error, then the Chapman-Enskog method alone doesn't allow to determine the numerical error for the equivalent macroscopic equation. Also, the required approximations allowing the Chapman-Enskog development can be restrictive. For those reasons a new method establishing the equivalent macroscopic equation of the Lattice Boltzmann Method is introduced. It is the method proposed by Dubois [201] relying on the principle of Taylor expansion.
This method is based on the Multiple Relaxation Time approach which is an advanced collision model. For this reason, before proceeding to the presentation of Dubois's method itself, a discussion about advanced collision model will be leaded. In addition, the method is generalized to the case where a body force is introduced in the Lattice Boltzmann framework. For this reason, after the discussion about advanced collision model, a discussion about source term and body forces in Lattice Boltzmann method is proposed.

4.1. Advanced Collision Model

The choice of the collision model One of the most important one is the BGK collision operator:

$$f_i^* = f_i - \frac{1}{\tau}\left(f_i - f_i^{eq}\right) \tag{4.1}$$

It is common to write the collision operator as follow:

$$f_i^* = f_i^{eq} + \left(1 - \frac{1}{\tau}\right)\left(f_i - f_i^{eq}\right) \tag{4.2}$$

But this collision operator suffers from a lack of numerical stability particularly when dealing with high shear stress. More generally speaking, the number of degree of freedom in the lattice Boltzmann method is higher than the number of fields of interest. For instance, in an isothermal D_2Q_9 scheme, the desired moments are the density ρ, the momentum in the x-direction ρu_x and the momentum in the y-direction ρu_y, which leaves 6 remaining degrees of freedom. The consequence is the existence of "ghost modes" which follow their own conservation equation and evolve freely among space. The practical consequence of those "ghost modes" is the appearance of spurious currents that reduces both accuracy and numerical stability.

4.1.1. Multiple Relaxation Time

Proposed by D'Humieres et al. [202], the Multiple Relaxation Time (MRT) approach intends to address this issue. The idea is that any value expressed in the microscopic velocity space can be projected into the moments space through a mathematical projection. For instance, the moments j of the distribution function can be defined as:

$$m_j = \sum_i M_{ji} f_i \tag{4.3}$$

with M the transformation matrix from the population function to the moments function. The choice of the transformation matrix is a subject of discussion in itself, but some choices are often made such

as $M_{0i} = 1$, or $M_{\alpha i} = \xi_{\alpha,i}$, to ensure that $m_0 = \rho$, $m_\alpha = \rho u_\alpha$. By applying the transformation operation to Eq. (4.2) the BGK operator can be expressed in the moments space as:

$$m_j^* = m_j^{eq} + \left(1 - \frac{1}{\tau}\right)\left(m_j - m_j^{eq}\right) \tag{4.4}$$

It is interesting to not that: $m_0^* = m_0^{eq}$ and $m_\alpha^* = m_\alpha^{eq}$
It is a common practice to divide the distribution functions (collided f_i^* and non-collided f_i) into an equilibrium counterpart and a non equilibrium counterpart $f_i = f_i^{eq} + f_i^{neq}$. We see that the contribution of the collision phase to the non-equilibrium part is driven by the relaxation time. But in practice, only the second moments of the non-equilibrium function is interesting (as it is linked with the stress tensor, as discussed in Section 1.2.2, more precisely Eq .(1.48)), but the other moments tend to produce spurious currents. The idea of the Multiple Relaxation Times is to attribute different relaxation times depending with the considered moment. For the moments of interest (i.e. the 2^{nd} order moments) the relaxation time are set in order to match the desired physic, and for the other ones, the relaxation time are set very large to assign a large viscosity to the non-desired moments. It is reminded here that the viscosity is given by: $\nu = \Delta t \rho c_s^2 (\tau - 1/2)$, then viscosity is proportional to the relaxation time. The MRT collision operation becomes:

$$f_i^* = f_i^{eq} + \sum_{jk}\left(M_{ij}^{-1} K_j M_{jk}(f_k - f_k^{eq})\right) \tag{4.5}$$

where M is the change of basis matrix between the microscopic velocities space and the moment space, M^{-1} the inverse of the M matrix and K is a vector that attributes a relaxation time to each moments:

$$K_j = 1 - \frac{1}{\tau_j} \tag{4.6}$$

with τ_j the relaxation time corresponding to the j^{th} moment. The choice of the moments base is crucial and is a subject of discussion in itself, the most obvious choice is to take the Hermite's polynomial moment. If this choice is made, then the matrix M is given by:

$$M_{ji} = H_{j,i} \tag{4.7}$$

Then the j^{th} line of the matrix corresponds to the j^{th} moments. The raw moment matrix is also commonly used. Obviously, an infinite number of bases are possible. D'Humières et al. proposed a matrix constructed through the Gram-Schmidt algorithm [202]. De Rosis, proposed a denser non-orthogonal matrix [203].
A popular MRT variant is the central moments. This type of collision operator intends to tackle the lack of Galilean invariance issue observed for Lattice Boltzmann Method. Always in the same idea of tranposing the collision phase into the moment space, Geier et al. [204] proposed to express the moments as functions of the relative velocity regarding the mean flow, i.e., $\vec{v} = \vec{\xi} - \vec{u}$. For instance, in his original work the raw moments are used but expressed with the relative velocity. Expressed in the more general MRT formalism, it comes that the matrix M also depends with the mean velocity $\vec{u}$ such as:

$$M_{\alpha\beta\gamma,i} = (\xi_{x,i} - u_x)^\alpha (\xi_{y,i} - u_y)^\beta (\xi_{z,i} - u_z)^\gamma \tag{4.8}$$

These models were originally named the cascaded moment method, and allowed to improve stability at high Reynolds numbers. The implementation was originally complex and though difficult to generalise to other physics (such as multiphase flows, compressible flows, etc...) or other schemes. The formulation was simplified by Lycett-Brown and Luo [195] in a multiphase context and then by Dubois et al. in a general framework [205]. This formulation has been shown to be more numerically stable than commonly used MRT model [206]. A last method that relies on the MRT principle, was proposed by Seeger et al. [207] who proposed an approach that relies on the cumulant approach that also showed to be more stable than MRT base schemes based on raw moments [208]

Relaxation times value

In the MRT framework, the value of the higher relaxation times hasn't been discussed so far. It is a usual practice to simply put them at a relatively high value. Anyway, specific values have already been discussed in the literature.
The term $\Lambda = (\tau_{\alpha\beta-1/2})(\tau_{\alpha\beta\gamma} - 1/2)$, where $\tau_{\alpha\beta}$ and $\tau_{\alpha\beta\gamma}$ are relaxation times respectively linked to the Hermite polynomials $H_{\alpha\beta}$ and $H_{\alpha\beta\gamma}$, is called the magic number. It is a common practice to set this number as a constant value, and this value has shown to influence greatly the stability of the simulation [209–212]. It can be shown [209] that setting $\Lambda = 1/12$ allows to suppress a truncation error proportional to Δt^2 making LBM to be accurate up to the third order for steady cases. This method showed to be efficient in a multiphase framework [213]. In practice, the value of $\Lambda = 1/4$ allows a better numerical stability [214].

4.1.2. Regularized Collision Operators

In the mean time, a regularized algorithm was proposed by Latt [215]. The idea is similar to the MRT collision scheme, the non-equilibrium part of the collided population is projected into the moments space. Rather than assigning a relaxation time to every moment, the useful moments (the second order ones) are kept, but higher orders are simply truncated. To do so, the Hermite's polynomial base must be used since it is an orthogonal base. This is possible thanks to the Hermite's polynomial orthogonality property. In this algorithm, the collision step Eq. (4.2) is modified to:

$$f_i^* = f_i^{eq} + \left(1 - \frac{1}{\tau}\right) f_i^{neq} \tag{4.9}$$

with f_i^{neq} the non-equilibrium function. It is calculated by projecting the non-equilibrium part of the population function into the moments space. The non-equilibrium moments are defined through:

$$m_*^{neq} = \sum_i H_{*,i}(f_i - f_i^{eq}) \tag{4.10}$$

The non-equilibrium function is calculated only using moments from the second order in Hermite's polynomial. f_i^{neq} is finally calculated through:

$$f_i^{neq} = \frac{w_i}{2c_s^4} \sum_{\alpha\beta} H_{\alpha\beta,i} m_{\alpha\beta}^{neq} \tag{4.11}$$

where $\sum_{\alpha\beta}$ is the sum over the second order indexes. For instance in D_2Q_9 there are three 2^{nd} order Hermite's polynomials: H_{xy}, H_{xx}, H_{yy}, then the previous equation reads:

$$f_i^{neq} = w_i \left(\frac{H_{xy,i} m_{xy}^{neq}}{c_s^4} + \frac{H_{xx,i} m_{xx}^{neq} + H_{yy,i} m_{yy}^{neq}}{2c_s^4} \right) \tag{4.12}$$

Giving the orthogonality property of the Hermite's polynomials, it comes that the moments of order 3 and 4 of the f^{neq} distribution are equal to 0. It is said that these moments have been regularized. This method increases stability by filtering non-hydrodynamic modes [216]. To summarize, the regularized collision operator is equivalent to a MRT scheme where $\tau_{\alpha\beta} = \tau$ and $\tau_j = 1$ otherwise. The M matrix is formed by the Hermite's polynomial. The regularized collision being a particular case of the MRT, the principal interest to use regularized operator is numerical efficiency. In the MRT scheme all the moment space must be considered while only the 2^{nd} order polynomials can be considered in the regularized approach.

Recursived Regularized collision operator

This model could be improved through a recursive mechanism. The idea of recursivity was introduced by Malaspinas [217]. He pointed out that the successive moments of the equilibrium function follow recursive relationships. If we note $a^{(n)}$ the moments of order n of the equilibrium function, then for $n > 2$ the following relationship is true:

$$m^{eq}_{\alpha_1,\alpha_2...\alpha_n} = m^{eq}_{\alpha_1,\alpha_2...\alpha_{n-1}} u_{\alpha_n} + \left(u_{\alpha_1}...u_{\alpha_{n-2}} m^{eq}_{\alpha_{n-1}\alpha_n} + perm\left(\alpha_n\right) \right) \tag{4.13}$$

where $perm\left(\alpha_n\right)$ stands for all the cyclic index permutations of indexes from α_1 to α_{n-1}. Malaspinas pointed out that both accuracy and numerical stability of a Lattice Boltzmann numerical scheme are related to the recursivity relationships: the more these relationships are verified, the better the performance of the scheme is.
The principle of the recursive regularized operator is to assume that the recursivity relationships are also verified for the non-equilibrium moment, which allows to calculate moments higher than the order 2 with low computational cost. Expressed thanks to the recursive relationship, the 3^{rd} order Hermite polynomial reads:

$$m^{neq}_{\alpha\alpha\beta} = 2u_\alpha m^{neq}_{\alpha\beta} + u_\beta m^{neq}_{\alpha\alpha} \tag{4.14}$$

Then the non-equilibrium function is given by:

$$f^{neq}_i = w_i \left(\sum_{\alpha\beta} \frac{H_{\alpha\beta}}{2c_s^4} m^{neq}_{\alpha\beta} + \sum_{\alpha\beta\gamma} \frac{H_{\alpha\beta\gamma}}{6c_s^6} a^{neq}_{\alpha\beta\gamma} \right) \tag{4.15}$$

with $\sum_{\alpha\beta\gamma}$ being the sum on all the 3^{rd} order Hermite polynomials. For instance, in D_2Q_9 the 3^{rd} order Hermite polynomial are: H_{xxy}, H_{xxx}, H_{yyx}, H_{yyy}. Remember that this methods is limited by the number of microscopic velocities that are used. In particular, in the most commonly used velocity sets (D_2Q_9, D_3Q_{19} and D_3Q_{27}) the moments linked to the polynomial $H_{\alpha\alpha\alpha}$ (α being a direction of space) cannot be calculated as discussed in Section 1.3.2. When the regularized operator is coupled with the recursive approach, this new collision operator is refereed to as RR.

Hybrid Recursived Regularized collision operator

Finally, an other mechanism can be added to the RR collision operator [218]. In practice, the 2^{nd} order non-equilibrium distribution function is linked with the stress tensor as discussed in Section 1.2.2. Then there are two ways to calculate the non-equilibrium function, the first one is the one proposed earlier (Eq. (4.10)) and the other one consists in calculating the stress tensor:

$$m^{FD,neq}_{\alpha\beta} = \rho c_s^2 \tau \left(\partial_\alpha u_\beta + \partial_\beta u_\alpha \right) \tag{4.16}$$

with the spatial derivative terms calculated through a finite difference scheme. In the Hybrid Regularized Recursive (HRR) scheme, the 2^{nd} order non-equilibrium moment is calculated by a combination of the two approaches:

$$m^{neq}_{\alpha\beta} = \sigma_{HRR} m^{LBM,neq}_{\alpha\beta} + (1 - \sigma_{HRR}) m^{FD,neq}_{\alpha\beta} \tag{4.17}$$

where $m^{LBM,neq}_{\alpha\beta}$ is the non equilibrium moment calculated through Eq. (4.10), and σ_{HRR} is a real number which value is included between 0 and 1. The value of σ_{HRR} corresponds to the rate of the non-equilibrium moment that will come from the finite difference scheme or from the LBM scheme. For example, if σ_{HRR} is equal to 1, then the HRR scheme is strictly equivalent to the RR one, and when σ_{HRR} is equal to 0, the non-equilibrium part of the distribution function is fully calculated

through the Finite Difference scheme. This approach allows to introduce a small amount of numerical dissipation through the Finite Difference, which improves the numerical stability. Common values for σ_{HRR} are $\sigma_{HRR} = 0.98$ to 0.99. This collision operator increases greatly LBM numerical stability, allowing the method to cover a large range of applications, such as aeroacoustic [219] or compressible flows [220].

4.1.3. Bulk viscosity and MRT

A major property of the MRT-like (including regularized) collision operator is the capability to freely set bulk viscosity. The general form of the stress tensor is given by:

$$\mu \left(\partial_\alpha u_\beta + \partial_\beta u_\alpha\right) + \left(\mu_b - \frac{2}{D}\mu\right) \partial_\gamma u_\gamma \tag{4.18}$$

with D the dimension of the system. As discussed in Section 1.2.2, in the classic BGK athermal framework, $\mu = \mu_b$ (Eq. (1.57)), and in the thermal framework $\mu_b = 0$ (Eq. (1.51)). In a MRT athermal framework, it is possible to freely set the bulk viscosity. The present method will be illustrated in a D_2Q_9 framework for a better comprehension. The common practice is to set a similar relaxation time for all the second order polynomials (in D_2Q_9 H_{xx}, H_{yy} and H_{xy}), that are linked to the value of the dynamic viscosity. It must be noted that the 2^{nd} order Hermite polynomials form a partition of the polynomial space and that $\{H_{xx}, H_{yy}, H_{xy}\}$ is a base of this sub-space. To freely set the bulk viscosity, an alternative rotated base must be used: $\{H_{xy}, \frac{H_{xx}+H_{yy}}{2}, \frac{H_{xx}-H_{yy}}{2}\}$. A relaxation time is attributed to H_{xy} and $\frac{H_{xx}-H_{yy}}{2}$ (noted τ_ν) and a second relaxation time to $\frac{H_{xx}+H_{yy}}{2}$ (noted τ_b). For example, in a regularized framework, the collision operator writes

$$f_i^* = f_i^{eq} + w_i \left[\left(1 - \frac{1}{\tau_\nu}\right)\left(\frac{H_{xy,i}}{c_s^4} m_{xy}^{neq} + \frac{H_{xx,i} - H_{yy,i}}{2c_s^4} m_\nu^{neq}\right) + \left(1 - \frac{1}{\tau_b}\right) \frac{H_{xx,i} + H_{yy,i}}{2c_s^4} m_b^{neq}\right] \tag{4.19}$$

with $m_b^{neq} = \sum_i (f_i - f_i^{eq}) \frac{H_{xx,i} + H_{yy,i}}{2}$ and $m_\nu^{neq} = \sum_i (f_i - f_i^{eq}) \frac{H_{xx,i} - H_{yy,i}}{2}$ and $m_{xy}^{neq} = \sum_i (f_i - f_i^{eq}) H_{xy,i}$. It can be shown than the equivalent macroscopic equation is given as follow:

$$\partial_t \rho u_\alpha + \partial_\beta \left(\rho u_\alpha u_\beta + \rho c_s^2 \delta_{\alpha\beta}\right) = \partial_\beta \left(\rho c_s^2 (\tau_\nu - 1/2) \left(\partial_\alpha u_\beta + \partial_\beta u_\alpha\right) + \rho c_s^2 (\tau_b - \tau_\nu) \partial_\gamma u_\gamma\right) \tag{4.20}$$

In this framework, the bulk dynamic viscosity is given by $\mu_b = \rho c_s^2 (\tau_b - 1/2)$ and the shear dynamic viscosity is given by $\mu_\nu = \rho c_s^2 (\tau_\nu - 1/2)$.

Traceless operator

In the standard LBM, bulk viscosity is equal to the shear viscosity through $\nu_b = \nu$, but in practice the bulk viscosity is often equal to 0. It has been shown that it is the case in the mono atomic case, but this is also the case for commonly found gas (air for example). The Stokes assumption that consists in assuming that $\nu_b = 0$ is a common assumption. Two different ways to set $\nu_b = 0$ are addressed in this paragraph. The first way would be to use the base presented in this section and to impose $\tau_b = 1/2$. Another method to set bulk viscosity equal to zero was presented by Farag et al. [162]. The idea consists in regularizing the moment linked to $\frac{H_{xx,i} + H_{yy,i}}{2}$. To do so, a smart step is added to the classical regularization process. The 2^{nd} order non-equilibrium moments are first calculated through Eq. (4.10). (For instance $m_{xx}^{neq} = \sum_i H_{xx,i}(f_i - f_i^{eq})$), and then the diagonal moments are modified through:

$$m_{\alpha\beta}^{neq,*} = m_{\alpha\beta}^{neq} - \frac{1}{D} m_{\gamma\gamma}^{neq} \delta_{\alpha\beta} \tag{4.21}$$

D being the dimension of the system. The non-equilibrium distribution function is then calculated thanks to this edited moments: $f_i^{neq,*} = \sum_{\alpha\beta} \frac{w_i}{2c_s^4} H_{\alpha\beta} m_{\alpha\beta}^{neq,*}$. It can be shown that $\sum_i f_i^{neq,*} H_{xy,i} = \sum_i f_i^{neq} H_{xy,i}$, $\sum_i f_i^{neq,*} \frac{H_{xx,i} - H_{yy,i}}{2} = \sum_i f_i^{neq} \frac{H_{xx,i} - H_{yy,i}}{2}$, and $f_i^{neq,*} \frac{H_{xx,i} + H_{yy,i}}{2} = 0$. This shows that the moment linked to $\frac{H_{xx} + H_{yy}}{2}$ has been correctly regularized as desired. it must be recalled that the regularization of a given moment is equivalent to set the relaxation time associated to its moment to 1 in a MRT process, then the traceless operator is equivalent to setting the bulk dynamic viscosity to $\mu_b = \rho c_s^2 \frac{\Delta t}{2}$, which is not equal to 0. In practice, a corrective term is added in order to get rid of this spurious bulk viscosity induced by this scheme.

4.2. Body Force in LBM

4.2.1. Body force schemes

Including a source term in the Boltzmann equation allows to widen the range of applicability of LBM, considering for example mass production, body force, gravity, or adding an eventual correction term. More specifically in the multiphase framework, surface tension can be modeled through a body force [135]. This was originally present in the Boltzmann work, since a term taking into account a body force $\vec{F}$ can be included:

$$\partial_t f + \xi_\alpha \partial_\alpha f + F_\alpha \frac{\partial f}{\partial \xi_\alpha} = \Omega \tag{4.22}$$

In practice, several schemes were originally proposed to transpose this scheme into a LBM framework. Different schemes proposed through out the literature are presented here.

Shan and Chen scheme

One of the first method was proposed by Shan and Chen in a multiphase framework [26], and consists in modifying the velocity used to calculate the equilibrium function (Eq. (1.80)). The equilibrium function is calculated using the following velocity:

$$u_\alpha^{eq} = u_\alpha + \frac{F_\alpha \tau}{\rho} \tag{4.23}$$

An important behaviour common to most of the methods intending to include a body force is that it modifies the value of the 1^{st} order of the distribution function. As pointed out by Shan and Doolen [221], the first order moment writes:

$$\sum_i f_i \xi_{\alpha,i} = \rho u_\alpha - \frac{\Delta t F_\alpha}{2} \tag{4.24}$$

Which modifies the way velocity is calculated. Even if this method is the first that has been proposed, it is barely used in practice. Two other ones are much more popular and are still used nowadays.

He's scheme

The first one was proposed by He et al. [53], then it is refereed as "He's scheme". In this one, the term $F_\alpha \frac{\partial f}{\partial \xi_\alpha}$ of Eq. (4.22) that allows to introduce a force term in the Boltzmann equation is used. In this scheme, it is assumed that:

$$\frac{\partial f}{\partial \xi_\alpha} \approx \frac{\partial f^{eq}}{\partial \xi_\alpha} = -\frac{\xi_\alpha - u_\alpha}{c_s^2} f^{eq} \tag{4.25}$$

Previous equality was obtained by assuming the equilibrium function is equal to the Maxwell-Boltzmann distribution given in Eq. (A.15). As the formulation of f^{eq} is known, a source term introducing a body force can be introduced. In a BGK framework, the collision step is modified to:

$$f_i^* = f_i - \frac{1}{\tau}(f_i - f_i^{eq}) + S_i \tag{4.26}$$

with

$$S_i = \left(1 - \frac{1}{2\tau}\right) F_\alpha \frac{(\xi_{\alpha,i} - u_\alpha)}{c_s^2} f_i^{eq} \tag{4.27}$$

Similarly as the Shan and Chen scheme, the velocity should be calculated through

$$u_\alpha = \frac{\sum_i f_i \xi_{\alpha,i}}{\rho} + \frac{F_\alpha \Delta t}{2\rho} \tag{4.28}$$

Guo's scheme

The second scheme often used in the literature was first introduced by Ladd and Verberg [222] and then improved by Guo [148]. It is often refereed as "Guo's scheme". In this approach, the forcing term is formed by an expansion in a power series in the particle velocity:

$$S_i = w_i \left(1 - \frac{1}{2\tau}\right) \left[\frac{\xi_{\alpha,i} - u_\alpha}{c_s^2} + \frac{\xi_{\alpha,i}\xi_{\beta,i}u_\beta}{c_s^4}\right] F_\alpha \tag{4.29}$$

w_i being the coefficients introduced in Section 1.3.2. Similarly as for the He's scheme, the first moments of the distribution function are modified. The difference between Guo's and He's scheme relies in the moments of order higher than 2. At this point it is interesting to give the moments of the S_i terms:

$$\begin{aligned} \sum_i S_i &= 0 \\ \sum_i \xi_{\alpha,i} S_i &= F_\alpha \\ \sum_i \xi_{\alpha,i}\xi_{\beta,i} S_i &= u_\alpha F_\beta + u_\beta F_\alpha \end{aligned} \tag{4.30}$$

It could be shown through a Chapman-Enskog method or a Taylor expansion that the value of the 2^{nd} order moment given here must take this form to correct an error appearing in the stress tensor otherwise.

4.2.2. Body force and MRT schemes

It should be noted that when using a MRT or regularized collision model, both the formulation of those schemes and the formulation of the source term must be modified. First of all, it can be seen that in both Guo's and He's scheme, the relaxation time is involved in the formulation. In the MRT case, relaxation time is no longer unique to all moments. This is taken into account by changing the formulation of the source term, and removing the relaxation term's contribution. For example the Guo's source term becomes:

$$S_i = w_i \left[\frac{\xi_{\alpha,i} - u_\alpha}{c_s^2} + \frac{\xi_{\alpha,i}\xi_{\beta,i}u_\beta}{c_s^4}\right] F_\alpha \tag{4.31}$$

The expression of the collision term is also modified. The MRT collision term becomes:

$$m_j^* = m_j^{eq} + (1 - 1/\tau_j)\left(m_j - m_j^{eq} + 0.5\sum_i M_{ji}S_i\right) + 0.5\sum_i M_{ji}S_i \tag{4.32}$$

Similarly in the recursive collision model, the expression of the non-equilibrium function is also modified, and it becomes:

$$m_*^{neq} = \sum_i H_{*,i}(f_i - f_i^{eq} + 0.5S_i) \tag{4.33}$$

To understand this, we have shown in Section 1.3 that the distribution function f_i is actually not solution of the Boltzmann equation, but the function $\bar{f}_i = f_i - \frac{1}{2\tau}(f_i - f_i^{eq})$ is. Similarly, when introducing a source term, it is the population defined by $\tilde{f}_i = f_i - \frac{1}{2\tau}\Omega_i - \frac{\Delta t S_i}{2}$ that is solution of the equation:

$$\partial_t \tilde{f}_i + \xi_\alpha \partial_\alpha \tilde{f}_i = -\frac{1}{\tau - 1/2}\left(\tilde{f}_i - f_i^{eq}\right) + S_i \tag{4.34}$$

As a consequence, the macroscopic velocity solution of the Navier-Stokes equation is the first order moment of $\tilde{f}_i$. For this reason:

$$\rho u_\alpha = \sum_i \tilde{f}_i = \sum_i \xi_{\alpha,i}\left(f_i + \frac{\Delta t S_i}{2}\right) = \sum_i \xi_{\alpha,i} f_i + \frac{\Delta t F_\alpha}{2} \tag{4.35}$$

4.2.3. Correction terms in LBM

It has been pointed out that for the most commonly used velocity sets (i.e. D_2Q_9, D_3Q_{19} or D_3Q_{27}) the number of degrees of freedom is too low to allow a perfect prediction of the Navier-Stokes equations to the order 2. For instance, in D_2Q_9 for a "classic" LBM scheme, a Mach cubed error appears, taking the form:

$$Er_{\alpha}^{Mach} = -\partial_{\beta}\partial_{\gamma}\rho u_{\alpha}u_{\beta}u_{\gamma} \tag{4.36}$$

As this term takes the form of two successive spatial derivative, it can also be interpreted as a pressure tensor. This spurious pressure term can be defined:

$$p_{\alpha\beta}^{Mach} = \partial_{\gamma}\rho u_{\alpha}u_{\beta}u_{\gamma} \tag{4.37}$$

A corrective pressure can be introduced through a source term, equals to the opposite of this error term. The spatial derivative terms can be calculated through a finite difference scheme. It can be shown through a Taylor expansion that to introduce a pressure tensor, the corrective source term $S_{er,i}$ should have the following moments:

$$\begin{aligned} \sum_i S_{er,i} &= 0 \\ \sum_i \xi_{\alpha} S_{er,i} &= 0 \\ \sum_i \xi_{\alpha}\xi_{\beta} S_{er,i} &= p_{\alpha\beta}^{Mach} \end{aligned} \tag{4.38}$$

To obtain such an error term, one can simply project it into the Hermite polynomial space, like:

$$S_{er,i} = p_{\alpha\beta}^{Mach}\frac{H_{\alpha\beta,i}}{2c_s^4} \tag{4.39}$$

This strategy has been presented for the Mach error, but it can be generalised to any spurious term.

4.3. Taylor expansion

In Section 1.2.2, we showed how to recover the macroscopic equation solved by the moments of a distribution function whose behavior is described by the Boltzmann equation. As it has been shown that the distribution function f_i calculated through a Lattice Boltzmann Method is solution of a Boltzmann Equation to the 2^{nd} order in Δt, the Chapman-Enskog method shows that the moments of f_i are also solution of a Navier-Stokes system. But this approach has two major drawbacks. First of all, f_i is solution of a Boltzmann equation only up to the order Δt^2, the higher-order errors cannot be determined. Furthermore, the Chapman-Enskog method itself has theoretical weaknesses. As pointed out by Farag et al. [162], the hypothesis that $\iiint f^{(n)} d\vec{\xi} = \iiint \xi_\alpha f^{(n)} d\vec{\xi} = 0$ for $n > 0$ is a strong hypothesis. On another hand, the hypothesis of the existence of two time scales is also a limiting hypothesis. For theses two reasons, there is a real need for another method allowing to determine the equivalent equation of the Lattice Boltzmann Method.
For this reason, methods based on the Taylor expansion were proposed in order to obtain the equivalent macroscopic equation of the LB method. The first one was proposed by Holdych [223] that could recover the same macroscopic equations obtained through the Chapman-Enskog method. The default of this approach is that similarly as the Chapman-Enskog method, this demonstration relies on the hypothesis that two different time scales exist. Later Dubois [201] proposed a method that allow to determine properly the equivalent equation of the Lattice Boltzmann algorithm up to the order 3. It allows to determine the equation solved by the moments of the population f_i. This development is presented here.
As this development takes place in a Multiple Relaxation Time (MRT) framework, the moments m_j of the distribution function f_i are defined as

$$\sum_i M_{ji} f_i = m_j \tag{4.40}$$

with M the transformation matrix from the population function basis to the moments function basis. To fit the MRT formalism, a specific relaxation time must also be attributed to each moment. In the method presented in the main text, a regularized collision model is used which can be translated in a MRT framework. An example of matrix M, based on a Hermite polynomial based is proposed here:

$$M_{\alpha,i} = H_{\alpha,i} \tag{4.41}$$
$$M_{\alpha\beta,i} = H_{\alpha\beta,i} \tag{4.42}$$
$$M_{\alpha\beta\gamma,i} = H_{\alpha\beta\gamma,i} \tag{4.43}$$
$$M_{\alpha\beta\gamma\mu,i} = H_{\alpha\beta\gamma\mu,i} \tag{4.44}$$

Relaxation times must be attributed to each moments. For instance in the regularized framework, this comes as: $\tau_{xy} = \tau_\nu$ (linked with the shear viscosity), τ_b is linked with the bulk viscosity and other relaxation times are set to 1, i.e.: $\tau_0 = \tau_\alpha = \tau_{\alpha\beta\gamma} = \tau_{\alpha\beta\gamma\mu} = 1$. The inverse-matrix of M is noted M^{-1}. It respects that:

$$f_i = \sum_i M^{-1}_{ij} m_j \tag{4.45}$$

For the sake of clarity, the Lattice-Boltzmann algorithm is reminded and adapted to the MRT formalism. The population at the time $t + 1$ is calculated from the collided function through the streaming step:
Streaming step

$$f_i(x, t + \Delta t) = f_i^*(x - \xi_i \Delta t, t) \tag{4.46}$$

where f_i^* is the population function obtained after collision. It is calculated from the collided moments through: $f_i^* = \sum_i M_{ij}^{-1} m_j$. The moments m_j^* are obtained through the collision step: Collision step:

$$m_j^* = m_j^{eq} + (1 - \frac{1}{\tau_j}) \left(m_j - m_j^{eq} + \frac{1}{2} S_j \right) + \frac{1}{2} S_j \tag{4.47}$$

where m_j^{eq} is the j^{th} moment of the equilibrium function and S_j is the j^{th} moment of the source term. In agreement with Dubois's [201], the following tensors are defined:

$$\Lambda_{j,\alpha}^k = \sum_i M_{ji} \xi_{\alpha,i} M_{ik}^{-1} \tag{4.48}$$

$$\Lambda_{j,\alpha\beta}^k = \sum_i M_{ji} \xi_{\alpha,i} \xi_{\beta,i} M_{ik}^{-1} \tag{4.49}$$

$$\Lambda_{j,\alpha\beta\gamma}^k = \sum_i M_{ji} \xi_{\alpha,i} \xi_{\beta,i} \xi_{\gamma,i} M_{ik}^{-1} \tag{4.50}$$

These polynomials allow to characterise the base M. For instance, $\Lambda_{j,\alpha}^k$ is the projection of the polynomial M_j multiplied by ξ_α in the base M_k. For instance, $M_{0i} = 1$, then $M_{0i}\xi_{\alpha,i} = \xi_{\alpha,i}$. The proposed base M is orthogonal and it happens that $\xi_\alpha = M_\alpha$, then $\Lambda_{j,\alpha}^k = \delta_{\alpha k}$. In the original work, a source term introducing a body force was not considered. In order to make this development slightly more general, a body force introduced through a Guo's scheme [148] is added. It was underlined in Section 4.2 that when a body force is introduced through a Guo's scheme, the calculation of the momentum is modified, since the first moment of the population f_i is given by: $m_\alpha = \rho u_\alpha - \frac{\Delta t}{2} F_\alpha$. The justification for this relationship is demonstrated in the present work.
The last useful notation used in this section is:

$$\Pi_j^{eq} = \partial_t \left(m_j^{eq} + (\tau_j - 1/2) S_j \right) + \partial_\alpha \sum_k \left(\Lambda_{j,\alpha}^k \left(m_k^{eq} + (\tau_k - 1/2) S_k \right) \right) \tag{4.51}$$

It can be shown that this term corresponds to the moments of the non-equilibrium part of the population function: $f_i - f_i^{eq}$. Also, it can be shown that $\Pi_{\alpha\beta}^{eq}$ is the stress tensor.
Similarly as in the Chapman-Enskog method, equivalent macroscopic equation are calculated through a recursive approach, it means that in order to determine the equivalent macroscopic equation at the order Δ^n, the knowledge of the equivalent macroscopic equation at the order Δt^{n-1} is necessary. The equivalent macroscopic equation are given order by order, but the detail of the calculation are available in appendix.

4.3.1. 0^{th} *order*

By developing (4.47) and (4.46), 0^{th} order equations can be obtained. It can be shown that up to the order 1 in Δt the moments m_j and the collided moments m_j^* are equivalent:

$$m_j = m_j^* + O(\Delta t) \tag{4.52}$$

Similarly, m_j and m_j^{eq} are showed to be related through:

$$m_j = m_j^{eq} + \left(\tau_j - \frac{1}{2} \right) S_j + O(\Delta t) \tag{4.53}$$

Through the Chapman-Enskog method the following relationship was obtained: $f_i = f_i^{eq} + O(Kn)$. It appears that the development in Δt in the present approach is very similar to the development in Knudsen number in the Chapman-Enskog approach.

4.3.2. $1^{st} order$

The collision and streaming equations (4.47)(4.46) can then be developed to the order 1 in Δt. Similarly as in the Chapman-Enskog method, the lower order equations C.17 are necessary to obtain an equivalent macroscopic equation. Similarly as the Chapman-Enskog method, two equations can be obtained. One for the mass conservation (the moment m_0) and one for momentum (the 1^{st} order moment m_α). The mass conservation equation is given by:

$$\partial_t m_0 + \partial_\alpha m_\alpha^{eq} = O(\Delta t) \tag{4.54}$$

The momentum conservation equation is given by:

$$\partial_t m_\alpha + \partial_\beta \left(m_{\alpha\beta}^{eq} + c_s^2 m_0^{eq} \delta_{\alpha\beta} \right) = F_\alpha + O(\Delta t) \tag{4.55}$$

It can be seen that LBM solves an Euler system up to the order Δt. The present equation system corresponds to the system obtained at the order 1 in Knudsen number through the Chapman-Enskog method.
Similarly as in the Chapman-Enskog method, the knowledge of the non-equilibrium part of the moments is necessary. It is given by the following formula:

$$m_j = m_j^{eq} + (\tau_j - 1/2) S_j - \Delta t \tau_j \left(\partial_t m_j^{eq} + \partial_\alpha \left(\sum_k \Lambda_{j,\alpha}^k m_k^{eq} \right) \right) + O(\Delta t^2) \tag{4.56}$$

It can be seen that the non-equilibrium part of the population function is linked with the temporal and spatial derivative of the equilibrium moments.

4.3.3. $2^{nd} order$

It can be shown, that up to the order 2, the Lattice Boltzmann scheme is equivalent to the following system:

$$\partial_t m_0 + \partial_\alpha m_\alpha^{eq} = O(\Delta t^2) \tag{4.57}$$

The first thing to notice, is that if $m_0 = \rho$ and $m_\alpha^{eq} = \rho u_\alpha$, then the mass conservation equation is retrieved up to the order 2. A similar result can be obtained through a Chapman-Enskog method.
The momentum conservation equation is given by:

$$\partial_t \left(m_\alpha + \frac{\Delta t}{2} F_\alpha \right) + \partial_\beta \left(m_{\alpha\beta}^{eq} + m_0^{eq} c_s^2 \delta_{\alpha\beta} + (\tau_{\alpha\beta} - 1/2) S_{\alpha\beta} \right) = \Delta t (\tau_{\alpha\beta} - 1/2) \Pi_{\alpha\beta}^{eq} + F_\alpha + O(\Delta t^2) \tag{4.58}$$

A first thing to notice, is that the term in the temporal derivative is $m_\alpha + \frac{\Delta t}{2} F_\alpha$. Then in order to retrieve the Navier-Stokes momentum conservation equation, the f_i 1^{st} moment must respect $\rho u_\alpha = m_\alpha + \frac{\Delta t}{2} F_\alpha$, which is the relationship that was introduced in the body force Section 4.2. In the present work, this relationship could be retrieved "a priori".
It can be shown that $S_j = O(\Delta t)$ (discussed in Appendix C.1), the consequence is that:

$$\Pi_{\alpha\beta}^{eq} = \partial_t m_{\alpha\beta}^{eq} + \partial_\gamma \sum_k \left(\Lambda_{j,\alpha}^k m_k^{eq} \right) + O(\Delta t) \tag{4.59}$$

The previous expression is base dependant, using the base M proposed in example (which is the Hermite's polynomial base) it becomes:

$$\Pi_{\alpha\beta}^{eq} = \partial_t m_{\alpha\beta}^{eq} + \partial_\gamma \left(m_{\alpha\beta\gamma}^{eq} + c_s^2 \left(m_\alpha^{eq} \delta_{\beta\gamma} + m_\beta^{eq} \delta_{\alpha\gamma} \right) \right) \tag{4.60}$$

which is similar to what is obtained through a Chapman-Enskog method.
The current Taylor expansion showed how a Lattice Boltzmann method allows to solve a Navier-Stokes system.
The current determination of the equivalent macroscopic equation process can be extended to the order 3, allowing to know the numerical errors implied by the LBM scheme. Similarly as previously, the knowledge of the development of m_j up to Δt^3 is necessary:

$$m_j^* = m_j^{eq} + (\tau_j - 1/2)S_j - \Delta t\,(\tau_j - 1)\,\Pi_j^{eq} \\ - \Delta t^2\,(\tau_j - 1)\left((\tau_j - 1/2)\partial_t \Pi_j^{eq} + \partial_\alpha \sum_k (\tau_k - 1/2)\Lambda_{j,\alpha}^k \Pi_k^{eq}\right) + O(\Delta t^3) \quad (4.61)$$

4.3.4. $3^{rd}order$

Finally, the Δt^2 error can be determined for the mass conservation equation:

$$\partial_t m_0 + \partial_\alpha m_\alpha^{eq} = \Delta t^2 \partial_\alpha \left(\frac{1}{12}\partial_\beta \Pi_{\alpha\beta}^{eq} - \frac{1}{6}\partial_t F_\alpha\right) + O(\Delta t)^3 \quad (4.62)$$

It comes from the last equation that the Δt^2 error for the mass conservation equation is proportional to $\Pi_{\alpha\beta}^{eq}$ which corresponds to the stress tensor. It is also proportional to the time derivative of the body force. For the momentum conservation equation, up to the order three it is given by:

$$\partial_t \left(m_\alpha + \frac{\Delta t}{2}F_\alpha\right) + \partial_\beta \left(m_{\alpha\beta}^{eq} + m_0^{eq} c_s^2 \delta_{\alpha\beta} + (\tau_{\alpha\beta} - 1/2)\,S_{\alpha\beta}\right) \\ = \Delta t(\tau_{\alpha\beta} - 1/2)\Pi_{\alpha\beta}^{eq} + F_\alpha \\ + \Delta t^2 \partial_\beta \left[\left(\left[\tau_{\alpha\beta} - \frac{1}{2}\right]^2 - \frac{1}{6}\right)\partial_t \Pi_{\alpha\beta}^{eq} + \left(\left[\tau_{\alpha\beta\gamma} - \frac{1}{2}\right]\left[\tau_{\alpha\beta} - \frac{1}{2}\right] - \frac{1}{12}\right)\partial_\gamma \Pi_{\alpha\beta\gamma}^{eq}\right] \\ - \frac{\Delta t^2}{6}\left[\partial_t^2 F_\alpha + c_s^2 \partial_{\beta\gamma}\left(F_\alpha \delta_{\beta\gamma} + F_\beta \delta_{\alpha\gamma} + F_\gamma \delta_{\alpha\beta}\right)\right] + O(\Delta t^3) \quad (4.63)$$

The Δt^2 error has three counterparts. One is equal to the temporal derivative of the stress tensor $\partial_t \Pi_{\alpha\beta}^{eq}$, one is equal to the spatial derivative of the third moments of the non-equilibrium distribution, and the last one is a composition of derivatives of the body force.
As it was already discussed, the second component of the Δt^2 error can be cancelled. As it is proportional to the so-called magic number [210], this error term can be cancelled by choosing:

$$\tau_{\alpha\beta\gamma} = 1/2 + \frac{1}{12\tau_{\alpha\beta} - 6} \quad (4.64)$$

Chapter 5

Colour Gradient algorithm theoretical analysis

Overview

5.1. Algorithm reformulation 96
5.2. Equation of State Operator 99
5.2.1. Discussion 99
5.2.2. Numerical illustration 103
5.3. Recoloration equivalent phase field equation 105
5.3.1. Discussion 105
5.3.2. Numerical illustration 106

Among the presented Lattice Boltzmann methods, HCZ methods showed the best qualities in term of numerical stability and application range. Unfortunately, such methods take place in an incompressible framework, which limits their interest for fuel atomization in aeroengines. In particular, acoustics waves are known to influence greatly the atomization process [7, 8, 224–227] in break up jet cases. For this reason, the need for a compressible multiphase simulation method is strong. In addition, thermal effects are also of paramount importance when dealing with injector applications. For this reason, there is also a need for a numerical scheme able to include non-perfect equation of state.
Among the Lattice Boltzmann methods described in Chapter 3, pseudo-potential methods and free-energy methods fulfill these conditions since they allow to introduce an equation of state, and belong to compressible methods. They can moreover be generalized to thermal flows. For the pseudo-potential method, it could be an interesting subject of investigation to transpose methods such as the one proposed by Pelletier et al. [120, 127] in a pseudo-potential framework. The generalization to free-energy method to has already been investigated by Verdier et al. [228].
On the other hand, adding a non-perfect equation of state in the colour-gradient framework is not straightforward. As pointed out in Section 3.2, the equation of state generally used in colour-gradient methods induces spurious compressible phenomena. Another drawback of the colour gradient method is the fact that the equivalent phase field equation is not known, which limits its generalization to other physics.
In this chapter, an analysis of the colour gradient algorithm is proposed. A link between these methods and phase-field methods (presented in Section 2.2.1) is also proposed. Also, in this chapter, it is proposed that color gradient equilibrium function is similar to Pooley's equilibrium scheme [156]. Pooley et al. [156] proposed their equilibrium scheme based on an empirical argument. They pointed out that this precise scheme allows to minimize spurious currents in the interface. In this chapter, a theoretical argument is added to justify this mechanism. It is demonstrated that the discussed operator maximizes the degree of isotropy, eliminating an error proportional to Δt^2.
Finally, based on Dubois's work [201], an equivalent equation for the recoloration phase is proposed. It is shown how the color-gradient algorithm allows to solve a Chiu and Lin [47] phase field equation.

5.1. Algorithm reformulation

As described in Section 3.2, in colour gradient the fluid is described thanks to two populations R_i and B_i corresponding to a red phase and a blue phase [159]. Their 0^{th} moment corresponds to the density of each phase, then if we note Y_1 and Y_2 the red and blue mass fraction respectively, it comes:

$$\sum_i R_i = \rho Y_1 \quad \text{and} \quad \sum_i B_i = \rho Y_2 \tag{5.1}$$

It is proposed to consider two populations f_i and g_i such as:

$$f_i = R_i + B_i \; and \; g_i = R_i - B_i \tag{5.2}$$

which are linked to the total mass ρ, the phase field ϕ and the total momentum $\rho\vec{u}$ through:

$$\sum_i f_i = \rho \; and \; \sum_i f_i \xi_\alpha u_\alpha = \rho u_\alpha \tag{5.3}$$

$$\sum_i g_i = \rho\phi \tag{5.4}$$

Leclaire's et al. [159] algorithm detailed in Section 3.2 can be re-expressed only in term of f_i and g_i.

f_i: stream and collide

It can be shown that f_i follows a classical stream and collide algorithm. The collide step is given by:

$$f_i^* = f_i^{eq} + \left(1 - \frac{1}{\tau}\right)(f_i - f_i^{eq} + 0.5S_i) + 0.5S_i \tag{5.5}$$

with S_i being the source term that introduces surface tension and correction term. Its formulation is given Eq.(3.52), but this term is not central in the current discussion. f_i^{eq} is the equilibrium function. The formulation given in Section 3.2 (Eq. (3.75)) is the one proposed by Leclaire et al. [150], it can actually be reformulated to:

$$f_i^{eq} = \rho w_i \left(1 + \frac{u_\alpha H_{\alpha,i}}{c_s^2} + \frac{u_\alpha u_\beta H_{\alpha\beta}}{2c_s^4}\right) + \left(p - \rho c_s^2\right)\frac{w_i - \delta_{i,0}}{c_s^2} \tag{5.6}$$

with p the pressure given by:

$$p = \rho\left(\left(\frac{1+\phi}{2}\right)c_s^{(R)2} + \left(\frac{1-\phi}{2}\right)c_s^{(B)2}\right) \tag{5.7}$$

It can be noticed that Eq.(5.6) is identical to the equilibrium function given by Pooley et al. [156] (Eq. (3.21)), which was not straightforward using previous formulations (from Grunau et al. [164], Eq. (3.75) or from Leclaire et al. [159] given Eq. (3.69) for example). The streaming step is simply given by:

$$f_i(x + \xi_{\alpha,i}\Delta t, t + \Delta t) = f_i^*(x,t) \tag{5.8}$$

Note that f_i is only involved in the computation of the total mass and momentum, while the recoloration process, described hereafter (Eq. (6.16)), only involves g_i.

g_i: stream and recolor

After reformulation, it comes that the g_i function calculated through a stream and recolor algorithm is given by:

$$g_i^* = \phi f_i^* + \Omega_i^{(3)} \tag{5.9}$$

with $\Omega_i^{(3)}$the collision operator accounting for phase segregation. The g_i function is then streamed:

$$g_i(x + \xi_{\alpha,i}\Delta t, t + \Delta t) = g_i^*(x,t) \tag{5.10}$$

The recoloration operator $\Omega_i^{(3)}$ can also be reformulated. The formulation given in Leclaire et al. [159] is strictly equivalent to:

$$\Omega_i^{(3)} = w_i \frac{p(1-\phi^2)}{2c_s^2 W}\frac{\xi_{\alpha,i}\partial_\alpha\phi}{|\vec{\xi_i}||\vec{\nabla}\phi|} \tag{5.11}$$

where W has the dimension of a length (m) and corresponds to the characteristic width of the interface. It is useful to give $\Omega_i^{(3)}$ two first moments:

$$\sum_i \Omega_i^{(3)} = 0 \tag{5.12}$$

$$\sum_i \Omega_i^{(3)}\xi_{\alpha,i} = \frac{p\left(1-\phi^2\right)}{2W}\frac{\partial_\alpha\phi}{|\vec{\nabla}\phi|} \tag{5.13}$$

Note that $\Omega_i^{(3)}$ 0^{th} moment given Eq. (5.12) is equal to 0 in order to ensure that no mass transfer occurs between phase 1 and phase 2.
The equilibrium function present formulation, given Eq. (5.6), makes stand out the mechanism that

allows to introduce pressure in colour gradient algorithm. It comes that the equilibrium function used in colour gradient algorithm can be associated to a Pooley's equilibrium scheme [156] given Eq. (3.21). The reformulation of the recoloration term Eq. (5.11) stresses the role played by the equation of state, making straightforward the generalization of the colour gradient method to an arbitrary equation of state under the form $p = f(\rho, \phi)$.

5.2. Equation of State Operator

It has been shown in the previous subsection that the color-gradient algorithm can be reformulated in such a way that mass and momentum are described by a single population f_i. Thanks to this reformulation, colour gradient algorithm can be compared to other methods such as free energy or HCZ.
As it was pointed out in Section 3.1.3, the ability to introduce an arbitrary equation of state is required for the considered multiphase flows. Among the available tools in Lattice Boltzmann methods to introduce an equation of state, one of them is the equilibrium scheme. The general principle of the equilibrium scheme is to write the equilibrium such as:

$$f_i^{eq} = f_i^{eq,0} + \left(p - \rho c_s^2\right) E_i \tag{5.14}$$

where E_i is an operator discussed in the following, and $f_i^{eq,0}$ the classical equilibrium function from He et al. [53]

$$f_i^{eq,0} = \rho w_i \left(1 + \frac{u_\alpha H_{\alpha,i}}{c_s^2} + \frac{u_\alpha u_\beta H_{\alpha\beta,i}}{2c_s^4}\right) \tag{5.15}$$

In this Section, the formulation of E_i presented in Eq. (5.14) is discussed. A $D2Q9$ framework is considered here, but the discussion can be extended to other lattices ($D3Q19$, $D3Q27$, etc...).

5.2.1. Discussion

In $D2Q9$, an operator E_i is defined through its 9 values corresponding to each microscopic velocities. It can also be defined through 9 independent moments. In order to determine these moments, the equivalent macroscopic equations are determined, and the operator E_i's moments are chosen to satisfy the desired physics. In the present case, the operator E_i is aimed to introduce a pressure gradient $\partial_\alpha p$ into the momentum conservation equation. It can be shown through a Taylor expansion that the two equivalent macroscopic equations while using the equilibrium function Eq.(5.14) are:

$$\partial_t \left(\rho + (p - \rho c_s^2) \sum_i H_{0,i} E_i\right) + \partial_\alpha \left(\rho u_\alpha + (p - \rho c_s^2) \sum_i H_{\alpha,i} E_i\right) = 0 \tag{5.16}$$

$$\begin{aligned}
&\partial_t \left(\rho u_\alpha + (p - \rho c_s^2) \sum_i H_{\alpha,i} E_i\right) + \partial_\beta \left(\rho u_\alpha u_\beta + \rho c_s^2 \delta_{\alpha\beta} + \underbrace{(p - \rho c_s^2) \sum_i \left(H_{\alpha\beta,i} + c_s^2 H_{0,i} \delta_{\alpha\beta}\right) E_i}_{(1)}\right) \\
&= \Delta t \left(\tau - 1/2\right) \partial_\beta \left[\underbrace{-\partial_\gamma \rho u_\alpha u_\beta u_\gamma}_{Mach\ error} + \underbrace{Er_{\alpha\beta}}_{EOS\ error} + \underbrace{\rho c_s^2 \left[\partial_\alpha u_\beta + \partial_\beta u_\alpha\right]}_{stress\ tensor} + \right. \\
&\left. \sum_i \left[\underbrace{H_{\alpha\beta,i} \partial_t (p - \rho c_s^2)}_{(2)} + \underbrace{\left[H_{\alpha\beta\gamma,i} + c_s^2 \left(H_\alpha \delta_{\beta\gamma} + H_\beta \delta_{\alpha\gamma}\right)\right] \partial_\gamma (p - \rho c_s^2)}_{(3)}\right] E_i\right]
\end{aligned} \tag{5.17}$$

where red terms corresponds to terms introduced by the Equation of State operator E_i. In order to guaranty mass conservation and momentum conservation, the operator E_i must respect:

$$\sum_i H_{0,i} E_i = 0 \tag{5.18}$$

$$\sum_i H_{\alpha,i} E_i = 0 \tag{5.19}$$

In addition, in the right equation of the momentum conservation the term noted (3) can be cancelled by imposing:

$$\sum_i H_{\alpha\beta\gamma,i} E_i = 0 \tag{5.20}$$

Finally, the term noted (1) shows that to introduce the pressure gradient in the momentum conservation equation, the operator must respect:

$$\sum_i H_{\alpha\beta,i} E_i = \delta_{\alpha\beta} \tag{5.21}$$

Note that the term noted (2) is not cancelled. This term is a spurious term and should be removed in order to accurately simulate the stress tensor. To do so, an original temporal correction is proposed in Chapter 6.

Thanks to Eqs. (5.18, 5.19, 5.20, 5.21), the moments linked to the Hermite's polynomials H_0, H_x, H_y, H_{xy}, H_{xx}, H_{yy}, H_{xxx}, H_{xxy}, H_{yyx} and H_{yyy} are determined, which is a total of 10 moments. In a $D2Q9$ framework, it should be enough moments to entirely determine the operator E_i. But, it was pointed out in Section 1.3.2.1 that in $D2Q9$ the moments H_α and $H_{\alpha\alpha\alpha}$ are not independent, involving that only 8 independent moments can be determined. One more condition is then required to fully determine E_i to determine completely the operator E_i. Which means that the E_i operators that fulfill the conditions given Eqs. (5.18, 5.19, 5.20, 5.21) form a one dimensional space. In this work, the moment related to H_{xxyy} is considered to determine E_i.
To build their operator, Pooley's et al. [156] investigated this $1D$ space measuring the amount of spurious current produced by each possible operator, and chosen the one producing the less amount of current. In Pooley's et al. [156] work, a specific operator E_i among the $1D$ space is characterized by a factor p. Figure 5.1 extracted from Pooley et al. depicts the maximum spurious velocity as a function of the parameter p. It can be shown that the minimum spurious velocity is reached for $p = 1/12$. The operator chosen by Pooley et al. [156] consequently follows:

$$E_i = \frac{w_i - \delta_{i,0}}{c_s^2} \tag{5.22}$$

This choice relies on an empirical result. In the present work, a theoretical argument is proposed to support Pooley's et al. [156] result.

Theoretical result

It was proposed in Section 4.3 Eq. (4.63) that the Δt^2 error of the momentum conservation equation is given by:

$$Er_{\Delta t^2} = \partial_\beta \left(\left(\left[\tau_{\alpha\beta} - \frac{1}{2} \right]^2 - \frac{1}{6} \right) \partial_t \Pi^{eq}_{\alpha\beta} + \left(\left[\tau_{\alpha\beta\gamma} - \frac{1}{2} \right] \left[\tau_{\alpha\beta} - \frac{1}{2} \right] - \frac{1}{12} \right) \partial_\gamma \Pi^{eq}_{\alpha\beta\gamma} \right) \tag{5.23}$$

In the present chapter, Leclaire et al. [159] algorithm is considered, which relies on a BGK collision operator, for which $\tau_{\alpha\beta} = \tau_{\alpha\beta\gamma} = \tau$. The expression for $\Pi^{eq}_{\alpha\beta\gamma}$ is reminded here:

$$\Pi^{eq}_{\alpha\beta\gamma} = \partial_t m^{eq}_{\alpha\beta\gamma} + \partial_\mu \left(m^{eq}_{\alpha\beta\gamma\mu} + \left[m^{eq}_{\alpha\beta} \delta_{\gamma\mu} + m^{eq}_{\alpha\gamma} \delta_{\beta\mu} + m^{eq}_{\beta\gamma} \delta_{\alpha\mu} \right] c_s^2 \right) \tag{5.24}$$

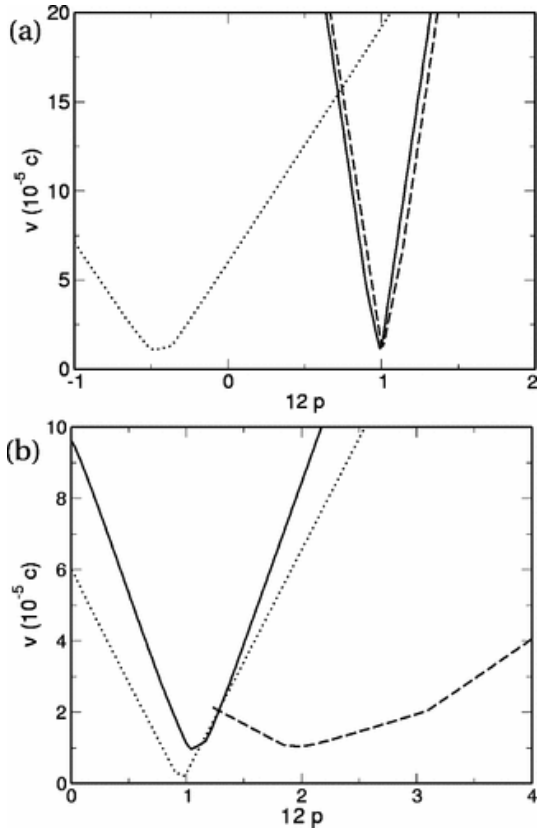


Figure 5.1. – The maximum spurious velocity (in Lattice Boltzmann Units) for a static bubble as a function of the parameter p (Figure (a) plain line) from Pooley et al. [156]

By injecting previous equation Eq. (5.24) into Eq. (5.23), it comes that the Δt^2 error at steady state (i.e. when $\partial_t = 0$) becomes:

$$Er_{\Delta t^2} = \partial^3_{\beta\gamma\mu}\left[\left(\left[\tau - \frac{1}{2}\right]^2 - \frac{1}{12}\right)\left(m^{eq}_{\alpha\beta\gamma\mu} + \left[m^{eq}_{\alpha\beta}\delta_{\gamma\mu} + m^{eq}_{\alpha\gamma}\delta_{\beta\mu} + m^{eq}_{\beta\gamma}\delta_{\alpha\mu}\right]c_s^2\right)\right] \tag{5.25}$$

In the absence of mean flow, i.e. if $\vec{u} = 0$, Eq. (5.6) shows that the values of the moments of the equilibrium function (the m^{eq}_*) only depend with p and ρ. Per construction, in absence of mean flow, second moment of the equilbirum function is:

$$m^{eq}_{\alpha\beta} = (p - \rho c_s^2)\delta_{\alpha\beta} \tag{5.26}$$

Also, the values of the 4^{th} order moments of the equilibrium function only depends on the moments of the operator E_i

$$m^{eq}_{\alpha\beta\gamma\mu} = \sum_i H_{\alpha\beta\gamma\mu,i}E_i\left(p - \rho c_s^2\right) \tag{5.27}$$

It comes that the Δt^2 error can be partially cancelled with a wise choice of E_i H_{xxyy} moment. In these conditions (steady flow and no mean velocity) it is possible to nullify the Δt^2 error, (i.e., to impose $Er_{\Delta t^2} = 0$) by setting:

$$\sum_i H_{\alpha\beta\gamma\mu,i}E_i = -c_s^2\left(\delta_{\alpha\beta}\delta_{\gamma\mu} + \delta_{\alpha\gamma}\delta_{\beta\mu} + \delta_{\alpha\mu}\delta_{\beta\gamma}\right) \tag{5.28}$$

In practice, due to the limitation of the $D2Q9$ scheme discussed in Section 1.3.2.1, only the moment linked to $H_{xxyy,i}$ can be imposed. Applying the previous equation to $H_{xxyy,i}$, it comes that the Δt^2

error can be reduced by setting:

$$\sum_i H_{xxyy,i} E_i = -c_s^2 \tag{5.29}$$

Thanks to this last condition, the E_i operator can be fully determined. By projecting the conditions given in Eqs.(5.18, 5.19, 5.21, 5.20, 5.29) into the Hermite polynomial space, an optimum operator, noted $E_i^{(iso)}$ can be defined by:

$$E_i^{(iso)} = \frac{H_{xx,i} + H_{yy,i}}{2c_s^2} - \frac{H_{xxyy,i}}{4c_s^6} \tag{5.30}$$

It happens that this last operator, determined only by theoretical arguments coincides with Pooley's operator Eq. (5.22). In the $E_i^{(iso)}$ notation, "iso" stands for isotropic. This notation is justified in the next section.

Links with isotropy

It can be shown that the previous operator $E_i^{(iso)}$ also respects isotropic conditions. The eight first moments were determined to ensure that mass and momentum conservation are accurately predicted, yielding conditions Eqs.(5.18, 5.19, 5.21, 5.20). And these conditions can be expressed in term of raw moments (raw moments are defined Appendix A.4 Eq. (A.30)):

$$\sum_i E_i = 0 \tag{5.31}$$

$$\sum_i \xi_{\alpha,i} E_i = 0 \tag{5.32}$$

$$\sum_i \xi_{\alpha,i}\xi_{\beta,i} E_i = \delta_{\alpha\beta} \tag{5.33}$$

$$\sum_i \xi_{\alpha,i}\xi_{\beta,i}\xi_{\gamma,i} E_i = 0 \tag{5.34}$$

A detailed discussion about isotropy has been conducted in Section 1. It must be noted that the present Eqs. (5.31,5.32,5.33,5.34) comply with isotropic conditions (namely Eq.(1.97) or Eq.(1.67)). This means the present operator E_i reaches a 3^{rd} degree of isotropy to satisfy the correct resolution of mass and momentum conservation equations.
Let us focus on the 4^{th} moments. It should be noted that the product of 4 microscopic velocities can be expressed as a function of the Hermite polynomials:

$$\begin{aligned}\xi_{\alpha,i}\xi_{\beta,i}\xi_{\gamma,i}\xi_{\mu,i} = H_{\alpha\beta\gamma\mu,i} + c_s^2 \left(H_{\alpha\beta,i}\delta_{\gamma\mu} + H_{\alpha\gamma,i}\delta_{\beta\mu} + H_{\alpha\mu,i}\delta_{\beta\gamma} + H_{\beta\gamma,i}\delta_{\alpha\mu} + H_{\beta\mu,i}\delta_{\alpha\gamma} + H_{\gamma\mu,i}\delta_{\alpha\beta}\right) \\ + c_s^4 \left(\delta_{\alpha\beta}\delta_{\gamma\mu} + \delta_{\alpha\gamma}\delta_{\beta\mu} + \delta_{\alpha\mu}\delta_{\beta\gamma}\right)\end{aligned} \tag{5.35}$$

By injecting Eqs.(5.18, 5.21, 5.28) into Eq. (5.35), it comes that $E_i^{(iso)}$ 4^{th} order raw moments are given by:

$$\sum_i \xi_{\alpha,i}\xi_{\beta,i}\xi_{\gamma,i}\xi_{\mu,i} E_i^{(iso)} = c_s^4 \left(\delta_{\alpha\beta}\delta_{\gamma\mu} + \delta_{\alpha\gamma}\delta_{\beta\mu} + \delta_{\alpha\mu}\delta_{\beta\gamma}\right) \tag{5.36}$$

According to the discussion of Section 1, and Eq. (1.67), it can be concluded that E_i^{iso} also reaches a 4^{th} degree of isotropy. Interestingly, this operator E_i^{iso} allowing to cancel the Δt^2 error $Er_{\Delta t^2}$ Eq. (5.23), is the one which reaches the highest degree of isotropy.
It can be verified that:

$$E_i^{(iso)} = \frac{w_i - \delta_{i,0}}{c_s^2} \tag{5.37}$$

it comes that $E_i^{(iso)}$ has the same degree of isotropy that w_i, i.e. the same degree of isotropy that the chosen velocity set. It means that $E_i^{(iso)}$ reaches the maximum level of isotropy possible in a $D2Q9$ framework.

Transposition to 3D

The present discussion can be generalised to $3D$ velocity sets. The most commonly used velocity sets are $D3Q19$ and $D3Q27$. In $D3Q19$ an operator is entirely defined when the moments associated to the following Hermite's polynomial are defined: H_0, H_x, H_y, H_z, H_{xx}, H_{xy}, H_{xz}, H_{yy}, H_{yz}, H_{zz}, H_{xxx}, H_{yyy}, H_{zzz}, H_{xyy}, H_{yzz}, H_{xzz}, H_{xxyy}, H_{xxzz} and H_{yyzz}.
It happens that in $D3Q19$, the different conditions proposed in the previous section (Eqs. (5.18, 5.19, 5.21, 5.20, 5.29)) cannot simply be projected into Hermite's polynomial basis. More specifically, while Eq. (5.37) stays true in $3D$, Eq. (5.30) is no longer verified:

$$E_i^{(iso)} = \frac{w_i - \delta_{i,0}}{c_s^2} \neq \frac{H_{xx,i} + H_{yy,i} + H_{zz,i}}{2c_s^4} - \frac{H_{xxyy,i} + H_{yyzz,i} + H_{xxzz,i}}{4c_s^6} \tag{5.38}$$

Eqs. (5.18, 5.19, 5.21, 5.20, 5.29) cannot be expressed in the Hermite's polynomial basis since Hermite's polynomials loose their orthogonality property in $D3Q19$ as discussed in Section 1.3.2.2, then the polynomial noted X defined Eqs. (1.77, 1.78, 1.79) must be used.

$$E_i^{(iso)} = X_{xx,i} + X_{yy,i} + X_{zz,i} - c_s^2 \left(X_{xxyy,i} + X_{yyzz,i} + X_{xxzz,i}\right) \tag{5.39}$$

It can still be useful to expressed it in term of Hermite's polynomials. It is given by:

$$E_i^{(iso)} = \frac{H_{xx,i} + H_{yy,i} + H_{zz,i}+}{3c_s^4} - \frac{H_{xxyy,i} + H_{yyzz,i} + H_{xxzz,i}}{3c_s^6} \tag{5.40}$$

5.2.2. Numerical illustration

The efficiency of the isotropic formulation $E_i^{(iso)}$ can be evaluated through the testcase of a static droplet. In a squared box with periodical boundary conditions, a spherical droplet of density $\rho_1 = 10kg.m^{-3}$ is set into an atmosphere of a lower density fluid ($\rho_2 = 1kg.m^{-3}$). The surface tension is set to 0, and the velocity field is initiated at 0 in all the domain. Giving the absence of phenomena able to animate the fluids, the flow is supposed to stay still, which makes it ideal to observe the spurious currents induced by the numerical scheme. The other parameters of the case are given afterward. The space step is $\Delta x = 0.001m$, the number of points in the x and y directions are $N_x = N_y = 128$ and the time step is $\Delta t = 1,6638.10^{-6}s$. The radius of the droplet is a multiple of the grid size: $R = 20\Delta x$ and so does the width of the interface $W = 2\Delta x$ (as a reminder, W is the parameter of the collision term in the recoloration operation Eq. (5.11)). The shear viscosity of the fluids are set equal, and the bulk viscosity is equal to the shear viscosity: $\nu_1 = \nu_2 = \nu_{b,1} = \nu_{b,1} = 0.001m^2.s^{-2}$.
Two cases are compared, one with E_i defined with $\sum_i H_{xxyy}E_i = 0$, and a second one with the isotropic operator $E_i^{(iso)}$. In Fig. 5.2, the spurious currents induced by the two methods are compared after 2000 iterations. The location of the interface is given by the line $\phi = 0$, and the velocity field is represented with arrows, whose length has a scale of $1m.s^{-1}$. In the non-isotropic case, it can be seen that strong spurious currents appear in the interface, reaching a maximum value of velocity of $53m.s^{-1}$. These spurious currents are strong enough to deform the interface shape. Around 4000 iterations, numerical instabilities led to the failure of the computation. In the isotropic case, the spurious currents are not visible (the maximum value of spurious velocity is $1.210^{-3}m.s^{-1}$), and the initial shape of the droplet is preserved. This illustrates the capability of this isotropic operator to reduce drastically the spurious currents. Note that the value $\sum_i H_{xxyy}E_i = 0$, for the non-isotropic operator has been chosen arbitrarily, and similar results can be obtained for other values different from $-c_s^2$.

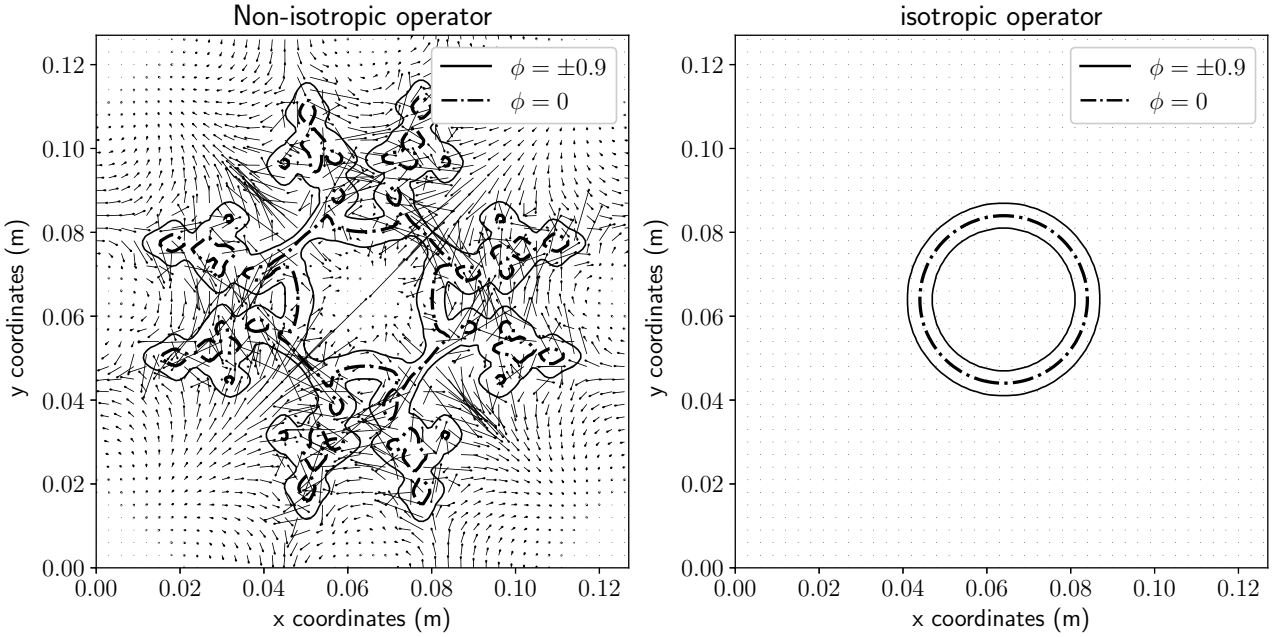


Figure 5.2. – Case of a static bubble in a quiescent atmosphere with two different operators, one without the isotropic condition, i.e. $\sum_i H_{xxyy,i} = 0$ (left), and one with it (right). The interface is represented by the $\phi = 0$ isolines and the velocity field by arrows of length scaled by $1m.s^{-1}$

5.3. Recoloration equivalent phase field equation

One of the major drawback of the colour-gradient algorithm is that the interface dynamics is not known. In particular, and contrary to other two populations methods (such as HCZ, free energy), the equivalent phase field equation was not known until recently [45].
It was discussed in Section 4.3 that two methods were proposed among the literature to determine the equivalent macroscopic equation of a Lattice Boltzmann Method, one from Holdych et al. [223] and one from Dubois [201]. The first approach relies on the assumlption that two different time scale exist. This assumption is particularly strong and is not required in Dubois's work.
The work of Subhedar et al. [45] relies on Holdych's [223] approach, which can limits the theoretical foundings of the result. To compensate this issue, the colour gradient equivalent phase field equation is determined based on Dubois's [201] work.

5.3.1. Discussion

As pointed out in Section 5.1, Leclaire et al. [159] original algorithm can be recast to involve a population function g_i (defined Eq. (5.2)) dedicated to the phase field prediction, so that $\sum_i g_i = \rho\phi$. The new formulation for the recoloration phase is reminded here. The recolored function g_i^* is calculated following:

$$g_i^* = \phi f_i^* + \Omega_i^{(3)} \tag{5.41}$$

where f_i^* is the collided main population function, and $\Omega_i^{(3)}$ is the forcing term accounting for phase segregation. This population is then streamed:

$$g_i(x, t + \Delta t) = g_i(x - \xi_{\alpha,i}\Delta t, t) \tag{5.42}$$

Through a Taylor expansion inspired by Dubois [201] which details are given in Appendix D, it can be shown that the equivalent macroscopic equation up to the order 1 in Δt is (Eq. (D.7)):

$$\partial_t \phi m_0^{eq} + \partial_\alpha \left(\phi m_\alpha^{eq} + S_\alpha^{(3)}\right) = O(\Delta t) \tag{5.43}$$

where $S_j^{(3)}$ corresponds to the $\Omega_i^{(3)}$ moments. To be more precise: $\sum_i \xi_{\alpha,i}\Omega_i^{(3)} = S_\alpha^{(3)}$. Eq. (5.43) can then be extended to the order 2 in Δt^2 (cf Appendix D):

$$\partial_t \phi m_0^{eq} + \partial_\alpha \left(\phi m_\alpha^{eq} + S_\alpha^{(3)}\right) = \frac{\Delta t}{2}\left[\partial_t\left(\phi m_\alpha^{eq}\right) + \partial_\beta\left(\phi m_{\alpha\beta}^{eq}\right)\right] + O(\Delta t^2) \tag{5.44}$$

Using the expression of $S_\alpha^{(3)}$ (Eq. (5.13)) and m_j^{eq} (Eq. (5.6)), it can be shown that the equivalent macroscopic equation for the recoloration is given by:

$$\partial_t \rho\phi + \partial_\alpha(\rho\phi u_\alpha) = \partial_\alpha\left[\frac{p\Delta t}{2}\left(\partial_\alpha\phi - \frac{1-\phi^2}{W}\frac{\partial_\alpha\phi}{|\vec{\nabla}\phi|}\right)\right] + O(\Delta t^2), \tag{5.45}$$

The right-side of Eq. (5.45) is related to the interface itself, and involves a diffusive term $\partial_\alpha\left(\frac{p\Delta t}{2}\partial_\alpha\phi\right)$, and an anti-diffusive term $-\partial_\alpha\left(\frac{p\Delta t}{2}\frac{1-\phi^2}{W}\right)$. The two effects are antagonist and can eventually compensate each other, meaning that the interface width can be controlled. Actually, in the case of a steady flat interface in a quiescent flow, the interface stabilizes in a hyperbolic tangent profile:

$$\phi = \tanh\left(\frac{x - x_\epsilon}{W}\right) \tag{5.46}$$

with x_ϵ the location of the interface $\phi = 0$. It comes from the fact that in the steady and with no velocity case, Eq. (5.45) reduces to:

$$\partial_x \left[\partial_x \phi - \frac{1-\phi^2}{W} \right] = 0 \tag{5.47}$$

which solution is a hyperbolic tangent. Since $tanh(2.65) \approx 0.99$ the terminal thickness of the interface can be approximated at $2x2.65 = 5.3W$. It is interesting to notice that the anti-diffusion force is simulated through the third collision term $\Omega^{(3)}$, while the diffusive term is induced by the recoloration step. It shows that the recoloration scheme allows to solve an advection-diffusion type equation in a LBM framework in an efficient way. A drawback of this method is that the diffusion rate (i.e., the $\frac{p\Delta t}{2}$ factor in Eq. (5.45)) is implied by the numerical scheme and then cannot be set freely.
An important result is that Eq. (5.45) corresponds to the compressible counterpart of the Chiu and Lin Allen-Cahn equation [47] discussed in Section 2.2.1.3, given Eq. (2.43). Its formulation is remembered here:

$$\partial_t \rho\phi + \partial_\alpha \left(\rho\phi u_\alpha\right) = M_{CL}\partial_\alpha \left[\partial_\alpha \phi - \frac{1-\phi^2}{W} n_\alpha \right] \tag{5.48}$$

with M_{CL} the so-called mobility factor and n_α the interface normal vector. In the colour-gradient context, as shown by Eq. (5.45), the mobility factor is given by:

$$M_{CL} = \frac{p\Delta t}{2} \tag{5.49}$$

and the normal vector is given by:

$$n_\alpha = \frac{\partial_\alpha}{|\vec{\nabla}\phi|} \tag{5.50}$$

It was discussed in Section 2.2.1.4 that Allen-Cahn equation is mass conservative, which supports the mass conservation property of the colour-gradient method already underlined by D'ortona [173] and Latva-Kokko [172].

5.3.2. Numerical illustration

Let us now conduct a study in the density matched case to highlight the influence of the mobility parameter M_{CL}. It is first interesting to note, that in the density match case ($\rho_1 = \rho_2$), Eq. (5.45) reduces to:

$$\partial_t \phi + \partial_\alpha(\phi u_\alpha) = \partial_\alpha \left[M \left(\partial_\alpha \phi - \frac{1-\phi^2}{W} n_\alpha \right) \right] \tag{5.51}$$

which corresponds to Chiu and Lin [47] Allen-Cahn equation for incompressible flows, where M is a constant also called the mobility factor (but different from the mobility factor M_{CL} given in Eq. (5.48)) given by:

$$M = \frac{p\Delta t}{2\rho}. \tag{5.52}$$

In this section, the M formulation is preferred since it has the dimension of a diffusion term ($m^2.s^{-1}$), which fits its physical effects.
The influence of the mobility factor is investigated through the case of a flat interface. First of all, a convergence analysis is held to recover Eq. (5.45), and then the impact of the mobility on the interface dynamics is investigated. The flat interface case is described as follow. The domain is a rectangular box with only few points ($Nx = 5$) in the short side, $Ny = \frac{L}{\Delta x}$ in the long side. The physical length of the domain is constant for all cases: $L = 1m$, and the space step Δx is used to set the mobility

factor M though Eq. (5.52). The boundary conditions are set periodic for the long side (normal to the x direction) and to wall conditions for the short side (along the x direction). Two phases are initialized in two equal volume of space such as:

$$\begin{cases} \phi(y, t=0) = -1 & 0 < y < \dfrac{L}{2} \\ \phi(y, t=0) = 1 & \dfrac{L}{2} < y < L \end{cases} \tag{5.53}$$

The interface is initially infinitely sharp. The interface widens under the effect of diffusion until it reaches its terminal thickness.
First, the grid convergence is investigated. The characteristic length of the interface is set to $W = 0.1m$. As seen in Eq. (5.46), the solution at steady state should be a tangent hyperbolic profile. Then a $L2$ error can be defined as:

$$L2 = \frac{\sqrt{\sum_j^{Ny} (\phi(j) - \tanh \frac{j\Delta x - y_\epsilon}{W})^2}}{Ny} \tag{5.54}$$

It was stated in Eq. (5.45) that ϕ is solution of the Allen-Cahn equation with an error proportional to Δt^2 which is itself proportional to Δx^2. This can be verified by plotting the L2-error in a log-log diagram as in Fig. 5.3. The L2 error follows nicely the expected tendency, which supports the theoretical result of Eq. (5.45).
To study the dynamics on the interface, the same set up is used chosing $W = 2.5\Delta x$. As previously,

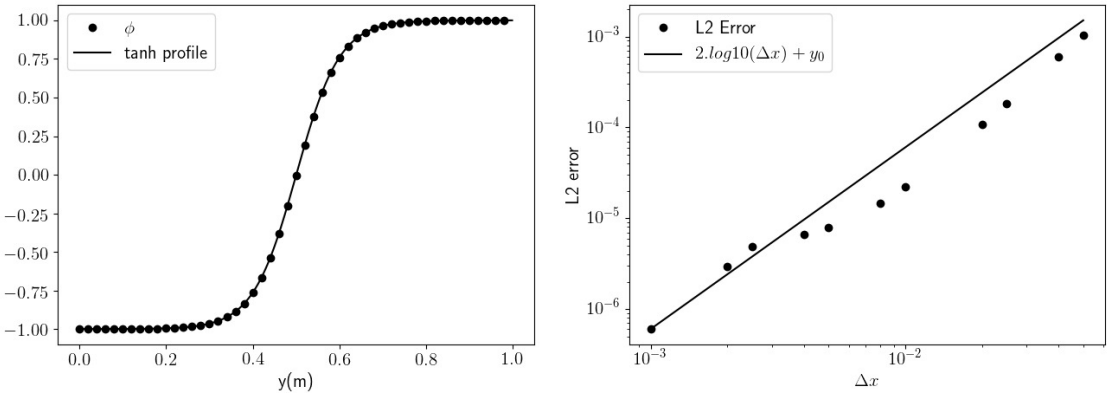


Figure 5.3. – Visualization of a phase field profile after grid convergence (left). L2 error expressed as a function of the spatial step Δx compared with a straight line of slope=2 in a log-log scale.

the case is performed for different values of Δx in order to compare the results with different values of the mobility factor M. Assuming that the profile of the interface at any time corresponds to a tangent hyperbolic profile: $\phi(x,t) = tanh(\dfrac{x - x_\epsilon}{W(t)})$, the value of $W(t)$ can be determined at any time by proceeding through a least square algorithm. For clarity issues, W_0 now denotes the final value of the interface thickness (which corresponds to the W term in the recoloration phase Eq. (5.11)). As the system only depends on W_0 and M, a non-dimensional time scale can be defined: $\tau_{int} = \dfrac{W_0^2}{2M}$. The evolution of the ratio W/W_0 is represented on Fig. (5.4) as a function of the dimensionless time: t/τ_{int}. It can be seen that the different profiles of interface thickening nicely superimpose on each other, evidencing that the evolution of the interface is driven by τ_{int} and W_0. Thanks to this analysis, it can be seen that the interface reaches 99% of its final thickness around $t = 5.6\tau_{int}$. It was pointed

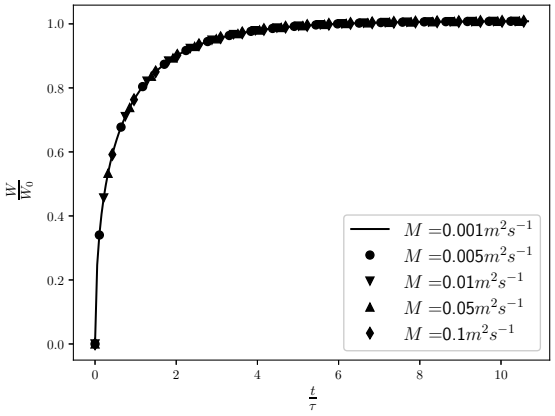


Figure 5.4. – Time evolution of the non-dimensional interface thickness for different mobility factors M as a function of dimensionless time.

out Section 5.3.1 that the mobility factor (and consequently the interface thickening characteristic time) is imposed by the numerical scheme, which could result in thickening of the interface slower than the flow characteristic time. To answer that issue, it is interesting to write τ_{int} as a function of the dimensionless interface final width $\tilde{W}_0$ defined as $\tilde{W}_0 = \dfrac{W_0}{\Delta x}$:

$$\tau_{int} = \frac{\tilde{W}_0 \rho c_s^2 \Delta t}{p} \tag{5.55}$$

In this equation it is straightforward that the characteristic time of thickening can be reduced by reducing the time step, i.e. by refining the mesh. It shows that a grid fine enough allows to compensate the fact to not be able to set the interface thickening characteristic time.

Chapter 6

Improved algorithm

Overview

6.1. Improved algorithm 110
6.1.1. Targeted macroscopic equations 110
6.1.2. Algorithm presentation 111
6.1.3. Correction term justification 114
6.2. Numerical Results 118
6.2.1. Poiseuille Flow 118
6.2.2. Laplace test 119
6.2.3. Oscillating droplet 120
6.2.4. Rayleigh-Taylor instability 123

A theoretical framework for the color gradient method has been provided in Chapter 5, for which a macroscopic equation for the recoloration has been provided. A detailled investigation for the operator E_i allowing to introduce an equation of state has also been provided, evidencing the need for an isotropic operator.
In the present Chapter, relying on the theoretical background provided in Chapter 5, a color-gradient framework is described, for which further improvements are proposed to deal with practical issues. Validations and numerical results are then provided for this improved algorithm.

6.1. Improved algorithm

6.1.1. Targeted macroscopic equations

The present algorithm allows to solve three macroscopic equations reminded hereafter. First, the continuity equation reads:

$$\partial_t \rho + \partial_\alpha \rho u_\alpha = 0 \tag{6.1}$$

The momentum conservation equation is then addressed:

$$\partial_t \rho u_\alpha + \partial_\beta \left(\rho u_\alpha u_\beta + p\delta_{\alpha\beta} + p^\sigma_{\alpha\beta} \right) = \mu \left(\partial_\alpha u_\beta + \partial_\beta u_\alpha \right) + \left(\mu_b - \mu \right) \partial_\gamma u_\gamma \tag{6.2}$$

where μ_b is the bulk viscosity, μ the shear viscosity, $p^\sigma_{\alpha\beta}$ the tensor introducing surface tension (detailed afterward Eq. (6.5)), and p the pressure which expression is discussed afterward.

The phase field equation is finally resolved following:

$$\partial_t \rho\phi + \partial_\alpha \left(\rho\phi u_\alpha \right) = \partial_\alpha \left[\frac{p\Delta t}{2} \left(\partial_\alpha \phi - \frac{1-\phi^2}{W} \frac{\partial_\alpha \phi}{|\vec{\nabla}\phi|} \right) \right] \tag{6.3}$$

Surface tension

In the present algorithm, surface tension is modeled using Gueyffier et al. [136] stress tensor. Surface tension is given as:

$$F^\sigma_\alpha = \partial_\beta p^\sigma_{\alpha\beta} \tag{6.4}$$

where the tensor $p^{sigma}_{\alpha\beta}$ is given by:

$$p^\sigma_{\alpha\beta} = \frac{\sigma}{2|\vec{\nabla}\phi|} \left[\partial_\alpha \phi \partial_\beta \phi - |\vec{\nabla}\phi| \delta_{\alpha\beta} \right] \tag{6.5}$$

Equation of State

To close the above system, a thermodynamic closure is required, which can be generically written as:

$$p = f(\rho, Y_1) = g(\rho, \phi). \tag{6.6}$$

Note that the equation of state (EOS) necessarily differs from $p = \rho c_s^2$ (c_s being the speed of sound), classically used in athermal Lattice-Boltzmann modelling [54]. In the classical color gradient formulation[164], the closure relation reads:

$$p = \rho Y_1 c_1^2 + \rho Y_2 c_2^2, \tag{6.7}$$

where c_k is the speed of sound in the k^{th} phase, and Y_k is the k^{th} phase mass fraction. c_1 and c_2 are chosen to ensure mechanical equilibrium. This equation of state proposed by Grunau et al. [164] presents a major drawback for high density ratios, as it implies

$$\frac{c_2^2}{c_1^2} = \frac{\rho_1}{\rho_2}. \tag{6.8}$$

This drawback can easily be illustrated considering the liquid-air system: for a density ratio of 1000, the air sound speed $c_{s,2} = 347m.s^{-1}$ would imply a liquid sound speed of $c_{s,2} = 11m.s^{-1}$. In such conditions, any liquid flow speed above $3m.s^{-1}$ would correspond to a local Mach number over 0.3, and therefore create non-physical compressible effects. To circumvent this limitation, an Equation Of State (EOS) is used, inspired from the Stiffened Gas formulation [229] $p = \rho(c_p - c_v)T - p_\infty$ for each phase, where p_∞ accounts for the attractive forces in the liquid. Assuming an isothermal fluid, the equation of state in each phase k only differs from the classical athermal EOS used in LBM by $p_{\infty,k}$, as:

$$p_k = \rho_k c_k^2 - p_{\infty,k}. \tag{6.9}$$

Note that $p_{\infty,k}$, c_k are constants of the flows. Finally, a mixture equation of state for the two-phase flow by assuming mechanical equilibrium [119, 230], is derived:

$$p = p_k, \forall k, \tag{6.10}$$

yielding

$$\frac{1}{\rho} = \frac{Y_1}{\rho_1} + \frac{Y_2}{\rho_2} = \frac{Y_1 c_1^2}{p + p_{\infty,1}} + \frac{Y_2 c_2^2}{p + p_{\infty,2}}, \tag{6.11}$$

which can be inverted to explicitly provide the expression required in Eq. (6.6), e.g.

$$p = \frac{1}{2}\left(\rho\hat{c}^2 - p_{\infty,1} - p_{\infty,2} + \sqrt{(p_{\infty,2} - p_{\infty,1} + \rho\bar{c}^2)^2 + \rho^2(1-\phi^2)c_1^2 c_2^2}\right) \tag{6.12}$$

where $\hat{c}^2 = \frac{c_1^2 + c_2^2}{2} + \phi\frac{c_1^2 - c_2^2}{2}$ and $\bar{c}^2 = \frac{c_1^2 - c_2^2}{2} + \phi\frac{c_1^2 + c_2^2}{2}$. Derivation of Eqs. (6.11, 6.12) and proof of the pressure's positivity can be found in Chiapolino, Boivin et Saurel [123] in the more general non-isothermal case. Note nonetheless that the present work is compatible with any other EOS which can be written under the generic form Eq. (6.6).

6.1.2. Algorithm presentation

In Chapter 5, it was pointed out that the colour gradient algorithm can equivalently be expressed through a f_i and g_i functions (defined Eq. (5.2)), respectively corresponding to total mass and mass phase field, rather than to R_i and B_i corresponding to each phase mass fraction. In the present method, the flow description through the distribution functions f_i and g_i is considered. As pointed out in Section 5.1, such formalism allows to only involve g_i in the recoloration step, while both R_i and B_i are involved in the original formulation. The computational cost associated to the recoloration step is then divided by two.
As previously said, f_i allows to calculate both the total mass and the total momentum, then its moments of interest are given by:

$$\sum_i f_i = \rho \quad \text{and} \quad \sum_i \xi_{\alpha,i} f_i = \rho u_\alpha \tag{6.13}$$

while g_i allows to calculate the phase field function, and its moment of interest is:

$$\sum_i g_i = \rho\phi \tag{6.14}$$

The algorithm is then given by the three following steps:

Step 1: collision:

$$f_i^* = f_i^{eq} + \Omega_i^{(1)} + \Omega_i^{(2)} + \frac{1}{2}S_i, \tag{6.15}$$

where $\Omega_i^{(1)}$ is the collision operator, $\Omega_i^{(2)}$ is the surface tension operator, and S_i is a forcing term, also detailed later. These different operators are detailed afterward (Eqs. (6.31)(6.35)).

Step 2: recoloration. The recoloration step writes now:

$$g_i^* = \phi f_i^* + \Omega_i^{(3)} \tag{6.16}$$

with $\Omega_i^{(3)}$the collision operator accounting for phase segregation, further detailed in Eq(6.34).

Step 3: streaming. Both f_i and g_i populations are then streamed, through

$$f_i(x + \xi_{\alpha,i}\Delta t, t + \Delta t) = f_i^*(x,t) \tag{6.17}$$
$$g_i(x + \xi_{\alpha,i}\Delta t, t + \Delta t) = g_i^*(x,t) \tag{6.18}$$

The equilibrium function, the collision terms, and the force term S_i for the revised color gradient method are provided in the following.

Equilibrium function

The equilibrium function considered here reads:

$$f_i^{eq} = \rho w_i \left(H_{0,i} + u_\alpha \frac{H_{\alpha,i}}{c_s^2} + u_\alpha u_\beta \frac{H_{\alpha\beta,i}}{2c_s^4} \right) + (p - \rho c_s^2) \left(E_i^{(iso)} + u_\alpha \frac{w_i H_{\beta\beta\alpha,i}}{2c_s^6} \right) \tag{6.19}$$

where the first terms correspond to the classical formulation[53], and the last one allows to consider an arbitrary EOS (e.g. when $p \neq \rho c_s^2$). It is reminded that the moment m_*^{eq} associated to the Hermite polynomial H_* is defined by

$$m_*^{eq} = \sum_i H_{*,i} f_i. \tag{6.20}$$

The equilibrium function of (Eq. (6.19)), is designed so that its low-order moments follow:

$$m_0^{eq} = \rho \tag{6.21}$$

$$m_\alpha^{eq} = \rho u_\alpha \tag{6.22}$$

The second-order moment is obtained by pointing out that the macroscopic equation corresponding to the equilibrium part follows [231]:

$$\partial_t m_\alpha^{eq} + \partial_\beta \left(m_{\alpha\beta}^{eq} + m_0 c_s^2 \delta_{\alpha\beta} \right) = F_\alpha + O(\Delta t), \tag{6.23}$$

corresponding to the Eulerian part of the momentum equation:

$$\partial_t \rho u_\alpha + \partial_\beta \left(\rho u_\alpha u_\beta + p\delta_{\alpha\beta} \right) = 0. \tag{6.24}$$

Comparing the two previous equations, the second order moment of the equilibrium has to be:

$$m_{\alpha\beta}^{eq} = \rho u_\alpha u_\beta + (p - \rho c_s^2)\delta_{\alpha\beta} \tag{6.25}$$

The definition of the third moment depends on the velocity set ($D2Q9$, $D3Q15$, etc...). As discussed in Section 1.3, in a Lattice Boltzmann framework, the number of discrete velocities is directly related to the number of moments that are correctly recovered. In particular, in $D2Q9$ not all three order moments (i.e. the moments related to the third degree Hermite's polynomials: H_{xxx}, H_{xxy}, H_{xyy} and

H_{yyy}) can be correctly recovered: $\sum_i w_i H_{xxx,i} f_i^{eq} = \sum_i w_i H_{yyy,i} f_i^{eq} = 0$ for all f_i^{eq}. The consequence is that, while the third moments of f_i^{eq} should be

$$m_{\alpha\beta\gamma}^{eq} = (p - \rho c_s^2)(u_\alpha \delta_{\beta\gamma} + u_\beta \delta_{\alpha\gamma} + u_\gamma \delta_{\alpha\beta}), \tag{6.26}$$

due to the $D2Q9$ limitations, it actually reads:

$$\begin{cases} m_{\alpha\alpha\beta}^{eq} = (p - \rho c_s^2) u_\beta & \alpha \neq \beta \\ m_{\alpha\alpha\alpha}^{eq} = 0 & \text{otherwise} \end{cases} \tag{6.27}$$

This problem has already been discussed by Wen et al. [161], and the proposed solution is to adopt the forcing strategy proposed by Li et al. [160] for the color-gradient framework, leading to a forcing term S_{Sp}, detailed hereafter in Eq. (6.37).

Collision step: $\Omega_i^{(1)}$

In LB methods, the collision term $\Omega_i^{(1)}$ relaxes the population towards the so-called equilibrium distribution function Eq. (6.19). In practice, the BGK collision operator [50] is quite limited in terms of stability [217]. To enhance stability, a regularized collision operator [217] is used in this study. The effect of the bulk viscosity is also accounted for following the method by Renard et al [232].

The proposed collision term reads:

$$\Omega_i^{(1)} = \left(1 - \frac{1}{\tau_\nu}\right)\left(f_{xy,i}^{r,neq} + f_{\nu,i}^{r,neq}\right) + \left(1 - \frac{1}{\tau_b}\right) f_{b,i}^{r,neq} \tag{6.28}$$

where $f_{\nu,i}^{r,neq}$, $f_{b,i}^{r,neq}$ and $f_{xy,i}^{r,neq}$ are the projections of the non-equilibrium counterpart of the population function on respectively the H_ν and H_b polynomials:

$$f_{k,i}^{r,neq} = \frac{H_{k,i}}{c_s^4} \sum_i \left(f_i - f_i^{eq} + \frac{1}{2} S_i\right) H_{k,i}, \quad k = \nu, b, xy. \tag{6.29}$$

where S_i is a source term detailled Eq. (6.35) that introduces volumic forces, surface tension and correction terms. The dimensionless relaxation times (τ_ν, τ_b) depend on the kinematic viscosity ν and bulk viscosity ν_b following:

$$\tau_\nu = \frac{\rho\nu}{p\Delta t} + \frac{1}{2} \qquad \tau_b = \frac{\rho\nu_b}{p\Delta t} + \frac{1}{2} \tag{6.30}$$

Collision step: $\Omega_i^{(2)}$

The collision term $\Omega_i^{(2)}$ introduces surface tension to the model:

$$\Omega_i^{(2)} = \frac{\sigma w_i}{4|\vec{C}|c_s^4} \left(\frac{\left(2C_x C_y H_{xy,i} + (C_x^2 - C_y^2) H_{\nu,i}\right)}{\tau_\nu} - \frac{(C_x^2 + C_y^2) H_{b,i}}{\tau_b} \right) \tag{6.31}$$

This operator is a reformulation of the one proposed by Liu et al. [44], taking into account the different relaxation times for the moments of H_ν and H_b. $\vec{C}$ refers to the colour gradient that gave the method's name and σ is the surface tension $(kg.s^{-2})$. The colour gradient can be seen as an approximation of the spatial gradient of the phase field as showed by Leclaire et al. [150]. Among the discretization schemes proposed in [150], we chose the one providing the highest level of isotropy while involving only the first neighbours:

$$C_\alpha(x,t) = \sum_i \frac{w_i \xi_{\alpha,i} \phi(x + \xi_{\alpha,i}\Delta t, t)}{c_s^2} = \Delta t \partial_\alpha \phi + O(\Delta t^2) \tag{6.32}$$

When $\tau_\nu = \tau_b = \tau$, this formulation is equivalent to the one proposed by Reis & Phillips [43], where the operator $\Omega_i^{(2)}$ is designed in order to guarantee

$$\sum_i \xi_{\alpha,i}\xi_{\beta,i}\Omega_i^{(2)} = \frac{p^\sigma_{\alpha\beta}}{\tau} \tag{6.33}$$

with $p^\sigma_{\alpha\beta}$ the pressure tensor introducing surface tension proposed as by Gueyffier et al. [136].

Recoloration step: $\Omega_i^{(3)}$

The recoloration step applies to the phase-field population g_i (Eq. (6.16)) and reads

$$\Omega_i^{(3)} = w_i \frac{p(1-\phi^2)}{2W} \frac{\xi_{\alpha,i}\partial_\alpha \phi}{c_s^2 |\vec{\nabla}\phi|} \tag{6.34}$$

where W has the dimension of a length (m) and corresponds to the characteristic width of the interface (see Section 5.3). This term was originally proposed by Latva-Kokko [172] inspired by the work of D'Ortona [173] and later improved by Halliday et *al.* [174]. The present formalism is strictly equivalent to the one proposed by Halliday et *al.* [174].

Forcing term S_i

In this work, the forcing term consists in three contributions:

$$S_i = S_{F,i} + S_{Sp,i} + S_{t,i}. \tag{6.35}$$

S_F is a source term accounting for potential volume forces, e.g. gravity. Given a force F_α, S_F writes:

$$S_{F,i} = w_i \left(F_\alpha \frac{H_{\alpha,i}}{c_s^2} + (u_\alpha F_\beta + u_\beta F_\alpha) \frac{H_{\alpha\beta,i}}{2c_s^4} \right). \tag{6.36}$$

S_{Sp} is a corrective term which corrects the error stemming from the third order moment, improperly resolved on the D2Q9 lattice [160, 161, 233]:

$$S_{Sp,i} = w_i \left(3\frac{\partial_y[(p-\rho c_s^2)u_y] - \partial_x[(p-\rho c_s^2)u_x]}{2c_s^4} H_{\nu,i} - \frac{\partial_y[(p-\rho c_s^2)u_y] + \partial_x[(p-\rho c_s^2)u_x]}{2c_s^4} H_{b,i} \right) \tag{6.37}$$

This expression corresponds to the correction introduced by Wen et al.[161] recast in the present formalism. The derivative terms are calculated with the scheme proposed in Eq. (6.32).

Finally, a novel temporal correction term is proposed in this work:

$$S_{t,i} = \left[p(x,t) - p(x,t-\Delta t) + (\rho(x,t) - \rho(x,t-\Delta t))c_s^2 \right] E_i. \tag{6.38}$$

The derivation of Eqs. (6.37, 6.38) is provided in Section 6.1.3.

6.1.3. Correction term justification

It has been known since the work of Holdych [154], that when the EOS of state is modified through an equilibrium scheme (i.e. by putting the equilibrium function into the form $f_i^{eq} = f_i^{eq,0} + (p - \rho c_s^2)E_i$ or other equivalent scheme), an error term appears in the stress tensor, at the first order in Δt. In such a case, the macroscopic conservation equation follows:

$$\partial_t \rho u_\alpha + \partial_\beta \left(\rho u_\alpha u_\beta + p\delta_{\alpha\beta} \right) = \partial_\beta \left(\Delta t \left(\tau - 1/2 \right) \left[\rho c_s^2 \left(\partial_\alpha u_\beta + \partial_\beta u_\alpha \right) + Er_{\alpha\beta} \right] \right) O(\Delta t^2), \tag{6.39}$$

where the error $Er_{\alpha\beta}$ is given by:

$$Er_{\alpha\beta} = \underbrace{u_\alpha \partial_\beta \left(p - \rho c_s^2\right) + u_\beta \partial_\alpha \left(p - \rho c_s^2\right)}_{Spatial\ error} + \underbrace{\partial_t \left(p - \rho c_s^2\right) \delta_{\alpha\beta}}_{temporal\ error} \tag{6.40}$$

It comes that this error can be divided into a spatial component (a component made of spatial derivatives) and a temporal component (a component made of temporal derivative). Leclaire et al. [159] following the work of Che Sidick [158] proposed an enhancement of the equilibrium function that aims to correct the spatial component of the error $Er_{\alpha\beta}$ given in Eq. (6.40). Note that this enhancement of the equilibrium function could be expressed under the form of a source term, as all the correction terms in this study. In these two approaches [158, 159], the temporal components are not corrected and are considered negligible.
An alternative way to correct the error $Er_{\alpha\beta}$ was proposed in the literature. To understand it, it is useful to point out a less straightforward split of the $Er_{\alpha\beta}$ error. $Er_{\alpha\beta}$'s expression can be manipulated to give:

$$\begin{aligned} Er_{\alpha\beta} = \underbrace{\partial_\alpha \left(p - \rho c_s^2\right) u_\beta + \partial_\beta \left(p - \rho c_s^2\right) u_\alpha - \partial_\gamma \left((p - \rho c_s^2) u_\gamma\right) \delta_{\alpha\beta}}_{Er^{rec}_{\alpha\beta}} \\ + \underbrace{\left[\partial_t \left(p - \rho c_s^2\right) + \partial_\gamma \left((p - \rho c_s^2) u_\gamma\right)\right] \delta_{\alpha\beta}}_{Er^{cons}_{\alpha\beta}} \end{aligned} \tag{6.41}$$

where $Er^{rec}_{\alpha\beta}$ and $Er^{cons}_{\alpha\beta}$ correspond to two distinct errors. It is detailed hereafter that $Er^{rec}_{\alpha\beta}$ comes from the breaking of the recursive relationships between the moments of the equilibrium functions, and $Er^{cons}_{\alpha\beta}$ from the fact that the evolution of the pressure p is not determined by a conservation equation.

A discussion about recursivity

As pointed out by Malaspinas et al. [217], the moments of the equilibrium function for a classical LBM model respects the following relationships:

$$m^{eq}_{\alpha_1 \ldots \alpha_n} = m^{eq}_{\alpha_1 \ldots \alpha_{n-1}} u_{\alpha_n} + \left(u_{\alpha_1} \ldots u_{\alpha_{n-2}} m^{eq}_{\alpha_n \alpha_n} + perm(\alpha_n)\right) \tag{6.42}$$

with $perm(\alpha_n)$ being all the cyclic index permutations of indexes from α_1 to α_{n-1}. Then by setting:

$$m^{eq}_{\alpha\beta} = \rho u_\alpha u_\beta + (p - \rho c_s^2) \tag{6.43}$$

without setting

$$m^{eq}_{\alpha\beta\gamma} = \rho u_\alpha u_\beta u_\gamma + (p - \rho c_s^2)(u_\alpha \delta_{\beta\gamma} + u_\beta \delta_{\alpha\gamma} + u_\gamma \delta_{\alpha\beta}) \tag{6.44}$$

the recursive relationships are broken. The practical consequence is the appearance of the $Er^{rec}_{\alpha\beta}$ error in the momentum conservation equation. To address this issue, Li et al [160] proposed to heal the scheme's recursivity by imposing Eq. (6.44).
In the case of a perfect scheme (i.e. a microscopic velocity set with an infinite number of velocities), Li et al. [160] would be preferred: the source term proposed in Leclaire et al. [159] needs the computation of a gradient term ($\vec{\nabla}\left(p - \rho c_s^2\right)$), which is a price to pay in term of computational efficiency, since spatial gradient at given point requires the knowledge of (at least) the first neighbours. Moreover, one of the advantages of a LBM scheme is the fact that locality is only broken during the streaming phase, which makes LBM a good candidate for parallelization. By adding a non-local term, this potential of parallelization decreases.

In practice, Li et al. [160] method still needs corrections. In $D2Q9$ for example m^{eq}_{xxx} and m^{eq}_{yyy} cannot be imposed, then Eq. (6.44) cannot be verified for $\alpha\beta\gamma = xxx$ and $\alpha\beta\gamma = yyy$, which implies that recursivity cannot be fully restored.

The other counterpart of the error, $Er^{cons}_{\alpha\beta}$, is not often discussed. In Li et al. [160], it is divided into a temporal and a spatial component, the temporal component is considered negligible and the spatial component is corrected through a source term. It must be noted that $Er^{cons}_{\alpha\beta}$ can be reduced. Noting that LBM is mass conservative, i.e. that $\partial_t\rho + \partial_\alpha\rho u_\alpha = 0$, it comes that $Er^{cons}_{\alpha\beta}$ reduces to:

$$Er^{cons}_{\alpha\beta} = \left[\partial_t p + \partial_\gamma \left(p u_\gamma\right)\right]\delta_{\alpha\beta} \tag{6.45}$$

This error looks like the left hand side of a "p conservation equation", that is why $Er^{cons}_{\alpha\beta}$ is said to be an error occuring from the fact that p doesn't follow a conservation equation. In the general case, this error cannot be simply calculated and cannot be considered negligible neither. It was pointed out by Renard et al. [232], that in a compressible framework, when p follows the perfect gas equation of state ($p = \rho r T$, T being the temperature and r the specific constant of the gas), $Er^{cons}_{\alpha\beta}$ reduces to a spatial derivative error, and then can be corrected through a source term. A source term allowing to correct both $Er^{cons}_{\alpha\beta}$ and $Er^{rec}_{\alpha\beta}$ is proposed hereinafter.

Source term for the enhanced algorithm

The enhanced algorithm being different from Leclaire et al. [159]'s algorithm, the error term $Er_{\alpha\beta}$'s formulation is different as well. If we suppose that no correction term is introduced (i.e. that Eq. (6.35) is modified to $S_i = 0$), then it can be shown through a Taylor-expansion detailed in Appendix D.2 that the enhanced algorithm equivalent macroscopic equation is given by:

$$\begin{aligned}\partial_t\rho u_\alpha + \partial_\beta\left(\rho u_\alpha u_\beta + p\delta_{\alpha\beta}\right) &\\ = \Delta t\partial_\beta\left(p(\tau_\nu - 1/2)\left(\partial_\alpha u_\beta + \partial_\beta u_\alpha\right) + p(\tau_b - \tau_\nu)\partial_\gamma u_\gamma + Er_\alpha\delta_{\alpha\beta}\right)&\\ + O(\Delta t^2)&\end{aligned} \tag{6.46}$$

With

$$\begin{aligned}Er_\alpha = &\underbrace{-(\tau_\nu - 1/2)3\partial_\alpha\left((p - \rho c_s^2)u_\alpha\right) + \frac{3}{2}\left(\tau_\nu - \tau_b\right)\partial_\gamma\left((p - \rho c_s^2)u_\gamma\right)}_{lack\ of\ recursivity}\\ &+ \underbrace{(\tau_b - 1/2)\left(\partial_t(p - \rho c_s^2) + \partial_\gamma\left((p - \rho c_s^2)u_\gamma\right)\right)}_{Not\ conservative}\end{aligned} \tag{6.47}$$

In practice, similarly as in Leclaire et al. [159], Er_α is divided in a spatial error and a temporal error:

$$Er = Er_t + Er_{Sp} \tag{6.48}$$

$$Er_t = (\tau_b - 1/2)\partial_t(p - \rho c_s^2) \tag{6.49}$$

$$Er_{Sp} = 3(\tau_\nu - 1/2)\frac{\partial_\gamma(p - \rho c_s^2)u_\gamma - \partial_\alpha(p - \rho c_s^2)u_\alpha}{2} - (\tau_b - 1/2)\frac{\partial_\gamma(p - \rho c_s^2)u_\gamma}{2} \tag{6.50}$$

The forcing term S_{Sp} and S_t given in Eqs. (6.37)(6.38) aims to correct Er_{Sp} and Er_t respectively.

- S_{Sp} corrects the spatial counterpart of the error, it then must guaranty:

$$\sum_i H_{\nu,i}S_{Sp,i} = 3\frac{\partial_y(p - \rho c_s^2)u_y - \partial_y(p - \rho c_s^2)u_y}{2} \tag{6.51}$$

$$\sum_i H_{b,i}S_{Sp,i} = \frac{\partial_\gamma(p - \rho c_s^2)u_\gamma}{2} \tag{6.52}$$

All the other moments must be 0.

– S_t aims to correct the temporal component of the error. It must respect:

$$\sum_i H_{b,i} S_{t,i} = \partial_t (p - \rho c_s^2) \tag{6.53}$$

and the 0^{th}, 1^{st} and 3^{rd} moments are set to 0. Eq. (6.53) can equally be expressed as $\sum_i S_{t,i} H_{\alpha\beta,i} = \partial_t (p - \rho c_s^2)\delta_{\alpha\beta}$, which corresponds to Eq. (5.21). It means that the conditions used to defined S_t are similar to the conditions used to define the operator E_i (Eqs. (5.18, 5.19, 5.21, 5.20)). For this reason, and as discussed in Section 5.2, the operator $E_i^{(iso)}$ must be used for a better numerical stability:

$$S_{t,i} = \partial_t \left(p - \rho c_s^2\right) E_i^{(iso)} \tag{6.54}$$

The stencil used to approximate $\partial_t(p - \rho c_s^2)$ is now discussed. When taking S_i into consideration, Eq. (6.46) is modified to:

$$\begin{aligned}\partial_t \rho u_\alpha + \partial_\beta \left(\rho u_\alpha u_\beta + p\delta_{\alpha\beta}\right) = \Delta t \partial_\beta \Big(& p(\tau_\nu - 1/2)\left(\partial_\alpha u_\beta + \partial_\beta u_\alpha\right) + p(\tau_b - \tau_\nu)\partial_\gamma u_\gamma \\ & + \left(Er_t + Er_{Sp}\right)\delta_{\alpha\beta} - \sum_i \left[(\tau_b - 1/2)\left(St_i + Sp_i\right) + (\tau_\nu - 1/2)\, Sp_i\right] \Big) \\ & + O(\Delta t^2)\end{aligned} \tag{6.55}$$

Noting that Δt is in factor of the right hand side of Eq. (6.55), it comes that in order to recover the momentum conservation equation to the order 2 in Δt, $S_{Sp,i}$ and $S_{t,i}$ must ensure:

$$\left(Er_t + Er_{Sp}\right)\delta_{\alpha\beta} - \sum_i \left[(\tau_b - 1/2)\left(St_i + Sp_i\right) + (\tau_\nu - 1/2)\, Sp_i\right] = O(\Delta t) \tag{6.56}$$

When isolating only the temporal component of Eq. (6.56) , and injecting Eq. (6.49) it comes that:

$$\sum_i S_{t,i} H_{b,i} = Er_t + O(\Delta t) = \partial_t (p - \rho c_s^2) + O(\Delta t) \tag{6.57}$$

It comes that the temporal derivative in the temporal correction term can only be estimated with a Δt precision. The following expression is then chosen for S_t

$$S_{t,i}(x,t) = \left[p(x, t+\Delta t) - p(x,t) - c_s^2\left(\rho(x, t+\Delta t) - \rho(x,t)\right)\right] E_i^{(iso)} \tag{6.58}$$

On a side note, the attentive reader would underlined that the Li et al's scheme [160] used in this work requires the calculation of a gradient term as in the scheme proposed by Leclaire et al. [159]. This would make these two schemes equivalent in term of numerical efficiency. But the performances of these two models are in practice not similar. If not corrected, the error term Er leads to the growth of a spurious shear stress in the interface which leads to a non continuous velocity field across the interfacial region. The higher the density ratio is, the more this spurious stress in the interface becomes significant. At high density ratio (i.e. up to 100) the model proposed in Leclaire et al. [159] doesn't allow to correct the velocity jump, and the continuity of the velocity field across the interface no longer holds.
To illustrate this last statement, the effect of the different corrections through the schemes of Leclaire et al. [159] and Li et al. [160] are investigated on a two-phase Poiseuille flow in the following section.

6.2. Numerical Results

6.2.1. Poiseuille Flow

The considered test case consists in a rectangular $2D$ box, discretized in a $N_x = 5 * N_y = 200$ mesh. Two separated phases coexist in the channel, the denser fluid 1 is located in a band of width $2a$ surrounded by two bands of width $b - a$ of the fluid 2, a and b being geometrical values given by $a = \frac{\Delta x N y}{2}$ and $b = \frac{\Delta x N y}{4}$. The system is invariant along the x-axis. Placing that the origin of the y-axis in the middle of the box, the initial phase field profile is given by $|y| < a$: $\phi = 1$ and when $a < |y| < b$: $\phi = -1$. The boundaries normal to the x-axis are set as walls, and the boundaries normal to the y-axis are periodic. Finally, a constant volumic force, which simulates a constant pressure gradient G, is applied. The expression of the force is given by $\vec{F} = G\vec{e_x}$. The norm of this force is given by $G = 9.81 kg.m^{-1}.s^{-2}$ An illustration is proposed in Fig. 6.1. Other usefull parameters that were used for the testcase are given afterward. The spatial step is set to $\Delta x = 0.001m$. The density ratio is set to 100, with densities of $\rho_{1,0} = 1 kg.m^{-3}$ and $\rho_{2,0} = 0.01 kg.m^{-3}$, the kinematic viscosity of the fluids are identical: $\nu_1 = \nu_2 = 1.666667 m^2.s^{-1}$, and the bulk viscosity is set equal to the shear viscosity: $\nu_{b,1} = \nu_{b,2} = \nu_1$. The speed of sound in both fluids is identical and equal to the speed of sound in air at ambient temperature. Moreover the characteristic velocity c_s is set equal to the speeds of sound: $c_1 = c_2 = c_s = 347 m.s^{-1}$. The lighter fluid is supposed to have no coherent forces, then $p_{\infty,2} = 0$, and $p_{\infty,1}$ is chosen to guarantee mechanical equilibrium between the phases, i.e., $p_{\infty,1} = (\rho_{1,0} - \rho_{2,0}) c_s^2$. The surface tension is neglected $\sigma = 0$ which has no impact here, since the interfaces are planar in this Poiseuille flow. The interface thickness is set to $W = 1.6\Delta x$. The initial solution is implemented with a thick interface, i.e.:

$$\phi(x, y, 0) = \tanh\left(-\frac{|y| - a}{W}\right), \tag{6.59}$$

with W the interface thickness.

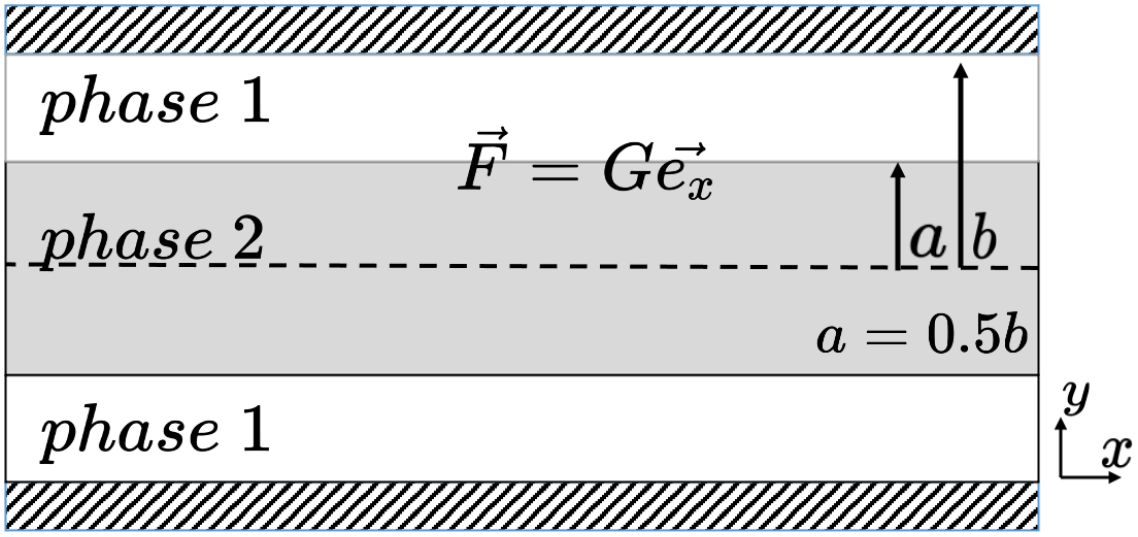


Figure 6.1. – Two-phase Poiseuille flow case

The analytical solution is known, as proposed in Huang and Lu [234]. Then the simulated field obtained can be compared to the analytical solution. Results are proposed in Fig. 6.2 where the analytical solution is also reported. Two simulation are conducted. In the first one, referred as "model 1", Leclaire's scheme is implemented, i.e. $S_{Sp} = 0$, $S_t = 0$ and a correction term is added to the equilibrium function given in Eq. (6.19) $f_i^{eq,(Leclaire)} = f_i^{eq} + \Phi_i$ with the expression of Φ given in

Leclaire et al. [159]. In the second one, referred as "model 2", the equilibrium presented Eq. (6.19) is used. As evidenced in Fig.6.2, a non-physical velocity jump appears at the interface for the Leclaire's

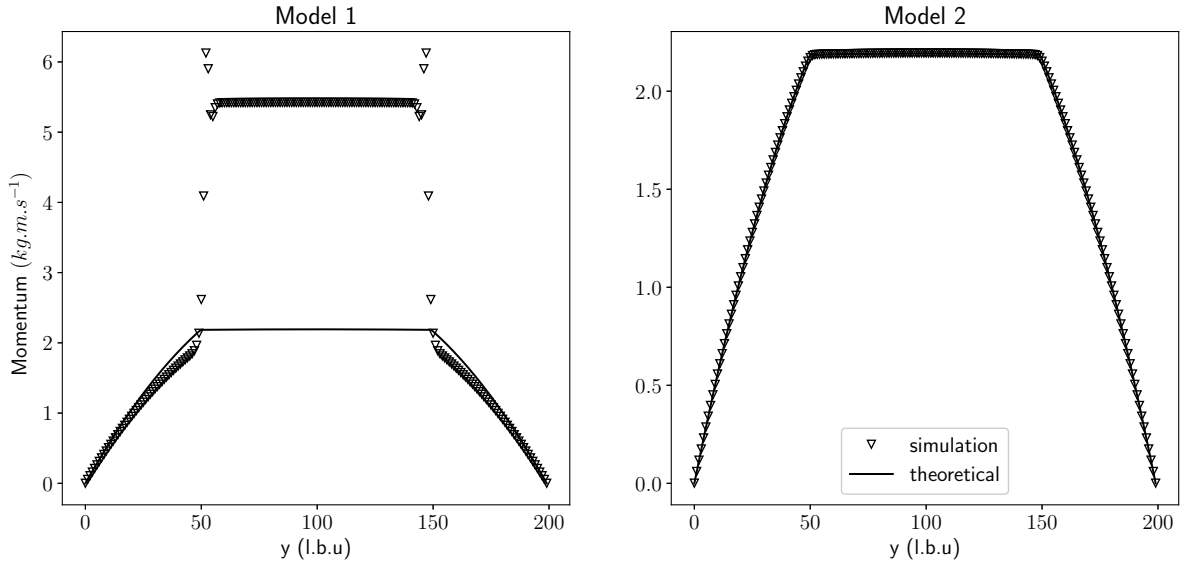


Figure 6.2. – Comparison between "model 1" inspired fom the scheme in Leclaire [159] (left), and "model 2" the present scheme inspired from Li [160] (right), for a two-phase Poiseuille flow at high density ratio case (100). Both are compared with the theoretical solution (solid line)

scheme, while the flow stays continuous across the interface with the proposed scheme.

6.2.2. Laplace test

One of the fundamental capability intended from a multiphase solver is the ability to accurately simulate surface tension. This behavior can be evaluated through the Laplace test. It consists in simulating a bubble or a droplet of a phase 1 in a quiescent atmosphere composed of phase 2. Due to surface tension, a pressure jump appears across the interface. In a 2D framework (which comes to simulate an infinite cylinder), the pressure jump is given by the following form of the Laplace law

$$p_1 - p_2 = \frac{\sigma_{exp}}{r} \tag{6.60}$$

r being the cylinder radius, p_1 the pressure outside the droplet/bubble, p_2 the pressure inside the droplet/bubble, σ_{exp} being the surface tension and r the radius of the cylinder. The test consists in comparing the value of the user set surface tension (in this case, the term σ in the surface tension operator $\Omega_i^{(2)}$ Eq. (6.31)), and the observed surface tension σ_{exp} calculated from the measured pressure jump across the interface and Eq. (6.60). This test is performed in a squared grid of size $Nx = 128$, $Ny = 128$, for a space step of $\Delta x = 0.0001m$. In this box, a bubble of radius r taking one value in the range of $(10, 15, 20, 25)\Delta x$, and with σ taking one value in $(1, 3, 5, 8)10^{-2}kg.s^{-2}$ (this relative narrow range of surface tension coefficient is motivated by the fact that the vast majority of practical cases falls into this interval, which excludes only extreme cases like mercury for instance). The density of the outside phase is the lowest and set to $\rho_2 = 1kg.m^{-3}$, while the other phase's density ρ_1 falls into the range: $(4, 10, 100, 1000)kg.m^{-3}$ The test is initialized by setting:

$$\phi(x, y, 0) = -\tanh\left(\frac{\sqrt{(x - x_0)^2 + (y - y_0)^2)} - r}{W_0}\right) \tag{6.61}$$

$W_0 = 1.3\Delta x$ being the initial interface thickness and (x_0, y_0) the coordinates of the center of the box. The other parameters of the simulation are: $c_1 = c_2 = c_s = 347m.s^{-1}$, $W = 1.6\Delta x$, $\nu_1 = \nu_2 = \nu_{b,1} = \nu_{b,2} = 0.001m^2.s^{-1}$. The results of these multiple tests are proposed in Fig. 6.3. It can be seen that

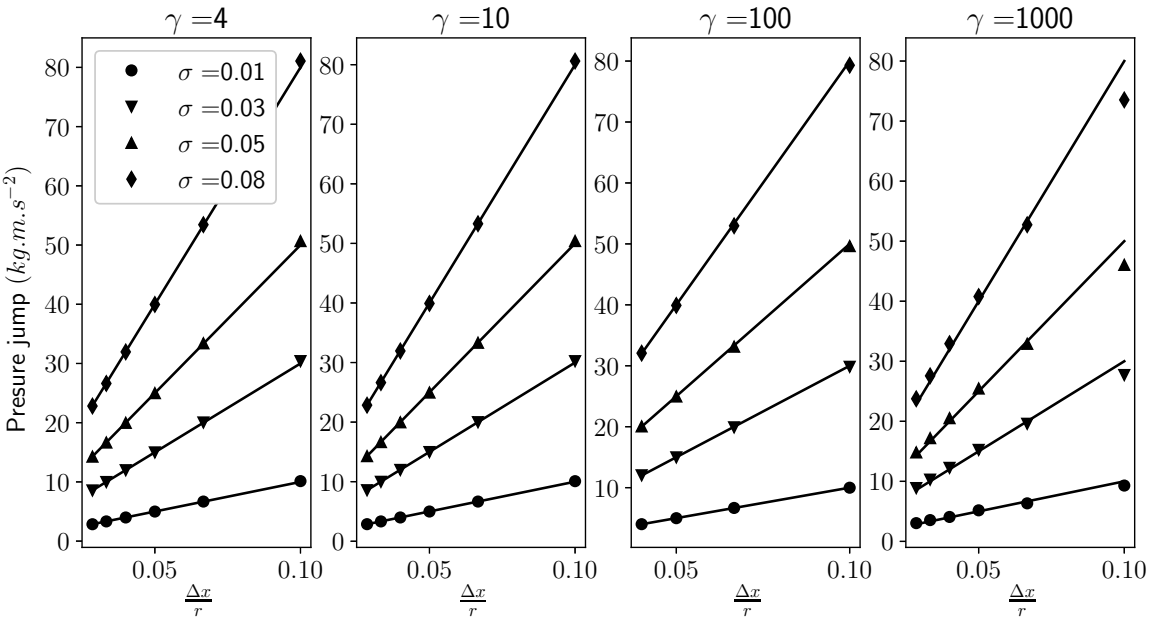


Figure 6.3. – Laplace test for a range of surface tension σ, and dimensionless radius $r/\Delta x$ for different density ratios γ. The value of the pressure jump $p_1 - p_2$ (dots) can be compared with $\frac{\sigma}{r}$ (plain curve)

the relationship of proportionality between the pressure jump and the dimensionless inverse radius $\Delta x/r$ is nicely recovered for a large range of density ratio, even as high as 1000. The accuracy of the pressure jump prediction is satisfying in most cases. Defining the relative error by:

$$E = 100\frac{|\sigma_{exp} - \sigma|}{\sigma} \quad \text{with } \sigma_{exp} = (p_1 - p_2)r \tag{6.62}$$

E is found systematically to be lower than 2% and can be as low as 0.007% for density ratio of 4, 10 and 100. For a density ratio of 1000 the error increases between 7% and 8% for the case where the radius is $r = 10\Delta x$, and higher for surface tension, and remains reasonable for the other cases. The values for the relative error are given in Table 6.1.

6.2.3. Oscillating droplet

If the previous test case allowed to evaluate the capability of the model to simulate surface tension in a static case, a dynamic case is now evaluated. The case of an ellipsoidal oscillating bubble is chosen. As in the previous case a denser phase 1 is put into a quiescent atmosphere composed of phase 2. The final shape of this droplet must be spherical. As the droplet is not initially in its equilibrium shape, surface tension initiates the contraction of the bubble to its final shape, but due to its own inertia, the bubble tends to oscillate around the spherical shape until viscous effects degrade the interface motion. The oscillation of a droplet has been studied by Lord Rayleigh [235], who proposed a theoretical value for a cylinder oscillation period when excited through different modes. When adapted to a 2D circle, this period is [236]:

$$T_{theo} = 2\pi\sqrt{\frac{(\rho_1 + \rho_2)r^3}{6\sigma}} \tag{6.63}$$

γ	σ	Droplet radius (l.b.u.) 10	15	20	25
4	0.01	1,36	0.207	0.0644	0.144
	0.03	1.34	0.201	0.0695	0.147
	0.05	1.34	0.201	0.0694	0.146
	0.08	1.34	0.202	0.0683	0.146
10	0.01	0.874	0.0195	0.168	0.164
	0.03	0.801	0.0502	0.177	0.167
	0.05	0.778	0.0578	0.180	0.169
	0.08	0.763	0.0617	0.181	0.170
100	0.01	0.101	0.148	0.0869	0.147
	0.03	0.550	0.490	0.140	0.244
	0.05	0.730	0.609	0.186	0.239
	0.08	0.861	0.683	0.223	0.221
1000	0.01	7.03	4.97	3.31	1.66
	0.03	7.62	2.02	1.59	2.07
	0.05	7.89	1.31	1.80	2.58
	0.08	8.09	1.12	1.95	2.91

Table 6.1. – Relative error E calculated with Eq(6.62) for different density ratios (γ), surface tension (σ in $kg.s^{-2}$) and for different droplet radii (expressed in l.b.u., i.e., as multiples of Δx)

The case is described as follows: in a squared box ($Nx = Ny = 128$), an ellipsoidal droplet is initialized in a quiescent atmosphere. The initial profile is given by:

$$\phi(x, y, 0) = -\tanh \frac{\sqrt{\frac{(x-x_0)^2}{a^2} + \frac{(y-y_0)^2}{b^2}} - R}{W_0} \tag{6.64}$$

where a and b are the semi-axis length of the ellipsoid, given by $a = \sqrt{\frac{3}{2}}$, $b = 1/a$, $W_0 = 1.1\Delta x$ is the initial interface width. R is the radius of the disk with the same area of the ellipse (i.e., the area of the ellipse is πR^2). The other parameters are: $\Delta x = 0.0001m$, $\nu_1 = \nu_2 = \nu_{b,1} = \nu_{b,2} = 0.0002m^2s^{-1}$, $W = 1.6\Delta x$, $\rho_2 = 1kg.m^{-3}$, $c_1 = c_2 = 347m.s^{-1}$. ρ_1 varies between $1kg.m^{-3}$ and $1000kg.m^{-3}$ All boundaries are periodic. An illustration of the setup is proposed Fig. 6.4.

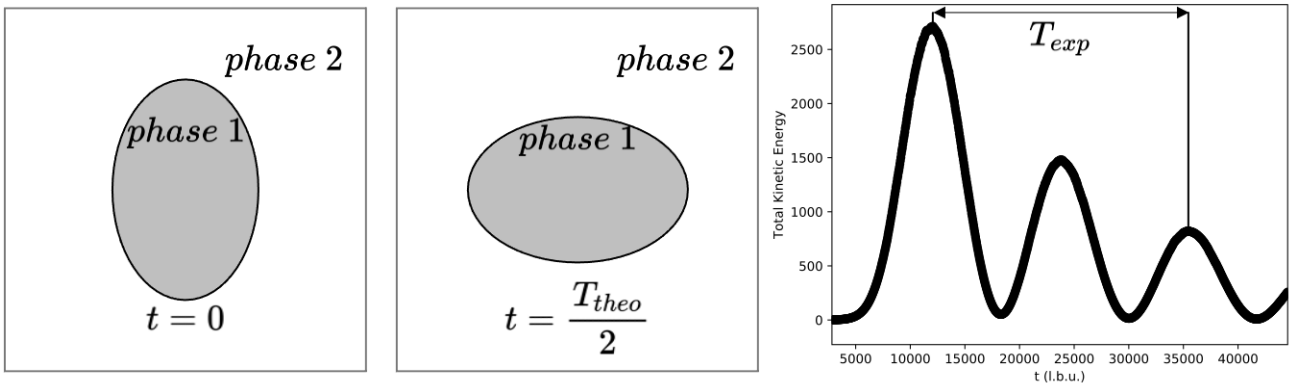


Figure 6.4. – Illustration of an oscillating ellipsoidal droplet between initial state (left) and half period state (centre). Time evolution of kinetic energy curve (right)

As explained by Rayleigh [235], the phenomenon of the oscillating droplet consists in a periodic transfer of energy between the kinetic energy and the surface tension energy. When the droplet is totally deformed, the kinetic energy is minimum and the surface tension energy is minimum when the sphere is into a spherical shape. As a consequence, the period of the phenomenon can easily be measured by plotting the kinetic energy of the system. The total kinetic energy (K_E) of the droplet is calculated through:

$$K_E = \sum_{i,j}^{N_x,N_y} \rho \frac{1+\phi}{2} \frac{u_x^2 + u_y^2}{2} \tag{6.65}$$

The temporal evolution of K_E is provided in Fig. 6.4. The period can then be determined by measuring the time between the extrema of this curve. From this measured period (noted T_{exp}), a numerical surface tension can be defined by inverting Eq.(6.63):

$$\sigma_{num} = \left(\frac{2\pi}{T_{exp}}\right)^2 \frac{(\rho_1+\rho_2)r^3}{6} \tag{6.66}$$

Then a relative error can be defined:

$$Er = 100\frac{|\sigma_{num} - \sigma|}{\sigma} \tag{6.67}$$

This analysis has been performed for different radii ($r = (15, 20, 25)\Delta x$), density ratio ($\gamma = (4, 10, 100)$ giving $\rho_2 = 1kg.m^{-3}$) and surface tension ($\sigma = (0.05, 0.07, 0.08)$). Moreover, this test case also allows to evaluate the gain in terms of numerical stability coming from the temporal correction (the counterpart of the source term given in Eq. (6.38)). The simulation is then performed twice, one with $S_t = 0$ (no correction) and one with S_t defined as in Eq. (6.38). The results are compiled in Table 6.2. It should be noted that the range of radii and surface tension is smaller than for the Laplace

		$\gamma = 4$				$\gamma = 10$				$\gamma = 100$			
		Correction		No correction		Correction		No correction		Correction		No correction	
radius	σ	σ_{exp}	Er	σ_{exp}	Er	σ_{exp}	Er	σ_{exp}	Er	σ_{exp}	Er	σ_{exp}	Er
	0.05	0.042	9.2	0.042	9.2	0.046	4.79	0.046	4.38	-	-	crash	
15	0.07	0.059	8.56	0.059	8.98	0.065	3.57	0.036	40.0	-	-	crash	
	0.08	0.068	8.38	0.068	8.80	0.075	4.79	0.040	42.3	-	-	crash	
	0.05	0.043	7.94	0.043	8.35	0.046	4.16	0.046	4.16	0.035	19.9	crash	
20	0.07	0.061	7.41	0.061	7.41	0.065	3.59	0.065	3.59	0.054	14.0	crash	
	0.08	0.070	7.28	0.070	7.28	0.075	3.42	0.075	3.22	0.065	10.8	crash	
	0.05	0.043	7.58	0.043	7.78	0.046	4.41	0.046	4.21	0.16	43.4	crash	
25	0.07	0.061	6.89	0.061	7.09	0.065	3.83	0.065	3.66	0.065	3.73	crash	
	0.08	0.070	6.74	0.070	6.74	0.074	3.67	0.075	3.47	0.073	4.72	crash	

Table 6.2. – Oscillation of an ellipsoidal droplet: comparison between expected surface tension σ and experimental value σ_{exp} The symbol "$-$" underlines a lack of oscillation and "*crash*" a lack of numerical stability.

test. This is due to the fact that all ellipsoidal droplets do not oscillate. In Fig. 6.4, it can be seen that the envelope of the kinetic energy oscillations decreases with time due to viscous dissipation. When this decrease is too sharp (i.e., when the characteristic time of the dissipation is shorter than the period of oscillation), the droplet does not oscillate. For this reason, systems with surface tension lower than $0.05kg.s^{-2}$, radii lower than $15\Delta x$, or density ratio of 1000 are not presented in this study. A possibility to simulate the oscillation of the cases would be to reduce the viscosity. In this study, it was set to $\nu = 2.10^{-4}m.s^{-2}$, but a lower value would lead to unstable behaviors.

First of all, it can be seen that the temporal correction allows a better robustness of the method at high density ratio. For a density ratio of 100, the absence of temporal correction implies the non-stability of the method. It should also be noted that, despite the absence of cases at a ratio density of 1000, they were simulated and found numerically unstable without the temporal correction. Otherwise, it can be seen that when the method is stable enough, the performances in terms of prediction are pretty similar in most cases. The trend seems to be that the higher surface tension is, the more precise the method is and the larger the radius of the droplet is, the more precise the method is. These two values are directly related to the amplitude of the oscillation: high oscillations lead to better precision. This explains the poor capability of prediction in the case $\gamma = 100$ for $r = 20$ and $r = 25$ for $\sigma = 0.05$: in all these cases, the oscillation is particularly weak, and the droplet is nearly not oscillating. In favorable cases, the performances of the method are very good since it can go as low as a 3.47% error. Giving the fact that Eq. (6.63) was obtained by assuming an inviscid system, it is reasonable to think that this performances could be enhanced in a less viscous simulation.

6.2.4. Rayleigh-Taylor instability

Previous cases showed that the method could accurately predict the interface behavior. Then the numerical robustness of the method can be interrogated. The Rayleigh Taylor instability is a good case for such investigation. This instability appears when a heavier fluid is put over a lighter one and when both of them are under the influence of a gravitational field. Under certain conditions, the interface is unstable which turns a small disturbance into non-linear behaviors and can lead to break-up for high Reynolds Number (Re) cases. In order to compare with the literature, the setup of He et al [53] is reproduced. In a rectangular box (Nx=256, Ny=1024) the, a fluid of density $\rho_1 = 3kg.m^{-3}$ is put up on a lighter fluid $\rho_2 = 1kg.m^{-3}$. The box width is $L = \Delta x Nx$. Defining the Atwood number (At) by:

$$At = \frac{\rho_1 - \rho_2}{\rho_1 + \rho_2} \tag{6.68}$$

this choice of density leads to $At = 0.5$. The phase field is initiated as:

$$\phi(x, y, 0) = \tanh \frac{y - y_0 - 0.2L \cos\left(\frac{-2\pi x}{L}\right)}{W_0} \tag{6.69}$$

y_0 being the vertical coordinate box center. As it can be seen, a single-mode initial perturbation is imposed. Moreover, a volume force is applied, taking the form:

$$\vec{F} = -\rho g \vec{e_y} \tag{6.70}$$

$\vec{e_y}$ being the vertical direction. In this case, no surface tension is included, then $\sigma = 0$. A characteristic velocity is given by $U_0 = \sqrt{Lg}$. In He et al. [53], the characteristic non-dimensional velocity is set to the value of 0.04 which gives $U_0 = 0.04\frac{\Delta x}{\Delta t}$ in the present study, as well as $L = 56.1m$. From this velocity, a Reynolds number can be determined:

$$Re = \frac{U_0 L}{\nu} = 2048 \tag{6.71}$$

Leading to the kinematic viscosity $\nu = 0.643m^2.s^{-1}$. Finally, a dimensionless time can be defined as:

$$t^* = t\sqrt{\frac{g}{L}} \tag{6.72}$$

The result of the simulation is illustrated in Fig. 6.5. The flow profiles obtained are similar to the one obtained through the HCZ method (He et al [53]). Compared to HCZ method, the present work

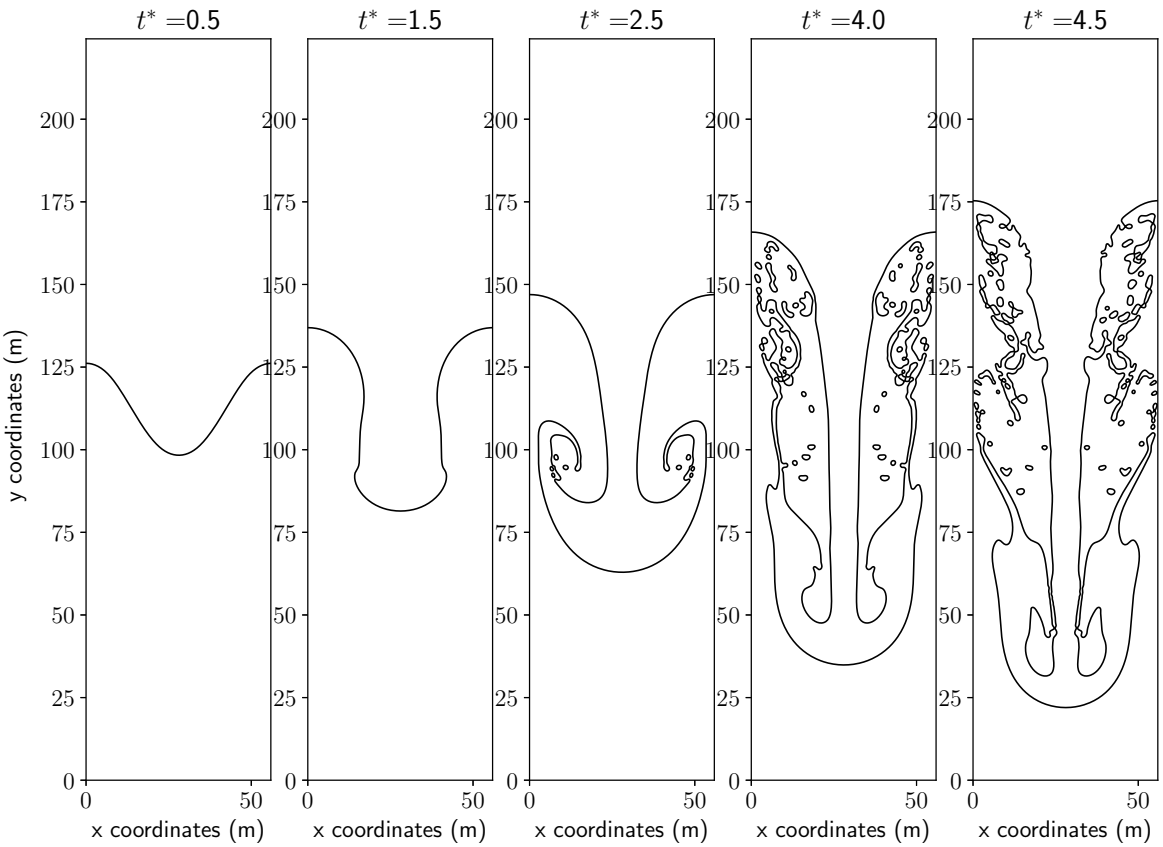


Figure 6.5. – Rayleigh-Taylor instability at various characteristic times t^*, Reynolds number is $Re = 2048$

tends to accentuate the atomization process since smaller structures appear. This results underlines the method capability to handle high Reynolds flows for a colour gradient method without the need for a high bulk viscosity. Moreover, as expected from a diffuse interface method, the break up into small structures, even in structures as complex as in the present work, does not affect the numerical stability.

Conclusion

This work focused on the investigation of Lattice Boltzmann Method applied to compressible multiphase flows, with a particular interest in accounting for compressible flows. Statistical physics basis were introduced, leading to a Lattice Boltzmann Methods basic principles presentation. A review of multiphase flows simulation's methods in a more general framework than Lattice Boltzmann Methods, as well as a comprehensive review of Lattice Boltzmann methods applied to multiphase flows was proposed. This last review showed the strong link between diffuse interface methods and Lattice Boltzmann Methods. The different methods allowing to introduce surface tension, to solve a phase field equation or to set a real gas equation of state were also listed.

In the present work, a Taylor expansion of a Lattice Boltzmann Method involving a body force was proposed. This expansion allows to determine a Lattice Boltzmann algorithm equivalent macroscopic equation in a more rigorous way than the widely used Chapman-Enskog method. In addition, the Taylor expansion allows to determine the LBM discretization error.
A theoretical analysis of the colour gradient method was proposed. Based on a Taylor's expansion, an expression for the Δt^2 colour gradient error term for the macroscopic equivalent momentum transport equation was proposed. Thanks to this expression, the form of the equilibrium function when accounting for a non-perfect equation of state was discussed. It turns out that the Hermite's fourth order moment of the equilibrium function is of prime importance, and a non-cautious choice can lead to severe instabilities at the interface location. A theoretical argument was added to the already known empirical argument that allows to choose carefully an accurate operator. In addition, the re-coloration phase equivalent macroscopic equation was established. It can be shown that re-coloration allows to solve a phase field equation as proposed in Chiu and Lin [47]. It was also shown that the recoloration scheme implies a natural thickening for which characteristic time was proposed.

Based on the theoretical analysis conducted along this manuscript, an improved colour gradient algorithm was proposed. In this algorithm, the stream and collide algorithm structure is preserved. As for other colour gradient methods, the knowledge of the first neighbours only is required, preserving LBM efficiency and scalability. The proposed model is used with a stiffened gas equation but can be generalised to an arbitrary equation of state, removing the nonphysical relationship between the speed of sound and the density ratio in the colour gradient original formulation.
Finally, an original temporal correction is proposed, allowing to improve numerical stability for high density ratio configurations. The algorithm efficiency and consistency was assessed on academical test-cases. The improved algorithm was shown to be stable for simple cases at density ratios as high as 1000. On a Rayleigh-Taylor test-case, the proposed algorithm method showed to be stable for Reynolds number as high as 3000, but is limited to low density ratios (around 3).

Perspectives

From this work, several perspectives can be foreseen.
The proposed operator to account for an equation of state can be generalised to other contexts than multiphase flows. In particular, modifying the Equation of State is also of importance in a compressible flows context, then this operator can be generalised to this framework.

It has been shown that re-coloration operator allows to solve a phase field equation in an efficient

way. The gain in term of computational time has not been evaluated properly nevertheless in comparison with other existing methods in the literature such as double distribution or hybrid methods. In addition, a stability comparison between these methods would also be of interest.
As all numerical methods, the present improved colour gradient algorithm induces the appearance of spurious currents at the interface location. This spurious currents production is a major concern since they are source of numerical instabilities. Their origin is still a subject of investigation since no general agreement exist on this subject. Jamet et al. [237] states that these spurious currents result from of a lack of chemical potential equilibrium in the interface while Lee and Fisher considered spurious current as a purely numerical issue [138]
As the present study takes place in a compressible framework, acoustic wave studies are of major importance. In particular, acoustic waves resulting from the numerical method is a subject of discussion in itself. Spurious acoustic waves tends to appear at the interface location and to stay in the domain when interacting with boundary conditions. Non Reflective Boundary Conditions must be investigated in order to tackle this issue and then increase numerical stability and physical accuracy.
Finally, for multiphase flow problems involving large gradients that lead to numerical instability, a fine mesh is required to ensure numerical stability. Yet, this fine mesh is required only at the interface location. An adaptive mesh refinement mechanism would allow both a stable simulation, and a significant computational cost reduction.

Appendices

Appendix A

Appendix A

A.1. pressure and internal energy

If the definition of the pressure is challenging in itself, the mechanical effect of the pressure is well known. When it is in contact with a wall, a fluid exerts a force proportionally to the contact surface between the wall and the fluid. Even if it is restrictive, pressure can then be interpreted as a surface force. The reason why fluids exert a force on an adjacent wall comes from the collision between in-coming particle and the wall. If the wall is assumed to exert no particular attractive or repulsive force on the particles, then when entering into contact with the wall, the particle will bounce-back. The bounce-back is supposed to be ideally elastic, i.e., the magnitude of the velocity is conserved, the particle will change its direction to the opposite one. This brutal change of direction leads to a force applied to the wall proportional to the momentum jump according to the 3^{rd} Newton principle.
To determine the link between pressure p and distribution function f, we will make the assumption that the fluid is at rest, making the state of the flow constant in space and time. Then in that demonstration, f is only a function of $\vec{\xi}$. More over, the spherical coordinates will be used, then $\vec{\xi}(\xi_x, \xi_y, \xi_z)$ can also be written $\vec{\xi}(|v|, \varphi, \theta)$. With $|v|$ the norm of the velocity (relatively to the main velocity), φ the azimuthal angle and θ the polar angle
We assume that a wall is placed normal to the z-direction, and is supposed to be at rest with the fluid, i.e. going at the speed $\vec{u}$. A particle travelling at the relative velocity $-v$ will impact the wall and change its momentum from $-mv$ to mv with m the mass of one particle, resulting to a momentum change of $2mv$. Now, let's consider an infinitesimal time length dt during which a certain number of particle will hit the wall. We consider particles whose velocity have an azimuthal angle φ, a polar angle $\pi + \theta$ and a norm (relatively to the wall) $|\vec{v}|$. Note that to hit the wall, the velocity must lean toward the wall, i.e. $\theta \in [0, -\pi]$. Such particles will hit the wall during the time interval dt if and only if they are included in the parallelepiped illustrated Figure A.1.

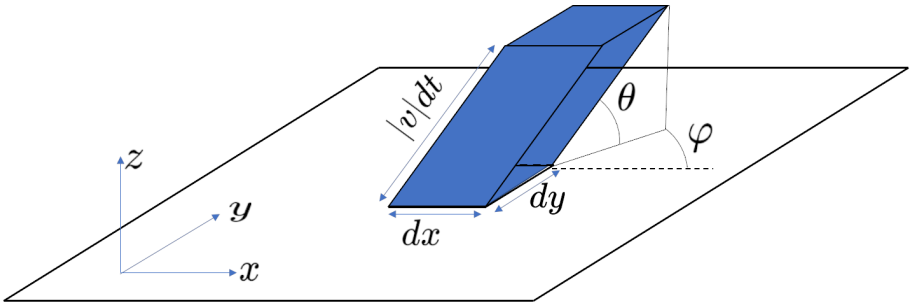


Figure A.1. – Illustration of a cone of particle hitting the surface of area dS

The quantity of particle included in this volume is expressed as:

$$|\vec{v}|dtcos(\theta)d\varphi d\theta d|\vec{v}|f(\vec{\xi}(|\vec{v}|, \varphi + \pi, -\theta))dxdy \tag{A.1}$$

Then the variation of momentum that was applied to the surface dS is equal to the previous quantity times the velocity of the particles projected on the z-direction, i.e.

$$2dS\frac{|\vec{v}|^4}{3}cos(\theta)sin(\theta)f(\vec{\xi}(|\vec{v}|, \varphi + \pi, -\theta))d\varphi d\theta d|\vec{v}|dtdxdy \tag{A.2}$$

To obtain the pressure, this expression must be integrated among the microscopic velocity space

$$p = \int_{|\vec{v}|=0}^{|\vec{v}|=+\infty}\int_{\varphi=0}^{\varphi=\pi}\int_{\theta=0}^{\theta=\pi} 2cos^2(\theta)sin(\theta)|\vec{v}|^4 f(\vec{\xi}(|\vec{v}|, \varphi + \pi, -\theta))d\varphi d\theta d|\vec{v}| \tag{A.3}$$

This expression cannot be reduced without an additional fundamental hypothesis: the hypothesis of isotropy. We assume that the distribution function is only function of the norm of the microscopic

velocity: $f(\vec{\xi}(|v|,\varphi,\theta)) = f(|v|)$. It allows to calculate the integrals as follow:

$$p = 2\int_{\varphi=0}^{\varphi=\pi}\int_{\theta=0}^{\theta=2\pi} cos^2(\theta)sin(\theta)d\varphi d\theta \int_{|\vec{v}|=0}^{|\vec{v}|=+\infty} |\vec{v}|^4 f(|\vec{v}|)d|\vec{v}| = \frac{4\pi}{3}\int_{|\vec{v}|=0}^{|\vec{v}|=+\infty} |\vec{v}|^4 f(|\vec{v}|)d|\vec{v}| \tag{A.4}$$

It happens that $4\pi = \int_{\varphi=0}^{\varphi=2\pi}\int_{\theta=0}^{\theta=\pi} cos(\theta)d\varphi d\theta$ which allows us to write:

$$p = \frac{1}{3}\int_{|\vec{v}|=0}^{|\vec{v}|=+\infty}\int_{\varphi=0}^{\varphi=\pi}\int_{\theta=0}^{\theta=2\pi} cos^2(\theta)sin(\theta)|\vec{v}|^4 f(|v|)d|\vec{v}| = \frac{1}{3}\iiint |\vec{v}|^2 f(\vec{\xi})d\vec{\xi} \tag{A.5}$$

Taking into consideration the definition of the internal energy Eq. 1.5 in this framework, the pressure is proportional to the internal energy :

$$p = \frac{2}{3}\rho e \tag{A.6}$$

A.2. Equilibrium function

Here, the demonstration of the form taken by the equilibrium function is proposed. The main hypothesis is that the equilibrium function must be isotropic. The partition function is normally function of $\vec{v}$, φ and θ. As it is isotropic, the partition function is only function of $|\vec{v}|$. The equilibrium function is now written $f^{eq}(|\vec{v}|)$. The next hypothesis is that the distribution function is the product of three function of the coordinates of the velocity:

$$f^{eq}(|\vec{v}|^2) = f_x^{eq}(v_x^2) f_y^{eq}(v_y^2) f_z^{eq}(v_z^2) \tag{A.7}$$

Then if we note $a(v_x^2) = ln(f_x^{eq}(v_x^2))$ and $b(|\vec{v}|^2) = ln(f^{eq}(|\vec{v}|^2))$, then we have

$$a(v_x^2) + a(v_y^2) + a(v_z^2) = b(v_x^2 + v_y^2 + v_z^2) \tag{A.8}$$

The partial derivative of the previous equation with respect to v_x^2 gives:

$$a'(v_x^2 + v_y^2 + v_z^2) = b'(v_x^2) \tag{A.9}$$

Then the derivative with respect to v_y^2 or v_z^2 gives: $a'' = 0$, and then:

$$ln(f^{eq}(|\vec{v}|)) = \alpha - \beta |\vec{v}|^2 \tag{A.10}$$

with α and β integration constants. Then:

$$f^{eq} = e^{\alpha} e^{-\beta |\vec{v}|^2} \tag{A.11}$$

The values of α and β are then deduced from the integral relationship that should respect any partition function. The integral of this partition function is still equal to the density, then:

$$\int f^{eq}(|\vec{v}|) d\vec{\xi} = e^{\alpha} \int_{-\infty}^{+\infty} \int_{-\infty}^{+\infty} \int_{-\infty}^{+\infty} e^{\left(-\beta\left(v_x^2 + v_y^2 + v_z^2\right)\right)} d\xi_x d\xi_y d\xi_z = \rho \tag{A.12}$$

Then $f^{eq}(|\vec{v}|) = \rho \left(\frac{\beta}{\pi}\right)^{\frac{3}{2}} e^{-\beta |\vec{v}|^2}$. By calculating the

$$\rho e = \rho \left(\frac{\beta}{\pi}\right)^{\frac{3}{2}} \int_{-\infty}^{+\infty} \int_{-\infty}^{+\infty} \int_{-\infty}^{+\infty} \left(v_x^2 + v_y^2 + v_z^2\right)^2 e^{\left(-\beta\left(v_x^2 + v_y^2 + v_z^2\right)\right)} d\xi_x d\xi_y d\xi_z = \frac{3\rho}{4\beta} \tag{A.13}$$

The value of β can then be deduced from Eq. (A.6), and by assuming the law of perfect gas:

$$\beta = \frac{1}{2rT} \tag{A.14}$$

Which finally gives us:

$$f^{eq} = \frac{\rho}{(2\pi r T)^{\frac{3}{2}}} e^{-\frac{|\vec{v}|^2}{2rT}} \tag{A.15}$$

A.3. From LBM to the Boltzmann Equation

In this section, the link between the LBM algorithm proposed by He and Luo [58] and the Boltzmann equation is proposed. A variable should be made, then $\bar{f}_i$ is introduced: $\bar{f}_i = f_i - \frac{1}{2\tau}\left(f_i - f_i^{eq}\right)$. This definition is included into Eq. (1.82) giving:

$$\begin{aligned} \bar{f}_i(x, t + \Delta t) = {} & \bar{f}_i(x - \xi_{\alpha,i}\Delta t, t) \\ & - \frac{1}{2\tau}\left(\left[f_i(x - \xi_{\alpha,i}\Delta t, t) - f_i^{eq}(x - \xi_{\alpha,i}\Delta t, t)\right] + \left[f_i(x, t + \Delta t) - f_i^{eq}(x, t + \Delta t)\right]\right) \end{aligned} \tag{A.16}$$

Giving the definition of $\bar{f}_i$, the following equation is true:

$$\frac{1}{\tau}\left(f_i - f_i^{eq}\right) = \frac{1}{\tau - 1/2}\left(\bar{f}_i - f_i^{eq}\right) \tag{A.17}$$

Taking into account Eq. (A.17) into Eq. (A.16), we obtain:

$$\begin{aligned}\bar{f}_i(x, t+\Delta t) = \bar{f}_i(x - \xi_{\alpha,i}\Delta t, t) - \\ \frac{1}{2(\tau - 1/2)}\left(\left[\bar{f}_i(x - \xi_{\alpha,i}\Delta t, t) - f_i^{eq}(x - \xi_{\alpha,i}\Delta t, t)\right] + \left[\bar{f}_i(x, t+\Delta t) - f_i^{eq}(x, t+\Delta t)\right]\right)\end{aligned} \tag{A.18}$$

Using the Taylor expansion to one order in Δt, i.e. giving $\bar{f}_i(x, t+\Delta t) = \bar{f}_i(x,t) + O(\Delta t)$, $\bar{f}_i(x - \xi_{\alpha,i}\Delta t, t) = \bar{f}_i(x,t) + O(\Delta t)$ (same expression is used for f_i^{eq}), Eq. (A.18) becomes:

$$\bar{f}_i = f_i^{eq} + O(\Delta t) \tag{A.19}$$

Then using: $\bar{f}_i(x, t+\Delta t) = \bar{f}_i(x,t) + \Delta t \partial_t \bar{f}_i(x,t) + O(\Delta t^2)$ and $\bar{f}_i(x - \xi_{\alpha,i}\Delta t, t) = \bar{f}_i(x,t) - \Delta t \xi_{\alpha,i}\partial_\alpha \bar{f}_i(x,t) + O(\Delta t^2)$ Eq. (A.18) becomes:

$$\Delta t\left[\partial_t \bar{f}_i + \xi_{\alpha,i}\partial_\alpha \bar{f}_i\right] = -\frac{1}{\tau - 1/2}\left(\bar{f}_i - f_i^{eq}\right) + \frac{\Delta t}{2(\tau - 1/2)}\left[\xi_\alpha \partial_\alpha(\bar{f}_i - f_i^{eq}) - \partial_t(\bar{f}_i - f_i^{eq})\right] + O(\Delta t^2) \tag{A.20}$$

Giving that according to Eq. (A.19), $\bar{f}_i - f_i^{eq} = O(\Delta t)$, then:

$$\partial_t \bar{f}_i + \xi_\alpha \partial_\alpha \bar{f}_i = \frac{1}{\Delta t(\tau - 1/2)}\left[\bar{f}_i - f_i^{eq}\right] + O(\Delta t) \tag{A.21}$$

Finally, using the Taylor expansion relationship to the order 2:

$$f_i(x, t+\Delta t) = f_i(x,t) + \Delta t \partial_t f_i(x,t) + \frac{\Delta t^2}{2}\partial_t^2 f_i(x,t) + O(\Delta t^3) \tag{A.22}$$

$$f_i(x - \xi_\alpha \Delta t, t) = f_i(x,t) - \Delta t \xi_\alpha \partial_\alpha f_i(x,t) + \xi_\alpha \xi_\beta \frac{\Delta t^2}{2}\partial^2_{\alpha\beta} f_i(x,t) + O(\Delta t^3) \tag{A.23}$$

Integrating Eq. (A.22) into Eq. (A.18), it comes:

$$\begin{aligned}\Delta t\left[\partial_t f_i + \xi_\alpha \partial_\alpha f_i\right] = -\frac{1}{(\tau - 1/2)}\left(\bar{f}_i - f_i^{eq}\right) - \frac{\Delta t^2}{2}\left[\partial_t^2 \bar{f}_i - \xi_\alpha \xi_\beta \partial^2_{\alpha\beta}\bar{f}_i\right] \\ + \underbrace{\frac{\Delta t}{2(\tau - 1/2)}\left[\partial_t(\bar{f}_i - f_i^{eq}) - \xi_\alpha \partial_\alpha(\bar{f}_i - f_i^{eq})\right]}_{(1)} - \underbrace{\frac{\Delta t^2}{2(\tau - 1/2)}\left[\partial_t^2\left(\bar{f}_i - f_i^{eq}\right) + \xi_\alpha\xi_\beta\partial^2_{\alpha\beta}\left(\bar{f}_i - f_i^{eq}\right)\right]}_{(2)} \\ + O(\Delta t^3)\end{aligned} \tag{A.24}$$

In the previous equation Eq. (A.24), giving that $\bar{f}_i = f_i^{eq} + (\Delta t)$ (Eq. (A.19)), we directly have $(2) = O(\Delta t^3)$. The expression of the value of $\bar{f}_i - f_i^{eq}$ allow to express (1) only in term of $\bar{f}_i$, by injecting Eq. (A.21) into (1):

$$\begin{aligned}(1) = \frac{\Delta t^2}{2(\tau - 1/2)}\left[\partial_t\left[(\tau - 1/2)\left[\partial_t \bar{f}_i + \xi_\beta \partial_\beta \bar{f}_i\right]\right] - \xi_\alpha \partial_\alpha\left[(\tau - 1/2)\left[\partial_t \bar{f}_i + \xi_\beta \partial_\beta \bar{f}_i\right]\right]\right] \\ = \frac{\Delta t^2}{2}\left[\partial_t^2 \bar{f}_i - \xi_\alpha \xi_\beta \partial^2_{\alpha\beta}\bar{f}_i\right]\end{aligned} \tag{A.25}$$

Injecting the expressions of (1) and (2) into Eq. (A.24), it becomes:

$$\partial_t \bar{f}_i + \xi_\alpha \partial_\alpha \bar{f}_i = -\frac{\Delta t}{\tau - 1/2}\left(\bar{f}_i - f_i^{eq}\right) + O(\Delta t^2) \tag{A.26}$$

A.4. CFL condition in LBM

In this appendix, the motivation behind the CFL condition usually imposed in the Lattice Boltzmann framework is presented here. In the classical LBM framework, the equilibrium function is given by:

$$f_i^{eq} = w_i \rho \left[1 + \frac{u_\alpha \xi_{\alpha,i}}{c_s^2} + u_\alpha u_\beta \frac{\xi_{\alpha,i}\xi_{\beta,i} - c_s^2 \delta_{\alpha\beta}}{2c_s^4} \right] \tag{A.27}$$

The attentive reader would have note that if in the thermal case, the order two in polynomial involved a pressure term, then it seems like no pressure term is involved in this model. Actually, a fundamental property of the Lattice Boltzmann method is the moment cascade.
To introduce this concept, we must distinguish the raw moments and the Hermite polynomial moments. The raw moments are defined as the successive moments of the partition function that takes the following form:

$$\mathcal{M}_{\alpha_1,\alpha_2,...,\alpha_n} = \int_{-\infty}^{+\infty} \xi_{\alpha_1}\xi_{\alpha_2}...\xi_{\alpha_n} f d\vec{\xi} \tag{A.28}$$

It is very important to note that the raw moments carry the physical meaning of the partition function, while the Hermite's polynomial moment are practical tools used to discretize the equilibrium function in the microscopic velocity space. To emphasize this point, we note that the macroscopic equation obtained through the Chapman-Enskog method can be written in term of raw moment. For instance, for the first moment:

$$\partial_t \mathcal{M}_\alpha^{eq} + \partial_\beta \mathcal{M}_{\alpha\beta}^{eq} = \tau \partial_\beta \left[\partial_t \mathcal{M}_{\alpha\beta}^{eq} + \partial_\gamma \mathcal{M}_{\alpha\beta\gamma}^{eq} \right] \tag{A.29}$$

$\mathcal{M}_*^{eq}$ being the raw moments of the equilibrium function. We noted that the Hermite's polynomial form an orthogonal basis in the polynomial space, but it is not the case for the raw polynomials. It means in concrete terms that a raw polynomial of order n will have moments at superior order. A raw polynomial of degree n is given by:

$$\mathcal{H}_{\alpha_1\alpha_2...\alpha_n} = \xi_{\alpha_1}\xi_{\alpha_2}...\xi_{\alpha_n} \tag{A.30}$$

Then, scalar products between different order polynomials are not equal to 0 in general, unlike the Hermite polynomial. For instance:

$$\int_{\infty}^{+\infty} w(\vec{\xi}) \mathcal{H}_{xx}(\vec{\xi}) \mathcal{H}_{xxxx}(\vec{\xi}) d\vec{\xi} = \frac{5}{9} \left(\frac{\Delta x}{\Delta t} \right)^2 \neq 0 \tag{A.31}$$

This lake of orthogonality can be clearly seen if we express the raw polynomial in term of Hermite polynomial. For instance:

$$\mathcal{H}_0 = H_0$$
$$\mathcal{H}_{xx} = H_{xx} + c_s^2 H_0$$

Then the non-orthogonality of $\mathcal{H}_0$ and $\mathcal{H}_{xx}$ becomes clear. But the last relationship illustrates the fact that in our framework the contribution to the total energy ($\mathcal{M}_{\alpha\beta}$) comes from the projection of the partition function on the moments $H_{\alpha\beta}$ but also from the moment H_0.
This explains why, despite the presence of no pressure term in the equilibrium function, in the formulation proposed by He et al. Eq. (A.15), the equivalent equation at the order 1 in Δt for the 1^{st} moment in Hermite is given by:

$$\partial_t \rho u_\alpha + \partial_\beta \left(\rho u_\alpha u_\beta + \rho (\sum_i \xi_\alpha \xi_\beta w_i) \right) = O(\Delta t) \tag{A.32}$$

In the present situation the system doesn't seem realistic as, in a isothermal framework, the term inside the derivative should take the following form: $\rho u_\alpha u_\beta + \rho c_s^2 \delta_{\alpha\beta}$. Then to retrieve this behavior

two solutions are possible. In the first case, we can add a second order term in the equilibrium function to "remove" the spurious term and "add" the desired one:

$$f_i^{eq} += \rho \left(c_s^2 - \sum_i \xi_\alpha \xi_\beta w_i \right) \delta_{\alpha\beta} \frac{H_{\alpha\beta}}{2c_s^4} \tag{A.33}$$

In practice, a second solution is chosen, constraint is imposed on the x_i and on the w_i to have:

$$\sum_i w_i \xi_\alpha \xi_\beta = c_s^2 \delta_{\alpha\beta\gamma} \tag{A.34}$$

It should be noted that the term $\sum_i w_i \xi_\alpha \xi_\beta$ depends with the numerical scheme. The question of the numerical scheme is detailed afterward, but the information to remember for the moment is that for the most commonly used scheme (D_2Q_9, D_3Q_{19} or D_3Q_{27} for instance), $\sum_i w_i \xi_\alpha \xi_\beta = \frac{\Delta x^2}{3\Delta t^2}$, then it comes that this term is linked to the ratio between the spatial step and the time step. It comes that the second solution for having the good pressure term consists in a condition on the Courant number (also called CFL number) that comes as:

$$\frac{\Delta x}{\Delta t} = \sqrt{3} c_s \tag{A.35}$$

Despite imposing a condition on the CFL number, the second solution is simpler and requires less computational effort, and also the first choice showed to reduce the numerical stability of the whole method. This discussion is an introduction to another discussion that will be addressed later in this document which is the practical solution to introduce an Equation of State in a Lattice Boltzmann system, which is not straightforward due to the moments cascade phenomenon described earlier.

A.5. Construction of the Hermite polynomials

The Hermite polynomials are an infinite family of polynomial defined from the weight function:

$$w(x) = \frac{1}{\sqrt{2\pi}} e^{\frac{-x^2}{2}} \tag{A.36}$$

Their are given by the successive derivative of this function; the n^{th} order Hermite polynomial (n being an integer) is given by:

$$H^{(n)} = (-1)^n \frac{1}{w} w^{(n)} \tag{A.37}$$

where $w^{(n)}$ is the n^{th} derivative of the function w. The first six polynomials are given by:

$$\begin{array}{cc} H^{(0)}(x) = 1 & H^{(1)}(x) = x \\ H^{(2)}(x) = x^2 - 1 & H^{(3)}(x) = x^3 - 3x \\ H^{(4)}(x) = x^4 - 6x^2 + 3 & H^{(5)}(x) = x^5 - 10x^3 + 15x \end{array} \tag{A.38}$$

They were introduced in a statistical mechanic framework by Grad [238]. The Hermite polynomial can then be generalised to a D spatial dimensions system. The Hermite polynomial in a multi-dimensional system is a tensor of rank n, it is given by:

$$\vec{H}^{(n)}_{x_1,x_2,...,x_n} = (-1)^n \frac{1}{w} \partial^{(n)}_{x_1,x_2,...,x_n} w \quad w(x) = \frac{1}{(2\pi)^{\frac{D}{2}}} e^{\frac{-x^2}{2}} \tag{A.39}$$

with x_1, x_2, x_n being dimensions of space include in $[1, D]$. For instance, $\vec{H}^{(3)}_{xxy} = (x^2 - 1)y$.
The interest of the Hermite polynomial is that they form an orthogonal base in the function base. We can define a product

$$\int_{-\infty}^{\infty} w(\vec{x}) \vec{H}^{(n)}_{\vec{\alpha}} \vec{H}^{(n)}_{\vec{\beta}} d^D \vec{x} = \Pi_{i=1}^{D} n_i! \delta^{(n+m)}_{\vec{\alpha}\vec{\beta}} = 0 \tag{A.40}$$

where δ is a Kronecker function, i.e., $\delta_{nm} = 1$ if $n = m$ and $\delta_{nm} = 0$ otherwise. In the previous equation $\vec{\alpha} = (\alpha_1, \alpha_2, ..., \alpha_n)$ and $\vec{\beta} = (\beta_1, \beta_2, ..., \beta_n)$ are vectors of size n and m respectively with α_k and β_k directions of space. For instance we can write $\vec{\alpha} = (x, y, y)$. Then $\delta^{(n+m)}_{\vec{\alpha}\vec{\beta}}$ is a generalization of the Kronecker operator which is equal to 1 if $\vec{\beta}$ is a permutation of $\vec{\alpha}$. For example for $\vec{\alpha} = (x, x, y)$ $\vec{\beta} = (x, y, z)$ then $\delta^{(6)}_{\vec{\alpha}\vec{\beta}} = 0$, but if $\vec{\alpha} = (x, y, y)$ and $\vec{\beta} = (y, x, y)$ then $\delta^{(6)}_{\vec{\alpha}\vec{\beta}} = 1$. To illustrate that:

$$\int w(\vec{x}) \vec{H}^{(2)(\vec{x})}_{xy} \vec{H}^{(3)(\vec{x})}_{xxy} = 0 \tag{A.41}$$

$$\int w(\vec{x}) \vec{H}^{(2)(\vec{x})}_{xx} \vec{H}^{(2)(\vec{x})}_{xx} = 2 \tag{A.42}$$

The fact that the Hermite polynomial forms an orthogonal bases allows the fact that any well behaved function h can be expressed as a series of Hermite polynomial:

$$h(\vec{x}) = w(\vec{x}) \sum_{n=0}^{\infty} \frac{1}{n!} a^{(n)} \vec{H} \quad \vec{a}^{(n)} = \int h(\vec{x}) \vec{H}^{(n)} d\vec{x} \tag{A.43}$$

By applying this rules, the equilibrium function can be expressed in term of Hermite polynomial:

$$f_i^{eq}(\rho, \vec{u}, T, \vec{\xi}) = w(\xi) \sum_{n=0}^{\infty} \frac{1}{n!} \vec{a}^{(n),eq}(\rho, \vec{u}, T) \vec{H}^{(n)}(\vec{\xi}) \tag{A.44}$$

with

$$\vec{a}^{(n),eq}(\rho,\vec{u},T)=\int f_i^{eq}(\rho,\vec{u},T,\vec{\xi})\vec{H}^{(n)}(\vec{\xi})d\vec{\xi} \tag{A.45}$$

It comes:

$$\begin{gathered}
a^{(0),eq}=\rho \\
a_\alpha^{(1),eq}=\rho u_\alpha \\
a_{\alpha\beta}^{(2),eq}=\rho u_\alpha u_\beta+\rho(rT-1)\delta_{\alpha\beta} \\
a_{\alpha\beta\gamma}^{(3),eq}=\rho=\rho\left[u_\alpha u_\beta u_\gamma+(rT-1)\left(u_\alpha\delta_{\beta\gamma}+u_\beta\delta_{\alpha\gamma}+u_\gamma\delta_{\alpha\beta}\right)\right]
\end{gathered} \tag{A.46}$$

$$\int_{-\infty}^{\infty} w(\vec{x})\vec{H}_{\vec{\alpha}}^{(n)}\vec{H}_{\vec{\beta}}^{(n)}d^D\vec{x}=\Pi_{i=1}^D n_i!\delta_{\vec{\alpha}\vec{\beta}}^{(n+m)}=0 \tag{A.47}$$

The attentive reader might have note an issue concerning the previous formulation, some terms are summed without having the same dimension (notably rT and 1). This is due to the fact than in the definition of the Hermite polynomial that doesn't take this physical consideration into account. For instance, $H_{xx}^{(2)}=\xi_x^2-1$ is not homogeneous. For this reason, in practice the definition of the weight function and the Hermite polynomial in the Lattice Boltzmann context is changed to:

$$\tilde{w}(\vec{\xi})=\frac{1}{\sqrt{2\pi}^{D/2}(rT)^D}e^{-\frac{|\vec{xi}|^2}{2rT}} \tag{A.48}$$

and

$$\vec{\tilde{H}}^{(n)}(\vec{\xi})=\frac{(-rT)^n}{w(\vec{\xi})}\vec{\nabla}^{(n)}w(\xi) \tag{A.49}$$

Then the Hermite polynomial expression are modified to:

$$\begin{gathered}
\tilde{H}^{(0)}=1 \quad \tilde{H}_\alpha^{(1)}(\vec{\xi})=\xi_\alpha \\
\tilde{H}_{\alpha\beta}^{(2)}(\vec{\xi})=\xi_\alpha\xi_\beta-rT\delta_{\alpha\beta} \quad \tilde{H}_{\alpha\beta\gamma}^{(3)}(\vec{\xi})=\xi_\alpha\xi_\beta\xi_\gamma-rT(\xi_\alpha\delta_{\beta\gamma}+\xi_\beta\delta_{\alpha\gamma}+\xi_\gamma\delta_{\alpha\beta}) \\
\tilde{H}_{\alpha\beta\gamma\mu}^{(4)}(\vec{\xi})=\xi_\alpha\xi_\beta\xi_\gamma\xi_\mu-rT\left(\xi_\alpha\xi_\mu\delta_{\beta\gamma}+\xi_\beta\xi_\mu\delta_{\alpha\gamma}+\xi_\gamma\xi_\mu\delta_{\alpha\beta}+\xi_\alpha\xi_\beta\delta_{\gamma\mu}+\xi_\alpha\xi_\gamma\delta_{\beta\mu}+\xi_\beta\xi_\gamma\delta_{\alpha\mu}\right) \\
+(rT)^2\left(\delta_{\beta\gamma}\delta_{\alpha\mu}+\delta_{\alpha\beta}\delta_{\gamma\mu}+\delta_{\alpha\beta}\delta_{\gamma\mu}\right)
\end{gathered} \tag{A.50}$$

Then the scalar product relationship is modified as follow:

$$\int_{-\infty}^{\infty} w(\vec{\xi})\vec{\tilde{H}}_{\vec{\alpha}}^{(n)}\vec{\tilde{H}}_{\vec{\beta}}^{(n)}d^D\vec{\xi}=\Pi_{i=1}^D n_i!(rT)^n\delta_{\vec{\alpha}\vec{\beta}}^{(n+m)}=0 \tag{A.51}$$

Then the expression of an arbitraty function h expressed as a serie of Hermite polynomial:

$$h(\vec{\xi})=\tilde{w}(\vec{\xi})\sum_{n=0}^{\infty}\frac{\vec{\tilde{a}}^{(n)}}{n!(rT)^n}\vec{\tilde{H}}^{(n)}(\vec{\xi}) \quad \vec{\tilde{a}}^{(n)}=\int h(\vec{\xi})\vec{\tilde{H}}^{(n)}(\vec{\xi})d\vec{\xi} \tag{A.52}$$

The new expressions of the integrals come as:

$$\begin{gathered}
a^{(0),eq}=\rho \\
a_\alpha^{(1),eq}=\rho u_\alpha \\
a_{\alpha\beta}^{(2),eq}=\rho u_\alpha u_\beta \\
a_{\alpha\beta\gamma}^{(3),eq}=\rho u_\alpha u_\beta u_\gamma
\end{gathered} \tag{A.53}$$

The attentive reader would have note that the Hermite polynomial as proposed in Eq. (A.50) are function of the temperature, it would mean that the velocity set, and then the grid length, would depend with the temperature. As it is obviously not possible, the Hermite polynomial need to be modified one more time with the athermal assumption. In this assumption, we define a reference temperature T_0 and the temperature will be constant for the weighted function. In an isothermal

framework, the Laplace constant is equal to 1: $\gamma = 1$ and then the speed of sound is equal to: $c_s = \sqrt{rT_0}$. Note that this reference speed corresponds to the speed of sound of the system if and only if the system is isothermal. The weighted function is given by:

$$w_{at}(\vec{\xi}) = \frac{(-c_s^2)^n}{\sqrt{2\pi}^{D/2} c_s^{2D}} e^{-\frac{|\vec{\xi}|^2}{2c_s^2}} \tag{A.54}$$

The expression of the Hermite polynomial (and the one that is used in practice) is given by:

$$\begin{array}{cc} H_0 = 1 & H_\alpha = \xi_\alpha \\ H_{\alpha\beta} = \xi_\alpha\xi_\beta - c_s^2\delta_{\alpha\beta} & H_{\alpha\beta\gamma} = \xi_\alpha\xi_\beta\xi_\gamma - c_s^2\left[\xi_\alpha\delta_{\beta\gamma} + \xi_\beta\delta_{\alpha\gamma} + \xi_\gamma\delta_{\alpha\beta}\right] \end{array} \tag{A.55}$$

The moments of the equilibrium function are then modified. To make the link with the discussion proposed in Chapter 5, temperature is expressed under the form a pressure term: $p = \rho r T$:

$$\begin{array}{c} a^{(0),eq} = \rho \\ a_\alpha^{(1),eq} = \rho u_\alpha \\ a_{\alpha\beta}^{(2),eq} = \rho u_\alpha u_\beta - [p - \rho c_s^2]\delta_{\alpha\beta} \\ a_{\alpha\beta\gamma}^{(3),eq} = \rho u_\alpha u_\beta u_\gamma + (p - \rho c_s^2)\left[u_\alpha\delta_{\beta\gamma} + u_\beta\delta_{\alpha\gamma} + u_\gamma\delta_{\alpha\beta}\right] \\ a_{\alpha\beta\gamma\mu}^{(4),eq} = \rho u_\alpha u_\beta u_\gamma u_\mu + (p - \rho c_s^2)\left[u_\alpha u_\mu\delta_{\beta\gamma} + u_\beta u_\mu\delta_{\alpha\gamma} + u_\gamma u_\mu\delta_{\alpha\beta} + u_\alpha u_\beta\delta_{\gamma\mu} + u_\alpha u_\gamma\delta_{\beta\mu} + u_\beta u_\gamma\delta_{\alpha\mu}\right] \\ +\rho\left[\left(\frac{p}{\rho}\right)^2 - c_s^4\right](\delta_{\alpha\beta}\delta_{\gamma\mu} + \delta_{\alpha\gamma}\delta_{\beta\mu} + \delta_{\beta\gamma}\delta_{\alpha\mu}) \end{array} \tag{A.56}$$

Appendix B

Appendix B

B.1. Allen-Cahn equation and Geier's scheme

The numerical schemes used to solve an Allen-Cahn equation is a widely discussed subject. In this context, Geier [239] proposed a scheme to solve this equation. This method is widely used in the literature, and in particular by the HCZ community [31][32][33][41]. In practice, we can show that this numerical scheme does not exactly solve an Allen-Cahn equation. To do so, a development that retrieves the equivalent macroscopic equation of the scheme is proposed. This numerical scheme is reminded here. It consists in a stream and collide algorithm, where the collision phase is given by:

$$h_i^* = h_i^{eq} + \left(1 - \frac{1}{\tau_\phi}\right)(h_i - h_i^{eq}) \tag{B.1}$$

with

$$h_i^{eq} = \phi w_i \left(1 + \frac{u_\alpha \xi_{\alpha,i}}{c_s^2} + u_\alpha u_\beta \frac{\xi_{\alpha,i}\xi_{\beta,i} - c_s^2 \delta_{\alpha\beta}}{2c_s^4}\right) + \Delta t \left(\tau_\phi - 1/2\right) \frac{4\phi(1-\phi)}{W} \xi_\alpha n_\alpha \tag{B.2}$$

with $n_\alpha = \dfrac{\partial_\alpha \phi}{|\vec{\nabla}\phi|}$, and W a value chosen by the user. The streaming step is given by:

$$h_i(\vec{x}, t + \Delta t) = h_i^*(\vec{x} - \Delta t \vec{\xi}, t) \tag{B.3}$$

The following notation is introduced. We note $m_j^{(h)}$ the moment of the function h associated to the Hermite's polynomial H_j. It is given by:

$$m_j^{(h)} = \sum_i H_{j,i} h_i^{eq} \tag{B.4}$$

Giving the definition of h_i^{eq}, the moments of the function can be deduced:

$$m_0^{(h)} = \phi \tag{B.5}$$

$$m_\alpha^{(h)} = \phi u_\alpha + \Delta t \left(\tau_\phi - 1/2\right) \frac{4\phi(1-\phi)}{W} n_\alpha \tag{B.6}$$

$$m_{\alpha\beta}^{(h)} = \phi u_\alpha u_\beta \tag{B.7}$$

Through the methodology proposed in Section 4.3, it can be shown that the equivalent macroscopic equation solved by ϕ

$$\partial_t m_0^{(h)} + \partial_\alpha m_\alpha^{(h)} = -\Delta t \left(\tau_\phi - 1/2\right) \left[\underbrace{\partial_t^2 m_0^{(h)}}_{(a)} - \partial_{\alpha\beta} \left(\underbrace{m_{\alpha\beta}^{(h)} + c_s^2 m_0^{(h)} \delta_{\alpha\beta}}_{(b)}\right)\right] + O(\Delta t^2) \tag{B.8}$$

The term on the right part of the equation must be determined to obtain the equivalent macroscopic equation:

$$(a) = \partial_t^2 m_0^{(h)} = -\partial_t \partial_\alpha \phi u_\alpha + O(\Delta t) = \partial_\alpha \left(-\phi \partial_t u_\alpha - u_\alpha \partial_t \phi\right) + O(\Delta t) \tag{B.9}$$

In the previous equation, the temporal derivative of the velocity $\partial_t u_\alpha$ appears. Then it comes that the macroscopic equivalent equation of the phase field also depends on the equation of the velocity. For this illustration to be relevant, a numerical scheme that solves the velocity field must be chosen. To be consistent with Section 3.5, the equation solved by the velocity in the scheme proposed by Fakhari et al. [32] is chosen. As a consequence, the temporal derivative of the velocity field is given by: $\partial_t u_\alpha = -u_\beta \partial_\beta u_\alpha - \frac{\mu}{\rho}\partial_\alpha \phi$. As a consequence, the expression of (a) can be deduced:

$$(a) = \partial_\alpha \left(\phi \left(u_\beta \partial_\beta u_\alpha + \frac{\mu}{\rho}\partial_\alpha \phi \right) + u_\alpha \partial_\beta \left(\phi u_\beta \right) \right) + O(\Delta t) = \partial_\alpha \left(\partial_\beta \phi u_\alpha u_\beta + \frac{\phi \mu}{\rho}\partial_\alpha \phi \right) + O(\Delta t) \quad \text{(B.10)}$$

Otherwise, the expression of (b) can be determined from the expression of h_i^{eq}:

$$\partial_{\alpha\beta} \left(\phi u_\alpha u_\beta + \phi c_s^2 \delta_{\alpha\beta} \right) \quad \text{(B.11)}$$

The final expression of the equivalent macroscopic equation is finally given by:

$$\partial_t \phi + \partial_\alpha \phi u_\alpha = \Delta t \partial_\alpha \left[(\tau_\phi - 1/2) \left(\left[c_s^2 - \frac{\phi \mu}{\rho} \right] \partial_\alpha \phi \right) - \frac{4\phi(1-\phi)}{W} n_\alpha \right] O(\Delta t^2) \quad \text{(B.12)}$$

From this development it comes that the expression of the chemical potential appears in the expression of the mobility factor. Then it is very likely that the hyperbolic tangent profile is not retrieve while using this method. On a side note, the surface tension term has been ignored in this development and it also has an influence on the form of the equivalent macroscopic expression. In practice, this term is very low relatively with other terms, then its influence on the field is neglected.
It should be noted that the thickening of the interface is not physical anyway, then it is not of the greatest importance for the Allen-Cahn equation to be strictly retrieved. The most important property that must be verified by the phase field equations are the mass conservation and the capability to stabilise the width of the interface, which is the case for the scheme proposed by Geier et al. [239].

Appendix C

Appendix C

C.1. Taylor expansion

The Taylor expansion allowing to determine LBM's equivalent macroscopic equation is detailled here. Some notations that were already given in Section 4.3 are reminded here for the sake of clarity. As Dubois' development takes place in a Multiple Relaxation Time (MRT) framework, the moments m_j of the distribution function f_i are defined as

$$\sum_i M_{ji} f_i = m_j \tag{C.1}$$

with M the transformation matrix from the population function basis to the moments function basis. To fit the MRT formalism, a specific relaxation time must also be attributed to each moment. In the method presented in the main text, a regularized collision model is used which can be translated in a MRT framework. An example of matrix M, based on a Hermite polynomial based is proposed here:

$$M_{\alpha,i} = H_{\alpha,i} \tag{C.2}$$
$$M_{\alpha\beta,i} = H_{\alpha\beta,i} \tag{C.3}$$
$$M_{\alpha\beta\gamma,i} = H_{\alpha\beta\gamma,i} \tag{C.4}$$
$$M_{\alpha\beta\gamma\mu,i} = H_{\alpha\beta\gamma\mu,i} \tag{C.5}$$

Noting that the present development is not base dependent, but the final equivalent macroscopic equations are. In the present Appendix, the base M will be used only in an illustration purpose, without any loss of generality.
Relaxation times must be attributed to each moments. For instance in the regularized framework, this comes as: $\tau_{xy} = \tau_\nu$ (linked with the shear viscosity), τ_b is linked with the bulk viscosity and other relaxation times are set to 1, i.e.: $\tau_0 = \tau_\alpha = \tau_{\alpha\beta\gamma} = \tau_{\alpha\beta\gamma\mu} = 1$. The inverse-matrix of M is noted M^{-1}. It respects that:

$$f_i = \sum_i M_{ij}^{-1} m_j \tag{C.6}$$

For the sake of clarity, the Lattice-Boltzmann algorithm is reminded and adapted to the MRT formalism. The population at the time $t+1$ is calculated from the collided function through the streaming step:
Streaming step

$$f_i(x, t+\Delta t) = f_i^*(x - \xi_i \Delta t, t) \tag{C.7}$$

where f_i^* is the population function obtained after collision. It is calculated from the collided moments through: $f_i^* = \sum_i M_{ij}^{-1} m_j$. The moments m_j^* are obtained through the collision step: Collision step:

$$m_j^* = m_j^{eq} + (1 - \frac{1}{\tau_j}) \left(m_j - m_j^{eq} + \frac{1}{2} S_j \right) + \frac{1}{2} S_j \tag{C.8}$$

where m_j^{eq} is the j^{th} moment of the equilibrium function and S_j is the j^{th} moment of the source term. In agreement with Dubois' [201], the following tensors are defined:

$$\Lambda_{j,\alpha}^k = \sum_i M_{ji} \xi_{\alpha,i} M_{ik}^{-1} \tag{C.9}$$

$$\Lambda^k_{j,\alpha\beta} = \sum_i M_{ji}\xi_{\alpha,i}\xi_{\beta,i}M^{-1}_{ik} \tag{C.10}$$

$$\Lambda^k_{j,\alpha\beta\gamma} = \sum_i M_{ji}\xi_{\alpha,i}\xi_{\beta,i}\xi_{\gamma,i}M^{-1}_{ik} \tag{C.11}$$

These polynomials allow to characterise the base M. For instance, $\Lambda^k_{j,\alpha}$ is the projection of the polynomial M_j multiplied by ξ_α in the base M_k. For instance, $M_{0i} = 1$, then $M_{0i}\xi_{\alpha,i} = \xi_{\alpha,i}$. The proposed base M is orthogonal and it happens that $\xi_\alpha = M_\alpha$, then $\Lambda^k_{j,\alpha} = \delta_{\alpha k}$. In Dubois's original work, a source term introducing a body force was not considered. Dubois's work is then generalized to the case when a body force is introduced through a Guo's scheme [148]. It was underline in Section 4.2 that when a body force is introduced through a Guo's scheme, the calculation of the momentum is modified, since the first moment of the population f_i is given by: $m_\alpha = \rho u_\alpha - \dfrac{\Delta t}{2}F_\alpha$. The justification for this relationship is demonstrated in the present work.
The last useful notation used in this section is:

$$\Pi^{eq}_j = \partial_t\left(m^{eq}_j + (\tau_j - 1/2)\,S_j\right) + \partial_\alpha \sum_k \left(\Lambda^k_{j,\alpha}\left(m^{eq}_k + (\tau_k - 1/2)\,S_k\right)\right) \tag{C.12}$$

It can be shown that this term corresponds to the moments of the non-equilibrium part of the population function: $f_i - f^{eq}_i$. Also, it can be shown that $\Pi^{eq}_{\alpha\beta}$ is the stress tensor. Eq. (C.8) can be manipulated to obtain:

$$m_j - m^*_j = \frac{1}{\tau_j}\left(m_j - m^{eq}_j\right) - \left(1 - \frac{1}{2\tau_j}\right)S_j \tag{C.13}$$

also, the following relationship will be used:

$$\Lambda^l_{j,\alpha\beta} = \sum_k (\Lambda^k_{j\alpha}\Lambda^\beta_{kl}) \tag{C.14}$$

Using Taylor expansion, Eq. (C.7) can be extended to:

$$\begin{aligned} &f_i(x,t) + \Delta t\partial_t f_i(x,t) + \frac{\Delta t^2}{2}\partial^2_t f_i(x,t) \\ &= f^*_i(x,t) - \Delta t\xi_{\alpha,i}\partial_\alpha f^*_i(x,t) + \frac{\Delta t^2}{2}\xi_{\alpha,i}\xi_{\beta,i}\partial_{\alpha\beta}f^*_i(x,t) + O(\Delta t^3) \end{aligned} \tag{C.15}$$

At the first order in Δt the last equation becomes $f_i = f^*_i + O(\Delta t)$. This equation is true for all the microscopic velocities i, then by using equation Eq. (C.1):

$$m_j = m^*_j + O(\Delta t) \tag{C.16}$$

By injecting this relationship in Eq. (C.13) and after small manipulations, it comes:

$$m_j = m^{eq}_j + \left(\tau_j - \frac{1}{2}\right)S_j + O(\Delta t) \tag{C.17}$$

C.1.1. 1^{st} Order

Developed at the order $O(\Delta t^2)$, and integrated in the moment space, Eq. (C.15) becomes:

$$(m_j - m^*_j) = -\Delta t\left(\partial_t m_j + \partial_\alpha\left(\sum_k \Lambda^k_{j,\alpha}m^*_k\right)\right) + O(\Delta t^2) \tag{C.18}$$

Using the collision relationship, Eq. (C.13), it comes:

$$\partial_t m_j + \partial_\alpha \left(\sum_k \Lambda^k_{j,\alpha} m^*_k \right) = \frac{1}{\Delta t} \left(\left(1 - \frac{1}{2\tau_j} \right) S_j - \frac{m_j - m_j^{eq}}{\tau_j} \right) \tag{C.19}$$

For $j = 0$, the previous equation can be simplified (giving $m_0 = \rho$, $m_0^{eq} = \rho$ and $S_0 = 0$). Moreover, the term $\Lambda^k_{j,\alpha}$ can be determined. Given $M_{0,i} = 1$ then $M_{ji}\xi_{\alpha,i} = M_{\alpha,i}$. Then:

$$\sum_k \Lambda^k_{j,\alpha} m^*_k = \sum_{ik} M_{ji}\xi_{\alpha,i} M^{-1}_{ki} m^*_k = \sum_k \left(\sum_i M_{\alpha,i} M^{-1}_{ik} \right) m^*_k = \sum_k \delta_{\alpha k} m^*_k = m^*_\alpha \tag{C.20}$$

By expressing m^*_j in term of m_j^{eq} and S_j through Eq. (C.16) and Eq. (C.17) it comes:

$$\partial_t m_0 + \partial_\alpha \left(m_\alpha^{eq} + \left(\tau_\alpha - \frac{1}{2} \right) S_\alpha \right) = O(\Delta t) \tag{C.21}$$

For $j = \alpha$, the sum term can also be simplified. M_{ji} becomes $M_{\alpha i}$. Then $M_{\alpha i}\xi_{\beta i} = \xi_\alpha \xi_\beta$. Then the product $\xi_\alpha \xi_\beta$ must be expressed in terms of vectors of the matrix M:

$$\xi_\alpha \xi_\beta = M_{\alpha\beta,i} + c_s^2 H_{0,i} \delta_{\alpha\beta} \tag{C.22}$$

In the case of the polynomial basis used in the main text, this expression is slightly more complicated and must be detailed for the different values of α and β:

$$\xi_x \xi_y = M_{xy,i} \tag{C.23}$$

$$\xi_x^2 = M_{b,i} + M_{\nu,i} + M_{0,i} c_s^2 \tag{C.24}$$

$$\xi_y^2 = M_{b,i} - M_{\nu,i} + M_{0,i} c_s^2 \tag{C.25}$$

As a consequence, $\Lambda^k_{j,\alpha}$ can be detailed:

$$\sum_k \Lambda^k_{j,\alpha} m^*_k = \sum_{ik} M_{ji}\xi_{\beta,i} M^{-1}_{ki} m^*_k = \sum_k \left(\sum_i M_{\alpha\beta,i} + c_s^2 M_{0i}\delta_{\alpha\beta} \right) m^*_k = m^*_{\alpha\beta} + m^*_0 c_s^2 \delta_{\alpha\beta} \tag{C.26}$$

Then using previous relationships Eqs. (C.16, C.17), Eq. (C.19) can be expressed for $j = \alpha$:

$$\partial_t m_\alpha + \partial_\beta \left(m^{eq}_{\alpha\beta} + c_s^2 m_0^{eq} \delta_{\alpha\beta} + \left(\tau_{\alpha\beta} - \frac{1}{2} \right) S_{\alpha\beta} \right) = \frac{1}{\Delta t} \left(\left(1 - \frac{1}{2\tau_\alpha} \right) S_\alpha - \frac{m_\alpha - m_\alpha^{eq}}{\tau_\alpha} \right) + O(\Delta t) \tag{C.27}$$

From the previous equation, a condition between the first moments m_α^{eq}, m_α and S_α stands out:

$$F_\alpha = \frac{1}{\Delta t} \left(\left(1 - \frac{1}{2\tau_\alpha} \right) S_\alpha - \frac{m_\alpha - m_\alpha^{eq}}{\tau_\alpha} \right) \tag{C.28}$$

To conclude with the first order, the following relationships can be obtained by manipulating both Eq. (C.17) and Eq. (C.8):

$$m^*_j = m_j^{eq} + (\tau_j - 1/2) S_j - \Delta t(\tau_j - 1) \left(\partial_t m_j + \partial_\alpha \left(\sum_k \Lambda^k_{j,\alpha} m^*_k \right) \right) + O(\Delta t^2) \tag{C.29}$$

$$m_j = m_j^{eq} + (\tau_j - 1/2) S_j - \Delta t \tau_j \left(\partial_t m_j + \partial_\alpha \left(\sum_k \Lambda^k_{j,\alpha} m^*_k \right) \right) + O(\Delta t^2) \tag{C.30}$$

C.1.2. 2^{nd} order

Eq. (C.15) when fully integrated into the moments space is given by:

$$\frac{1}{\tau_j}(m_j - m_j^{eq}) - \left(1 - \frac{1}{2\tau_j}\right) S_j = -\Delta t \left(\partial_t m_j + \partial_\alpha \left(\sum_k \Lambda_{j,\alpha}^k m_k^*\right)\right) - \frac{\Delta t^2}{2}\left(\partial_t^2 m_j - \partial_{\alpha\beta}\left(\sum_k \Lambda_{j,\alpha\beta}^k m_k^*\right)\right) + O(\Delta t^3) \quad \text{(C.31)}$$

Then this equation must be reduced for the two moments of interest: $j = 0$ and $j = \alpha$. First of all $\Lambda_{j,\alpha\beta}^k$ must be determined for $j = 0$. Giving $M_{ji} = 1$, it reduces to: $\Lambda_{0,\alpha\beta}^k = \sum_{ik} \xi_{\alpha,i}\xi_{\beta,i}M_{ik}^{-1}$ which has already been calculated Eq. (C.22):

$$\Delta t \left(\partial_t m_0 + \partial_\alpha m_\alpha^*\right) + \frac{\Delta t^2}{2}\left(\partial_t^2 m_0 - \partial_{\alpha\beta}\left(m_{\alpha\beta}^* + c_s^2 m_0^* \delta_{\alpha\beta}\right)\right) = O(\Delta t^2) \quad \text{(C.32)}$$

By expanding $\partial_t^2 m_0$ using Eq. (C.21), and by expanding m_α^*, the previous equation becomes:

$$\partial_t m_0 + \partial_\alpha \left(m_\alpha^{eq} + (\tau_\alpha - 1/2) S_\alpha\right) - \Delta t \left(\tau_\alpha - 1/2\right)\left(\partial_t m_\alpha + \partial_\beta\left(m_{\alpha\beta}^* + c_s^2 m_0^* \delta_{\alpha\beta}\right)\right) = O(\Delta t^2) \quad \text{(C.33)}$$

After few manipulations implying Eq. (C.27), and by integrating the relationship between the body force and the 1^{st} moments Eq. (C.28):

$$\partial_t m_0 + \partial_\alpha\left(m_\alpha + \frac{\Delta t}{2} F_\alpha\right) = O(\Delta t^2) \quad \text{(C.34)}$$

From the previous equation, it comes in a straightforward way that to ensure the mass conservation principle, the first moments of the density population must respect:

$$m_\alpha + \frac{\Delta t}{2} F_\alpha = \rho u_\alpha \quad \text{(C.35)}$$

which is the condition often found in the literature [148].
The same work should now be done for $j = \alpha$. Eq. (C.31) becomes

$$\partial_t m_\alpha + \partial_\beta\left(m_{\alpha\beta}^* + c_s^2 m_0^* c_s^2 \delta_{\alpha\beta}\right) + \Delta t\left(\partial_t^2 m_\alpha - \partial_{\alpha\beta}\left(\sum_k \Lambda_{\alpha,\beta\gamma}^k m_k^*\right)\right) = F_\alpha + O(\Delta t^2) \quad \text{(C.36)}$$

Giving that $M_{\alpha,i} = \xi_{\alpha,i}$ and that:

$$\xi_\alpha \xi_\beta \xi_\gamma = M_{\alpha\beta\gamma} + c_s^2(M_\alpha \delta_{\beta\gamma} + M_\beta \delta_{\alpha\gamma} + M_\gamma \delta_{\alpha\beta}) \quad \text{(C.37)}$$

It comes: $\sum_k \Lambda_{\alpha,\beta\gamma}^k m_k^* = m_{\alpha\beta\gamma}^* + c_s^2(m_\alpha^* \delta_{\beta\gamma} + m_\beta^* \delta_{\alpha\gamma} + m_\gamma^* \delta_{\alpha\beta})$ Using Eq. (C.29) to expand $m_{\alpha\beta}^*$ and Eq. (C.27) to expand $\partial_t^2 m_\alpha$, the following equation comes:

$$\partial_t\left(m_\alpha + \frac{\Delta t}{2} f_\alpha\right) + \partial_\beta\left(m_{\alpha\beta}^{eq} + m_0^{eq} c_s^2 \delta_{\alpha\beta} + ((\tau_{\alpha\beta} - 1/2) S_{\alpha\beta})\right) - \Delta t \left(\tau_{\alpha\beta} - 1\right)\partial_\beta\left(\partial_t m_{\alpha\beta} + \partial_\gamma \sum_k \Lambda_{\alpha\beta,\gamma}^k m_k^*\right) - \frac{\Delta t}{2}\left(\partial_t\left(m_{\alpha\beta}^* + m_0^* c_s^2 \delta_{\alpha\beta}\right) + \partial_\gamma\left(m_{\alpha\beta\gamma}^* + c_s^2(m_\alpha^* \delta_{\beta\gamma} + m_\beta^* \delta_{\alpha\gamma} + m_\gamma^* \delta_{\alpha\beta})\right)\right) = F_\alpha + O(\Delta t^2) \quad \text{(C.38)}$$

Giving $M_{\alpha\beta,i}\xi_{\gamma,i} = M_{\alpha\beta\gamma,i} + c_s^2\left(M_{\alpha,i}\delta_{\beta\gamma} + M_{\beta,i}\delta_{\alpha\gamma}\right)$ and by including Eq. (C.21), it comes:

$$\partial_t\left(m_\alpha + \frac{\Delta t}{2}F_\alpha\right) + \partial_\beta\left(m_{\alpha\beta} + m_0^{eq}c_s^2\delta_{\alpha\beta} + \left(\tau_{\alpha\beta} - 1/2\right)S_{\alpha\beta}\right) = \Delta t(\tau_{\alpha\beta} - 1/2)\Pi_{\alpha\beta} + f_\alpha + O(\Delta t^2) \quad \text{(C.39)}$$

with $\Pi_j = \partial_t m_j + \partial_\alpha \sum_k (\Lambda_{j,\alpha}^k m_k^*)$. It is also useful to define:

$$\Pi_j^{eq} = \partial_t\left(m_j^{eq} + \left(\tau_j - 1/2\right)S_j\right) + \partial_\alpha \sum_k \left(\Lambda_{j,\alpha}^k\left(m_k^{eq} + \left(\tau_k - 1/2\right)S_k\right)\right) \quad \text{(C.40)}$$

Noting that: $\Pi_{\alpha\beta} = \Pi_{\alpha\beta}^{eq} + O(\Delta t)$, the equation of conservation of momentum can be written as:

$$\partial_t\left(m_\alpha + \frac{\Delta t}{2}F_\alpha\right) + \partial_\beta\left(m_{\alpha\beta} + m_0^{eq}c_s^2\delta_{\alpha\beta} + \left(\tau_{\alpha\beta} - 1/2\right)S_{\alpha\beta}\right) = \Delta t(\tau_{\alpha\beta} - 1/2)\Pi_{\alpha\beta}^{eq} + F_\alpha + O(\Delta t^2) \quad \text{(C.41)}$$

To conclude with the 2^{nd} order, the following relationships can be obtained by manipulating Eq. (C.8) and Eq. (C.31):

$$m_j^* = m_j^{eq} + \left(\tau_j - 1/2\right)S_j - \Delta t\left(\tau_j - 1\right)\left(\partial_t m_j + \partial_\alpha\left(\sum_k \Lambda_{j,\alpha}^k m_k^*\right)\right) - \frac{\Delta t^2}{2}\left(\tau_j - 1\right)\left(\partial_t^2 m_j - \partial_{\alpha\beta}\left(\sum_k \Lambda_{j,\alpha\beta}^k m_k^*\right)\right) + O(\Delta t^3) \quad \text{(C.42)}$$

Using Eq. (C.16) and Eq. (C.14), the last term can be manipulated:

$$\begin{aligned}\partial_t^2 m_j - \partial_{\alpha\beta}\left(\sum_k \Lambda_{j,\alpha\beta}^k m_k^*\right) &= \partial_t^2 m_j + \underbrace{\partial_t\partial_\alpha\Lambda_{j,\alpha}^l m_l^* - \partial_t\partial_\alpha\Lambda_{j,\alpha}^l m_l}_{=O(\Delta t)} - \partial_{\alpha\beta}\sum_{kl}\Lambda_{j,\alpha}^l\Lambda_{j,\alpha\beta}^k m_k^* + O(\Delta t) \\ &= \partial_t\Pi_j - \partial_\alpha\Lambda_{j,\alpha}^l\Pi_l + O(\Delta t) = \partial_t\Pi_j^{eq} - \partial_\alpha\Lambda_{j,\alpha}^l\Pi_l^{eq} + O(\Delta t)\end{aligned} \quad \text{(C.43)}$$

By extending $\partial_t m_j$ and $\partial_\alpha\Lambda_{j,\alpha}^k m_k*$ using Eq. (C.29) and Eq. (C.30) and Eq. (C.42) reduces to:

$$m_j^* = m_j^{eq} + (\tau_j - 1/2)S_j - \Delta t\left(\tau_j - 1\right)\Pi_j^{eq} - \Delta t^2\left(\tau_j - 1\right)\left((\tau_j - 1/2)\partial_t\Pi_j^{eq} + \partial_\alpha\sum_k(\tau_k - 1/2)\Lambda_{j,\alpha}^k\Pi_k^{eq}\right) + O(\Delta t^3) \quad \text{(C.44)}$$

C.1.3. 3^{rd} Order

Eq. (C.15) can be extended to an additional order and then integrated to the moment space which gives:

$$\frac{1}{\tau_j}(m_j - m_j^{eq}) - \left(1 - \frac{1}{2\tau_j}\right)S_j = -\Delta t\left(\partial_t m_j + \partial_\alpha\left(\sum_k \Lambda_{j,\alpha}^k m_k^*\right)\right) - \frac{\Delta t^2}{2}\left(\partial_t^2 m_j - \partial_{\alpha\beta}\left(\sum_k \Lambda_{j,\alpha\beta}^k m_k^*\right)\right) - \frac{\Delta t^3}{6}\left(\partial_t^3 m_j + \partial_{\alpha\beta\gamma}\left(\sum_k \Lambda_{j,\alpha\beta\gamma}^k m_k^*\right)\right) + O(\Delta t^4) \quad \text{(C.45)}$$

For $j = 0$, the equation becomes:

$$\partial_t m_0 + \partial_\alpha \underbrace{m^*_\alpha}_{=m^{eq}_\alpha + \frac{\Delta t}{2} f_\alpha} - \frac{\Delta t}{2}\left(\underbrace{\partial^2_t m_0 - \partial_{\alpha\beta}(m^*_{\alpha\beta} + c_s^2 m^*_0 \delta_{\alpha\beta})}_{(1)}\right) - \frac{\Delta t^2}{6}\left(\underbrace{\partial^3_t m_0 + \partial_{\alpha\beta\gamma}\left(m^*_{\alpha\beta\gamma} + c_s^2(m^*_\alpha \delta_{\beta\gamma} + m^*_\beta \delta_{\alpha\gamma} + m^*_\gamma \delta_{\alpha\beta})\right)}_{(2)}\right) = O(\Delta t^3) \quad \text{(C.46)}$$

(1) can then be detailed by expanding $\partial^2_t m_0$ using Eq. (C.34) and $m^*_{\alpha\beta}$ using Eq. (C.29)

$$(1) = -\partial_\alpha \Big[\partial_t\left(m_\alpha + \frac{\Delta t}{2} f_\alpha\right) + \partial_\beta\left(m^{eq}_{\alpha\beta} + m^{eq}_0 c_s^2 \delta_{\alpha\beta} + (\tau_{\alpha\beta} - 1/2)\, S_{\alpha\beta} - \Delta t\,(\tau_{\alpha\beta} - 1)\,\Pi^{eq}_{\alpha\beta}\right)\Big] + O(\Delta t^2) \quad \text{(C.47)}$$

Which gives (using Eq. (C.41)):

$$(1) = -\partial_\alpha\left(F_\alpha + \partial_\beta \frac{\Delta t}{2}\Pi^{eq}_{\alpha\beta}\right) + O(\Delta t^2) \quad \text{(C.48)}$$

In (2), $\partial^3_t m_0$ can be developed by using Eq. (C.21) and Eq. (C.27) successively, which gives:

$$(2) = \partial_\alpha\Big[\partial_\beta\left(\partial_t\left(m^*_{\alpha\beta} + m^*_0 c_s^2 \delta_{\alpha\beta}\right) + \partial_\gamma\left(m^*_{\alpha\beta\gamma} + c_s^2\left(m^*_\alpha \delta_{\beta\gamma} + m^*_\beta \delta_{\alpha\gamma} + m^*_\gamma \delta_{\alpha\beta}\right)\right)\right) - \partial_t F_\alpha] + O(\Delta t) \quad \text{(C.49)}$$

Which can be reduced to:

$$(2) = \partial_\alpha\left(\partial_\beta \Pi^{eq}_{\alpha\beta} - \partial_t F_\alpha\right) + O(\Delta t) \quad \text{(C.50)}$$

By combining the expression of (1) and (2), the equation that is solved by the first moment of the main population is finally given by:

$$\partial_t m_0 + \partial_\alpha m^{eq}_\alpha = \Delta t^2 \partial_\alpha\left(\frac{1}{12}\partial_\beta \Pi^{eq}_{\alpha\beta} - \frac{1}{6}\partial_t F_\alpha\right) + O(\Delta t)^3 \quad \text{(C.51)}$$

Finally, for $j = \alpha$, Eq. (C.45) comes as:

$$\partial_t m_\alpha + \partial_\beta\left(m^*_{\alpha\beta} + m^*_0 c_s^2 \delta_{\alpha\beta}\right) + \frac{\Delta t}{2}\left(\underbrace{\partial^2_t m_\alpha - \partial_{\beta\gamma}\left(m^*_{\alpha\beta\gamma} + c_s^2\left(m^*_\alpha \delta_{\beta\gamma} + m^*_\beta \delta_{\alpha\gamma} + m^*_\gamma \delta_{\alpha\beta}\right)\right)}_{(1)}\right) + \frac{\Delta t^2}{6}\left(\underbrace{\partial^3_t m_\alpha + \partial_{\beta\gamma\mu}\sum_k \Lambda^k_{\alpha,\beta\gamma\mu} m^*_k}_{(2)}\right) + O(\Delta t^3) \quad \text{(C.52)}$$

$\sum_k \Lambda^k_{\alpha,\beta\gamma\mu} m^*_k$, can actually be expressed but was simply to long to be inserted in the same expression as the rest. It is given by:

$$\sum_k \Lambda^k_{\alpha,\beta\gamma\mu} m^*_k = m^*_{\alpha\beta\gamma\mu} + c_s^2(m^*_{\alpha\beta}\delta_{\gamma\mu} + m^*_{\alpha\gamma}\delta_{\beta\mu} + m^*_{\alpha\mu}\delta_{\beta\gamma} + m^*_{\beta\gamma}\delta_{\alpha\mu} + m^*_{\beta\mu}\delta_{\alpha\gamma} + m^*_{\gamma\mu}\delta_{\alpha\beta}) + m^*_0 c_s^4(\delta_{\alpha\beta}\delta_{\gamma\mu} + \delta_{\alpha\gamma}\delta_{\beta\mu} + \delta_{\alpha\mu}\delta_{\beta\gamma}) \quad \text{(C.53)}$$

To express (2), $\partial_t^3 m_\alpha$ must be expanded by using Eq. (C.21), then Eq. (C.27) and finally the definition of $\Pi_{\alpha\beta}$:

$$\begin{aligned}\partial_t^3 m_\alpha &= \partial_t^2 F_\alpha - \partial_\beta \partial_t^2 \left(m^*_{\alpha\beta} + m_0 c_s^2 \delta_{\alpha\beta}\right) + \partial_t \partial_{\beta\gamma} \left[\sum_k \left(\Lambda^k_{\alpha\beta,\gamma} m^*_k - \Lambda^k_{\alpha\beta,\gamma} m^*_k\right)\right] + O(\Delta t) \\ &= \partial_t^2 F_\alpha - \partial_\beta \partial_t \Pi_{\alpha\beta} + \partial_{\beta\gamma}\partial_t \left(m_{\alpha\beta\gamma^*} + \left[m^*_\gamma \delta_{\alpha\beta} + m_\alpha \delta_{\beta\gamma} + m^*_\beta \delta_{\alpha\gamma}\right] c_s^2\right) + O(\Delta t) \quad \text{(C.54)}\end{aligned}$$

By underlining that:

$$\sum_k \left(\Lambda^k_{\alpha,\beta\gamma\mu} m^*_k\right) = \sum_k \left(\Lambda^k_{\alpha\beta\gamma,\mu} m^*_k\right) + \left[m^*_{\alpha\mu}\delta_{\beta\gamma} + m^*_{\beta\mu}\delta_{\alpha\gamma} + m^*_{\gamma\mu}\delta_{\alpha\beta}\right] c_s^2 + m^*_0 \left[\delta_{\alpha\beta}\delta_{\gamma\mu} + \delta_{\alpha\gamma}\delta_{\beta\mu} + \delta_{\alpha\mu}\delta_{\beta\gamma}\right] c_s^4 \quad \text{(C.55)}$$

and that according to Eq. (C.27):

$$\partial_t m_\alpha + \partial_\beta (m_{\alpha\beta} + m_0 c_s^2 \delta_{\alpha\beta}) = F_\alpha + O(\Delta t) \quad \text{(C.56)}$$

(2) can be expressed as a composition of $\Pi^{eq}_{\alpha\beta\gamma}$ and $\Pi^{eq}_{\alpha\beta}$:

$$(2) = \left[\partial_t^2 F_\alpha + c_s^2 \partial_{\beta\gamma} \left(F_\alpha \delta_{\beta\gamma} + F_\beta \delta_{\alpha\gamma} + F_\gamma \delta_{\alpha\beta}\right)\right] + \partial_{\beta\gamma} \Pi^{eq}_{\alpha\beta\gamma} - \partial_\beta \partial_t \Pi^{eq}_{\alpha\beta} + O(\Delta t) \quad \text{(C.57)}$$

Developing $\partial_t^2 m_\alpha$ using Eq. (C.41), and developing $m_{\alpha\beta\gamma}$ using Eq. (C.44), (1) is expressed as:

$$(1) = \partial_t F_\alpha - \partial_\beta \left(\Pi_{\alpha\beta} + \Delta t \left[\left(\tau_{\alpha\beta} - 1/2\right) \partial_t \Pi^{eq}_{\alpha\beta} + \left(\tau_{\alpha\beta\gamma} - 1\right) \partial_\gamma \Pi^{eq}_{\alpha\beta\gamma}\right]\right) \quad \text{(C.58)}$$

By combining the expressions of (1), (2) and $m^*_{\alpha\beta}$ (Obtained through Eq. (C.44), the 2nd order equivalent equation to the algorithm comes as follow:

$$\begin{aligned}\partial_t \left(m_\alpha + \frac{\Delta t}{2} F_\alpha\right) + \partial_\beta \left(m_{\alpha\beta} + m_0^{eq} c_s^2 \delta_{\alpha\beta} + \left(\tau_{\alpha\beta} - 1/2\right) S_{\alpha\beta}\right) &= \Delta t(\tau_{\alpha\beta} - 1/2)\Pi^{eq}_{\alpha\beta} + F_\alpha \\ + \Delta t^2 \partial_\beta \left[\left(\left[\tau_{\alpha\beta} - \frac{1}{2}\right]^2 - \frac{1}{6}\right) \partial_t \Pi^{eq}_{\alpha\beta} + \left(\left[\tau_{\alpha\beta\gamma} - \frac{1}{2}\right]\left[\tau_{\alpha\beta} - \frac{1}{2}\right] - \frac{1}{12}\right) \partial_\gamma \Pi^{eq}_{\alpha\beta\gamma}\right] \\ - \frac{\Delta t^2}{6} \left[\partial_t^2 F_\alpha + c_s^2 \partial_{\beta\gamma} \left(F_\alpha \delta_{\beta\gamma} + F_\beta \delta_{\alpha\gamma} + F_\gamma \delta_{\alpha\beta}\right)\right] + O(\Delta t^3) \quad \text{(C.59)}\end{aligned}$$

Appendix D

Appendix D

D.1. Colour Gradient phase field equation

In this section, the equivalent macroscopic equation of the g_i population is determined. First of all, some value must be defined. The moments of the g_i population are noted:

$$m_j^{(g)} = \sum_i M_{ji} g_i \tag{D.1}$$

By definition of ϕ $m_0^{(g)} = \rho\phi$. As previously, the algorithm that is followed by the phase field population function should be slightly re-formulated. The recoloration is expressed in the moment space:

$$m_j^{(g),*} = \phi m_j^* + S_j^{(3)} \tag{D.2}$$

$$g_i(x, t + \Delta t) = g_i^*(x - \xi_{\alpha,i}, t) \tag{D.3}$$

By expanding the streaming relationship:

$$g_i + \Delta t \partial_t g_i + \frac{\Delta t^2}{2} \partial_t^2 g_i = g_i^* + \Delta t \partial_t g_i^* + \frac{\Delta t^2}{2} g_i^* + O(\Delta t^3) \tag{D.4}$$

Integrated into the moment space and by integrating Eq(C.29) the last expression can be expressed:

$$m_j^{(g)} = m_j^{(g),*} + O(\Delta t) = \phi \left(m_j^{eq} + (\tau_j - 1/2) S_j) \right) + S_j^{(3)} + O(\Delta t) \tag{D.5}$$

Eq(D.4) can be expressed at a higher degree:

$$m_j^{(g)} - m_j^{(g),*} = -\Delta t \left(\partial_t m_j^{(g)} + \partial_\alpha \sum_k \Lambda_{j,\alpha}^k m_k^{(g),*} \right) + O(\Delta t^2) \tag{D.6}$$

For $j = 0$, giving that $m_0^{(g)} = m_0^{(g),*} = \rho\phi$ previous equation becomes:

$$\partial_t m_0^{(g)} + \partial_\alpha \left(\phi(m_\alpha^{eq}) + (\tau_\alpha - 1/2) S_\alpha) + S_\alpha^{(3)} \right) = O(\Delta t) \tag{D.7}$$

Noting that $S_\alpha = \Delta t f_\alpha = O(\Delta t)$, $S_\alpha^{(3)} = O(\Delta t)$ and using the values of m_α^{eq} and $m_0^{(g)}$ it comes:

$$\partial_t \rho\phi + \partial_\alpha \rho\phi u_\alpha = O(\Delta t) \tag{D.8}$$

Now Eq(D.4) can be integrated into the moment space at its higher degree:

$$m_j^{(g)} - m_j^{(g),*} = -\Delta t \left(\partial_t m_j^{(g)} + \partial_\alpha \sum_k \Lambda_{j,\alpha}^k m_k^{(g),*} \right) - \frac{\Delta t}{2} \left(\partial_t^2 m_j^{(g)} - \partial_{\alpha\beta} \sum_k \Lambda_{j,\alpha\beta}^k m_k^{(g),*} \right) + O(\Delta t^2) \tag{D.9}$$

To express this equation for $j = 0$, $\partial_t^2 m_0^{(g)}$ must be expanded:

$$\begin{aligned}\partial_t^2 m_j^{(g)} &= -\partial_t\partial_\alpha \phi m_\alpha^{eq} + O(\Delta t) = -\partial_\alpha \left(u_\alpha \partial_t \rho\phi + \phi\rho\partial_t u_\alpha\right) + O(\Delta t) \\ &= \partial_\alpha \left(u_\alpha \partial_\beta \left(\rho\phi u_\beta\right) + \rho\phi u_\beta \partial_\beta u_\alpha + \phi\partial_\beta p\delta_{\alpha\beta}\right) + O(\Delta t) \\ &= \partial_{\alpha\beta}\rho\phi u_\alpha u_\beta + \partial_\alpha\left(\phi\partial_\alpha p\right) + O(\Delta t) \end{aligned} \tag{D.10}$$

To express the Δt^2, the spatial derivative must also be expressed:

$$\partial_{\alpha\beta}\sum_k \Lambda^k_{j,\alpha\beta} m_k^{(g),*} = m_{\alpha\beta}^{(g),*} + c_s^2 m_0^{(g),*}\delta_{\alpha\beta} = \partial_{\alpha\beta}(\rho\phi u_\alpha u_\beta + \phi p) + O(\Delta t) \tag{D.11}$$

Finally, the final equation is given by:

$$\partial_t\rho\phi + \partial_\alpha\rho\phi u_\alpha = \partial_\alpha\left[\frac{p\Delta t}{2}\partial_\alpha\phi - S_\alpha^{(3)}\right] + O(\Delta t^2) \tag{D.12}$$

This justifies the form of the collision term in the re coloration phase, to mimic the right term of the Allen-Cahn equation proposed by Chiu and Lin [47], the source term first moments must be:

$$S_\alpha^{(3)} = \frac{p\Delta t}{2}\frac{\left(1-\phi^2\right)}{W}\frac{\partial_\alpha\phi}{|\vec{\nabla}\phi|} \tag{D.13}$$

This justifies the form of the source term proposed in this work. The moment of the source term is projected in the Hermite's polynomial base:

$$\Omega_i^{(3)} = w_i\frac{S_\alpha^{(3)}H_{\alpha,i}}{c_s^2} \tag{D.14}$$

Which allows to recover Eq. (6.34). It is interesting to note that this operator is almost similar to the one originally proposed by D'Ortona [173] in 1995 and Latva-Kokko [172] in 2005. At the time, recoloration operator wasn't understood as a scheme allowing to solve a diffusion-advection equation for the phase field, and Chiu and Lin [47] only proposed their conservative form of the Allen-Cahn equation in 2011.

D.2. Improved algorithm equivalent equation

The conservation equation for momentum to the order 2 is given by Eq.(C.41). By expressing the moments of the equilibrium function, it comes as:

$$\partial_t\rho u_\alpha + \partial_\beta\left(\rho u_\alpha u_\beta + p\delta_{\alpha\beta} + p^\sigma_{\alpha\beta}\right) = \Delta t(\tau_{\alpha\beta} - 1/2)\partial_\beta\Pi^{eq}_{\alpha\beta} \tag{D.15}$$

Noting that in the previous expression, for the sake of clarity no volumic force are considered. This equation can be extended by determining the expression of $\Pi^{eq}_{\alpha\beta}$. This calculation is given for $\alpha = x$, the method being symmetrical for x and y direction the equation obtained for $y - direction$ is similar. $\partial_\beta\Pi^j_{x\beta}$ is given by:

$$\partial_\beta(\tau_{x\beta} - 1/2)\Pi^{eq}_{x\beta} = (\tau_\nu - 1/2)\left(\partial_x\Pi^{eq}_\nu + \partial_y\Pi^{eq}_{xy}\right) + \partial_x(\tau_b - 1/2)\Pi^{eq}_b \tag{D.16}$$

With

$$\Pi^{eq}_\nu = \partial_t\sum_i H_{\nu,i}f_i^{eq} + \partial_\gamma\sum_i H_{\nu,i}\xi_{\gamma,i}f_i^{eq} \tag{D.17}$$

$$\Pi^{eq}_{xy} = \partial_t\sum_i H_{xy,i}f_i^{eq} + \partial_\gamma\sum_i H_{xy,i}\xi_{\gamma,i}f_i^{eq} \tag{D.18}$$

$$\Pi_b^{eq} = \partial_t \sum_i H_{b,i} f_i^{eq} + \partial_\gamma \sum_i H_{b,i} \xi_{\gamma,i} f_i^{eq} \tag{D.19}$$

Giving that

$$H_{b,i}\xi_{\gamma,i} = \frac{H_{xx\gamma,i} + H_{yy\gamma,i}}{2} + c_s^2 H_{\gamma,i} \tag{D.20}$$

$$H_{\nu,i}\xi_{\gamma,i} = \frac{H_{xx\gamma,i} - H_{yy\gamma,i}}{2} + c_s^2 H_{x,i}\delta_{\gamma x} - c_s^2 H_{y,i}\delta_{\gamma y} \tag{D.21}$$

$$H_{xy,i}\xi_{\gamma,i} = H_{xy\gamma,i} + c_s^2 \left(H_{x,i}\delta_{\gamma y} + H_{y,i}\delta_{\gamma x}\right) \tag{D.22}$$

By integrating the definition of the equilibrium function Eq. (6.19), it gives:

$$\Pi_\nu^{eq} = \partial_t \left(\frac{\rho u_x^2 - \rho u_y^2}{2}\right) + \partial_x \left(\frac{(p - \rho c_s^2)u_x}{2} + \rho c_s^2 u_x\right) + \partial_y \left(\frac{(p - \rho c_s^2)u_y}{2} + \rho c_s^2 u_y\right) \tag{D.23}$$

$$\Pi_b^{eq} = \partial_t \left(\frac{\rho u_x^2 + \rho u_y^2}{2} + (p - \rho c_s^2)\right) - \partial_x \left(\frac{(p - \rho c_s^2)u_x}{2} - \rho c_s^2 u_x\right) + \partial_y \left(\frac{(p - \rho c_s^2)u_y}{2} - \rho c_s^2 u_y\right) \tag{D.24}$$

$$\Pi_{xy}^{eq} = \partial_t \rho u_x u_y + \partial_x \left((p - \rho c_s^2)u_y + \rho c_s^2 u_y\right) + \partial_y \left((p - \rho c_s^2)u_x + \rho c_s^2 u_x\right) \tag{D.25}$$

By merging Eqs. (D.23, D.24, D.25) into Eq. (D.16), the macroscopic equation that is solved by the scheme is:

$$\begin{aligned}\partial_t \rho u_\alpha + \partial_\beta \left(\rho u_\alpha u_\beta + p\delta_{\alpha\beta} + p^\sigma_{\alpha\beta}\right) = \\ \Delta t \partial_\beta \left(O(Ma^3) + (\tau_\nu - 1/2)p\left(\partial_\beta u_\alpha + \partial_\alpha u_\beta\right) + (\tau_b - \tau_\nu)p\partial_\gamma u_\gamma + Er_\alpha \delta_{\alpha\beta}\right)\end{aligned} \tag{D.26}$$

where the error term reads

$$\begin{aligned}Er_\alpha = -(\tau_\nu - 1/2)3\partial_\alpha \left((p - \rho c_s^2)u_\alpha\right) + \frac{3}{2}\left(\tau_\nu - \tau_b\right)\partial_\gamma \left((p - \rho c_s^2)u_\gamma\right) \\ + (\tau_b - 1/2)\left(\partial_t (p - \rho c_s^2) + \partial_\gamma \left((p - \rho c_s^2)u_\gamma\right)\right)\end{aligned} \tag{D.27}$$

and the term $O(Ma^3)$ is an error proportional to the Mach number [54].

List of Figures

0.1. Scheme of an aeronautical engine 2
0.2. Schematic of a pressure swirl injector in a combustion chamber 2
0.3. Atomization process in a pressure swirled injector. From Surya Prakash et al. [14] . . 3

1.1. Illustration of some possible velocities on a 2D cartesian grid 16
1.2. Properties of the principal velocity sets (from [54], which compiled informations from Succi [56] and Qian et d'Humières [55] 18
1.3. Illustration of a D_2Q_9 velocity set 19
1.4. Illustration of the D_3Q_{19} velocity set. (a) is the velocity set itself (b) projection in the (x, y) plane (c) projection in the (y, z) plane (d) projection in the (z, x) plane 20
1.5. Illustration of the classic athermal LBM algorithm proposed by He et Luo [59] 22
1.6. (a): Velocity set in the original "Maxwell model"; (b) An example of a collision at time t (From Hardy et al. [62]) 24
1.7. Hexagonal grid proposed by Frish et al [19] 25

2.1. Illustration of the flag system for a MAC algorithm 31
2.2. Splashing droplet into a denser and more viscous fluid. Figure from [78] 32
2.3. Illustration of an interface reconstruction process. (a) the reference phase field Y_1 with the actual interface location. (b) Reconstructed interface obtained through a SLIC algorithm (c) Reconstructed interface obtained through a piece wise linear method . . 33
2.4. Atomization of an air-water oscillating liquid jet with a VOF method. The open-source code Gerris [91] is used. Illustration from Schmidt et al. [90] 33
2.5. Simulation of the atomization of a liquid Diesel using ACLS method. Picture from Desjardins et al. [97] 35
2.6. Fragmentation of a liquid O_2 jet by a coaxial high-speed H_2 current. From Chiapolino et al. [123] 42
2.7. 3-equation simulation of a bubble coaslescence and separation confronted to experimental results [128]. Figure from Nayigizente et al. [127] 43

3.1. Topology obtained for the squared shape droplet test after 10.000 iterations for different degree of isotropy. Degree of isotropy 1 (left), degree of isotropy 2 (center) Degree of isotropy 4 (right) 53
3.2. Spurious current in the interface for a degree of isotropy 2 54
3.3. Illustration of the algorithm proposed by Leclaire et al. [159] 61
3.4. Illustration of a spinodal decomposition simulated by the RK LGA method (from [22]) 62
3.5. Illustration of the free energy algorithm proposed by Swift et al. [28] 69
3.6. Pseudo-potential algorithm inspired from Yuan and Schaefer [183] 73
3.7. Comparison between a Shan-Chen method and experimentation. Study of the impact of a droplet an a hydrophobic surface. Figure from Fei et al. [192] 75
3.8. Schematic of the HCZ algorithm from Fakhari et al. [31] 78
3.9. The evolution of the three-dimensional Rayleigh-Taylor instability with density ratio of 1000 and Reynold number of 3000. Figure from [41] 79

5.1. The maximum spurious velocity (in Lattice Boltzmann Units) for a static bubble as a function of the parameter p (Figure (a) plain line) from Pooley et al. [156] 101
5.2. Case of a static bubble in a quiescent atmosphere with two different operators, one without the isotropic condition, i.e. $\sum_i H_{xxyy,i} = 0$ (left), and one with it (right). The interface is represented by the $\phi = 0$ isolines and the velocity field by arrows of length scaled by $1m.s^{-1}$ 104
5.3. Visualization of a phase field profile after grid convergence (left). L2 error expressed as a function of the spatial step Δx compared with a straight line of slope=2 in a log-log scale. 107
5.4. Time evolution of the non-dimensional interface thickness for different mobility factors M as a function of dimensionless time. 108

6.1. Two-phase Poiseuille flow case 118
6.2. Comparison between "model 1" inspired fom the scheme in Leclaire [159] (left), and "model 2" the present scheme inspired from Li [160] (right), for a two-phase Poiseuille flow at high density ratio case (100). Both are compared with the theoretical solution (solid line) 119
6.3. Laplace test for a range of surface tension σ, and dimensionless radius $r/\Delta x$ for different density ratios γ. The value of the pressure jump $p_1 - p_2$ (dots) can be compared with $\frac{\sigma}{r}$ (plain curve) 120
6.4. Illustration of an oscillating ellipsoidal droplet between initial state (left) and half period state (centre). Time evolution of kinetic energy curve (right) 121
6.5. Rayleigh-Taylor instability at various characteristic times t^*, Reynolds number is $Re = 2048$ 124

A.1. Illustration of a cone of particle hitting the surface of area dS 130

List of Tables

2.1. Surface tension value for different fluids [132] 44

3.1. Maximum velocity corresponding to the spurious currents in the interface as a function of the degree of isotropy 53

6.1. Relative error E calculated with Eq(6.62) for different density ratios (γ), surface tension (σ in $kg.s^{-2}$) and for different droplet radii (expressed in l.b.u., i.e., as multiples of Δx) 121

6.2. Oscillation of an ellipsoidal droplet: comparison between expected surface tension σ and experimental value σ_{exp} The symbol "$-$" underlines a lack of oscillation and "$crash$" a lack of numerical stability. 122

Bibliography

[1] . European Union Aviation Safety Agency, "Eurocontrol and EEA European Aviation Environmental Repor https://www.easa.europa.eu/eaer/system/files/usr_uploaded/219473_EASA_EAER_2019_WEB_LOW-RES_190311.pdf.

[2] . Air Transport Action Group (ATAG), "Aviation benefits beyond borders." 2020.

[3] European Environmental Agency (EEA). https://www.eea.europa.eu/data-and-maps/data/data-viewers/greenhouse-gases-viewer.

[4] . Air Transport Action Group (ATAG), "Hydrogen-powered aviation a fact-based study of hydrogen technology, economics, and climate impact by 2050." 2020.

[5] J. J. Keller, "Thermoacoustic oscillations in combustion chambers of gas turbines," AIAA Journal, vol. 33, no. 12, pp. 2280–2287, 1995.

[6] I. Chterev and I. Boxx, "Effect of hydrogen enrichment on the dynamics of a lean technically premixed elevated pressure flame," Combustion and Flame, vol. 225, pp. 149–159, 2021.

[7] E. Lo Schiavo, D. Laera, E. Riber, L. Gicquel, and T. Poinsot, "Effects of liquid fuel/wall interaction on thermoacoustic instabilities in swirling spray flames," Combustion and Flame, vol. 219, pp. 86–101, 2020.

[8] T. Christou, B. Stelzner, and N. Zarzalis, "Influence of an oscillating airflow on the prefilming airblast atomization process," Atomization and Sprays, vol. 31, no. 3, pp. 1–14, 2021.

[9] T. Poinsot, "Prediction and control of combustion instabilities in real engines," Proceedings of the Combustion Institute, vol. 36, no. 1, pp. 1–28, 2017.

[10] A. H. Lefebvre and V. G. Mcdonell, Atomization and Sprays, Second Edition. CRC Press, 2017.

[11] C. Dumouchel, "On the experimental investigation on primary atomization of liquid streams," Experiments in Fluids, vol. 45, no. 3, pp. 371–422, 2008.

[12] A. Ficuciello, J. B. Blaisot, C. Richard, and F. Baillot, "Investigation of air-assisted sprays submitted to high frequency transverse acoustic fields: Droplet clustering," Physics of Fluids, vol. 29, no. 6, 2017.

[13] S. Dighe and H. Gadgil, "Atomization of acoustically forced liquid sheets," Journal of Fluid Mechanics, vol. 880, pp. 653–683, 2019.

[14] R. Surya Prakash, H. Gadgil, and B. N. Raghunandan, "Breakup processes of pressure swirl spray in gaseous cross-flow," International Journal of Multiphase Flow, vol. 66, pp. 79–91, 2014.

[15] https://www.claymath.org/millennium-problems/millennium-prize-problems.

[16] P. Sagaut, Large Eddy Simulation for Incompressible Flows. Springer Berlin Heidelberg, 2002.

[17] D. C. Wilcox, Turbulence Modeling for CFD. DCW Industries, Inc, 1993.

[18] N. Ashgriz, Handbook of Atomization and Sprays. Springer US, 1st ed., 2011.

[19] U. Frisch, B. Hasslacher, and Y. Pomeau, "Lattice-Gas Automata for the Navier-Stokes Equation," Physical Review Letters, vol. 56, no. 14, pp. 1505–1508, 1986.

[20] D. D'humières and P. Lallemand, "Lattice gas automata for fluid mechanics," Physica A: Statistical Mechanics and its Applications, vol. 140, no. 1-2, pp. 326–335, 1986.

[21] G. McNamara and G. Zanetti, "Use of the Boltzmann Equation to Simulate Lattice-Gas Automata," Physical Review Letters, vol. 61, no. 20, pp. 2332–2335, 1988.

[22] D. Rothman and J. Keller, "Immiscible Cellular-Automaton Fluids," Journal of Statistical Physics, vol. 52, no. 3/4, pp. 1119–1127, 1988.

[23] A. K. Gunstensen, D. H. Rothman, S. Zaleski, and G. Zanetti, "Lattice Boltzmann model of immiscible fluids," Physical Review A, vol. 43, no. 8, pp. 4320–4327, 1991.

[24] W. Shao and J. Li, "Review of Lattice Boltzmann Method Applied to Computational Aeroacoustics," Archives of acoustics, vol. 44, no. 2, pp. 215–238, 2019.

[25] X. Shan and H. Chen, "Lattice boltzmann model for simulating flows with multiple phases and components," Physical Review E, vol. 47, no. 3, pp. 1815–1820, 1993.

[26] X. Shan and H. Chen, "Simulation of non-ideal gases and liquid-gas phase transition by lattice boltzmann equation," Physical Review E, vol. 49, no. 4, pp. 2941–2948, 1994.

[27] M. Swift, W. Osborn, and J. Yeomans, "Lattice boltzmann simulation of nonideal fluids," Physical Review Letters, vol. 75, no. 5, pp. 830–833, 1995.

[28] M. Swift, E. Orlandini, W. Osborn, and J. Yeomans, "Lattice boltzmann simulations of liquid-gas and binary fluid systems," Physical Review E, vol. 54, no. 5, pp. 5041–5052, 1996.

[29] X. He, S. Chen, and R. Zhang, "A lattice boltzmann scheme for incompressible multiphase flow and its application in simulation of rayleigh-taylor instability," Journal of Computational Physics, vol. 152, pp. 642–663, 1999.

[30] A. Fakhari and T. Lee, "Multiple-Relaxation-Time lattice Boltzmann method for immiscible fluids at high Reynold numbers," Physical Review E, vol. 87, p. 023304, 2013.

[31] A. Fakhari, M. Geier, and T. Lee, "A mass-conserving lattice boltzmann method with dynamic grid refinement for immiscible two-phase flows," Journal of Computational Physics, vol. 315, pp. 434–457, 2016.

[32] A. Fakhari and D. Bolster, "Diffuse interface modeling of three-phase contact line dynamics on curved boundaries: A lattice Boltzmann model for large density and viscosity ratios," Journal of Computational Physics, vol. 334, pp. 620–638, 2017.

[33] A. Fakhari, T. Mitchell, C. Leonardi, and D. Bolster, "Improved locality of the phase-field lattice-Boltzmann model for immiscible fluids at high density ratios," Physical Review E, vol. 96, p. 053301, 2017.

[34] G. M., A. Fakhari, and T. Lee, "A conservatice phase-field lattice boltzmann model for interface tracking equation," Physical Review E, vol. 91, p. 063309, 2015.

[35] M. Wöhrwag, C. Semprebon, Mazloomi, A. Moqaddam, I. Karlin, and H. Kusumaatmaja, "Ternary free-energy entropic lattice boltzmann model with a high density ratio," Physical review Letters, vol. 120, p. 234501, 2018.

[36] S. Saito, A. De Rosis, A. Festuccia, A. Kaneko, Y. Abe, and K. Koyama, "Color-gradient lattice boltzmann model with monorthogonal central moments: hydrodynamic melt-jet breakup simulations," Physical Review E, vol. 98, pp. 013305–2948, 2018.

[37] Y. Yu, H. Liu, D. Liang, and Y. Zhang, "A versatile lattice Boltzmann model for immiscible ternary fluid flows," Physics of Fluids, vol. 31, no. 1, 2019.

[38] T. Inamuro, T. Echizen, and F. Horai, "Validation of an improved lattice Boltzmann method for incompressible two-phase flows," Computers and Fluids, vol. 175, pp. 83–90, 2018.

[39] S. Mukherjee, P. Berghout, and H. E. Van den Akker, "A lattice boltzmann approach to surfactant-laden emulsions," AIChE Journal, vol. 65, no. 2, pp. 811–828, 2019.

[40] H. Liu, Q. Kang, C. Leonardi, S. Schmieshek, A. Narvaez, B. Jones, J. Williams, A. Valocchi, and J. Harting, "Multiphase lattice boltzmann simulations for porous media applications," Comput Geosci, vol. 20, pp. 777–805, 2016.

[41] T. Mitchell, C. Leonardi, and A. Fakhari, "Development of a three-dimensional phase-field lattice boltzmann method for the study of immicible fluids at high density ratio," Int. J. multiphase flow, vol. 107, pp. 1–15, 2018.

[42] S. Leclaire, A. Parmigiani, B. Chopard, and J. Latt, "Three-dimensional lattice Boltzmann method benchmarks between color-gradient and pseudo-potential immiscible multi-component models," International Journal of Modern Physics C, vol. 28, no. 7, 2017.

[43] T. Reis and T. Phillips, "Lattice Boltzmann model for simulating immiscible two-phase flows," Journal of Physics A, vol. 40, pp. 4033–4053, 2007.

[44] H. Liu, A. Valocchi, and K. Q.J., "Three dimensionnal lattice boltzmann model for immiscible two phase flow simulations," Physical review E, vol. 85, no. 4, p. 046309, 2012.

[45] A. Subhedar, A. Reiter, M. Selzer, F. Varnik, and B. Nestler, "Interface tracking characteristics of color-gradient lattice boltzmann model for immiscible fluids," Physical Review E, vol. 101, p. 013313, 2020.

[46] Y. Sun and C. Beckermann, "Sharp interface tracking using the phase-field equation," Journal of Computational Physics, vol. 220, pp. 626–653, 2007.

[47] P. Chiu and Y.-T. Lin, "A conservative phase field method for solving compressible two phase flows," Journal of computational Physics, vol. 230, pp. 185–204, 2011.

[48] L. Boltzmann and S. G. Brush (translator), Lectures on gas theory. Berkeley: University of California Press, 1964.

[49] J. C. Maxwell, " V. Illustrations of the dynamical theory of gases. Part I. On the motions and collisions of perfectly elastic spheres ," The London, Edinburgh, and Dublin Philosophical Magazine and Journal of Science, vol. 19, no. 124, pp. 19–32, 1860.

[50] P. Bhatnagar, E. Gross, and M. Krook, "A Model for Collision Processes in Gases. I. Small Amplitude Processes in Charged and Neutral One-Component Systems," Physical Review, vol. 94, no. 3, pp. 511–525, 1954.

[51] S. Chapman and T. Cowling, The Mathematical Theory of Non-uniform Gases: An Account of the Kinetic Theory of Viscosity, Thermal Conduction and Diffusion in Gases. Cambridge University Press, 1st ed., 1970.

[52] G. Silva and V. Semiao, "First and second order forcing expansion in a atice boltzmann method reproducing isothermal hydrodynamics in artificial compressibility form," Journal of FLuid Mechanics, vol. 698, pp. 282–303, 2012.

[53] X. He, X. Shan, and D. G.D., "Discrete boltzmann equation model for nonideal gases," Physical Review E, vol. 57, no. 1, pp. R13–R16, 1998.

[54] T. Krüger, A. Kusumaatmaja, A. Kuzmin, O. Shardt, G. Silva, and E. Viggen, The Lattice Boltzmann Method, Principles and Practice. Springer Nature, 1st ed., 2017.

[55] Y. H. Qian, D. D'Humières, and P. Lallemand, "Lattice bgk models for navier-stokes equation," Epl, vol. 17, no. 6, pp. 479–484, 1992.

[56] S. Succi, The Lattice Boltzmann Equation for Fluid Dynamics and Beyond. Oxford university press, 1st ed., 2001.

[57] A. Kajzer and J. Pozorski, "A weakly Compressible, Diffuse-Interface Model for Two-Phase Flows," vol. 105, no. 2, pp. 299–333, 2020.

[58] X. He and L.-S. Luo, "A priori derivation of the lattice Boltzmann equation," Physical Review E, vol. 55, no. 6, pp. 6333–6336, 1997.

[59] X. He and L.-S. Luo, "Theory of the lattice Boltzmann method: From the Boltzmann equation to the lattice Boltzmann equation," Physical Review E, vol. 56, no. 6, pp. 6811–6817, 1997.

[60] X. He and L.-S. Luo, "Latice Boltzmann Model for the Incompressible Navier Stoke Equation," Journal of Statistical Physics, vol. 88, no. 3/4, pp. 927–944, 1997.

[61] J. Hardy and Y. Pomeau, "Thermodynamics and hydrodynamics for a modeled fluid," Journal of Mathematical Physics, vol. 13, no. 7, pp. 1042–1051, 1972.

[62] J. Hardy, Y. Pomeau, and O. De Pazzis, "Time evolution of a two-dimensional model system. I. Invariant states and time correlation functions," Journal of Mathematical Physics, vol. 14, no. 12, pp. 1746–1759, 1973.

[63] J. Hardy, O. De Pazzis, and Y. Pomeau, "Molecular dynamics of a classical lattice gas: Transport properties and time correlation functions," Physical Review A, vol. 13, no. 5, pp. 1949–1961, 1976.

[64] U. Frisch, D. D'humieres, B. Hasslacher, P. Lallemand, Y. Ves Pomeau, and J.-P. R. Ivet, "Lattice G as Hydrodynamics in Two and Three Dimensions," Complex Systems, vol. 1, pp. 649–707, 1987.

[65] J. Rivet and U. Frisch, "Automates sur gaz de réseau dans l'approximation de Boltzmann," C. R. Acad. Sci. Paris, Ser. II, vol. 302, no. 6, p. 267:, 1986.

[66] S. Wolfram, "Cellular automaton fluids 1: Basic theory," Journal of Statistical Physics, vol. 45, no. 3-4, pp. 471–526, 1986.

[67] A. S. Suiker and C. S. Chang, "Application of higher-order tensor theory for formulating enhanced continuum models," Acta Mechanica, vol. 142, no. 1, pp. 223–234, 2000.

[68] F. J. Higuera and J. Jiménez, "Boltzmann approach to lattice gas simulations," Epl, vol. 9, no. 7, pp. 663–668, 1989.

[69] S. Schmidt, O. Tammisola, L. Lesshafft, and K. Oberleithner, "Global stability and nonlinear dynamics of wake flows with a two-fluid interface," Journal of Fluid Mechanics, vol. 915, pp. 1–27, 2021.

[70] J. Eggers and E. Villermaux, "Physics of liquid jets," Reports on Progress in Physics, vol. 71, p. 036601, feb 2008.

[71] F. H. Harlow and J. E. Welch, "Numerical calculation of time-dependent viscous incompressible flow of fluid with free surface," Physics of Fluids, vol. 8, no. 12, pp. 2182–2189, 1965.

[72] J. E. Welch, F. H. Harlow, J. P. Shannon, and B. J. Daly, "The mac method: a computing technique for solving viscous, incompressible transient fluid-flow problems involving free surfaces," ., vol. ., 11 1968.

[73] S. Patankar, Numerical heat transfer and fluid flow. Taylor & Francis, 1st ed., 1980.

[74] A. A. Amsden and F. H. Harlow, "The smac method: A numerical technique for calculating incompressible fluid flows.," ., 1 1970.

[75] M. F. Tome and S. McKee, "GENSMAC: A computational marker and cell method for free surface flows in general domains," vol. 110, no. 1, pp. 171–186, 1994.

[76] N. Mangiavacchi, A. Castelo, M. F. Tome, J. A. Cuminato, M. Oliveira, and S. McKee, "An effective implementation of surface tension using the marker and cell method for axisymmetric and planar show," SIAM Journal of Scientific Computing, vol. 26, no. 4, pp. 1340–1368, 2005.

[77] S. McKee, M. F. Tomé, V. G. Ferreira, J. A. Cuminato, A. Castelo, F. S. Sousa, and N. Mangiavacchi, "The MAC method," Computers and Fluids, vol. 37, no. 8, pp. 907–930, 2008.

[78] F. S. de Sousa, N. Mangiavacchi, L. G. Nonato, A. Castelo, M. F. Tomé, V. G. Ferreira, J. A. Cuminato, and S. McKee, "A front-tracking/front-capturing method for the simulation of 3D multi-fluid flows with free surfaces," Journal of Computational Physics, vol. 198, no. 2, pp. 469–499, 2004.

[79] C. Hirt and B. Nichols, "Volume of fluid (VOF) method for the dynamics of free boundaries ," J. Comput. Phys., vol. 1, no. 39, pp. 201–225, 1981.

[80] W. Noh and P. Woodward, "SLIC (Simple Line Interface Calculation)," Proceeding of the Fifth international Conference on Numerical Methods in Fluid Dynamics, pp. 330–340, 1976.

[81] O. Ubbink and R. I. Issa, "A Method for Capturing Sharp Fluid Interfaces on Arbitrary Meshes," Journal of Computational Physics, vol. 153, no. 1, pp. 26–50, 1999.

[82] B. Lafaurie, C. Nardone, R. Scardovelli, S. Zaleski, and G. Zanetti, "Modelling merging and fragmentation in multiphase flows with SURFER," Journal of Computational Physics, vol. 113, no. 1, pp. 134–147, 1994.

[83] Y. Y. Tsui, S. W. Lin, T. T. Cheng, and T. C. Wu, "Flux-blending schemes for interface capture in two-fluid flows," International Journal of Heat and Mass Transfer, vol. 52, no. 23-24, pp. 5547–5556, 2009.

[84] J. K. Patel and G. Natarajan, "A generic framework for design of interface capturing schemes for multi-fluid flows," Computers and Fluids, vol. 106, pp. 108–118, 2015.

[85] D. L. Youngs, "Time-dependent multi-material flow with large fluid distortion.," ., no. January 1982, 1982.

[86] J. E. Pilliod and E. G. Puckett, "Second-order accurate volume-of-fluid algorithms for tracking material interfaces," Journal of Computational Physics, vol. 199, no. 2, pp. 465–502, 2004.

[87] S. J. Mosso, B. K. Swartz, D. B. Kothe, and S. P. Clancy, "Recent enhancements of volume tracking algorithms for irregular grids," Los Alamos National Laboratory , Los Alamos , NM ,LA_UR_96_277, no. October 1996, pp. 20–23, 1996.

[88] V. Dyadechko and M. Shashkov, "Moment-of-fluid interface reconstruction," Mathematical Modeling And Analysis, vol. 836, pp. 1–41, 2005.

[89] M. Sussman and E. G. Puckett, "A Coupled Level Set and Volume-of-Fluid Method for Computing 3D and Axisymmetric Incompressible Two-Phase Flows," Journal of Computational Physics, vol. 162, no. 2, pp. 301–337, 2000.

[90] S. Schmidt, O. Krüger, K. Göckeler, and C. O. Paschereit, "Numerical investigation of the breakup behavior of an oscillating two-phase jet," Physics of Fluids, vol. 30, no. 7, 2018.

[91] S. Popinet, "Gerris: A tree-based adaptive solver for the incompressible Euler equations in complex geometries," Journal of Computational Physics, vol. 190, no. 2, pp. 572–600, 2003.

[92] S. Osher and J. Sethian, "Front propagating with curvature dependent speed: algorithm based on Hamilton-Jacobi formulations," J. Comput. Phys., vol. 1, no. 79, pp. 12–49, 1988.

[93] W. Mulder, S. Osher, and J. A. Sethian, "Computing interface motion in compressible gas dynamics," Journal of Computational Physics, vol. 100, no. 2, pp. 209–228, 1992.

[94] M. Sussman, "A level set approach for computing solutions to incompressible two-phase flow," 1994.

[95] E. Olsson and G. Kreiss, "A conservative level set method for two phase flow," Journal of Computational Physics, vol. 210, no. 1, pp. 225–246, 2005.

[96] E. Olsson, G. Kreiss, and S. Zahedi, "A conservative level set method for two phase flow II," Journal of Computational Physics, vol. 225, no. 1, pp. 785–807, 2007.

[97] O. Desjardins, V. Moureau, and H. Pitsch, "An accurate conservative level set/ghost fluid method for simulating turbulent atomization," Journal of Computational Physics, vol. 227, no. 18, pp. 8395–8416, 2008.

[98] J. Van Der Waals and J. translation: Rowlinson, "The thermodynamic theory of capillarity under the hypothesis of a continuous density variation," Journal of Statistical Physic, vol. 20, pp. 197–244, 1979.

[99] D. Korteweg, "Sur la forme que prennent les équations du mouvements des fluides si l'on tient compte des forces capillaires causées par des variations de densité considérables mais continues et sur la théorie de la capilarité dans l'hypothèse d'une variation continue de la densité," Archive Néerlandaise des Sciences Exactes et Naturelles, vol. II, no. 6, pp. 1–24, 1901.

[100] J. Cahn and J. Hilliard, "Free energy of a nonuniform system. i. interfacial free energy," The jourenal of chemical physics, vol. 28, no. 2, pp. 830–833, 1957.

[101] J. W. Gibbs, "On the equilibrium of heterogeneous substances," American Journal of Science, vol. s3-16, no. 96, pp. 441–458, 1878.

[102] G. Caginalp, "Stefan and Hele-Shaw type model as asymptotic limits of the phase-field equations," Physical Review A, vol. 39, no. 11, pp. 5887–5896, 1989.

[103] W. J. Boettinger, J. A. Warren, C. Beckermann, and A. Karma, "Phase-field simulation of solidification," Annual Review of Materials Science, vol. 32, pp. 163–194, 2002.

[104] D. Nayigizente, Unsteady simulations of liquid / gas interfaces in real gas flows using the Second Gradient
PhD thesis, Université Paris-Saclay, 2021.

[105] J. W. Cahn, C. M. Elliott, and A. Novick-Cohen, "The CahnHilliard equation with a concentration dependent mobility: motion by minus the Laplacian of the mean curvature," European Journal of Applied Mathematics, vol. 7, no. 3, pp. 287–301, 1996.

[106] J. W. Cahn, "On spinodal decomposition," Acta Metallurgica, vol. 9, no. 9, pp. 795–801, 1961.

[107] S. M. Allen and J. W. Cahn, "Mechanisms of phase transformations within the miscibility gap of Fe-rich Fe-Al alloys," Acta Metallurgica, vol. 24, no. 5, pp. 425–437, 1976.

[108] L. K. Antanovskii, "A phase field model of capillarity," Physics of Fluids, vol. 7, no. 4, pp. 747–753, 1995.

[109] X. Yang, J. J. Feng, C. Liu, and J. Shen, "Numerical simulations of jet pinching-off and drop formation using an energetic variational phase-field method," Journal of Computational Physics, vol. 218, no. 1, pp. 417–428, 2006.

[110] J. Rubinstein and P. Sternberg, "Nonlocal reaction-diffusion equations and nucleation," IMA Journal of Applied Mathematics (Institute of Mathematics and Its Applications), vol. 48, no. 3, pp. 249–264, 1992.

[111] V. Joshi and R. K. Jaiman, "A positivity preserving and conservative variational scheme for phase-field modeling of two-phase flows," Journal of Computational Physics, vol. 360, pp. 137–166, 2018.

[112] S. Kwak, J. Yang, and J. Kim, "A conservative AllenCahn equation with a curvature-dependent Lagrange multiplier," Applied Mathematics Letters, p. 107270, 2021.

[113] D. A. Drew, "Averaged Field Equations for Two-Phase Media," Studies in Applied Mathematics, vol. 50, no. 2, pp. 133–166, 1971.

[114] M. Baer and J. Nunziato, "A two phase mixture theory for the deflagration-to-detonation transition (DDT) in reactive granular materials," Int. J. Multiphase Flow, vol. 12, no. 6, pp. 861–889, 1986.

[115] R. Saurel and R. Abgrall, "A simple method for compressible multifluid flows," SIAM J. Sci. Comput., vol. 21, no. 3, pp. 1115–1145, 1999.

[116] A. K. Kapila, R. Menikoff, J. B. Bdzil, S. F. Son, and D. S. Stewart, "Two-phase modeling of deflagration-to-detonation transition in granular materials: Reduced equations," Physics of Fluids, vol. 13, no. 10, pp. 3002–3024, 2001.

[117] Richard Saurel, F. Petitpas, and R. A. Berry, "Simple and efficient relaxation methods for interfaces separating compressible fluids, cavitating flows and shocks in multiphase mixtures," Journal of Computational Physics, vol. 228, no. 5, pp. 1678–1712, 2009.

[118] R. Saurel, F. Petitpas, and R. Abgrall, "Modelling phase transition in metastable liquids: Application to cavitating and flashing flows," vol. 607, pp. 313–350, 2008.

[119] R. Saurel, P. Boivin, and O. Le Métayer, "A general formulation for cavitating, boiling and evaporating flows," Computers & Fluids, vol. 128, pp. 53–64, 2016.

[120] M. Pelletier, T. Schmitt, and S. Ducruix, "A multifluid Taylor-Galerkin methodology for the simulation of compressible multicomponent separate two-phase flows from subcritical to supercritical states," Computers and Fluids, vol. 206, 2020.

[121] P. Gaillard, V. Giovangigli, and L. Matuszewski, "A diffuse interface Lox/hydrogen transcritical flame model," Combustion Theory and Modelling, vol. 20, no. 3, pp. 486–520, 2016.

[122] J. Carmona, Modélisation des phénomènes diphasiques dans des injecteurs aéronautiques de type Airblast. PhD thesis, INPT, 2021.

[123] A. Chiapolino, P. Boivin, and R. Saurel, "A simple and fast phase transition relaxation solver for compressible multicomponent two-phase flows," Computers and Fluids, vol. 150, pp. 31–45, 2017.

[124] M. Barret, E. Faucher, and J.-M. Herard, "Schemes to compute unsteady flashing flows," AIAA Journal, vol. 40, no. 5, pp. 905–913, 2002.

[125] T. Laroche, N. Odier, T. Schmitt, M. Pelletier, and B. Cuenot, "A diffuse interface method with real-gas thermodynamic equilibrium closure applied to capillary problems," in ICLASS 2021, 15^{th} Triennial International Conference on Liquid Atomization and Spray Systems, (Edinburgh, UK), 2021.

[126] D. Jamet, O. Lebaigue, N. Coutris, and J. M. Delhaye, "The Second Gradient Method for the Direct Numerical Simulation of Liquid-Vapor Flows with Phase Change," Journal of Computational Physics, vol. 169, no. 2, pp. 624–651, 2001.

[127] D. Nayigizente, S. Ducruix, and T. Schmitt, "Development of an interface thickening method for the direct numerical simulation of compressible liquid-vapor flows in the framework of the second gradient theory," Physics of Fluids, vol. 33, no. 5, 2021.

[128] N. Ashgriz and J. Y. Poo, "Coalescence and separation in binary collisions of liquid drops," Journal of Fluid Mechanics, vol. 221, pp. 183–204, 1990.

[129] O. Benoit, Ecoulements multiphasiques: des fondements aux méthodes d'ingénieries. Hermes Sciences Publication, 2006.

[130] G. J. Gittens, "Variation of surface tension of water with temperature," Journal of Colloid And Interface Science, vol. 30, no. 3, pp. 406–412, 1969.

[131] S. Sugden, "Vi.the variation of surface tension with temperature and some related functions," J. Chem. Soc., Trans., vol. 125, pp. 32–41, 1924.

[132] A. Adamson and A. Gast, Physical chemistry of surfaces. New York: Wiley, 6th ed., 1997.

[133] https://cameochemicals.noaa.gov.

[134] J. Kim, "A continuous surface tension force formulation for diffuse-interface models," Journal of Computational Physics, vol. 204, pp. 784–804, 2005.

[135] J. Brackbill, D. Kothe, and C. Zemach, "A continuum method for modeling surface tension," Journal of Computation Physics, vol. 100, pp. 335–354, 1992.

[136] D. Gueyffier, J. Li, R. Scardovelli, and S. Zaleski, "Volume-of-Fluid interface tracking with smoothed surface stress methods for three-dimensional flows," Journal of Computational Physics, vol. 152, pp. 423–456, 1999.

[137] D. Jamet, Étude des Potentialités de la Théorie du Second Gradient pour la Simulation Numérique Directe PhD thesis, 1998.

[138] T. Lee and P. Fisher, "Eliminating parasitic currents in the lattice boltzmann equation method for nonideal gases," Physical Review E, vol. 74, p. 046709, 2006.

[139] T. Lee and L. Liu, "Lattice Boltzmann simulations of micron-scale drop impact on dry surfaces," Journal of Computational Physics, vol. 229, no. 20, pp. 8045–8063, 2010.

[140] P. Lallemand, L. Luo, and Y. Peng, "A lattice boltzmann front-tracking method for interface dynamics with surface tension in two dimensions," Journal of Computational Physics, vol. 226, pp. 1367–1384, 2007.

[141] Y. Kwak and A. Nakano, "Hybrid Lattice-Boltzmann/Level-set Method for Liquid Simulation and Visualization," International Journal of Computational Science, vol. 6669, pp. 1–14, 2009.

[142] J. Becker, M. Junk, D. Kehrwald, G. Thömmes, and Z. Yang, "A combined lattice BGK/level set method for immiscible two-phase flows," Computers and Mathematics with Applications, vol. 58, no. 5, pp. 950–964, 2009.

[143] X. He, X. Shan, and G. D. Doolen, "Discrete Boltzmann equation model for nonideal gases," Physical Review E - Statistical Physics, Plasmas, Fluids, and Related Interdisciplinary Topics, vol. 57, no. 1, pp. R13–R16, 1998.

[144] R. R. Nourgaliev, T. N. Dinh, and B. R. Sehgal, "On lattice Boltzmann modeling of phase transition in an isothermal non-ideal fluid," Nuclear Engineering and Design, vol. 211, no. 2-3, pp. 153–171, 2002.

[145] H. Huang, M. Sukop, and X. Lu, Multiphase Lattice Boltzmann Methods: Theory and Application. Wiley Blackwell, 1st ed., 2015.

[146] Q. Li, K. Luo, Q. Kang, Y. He, Q. Chen, and Q. Liu, "Lattice boltzmann methods for multiphase flow and phase-change heat transfer," Progress in Energy and Combustion Science, vol. 52, pp. 62–105, 2016.

[147] C. Zhang, Z. Guo, and H. Liang, "On the formulations of interfacial force in the phase-field-based lattice Boltzmann method," International Journal for Numerical Methods in Fluids, vol. 93, no. 7, pp. 2225–2248, 2021.

[148] Z. Guo, C. Zheng, and B. Shi, "Discrete lattice effects on the forcing term in the lattice boltzmann method," Physical Review E, vol. 65, p. 046308, 2002.

[149] T. Lafarge, P. Boivin, N. Odier, and B. Cuenot, "Improved color-gradient method for lattice Boltzmann modeling of two-phase flows," Physics of Fluids, vol. 33, no. 8, p. 082110, 2021.

[150] S. Leclaire, M. Reggio, and J. Trépanier, "Isotropic color gradient for simulating very high-density ratios with a two-phase flow lattice Boltzmann model," Computers and fluids, vol. 48, pp. 98–112, 2011.

[151] X. Shan, "Analysis and reduction of the spurious current in a class of multiphase lattice Boltzmann models," Physical Review E - Statistical, Nonlinear, and Soft Matter Physics, vol. 73, no. 4, pp. 6–9, 2006.

[152] T. Lee and C. L. Lin, "A stable discretization of the lattice Boltzmann equation for simulation of incompressible two-phase flows at high density ratio," Journal of Computational Physics, vol. 206, no. 1, pp. 16–47, 2005.

[153] L. S. Luo, "Theory of the lattice Boltzmann method: Lattice Boltzmann models for nonideal gases," Physical Review E - Statistical Physics, Plasmas, Fluids, and Related Interdisciplinary Topics, vol. 62, no. 4, pp. 4982–4996, 2000.

[154] D. Holdych, D. Rovas, J. Georgiadis, and R. Buckius, "An improved hydrodynamics formulation for multiphase flow lattice-boltzmann models," International Journal of Modern Physics C, vol. 9, pp. 1393–1404, 12 1998.

[155] A. Wagner and Q. Li, "investigation of galilean invariance of multi-phase lattice boltzmann methods," Physica A, vol. 362, pp. 105–110, 2006.

[156] C. Pooley and K. Furtado, "Eliminating spurious velocities in the free-energy lattice boltzmann method," Physical Review E, vol. 77, p. 046702, 2008.

[157] C. Semprebon, T. Krüger, and H. Kusumaatmaja, "Ternary free-energy lattice boltzmann model with tunable surface tensions and contact angles," Physical Review E, vol. 93, p. 033305, 2016.

[158] N. Che Sidik and T. Tanahashi, "Two-phase flow simulation with lattice boltzmann method," J. Mekanikal, vol. 24, pp. 68–79, 2007.

[159] S. Leclaire, N. Pellerin, M. Reggio, and J.-Y. Trépanier, "Enhanced equilibrium distribution functions for simulating immiscible multiphase flows with variable density ratios in a class of lattice boltzmann models," International Journal of Multiphase Flow, vol. 57, pp. 159–168, 2013.

[160] Q. Li, K. Luo, Y. He, Y. Gao, and W. Tao, "Coupling lattice Boltzmann model for simulation of thermal flows on standard lattices," Physical Review E, vol. 85, p. 016710, 2012.

[161] Z. Wen, Q. Li, Y. Yu, and K. Luo, "Improved three-dimensional color-gradient lattice Boltzmann model for immiscible two-phase flows," Physical Review E, vol. 100, p. 023301, 2019.

[162] G. Farag, S. Zhao, T. Coratger, P. Boivin, G. Chiavassa, and P. Sagaut, "A pressure-based regularized lattice-Boltzmann method for the simulation of compressible flows," Physics of Fluids, vol. 32, no. 6, 2020.

[163] G. Farag, T. Coratger, G. Wissocq, S. Zhao, P. Boivin, and P. Sagaut, "A unified hybrid lattice-Boltzmann method for compressible flows: Bridging between pressure-based and density-based methods," Physics of Fluids, vol. 33, no. 8, 2021.

[164] D. Grunau, S. Chen, and K. Eggert, "A lattice Boltzman model for multiphase fluid flows," Physics of fluids A, vol. 5, no. 10, pp. 2557–2562, 1993.

[165] J. Tölke, M. Krafczyk, M. Schulz, and E. Rank, "Lattice boltzmann simulations of binary fluid flow through porous media," Phil. Trans. R. Soc. Lond. A, vol. 360, pp. 535–545, 2002.

[166] S. Leclaire, N. Pellerin, M. Reggio, and J.-Y. Trépanier, "Unsteady immiscible multiphase flow validation of a multiplerelaxation-time lattice boltzmann method," Journal of Physics A: Mathematical and Theoretical, vol. 47, p. 105501, 2014.

[167] K. Burgin, J. Spendlove, X. Xu, and I. Halliday, "Kinematics of chromodynamic multicomponent lattice Boltzmann simulation with a large density contrast," Physical Review E, vol. 100, no. 4, pp. 1–15, 2019.

[168] A. Hollis, I. Halliday, and R. Law, "Kinematic condition for multicomponent lattice Boltzmann simulation," Physical Review E, vol. 76, no. 2, pp. 1–6, 2007.

[169] S. Leclaire, A. Parmigiani, O. Malaspinas, C. B., and L. J., "Generalized three-dimensional lattice boltzmann color-gradient method for immiscible two-phase pore-scale imbition and drainage in porous media," Physical Review E, vol. 95, p. 033306, 2017.

[170] H. Huang, J. Huang, X. Lu, and M. Sukop, "On simulations of high-density ratio flows using color-gradient multiphase lattice Boltzmann models," International Journal of Modern Physics C, vol. 24, no. 4, p. 1350021, 2013.

[171] S. Saito, Y. Abe, and K. Koyama, "Lattice Boltzmann modeling and simulation of liquid jet breakup," Physical Review E, vol. 96, no. 1, pp. 1–18, 2017.

[172] M. Latva-Kokko and D. Rothman, "Diffusion properties of gradient-based lattice Boltzmann models of immiscible fluids," Physical review E, vol. 71, p. 056702, 2005.

[173] U. D'Ortona, D. Salin, M. Cieplak, R. Rybka, and J. Banavar, "Two-color nonlinear boltzmann cellular automate: Surface tension and wetting," Physical Review E, vol. 51, no. 4, pp. 3718–3728, 1995.

[174] I. Halliday, A. Hollis, and C. Care, "Lattice boltzmann algorithm for continuum multicomponent flow," Physical review E, vol. 76, p. 026708, 2007.

[175] S. Lishchuk, C. Care, and I. Halliday, "Lattice boltzmann algorithm for surface tension with greatly reduced microcurrents," Physical review E, vol. 67, p. 036701, 2003.

[176] S. V. Lishchuk, I. Halliday, and C. M. Care, "Multicomponent lattice Boltzmann method for fluids with a density contrast," Physical Review E - Statistical, Nonlinear, and Soft Matter Physics, vol. 77, no. 3, pp. 1–8, 2008.

[177] Y. Ba, H. Liu, Q. Li, Q. Kang, and J. Sun, "Multiple-relaxation-time color-gradient lattice Boltzmann model for simulating two-phase flows with high density ratio," Physical Review E, vol. 94, no. 2, pp. 1–15, 2016.

[178] S. Leclaire, M. Reggio, and J. Y. Trépanier, "Progress and investigation on lattice Boltzmann modeling of multiple immiscible fluids or components with variable density and viscosity ratios," Journal of Computational Physics, vol. 246, pp. 318–342, 2013.

[179] T. Inamuro, T. Ogata, S. Tajima, and N. Konishi, "A lattice boltzmann method sor incompressible two-phase flows with large density differences," Journal of Computational Physics, vol. 198, pp. 628–644, 2004.

[180] T. Inamuro, M. Yoshino, H. Inoue, R. Mizuno, and F. Ogino, "A lattice Boltzmann method for a binary miscible fluid mixture and its application to a heat-transfer problem," Journal of Computational Physics, vol. 179, no. 1, pp. 201–215, 2002.

[181] T. Inamuro, T. Yokoyama, K. Tanaka, and M. Taniguchi, "An improved lattice Boltzmann method for incompressible two-phase flows with large density differences," Computers and Fluids, vol. 137, pp. 55–69, 2016.

[182] K. Suzuki, T. Inamuro, A. Nakamura, F. Horai, K. L. Pan, and M. Yoshino, "Simple extended lattice Boltzmann methods for incompressible viscous single-phase and two-phase fluid flows," Physics of Fluids, vol. 33, no. 3, 2021.

[183] P. Yuan and L. Schaefer, "Equation of state in a lattice boltzmann model," Phys. Fluids, vol. 18, p. 042101, 2006.

[184] P. Yuan and L. Schaefer, "Equation of state in a lattice boltzmann model," Physics of fluids, vol. 18, p. 042101, 2006.

[185] M. Sbragaglia, R. Benzi, L. Biferale, S. Succi, S. K., and F. Toschi, "Geneleralized lattice boltzmann method with multirange pseudopotential," Physical Review E, vol. 75, no. 2, p. 026702, 2007.

[186] S. Gong and P. Cheng, "Numerical investigation of droplet motion and coalescence by an improved lattice Boltzmann model for phase transitions and multiphase flows," Computers and Fluids, vol. 53, no. 1, pp. 93–104, 2012.

[187] A. Zarghami, N. Looije, and H. Van Den Akker, "Assessment of interaction potential in simulating nonisothermal multiphase systems by means of lattice Boltzmann modeling," Physical Review E - Statistical, Nonlinear, and Soft Matter Physics, vol. 92, no. 2, pp. 1–18, 2015.

[188] R. Benzi, L. Biferale, M. Sbragaglia, s. Succi, and F. Toschi, "Mesoscopic modelling of a two-phase flow in the presence of boundaries: The contact angle," Physical Review E, vol. 74, no. 2, p. 021509, 2006.

[189] H. Huang, D. T. Thorne, M. G. Schaap, and M. C. Sukop, "Proposed approximation for contact angles in Shan-and-Chen-type multicomponent multiphase lattice Boltzmann models," Physical Review E - Statistical, Nonlinear, and Soft Matter Physics, vol. 76, no. 6, pp. 1–6, 2007.

[190] Q. Li and K. H. Luo, "Achieving tunable surface tension in the pseudopotential lattice Boltzmann modeling of multiphase flows," Physical Review E - Statistical, Nonlinear, and Soft Matter Physics, vol. 88, no. 5, pp. 1–10, 2013.

[191] A. Xu, T. S. Zhao, L. An, and L. Shi, "A three-dimensional pseudo-potential-based lattice Boltzmann model for multiphase flows with large density ratio and variable surface tension," International Journal of Heat and Fluid Flow, vol. 56, pp. 261–271, 2015.

[192] L. Fei, J. Du, K. Luo, S. Succi, M. Lauricella, and A. Montessori, "Modeling realistic multiphase flows using a non-orthogonal multiple-relaxation-time lattice boltzmann method," Physics of Fluids, vol. 31, p. 042105, 2019.

[193] M. E. Gurtin, D. Polignone, and J. Viñals, "Two-phase binary fluids and immiscible fluids described by an order parameter," Mathematical Models and Methods in Applied Sciences, vol. 06, pp. 815–831, sep 1996.

[194] T. Lee and L. Liu, "Wall boundary conditions in the lattice Boltzmann equation method for nonideal gases," Physical Review E - Statistical, Nonlinear, and Soft Matter Physics, vol. 78, no. 1, pp. 16–19, 2008.

[195] D. Lycett-Brown and K. H. Luo, "Multiphase cascaded lattice Boltzmann method," Computers and Mathematics with Applications, vol. 67, no. 2, pp. 350–362, 2014.

[196] A. Fakhari and T. Lee, "Finite-difference lattice Boltzmann method with a block-structured adaptive-mesh-refinement technique," Physical Review E - Statistical, Nonlinear, and Soft Matter Physics, vol. 89, no. 3, pp. 1–12, 2014.

[197] Y. Q. Zu and S. He, "Phase-field-based lattice Boltzmann model for incompressible binary fluid systems with density and viscosity contrasts," Physical Review E - Statistical, Nonlinear, and Soft Matter Physics, vol. 87, no. 4, pp. 1–23, 2013.

[198] K. Premnath and J. Abraham, "Lattice boltzmann model for axisymmetric multiphase flows," Physical Review E, vol. 71, p. 056706, 2005.

[199] M. McCracken and J. Abraham, "Multiple-relaxation time lattice-boltzmann model for multiphase flow," Physical Review E, vol. 71, p. 036701, 2005.

[200] M. McCracken and J. Abraham, "Simulations of liquid break up with an axisymmetric, multiple relaxation time index-function lattice boltzmann model," International Journal of Modern Physics C, vol. 16, no. 11, pp. 1671–1692, 2005.

[201] F. Dubois, "Equivalent partial differential equations of a lattice Boltzmann scheme," Computers and Mathematics with Applications, vol. 55, pp. 1441–1449, 2008.

[202] D. D'Humières, I. Ginzburg, M. Krafczyk, P. Lallemand, and L. Luo, "Multiple-relaxation time lattice boltzmann models in three dimensions," Philosophical Transactions of the Royal Society, vol. 360, pp. 437–451, 2002.

[203] A. De Rosis, "Nonorthogonal central-moments-based lattice Boltzmann scheme in three dimensions," Physical Review E, vol. 95, no. 1, pp. 1–16, 2017.

[204] M. Geier, A. Greiner, and J. G. Korvink, "Cascaded digital lattice Boltzmann automata for high Reynolds number flow," Physical Review E - Statistical, Nonlinear, and Soft Matter Physics, vol. 73, no. 6, pp. 1–10, 2006.

[205] F. Dubois, T. Fevrier, and B. Graille, "Lattice Boltzmann schemes with relative velocities," ., 2015.

[206] C. Coreixas, B. Chopard, and J. Latt, "Comprehensive comparison of collision models in the lattice Boltzmann framework: Theoretical investigations," Physical Review E, vol. 100, no. 3, 2019.

[207] S. Seeger and K. H. Hoffmann, "The cumulant method for computational kinetic theory," Continuum Mechanics and Thermodynamics, vol. 12, no. 6, pp. 403–421, 2000.

[208] M. Geier, M. Schönherr, A. Pasquali, and M. Krafczyk, "The cumulant lattice Boltzmann equation in three dimensions: Theory and validation," Computers and Mathematics with Applications, vol. 70, no. 4, pp. 507–547, 2015.

[209] I. Ginzburg, F. Verhaeghe, and D. D'Humières, "Study of simple hydrodynamic solutions with the two-relaxation-times lattice Boltzmann scheme," Communications in Computational Physics, vol. 3, no. 3, pp. 519–581, 2008.

[210] I. Ginzburg, "Truncation errors, exact and heuristic stability analysis of two-relaxation-times lattice boltzmann schemes for anisotropic advection-diffusion equation," Communications in Computational Physics, vol. 11, no. 5, pp. 1439–1502, 2012.

[211] D. D'Humières and I. Ginzburg, "Viscosity independent numerical errors for Lattice Boltzmann models: From recurrence equations to "magic" collision numbers," Computers and Mathematics with Applications, vol. 58, no. 5, pp. 823–840, 2009.

[212] G. Silva and V. Semiao, "Truncation errors and the rotational invariance of three-dimensional lattice models in the lattice Boltzmann method," Journal of Computational Physics, vol. 269, pp. 259–279, 2014.

[213] K. Pasieczynski and B. Chen, "Fluidfluid interactions in pseudopotential lattice Boltzmann models: Effects of model schemes and fluid properties," International Journal for Numerical Methods in Fluids, vol. 93, no. 5, pp. 1578–1605, 2021.

[214] I. Ginzburg, D. D'Humières, and A. Kuzmin, "Optimal stability of advection-diffusion lattice boltzmann models with two relaxation times for positive/negative equilibrium," Journal of Statistical Physics, vol. 139, no. 6, pp. 1090–1143, 2010.

[215] J. Latt and B. Chopard, "Lattice Boltzmann method with regularized pre-collision distribution functions," Mathematics and Computers in Simulation, vol. 72, no. 2-6, pp. 165–168, 2006.

[216] G. Wissocq, P. Sagaut, and J. F. Boussuge, "An extended spectral analysis of the lattice Boltzmann method: modal interactions and stability issues," Journal of Computational Physics, vol. 380, pp. 311–333, 2019.

[217] O. Malaspinas, "Increasing stability and accuracy of the lattice Boltzmann scheme: recursivity and regularization," ., pp. 1–31, 2015.

[218] J. Jacob, O. Malaspinas, and P. Sagaut, "A new hybrid recursive regularised bhatnagargrosskrook collision model for lattice boltzmann method-based large eddy simulation," Journal of Turbulence, vol. 19, no. 11, pp. 1051–1076, 2019.

[219] T. Astoul, G. Wissocq, J. F. Boussuge, A. Sengissen, and P. Sagaut, "Analysis and reduction of spurious noise generated at grid refinement interfaces with the lattice Boltzmann method," Journal of Computational Physics, vol. 418, p. 109645, 2020.

[220] F. Renard, Y. Feng, J. F. Boussuge, and P. Sagaut, "Improved compressible hybrid lattice Boltzmann method on standard lattice for subsonic and supersonic flows," Computers and Fluids, vol. 219, 2021.

[221] X. Shan and G. Doolen, "Multicomponent lattice-Boltzmann model with interparticle interaction," Journal of Statistical Physics, vol. 81, no. 1-2, pp. 379–393, 1995.

[222] A. J. C. Ladd and R. Verberg, "Lattice-Boltzmann Simulations of Particle-Fluid Suspensions," Journal of Statistical Physics, vol. 104, no. September, pp. 1191–1251, 2001.

[223] D. J. Holdych, D. R. Noble, J. G. Georgiadis, and R. O. Buckius, "Truncation error analysis of lattice Boltzmann methods," Journal of Computational Physics, vol. 193, no. 2, pp. 595–619, 2004.

[224] D. W. Davis and B. Chehroudi, "Shear-coaxial jets from a rocket-like injector in a transverse acoustic field at high pressures," 44th AIAA Aerospace Sciences Meeting and Exhibit, vol. 13, no. May, pp. 9173–9190, 2006.

[225] F. Baillot, J. B. Blaisot, G. Boisdron, and C. Dumouchel, "Behaviour of an air-assisted jet submitted to a transverse high-frequency acoustic field," Journal of Fluid Mechanics, vol. 640, pp. 305–342, 2009.

[226] A. Qi, L. Y. Yeo, and J. R. Friend, "Interfacial destabilization and atomization driven by surface acoustic waves," Physics of Fluids, vol. 20, no. 7, 2008.

[227] J. M. Apeloig, F. X. D'Herbigny, F. Simon, P. Gajan, M. Orain, and S. Roux, "Liquid-fuel behavior in an aeronautical injector submitted to thermoacoustic instabilities," Journal of Propulsion and Power, vol. 31, no. 1, pp. 309–319, 2015.

[228] W. Verdier, P. Kestener, and A. Cartalade, "Performance portability of lattice Boltzmann methods for two-phase flows with phase change," Computer Methods in Applied Mechanics and Engineering, vol. 370, p. 113266, 2020.

[229] O. L. Métayer, J. Massoni, and R. Saurel, "Élaboration des lois d ' état d ' un liquide et de sa vapeur pour les modèles d ' écoulements diphasiques Elaborating equations of state of a liquid and its vapor for two-phase flow models," International journal of thermal sciences, vol. 43, pp. 265–276, 2004.

[230] P. Boivin, M. Cannac, and O. Le Métayer, "A thermodynamic closure for the simulation of multiphase reactive flows," International Journal of Thermal Sciences, vol. 137, pp. 640–649, 2019.

[231] G. Farag, S. Zhao, G. Chiavassa, and P. Boivin, "Consistency study of lattice-boltzmann schemes macroscopic limit," Physics of Fluids, vol. 33, no. 3, p. 031701, 2021.

[232] F. Renard, Y. Feng, J. Boussuge, and P. Sagaut, "Improved compressible hybrid lattice boltzmann method on standard lattice for subsonic and supersonic flows," arXiv preprint arXiv:2002.03644, 2020.

[233] S. Guo, Y. Feng, and P. Sagaut, "Improved standard thermal lattice boltzmann model with hybrid recursive regularization for compressible laminar and turbulent flows," Physics of Fluids, vol. 32, no. 12, p. 126108, 2020.

[234] H. Huang and X. Lu, "Relative permeabilities and coupling effects in steady-state gas-liquid flow in porous media: A lattice Boltzmann study," Physic of fluids, vol. 21, p. 092104, 2009.

[235] L. Rayleigh, "On The Instability Of Jets," Proceedings of the London Mathematical Society, vol. s1-10, pp. 4–13, nov 1878.

[236] D. Fyfe, E. Oran, and M. Fritts, "Surface tension and viscosity with lagrangian hydrodynamics on a triangular mesh," Journal of Computational Physics, vol. 76, no. 2, pp. 349–384, 1988.

[237] D. Jamet, D. Torres, and J. U. Brackbill, "On the theory and computation of surface tension: The elimination of parasitic currents through energy conservation in the second-gradient method," Journal of Computational Physics, vol. 182, no. 1, pp. 262–276, 2002.

[238] H. Grad, "Note on Ndimensional hermite polynomials," Communications on Pure and Applied Mathematics, vol. 2, no. 4, pp. 325–330, 1949.

[239] M. Geier, A. Fakhari, and T. Lee, "Conservative phase-field lattice Boltzmann model for interface tracking equation," Physical Review E - Statistical, Nonlinear, and Soft Matter Physics, vol. 91, no. 6, pp. 1–11, 2015.